



**HAL**  
open science

# Neuronal properties and synaptic connectivity in rodent presubiculum

Jean Simonnet

► **To cite this version:**

Jean Simonnet. Neuronal properties and synaptic connectivity in rodent presubiculum. *Neurons and Cognition [q-bio.NC]*. Université Pierre et Marie Curie - Paris VI, 2014. English. NNT : 2014PA066435 . tel-02295014

**HAL Id: tel-02295014**

**<https://theses.hal.science/tel-02295014>**

Submitted on 24 Sep 2019

**HAL** is a multi-disciplinary open access archive for the deposit and dissemination of scientific research documents, whether they are published or not. The documents may come from teaching and research institutions in France or abroad, or from public or private research centers.

L'archive ouverte pluridisciplinaire **HAL**, est destinée au dépôt et à la diffusion de documents scientifiques de niveau recherche, publiés ou non, émanant des établissements d'enseignement et de recherche français ou étrangers, des laboratoires publics ou privés.



**THÈSE DE DOCTORAT  
DE L'UNIVERSITÉ PIERRE ET MARIE CURIE**

Spécialité Neurosciences  
École doctorale Cerveau – Cognition – Comportement

Présentée par :  
Jean Simonnet

Pour obtenir le grade de  
**DOCTEUR DE L'UNIVERSITÉ PIERRE ET MARIE CURIE**

Sujet de la thèse :

**Neuronal properties and synaptic  
connectivity in rodent presubiculum**

Soutenue le 23.09.2014  
devant le jury composé de :

Dr Jean-Christophe Poncer	Président
Dr Dominique Debanne	Rapporteur
Dr Maria Cecilia Angulo	Rapportrice
Pr Hannah Monyer	Examinatrice
Dr Bruno Cauli	Examineur
Dr Desdemona Fricker	Directrice de thèse

---

Université Pierre & Marie Curie - Paris 6  
Bureau d'accueil, inscription des doctorants  
et base de données  
Esc. G, 2ème étage  
15 Rue de l'école de médecine  
75270 - PARIS CEDEX 06

Tél. Secrétariat : 01 42 34 68 35  
Fax : 01 42 34 68 40  
Tél. pour les étudiants de A à EL : 01 42 34 68 41  
Tél. pour les étudiants de EM à MON : 01 42 34 68 41  
Tél. pour les étudiants de MOO à Z : 01 42 34 68 51  
E-mail : [scolarite.doctorat@upmc.fr](mailto:scolarite.doctorat@upmc.fr)



## Abstract

Cognitive functions rely on the generation and regulation of information in specialized neuronal networks. The presubiculum, a cortical area located between the hippocampus and the entorhinal cortex, is involved in signaling the sense of orientation in animals as well as in humans. Most presubicular neurons are Head Direction Cells, that is, they fire as a function of directional heading. The presubiculum constitutes a crucial crossroad for spatial information. Very few data exist on the functional organization of the presubiculum, but its 6-layered cytoarchitecture suggests that signals are not passively relayed but rather actively integrated and refined.

During my PhD, I studied the microcircuit elements of rodent presubiculum in the slice preparation, linking structure and physiology using patch clamp records.

First, I focused on rat principal neurons and distinguished 3 groups: a homogeneous population of regular spiking neurons in superficial layers, mostly pyramidal; intrinsically burst firing neurons of layer 4; and a very heterogeneous population of regular spiking neurons in deep layers. These populations constitute the primary elements for information processing in the presubiculum, and their diversity suggests a high computational power.

Then, I addressed the question of the inhibitory control in the presubiculum. Recordings were performed from slices of transgenic mouse strains that express fluorescent proteins in interneurons. We showed a continuum of diversity for parvalbumin- (PV) and somatostatin- (SST) containing interneurons, from the archetypical PV-positive fast spiking basket cells to the SST-positive low-threshold spiking Martinotti cells. Regarding the inhibition, the presubiculum seems to possess the complexity of all cortical areas.

Finally, I investigated the synaptic interactions of pyramidal cells and Martinotti cells in superficial layers, using dual patch clamp recordings. Martinotti cells provide low amplitude but reliable inhibition onto pyramidal cell dendrites. I found that the strength at the excitatory synapse was enhanced following repetitive stimulation at high frequency. Consequently, dendritic inhibition by presubicular Martinotti cells may act as a homeostatic response to sustained excitation.

My PhD work brought essential knowledge about the presubicular microcircuit. It has shed light on the different populations of principal neurons and GABAergic interneurons and has uncovered a feedback inhibitory loop that is recruited during sustained but not transient activity.



## Acknowledgments

First, I would like to thank the members of my Jury: Hannah Monyer, Jean Christophe Poncer, Bruno Cauli as well as Dominique Debanne and Maria Cecilia Angulo who have accepted to review this manuscript.

Je tiens à remercier Desdemona, qui m'a donné l'opportunité de travailler avec elle et qui m'a encadré tout au long de cette thèse. Tu as su me donner la liberté de travail dont j'avais besoin, et je te remercie de m'avoir permis d'exprimer mes idées et mes envies tout en ayant un oeil critique et avisé à chaque étape. Je pense que cela n'a pas été une chose facile avec mon caractère plutôt ombrageux... Difficile à convaincre notamment. Disons que nous avons eu un certain nombre de discussions passionnées sur la « bonne manip à faire » ou « la figure à montrer » ou « ce qu'il faut dire ». J'ai toujours pris cela dans le sens positif, à savoir que la confrontation de nos idées a toujours permis d'améliorer notre travail. Je voudrais aussi te remercier pour la compréhension dont tu as fait preuve, par rapport aux aléas de la vie qui ne concernent en rien le travail, mais qui l'impactent inévitablement. Enfin, je souhaite exprimer toute ma gratitude de m'avoir toujours soutenu tout au long de ces années.

Bien évidemment, cette thèse ne serait pas possible sans Richard, qui m'a ouvert les portes de son laboratoire et apporté son soutien quotidien. Vous avez su me prodiguer de très bons conseils durant toute cette thèse. S'il y a une chose que j'ai appris, c'est bien qu'un message simple est beaucoup plus fort. Faire des figures simples, des diapos simples, écrire des phrases courtes. « More is less ». Je tiens également à vous remercier de m'avoir toujours valorisé auprès de vos pairs.

Merci à tous les membres de l'équipe. Emmanuel, Michael, Ivan, Lim-Anna, Constanze, Roxanne, Caroline, Maja, Etienne, Juliane, Katia, Bertrand et Mérie. Vous m'avez tous beaucoup apporté sur le plan scientifique et humain. Je pense à Emmanuel qui m'a appris tout ce qu'il savait sur l'imagerie structurée ou l'immunohistochimie. Je pense à Caroline qui m'a beaucoup conseillé pour les doubles enregistrements. Je me rappelle du temps passé devant le poste d'enregistrement de Michael à regardé défiler les enregistrements. Je pense aussi aux bons moments passés autour d'une bière, ou lors des dégustations de vin. Une spéciale pour Mérie qui prend la relève auprès de Desdemona, et qui a du me supporter pendant cette dernière année, j'avoue que je n'ai pas toujours été très tendre et sûrement trop

exigent parfois.

Merci à Alberto et toute son équipe avec qui j'ai souvent interagi pour résoudre mes problèmes de souris, de tranches, de solution intra, ou d'oxygène. Je dois avoir une dette de café envers Charlotte qu'il faudra régler un de ces jours.

Merci à Claire et Stéphane ainsi qu'à leurs équipes, avec qui j'ai peut être moins interagi, mais qui ont apporté leur petit grain de sel de temps à autre.

Merci à Sean. Sean tu venais au labo pour travailler avec Desdemona et c'est vrai que nous discussions souvent de tes manips et j'ai pu t'aider de temps à autre quand tu avais des problèmes. Un jour, tu m'as simplement proposé de participer activement à ton projet. J'en ai été très touché. Cette collaboration m'a également permis d'améliorer mon anglais et tu as été très pédagogue de ce point de vue là.

Merci à l'animalerie du 105, de l'ICM, aux plateformes de génotypage et d'histologie pour leur aide et support technique.

Merci aux Ajités. William, Pinar, Morgane P, Fabian, Kevin, Tristan, Morgane B, Alizée, ... Je ne peux pas citer tous les noms, mais ils sauront se reconnaître. On a passé de très bons moments tous ensemble et belle dynamique a été créée à l'ICM. Continuez s'il vous plait !

Je souhaite remercier Patricia Oliviero qui a superbement organisé, avec moi, la retraite des Doc et PostDoc en 2013. Merci pour toutes les petites choses que tu as faites pour moi, ne change rien tu es géniale !

Merci à la promo de master/thèse et associés. Carole, Audrey, Patrick, Esther, Nico, Raphael, Béné, Isa... j'en oublie c'est sur... On a passé de très bons moments, souvent de détente il faut le reconnaître, mais cela a été important pour tenir tout au long de ces années.

Carole. On était à la fac à Orléans en licence, on est venu à Paris avec la ferme intention de faire une thèse en neuro. On peut dire que c'est mission accomplie. Je pense que ca aurait été plus difficile sans toi sur le plan moral. Tu as su être présente au moment ou j'en avais besoin. Même si l'on a fait des choses très différentes lors de nos thèses, nos discussions scientifiques m'ont aussi beaucoup apportées.

Merci à Y. Audrey. On travaillait sur des modèles similaires, avec les mêmes problèmes... Enfin j'avais les problèmes, tu avais les solutions. Je suis venu te voir à plusieurs reprises quand j'avais des soucis de tranches ou de stéréotaxie, et tu as toujours été d'une aide plus que précieuse. Je pense que tu m'as aussi beaucoup influencé, sans que je ne me rende vraiment compte, dans ma façon de travailler. Merci aussi pour m'avoir aidé avec la rédaction.

J'aimerais remercier ma famille et mes proches qui ont toujours cru en moi et qui m'ont soutenu dans ma démarche.

Enfin, je tiens à remercier Eugénia du fond du cœur, pour m'avoir supporté et soutenu, surtout pendant la rédaction qui, je dois l'avouer, fut difficile, autant pour moi que pour elle.



# Contents

<b>Abbreviations</b>	<b>5</b>
<b>Presentation</b>	<b>7</b>
<b>I Introduction</b>	<b>11</b>
<b>1 The presubiculum: Anatomy, function, microcircuit</b>	<b>15</b>
1.1 The presubicular cortex . . . . .	15
1.1.1 Anatomy . . . . .	15
1.1.2 What kind of cortex? . . . . .	17
1.2 Presubiculum and spatial orientation . . . . .	20
1.2.1 Head direction cells of the presubiculum . . . . .	20
1.2.2 Head Direction Circuit . . . . .	22
1.2.3 The presubiculum is a major contributor of spatial representation and memory . . . . .	26
1.3 Information processing in the presubicular microcircuit . . . . .	31
1.3.1 Anatomy and intrinsic excitability of presubicular neurons . . . . .	31
1.3.2 Interlaminar, intralaminar and modular organization . . . . .	33
1.3.3 Input and output relays in the presubicular microcircuit . . . . .	35
<b>2 How does a microcircuit work?</b>	<b>39</b>
2.1 Many integrative levels in neuronal networks . . . . .	39
2.2 Neuronal intrinsic excitability . . . . .	42
2.2.1 Resting membrane potential . . . . .	42
2.2.2 Neuronal passive properties . . . . .	42
2.2.3 Action potentials . . . . .	43
2.2.4 Firing properties . . . . .	44

2.3	Wiring a network: axonal conduction and regulation of information . . . . .	48
2.3.1	Axonal conduction velocity . . . . .	48
2.3.2	Analog information encoding in the axon . . . . .	49
2.4	Synaptic transfer and modulation of information in the presynaptic terminal . . . . .	54
2.4.1	Basic mechanism of neurotransmitter release . . . . .	54
2.4.2	Synchronous versus asynchronous release of neurotransmitter . . . . .	56
2.4.3	Short term presynaptic plasticity . . . . .	58
2.4.4	Voltage dependent regulation of synaptic activation . . . . .	66
2.4.5	Regulation of presynaptic function by extrinsic factors . . . . .	67
<b>II</b>	<b>Methods</b>	<b>69</b>
<b>III</b>	<b>Results</b>	<b>79</b>
	<b>ARTICLE 1. Cellular neuroanatomy of rat presubiculum</b>	<b>81</b>
	<b>ARTICLE 2. Properties of presubicular neurons that project to lateral mammillary nucleus or anterodorsal thalamus</b>	<b>101</b>
	<b>ARTICLE 3. A continuum of diversity of Parvalbumin or Somatostatin expressing interneurons in mouse presubiculum</b>	<b>111</b>
	<b>ARTICLE 4. Memory of past activity determines the recruitment of a Martinotti cell-mediated inhibitory feedback loop in mouse presubiculum</b>	<b>147</b>
<b>IV</b>	<b>Discussion</b>	<b>179</b>
<b>1</b>	<b>Building blocks of the presubiculum</b>	<b>183</b>
1.1	Did we correctly address the whole diversity of principal neurons? . . . . .	183
1.2	Interneuron diversity . . . . .	185
<b>2</b>	<b>Perspective: from neuronal diversity to function</b>	<b>187</b>
<b>3</b>	<b>Neurons that project to lateral mammillary (LMN) and anterodorsal thalamus (ADN): implication for the visual update of the head direction signal</b>	<b>189</b>

<b>4</b>	<b>Memory of past activity at the pyramidal cell-to-Martinotti cell synapse: properties and mechanisms</b>	<b>191</b>
4.1	Better define the dynamics of the plasticity, its specificity and variability	191
4.2	Mechanisms of activity dependent synaptic transfer at the pyramidal cell to Martinotti cell synapse? . . . . .	192
4.2.1	Activity dependent action potential broadening . . . . .	193
4.2.2	Modulation at the synapse . . . . .	195
4.2.3	The transfer rate increase may results from a synergistic mechanism . . . . .	196
<b>V</b>	<b>General conclusion</b>	<b>197</b>
<b>VI</b>	<b>Collaboration</b>	<b>201</b>
	<b>ARTICLE. Cellular anatomy, physiology and epileptiform activity in the CA3 region of Dcx knockout mice: a neuronal lamination defect and its consequences</b>	<b>203</b>
	<b>List of figures</b>	<b>219</b>
	<b>Bibliography</b>	<b>241</b>



# Abbreviations

## Anatomy

ADN	anterodorsal thalamus
AM	anteromedial thalamus
AV	anteroventral thalamus
CA	corpus ammonis
DG	dentate gyrus
dl	dorso-lateral
HF	hippocampal formation
DTN	dorso tegmental nucleus
LEA	lateral entorhinal cortex
LDN	laterodorsal thalamus
LMN	lateral mammillary nucleus
MEA	medial entorhinal cortex
PHR	parahippocampal region
PaS	parasubiculum
PER	Perirhinal cortex
PrOS	presubiculum
POR	Postrhinal cortex
PoS	postsubiculum = dorsal part of PrS
RSC	retrosplenial cortex
sub	subiculum
vm	ventro-medial

## Physiology

AP	action potential
DC	direct current
FS	fast spiking
LTS	low-threshold spiking
PTP	posttetanic potentiation
PPD	paired-pulse depression
PPF	paired-pulse facilitation
PPR	paired-pulse ratio
RP	resting pool
RRP	readily releasable pool

## Others

AMPA	$\alpha$ -Amino-3-hydroxy-5-methyl-4-isoxazolepropionic acid
AIS	axon initial segment
BAPTA	1,2-bis(2-aminophenoxy)ethane-N,N,N',N'-tetraacetic acid
DTX	dendrotoxin
EGTA	ethylene glycol tetraacetic acid
GABA	$\gamma$ Amino-Butyrique Acid
GPCR	G protein-coupled receptor
NMDA	N-Methyl-D-aspartic acid
PV	parvalbumin
PKC	protein kinase C
SST	somatostatine
TTX	tetrodotoxin

# Presentation



The presubiculum is an understudied cortical area located in the parahippocampal region and involved in spatial navigation. My supervisor, Desdemona Fricker, therefore proposed this thesis project on information encoding at the level of the presubicular microcircuit.

The presubiculum contains head direction cells, which fire as a function of animal's directional heading. The head direction signal is generated from vestibular information, in subcortical areas that project to the presubiculum. Besides, presubiculum receives visual information from visual and retrosplenial cortices. The convergence of the two types of information in the presubiculum lead to the update of the head direction signal with visual cues. The presubiculum then distributes a visual landmark control to subcortical areas as well as a major drive to the downstream entorhinal cortex. Consequently, the presubicular function deeply impacts the function of entorhinal cortex and hippocampus.

The six-layered organization of the presubiculum suggests a high computational power, implying that information is not passively relayed, but rather actively integrated and refined. But what happens when information enters the presubiculum has been unknown as the presubicular network and its components have never been studied in detail.

During my PhD, I studied the microcircuit elements of rodent presubiculum, using a model that allows a very precise investigation of neuronal and synaptic properties: the slice preparation. The underlying theme of my work was to use patch clamp records in whole cell configuration in order to obtain electrophysiological and morphological data on presubicular neurons and their connections.

A part of my work consisted in a description of the intrinsic electrophysiological and morphological properties of the different neurons in the presubiculum. My first project focused on principal neurons in rat, whereas the second study dealt with the diversity of GABAergic interneurons. I defined the "building blocks" of the presubiculum, an essential step in the understanding of information encoding in a network. I showed that the six layers of the presubiculum contain neurons with distinct biophysical properties and distinct dendritic and axonal arborizations, suggesting that different integrative capabilities exist within the network. Together with Mérie Nassar, we described the diversity of inhibitory interneurons, that are important elements for tuning cortical information. Our results suggest that the

presubiculum possesses all necessary elements for complex information treatment, as is the case in other cortical areas.

The last part of my work focused on the specific interactions between pyramidal cells and a subpopulation of interneurons, the Martinotti cells. I noticed an unusual form of plasticity at the excitatory synapse. The transfer of information was exquisitely low, as one action potential in the pyramidal cell rarely triggered a postsynaptic excitatory event in the Martinotti cell. However, sustained activity at high frequency was able to un-mute the synapse, which then became efficient to transfer information and summed events could fire the Martinotti cell. Presubicular head direction cells fire persistently as the head is turned in the cell's preferred direction. The excitatory synapses onto Martinotti cells of the presubiculum are therefore appropriately tuned to integrate and balanced the persistent intrinsic excitatory activity delivered by the presubicular microcircuit.

# Introduction



Two main parts in the introduction should acquaint the reader with the context of my research. The first part presents the presubiculum, its situation in the parahippocampal region, its anatomy and development. I then go over its function as a key relay for landmark information in the brain, and I eventually come back on the poor knowledge of its microcircuit. How does a microcircuit work? The second part reviews different elements that process the information in neuronal networks, from ions channels responsible for excitability to some of the principles of computation in microcircuits. I mainly develop the regulation of information from the spike generation to the plasticity of synaptic release, because it provides useful information for the last study of my PhD.



# 1 | The presubiculum: Anatomy, function, microcircuit

## 1.1 The presubicular cortex

### 1.1.1 Anatomy

The presubiculum is a cortical region of the hippocampal-parahippocampal formation in brain's temporal lobe. Hippocampus proper is subdivided into the Dentate Gyrus, Ammon's Horn (CA3, CA2, CA1) and Subiculum; The parahippocampal area is its continuation, composed of presubiculum, parasubiculum, entorhinal (medial and lateral parts), peri- and postrhinal cortices (Fig. 1; van Strien et al., 2009).

The presubiculum corresponds to Brodmann's area 27 and 48 (Brodmann, 1909), following the temporoventral-to-septodorsal hippocampal axis in rodents (Fig. 1). The most dorsal part, corresponding to Brodmann's area 48 is also called "Post-subiculum" (Brodmann, 1909; Rose and Woolsey, 1948; Blackstad, 1956). In the proximo-distal axis of the hippocampus (from dentate gyrus to subiculum), the presubiculum is located just next to subiculum and is then followed by the parasubiculum; these 3 areas being classically grouped together into the "subicular complex". Eventually, in its retrodorsal part, the presubiculum is bordered by retrosplenial cortex.

The presubiculum is easily distinguishable from its neighboring areas regarding anatomical features such as cytoarchitecture and topography of afferent fibers (Fig. 2, Ramon y Cajal, 1899; Brodmann, 1909; Rose and Woolsey, 1948; Blackstad, 1956).

Presubiculum is a 6-layered cortex. Layers were already described by Ramon y Cajal according to their neuronal content and density, from the pial surface to the white matter (Fig. 2C; Ramon y Cajal, 1899). This description of layer holds true for non-human primates and rodent presubiculum.

Layer 1, the molecular layer, is almost empty and contains only few putative interneurons, (Cajal's "short axon cells") and glial cells. Layer 2 is a thin layer of

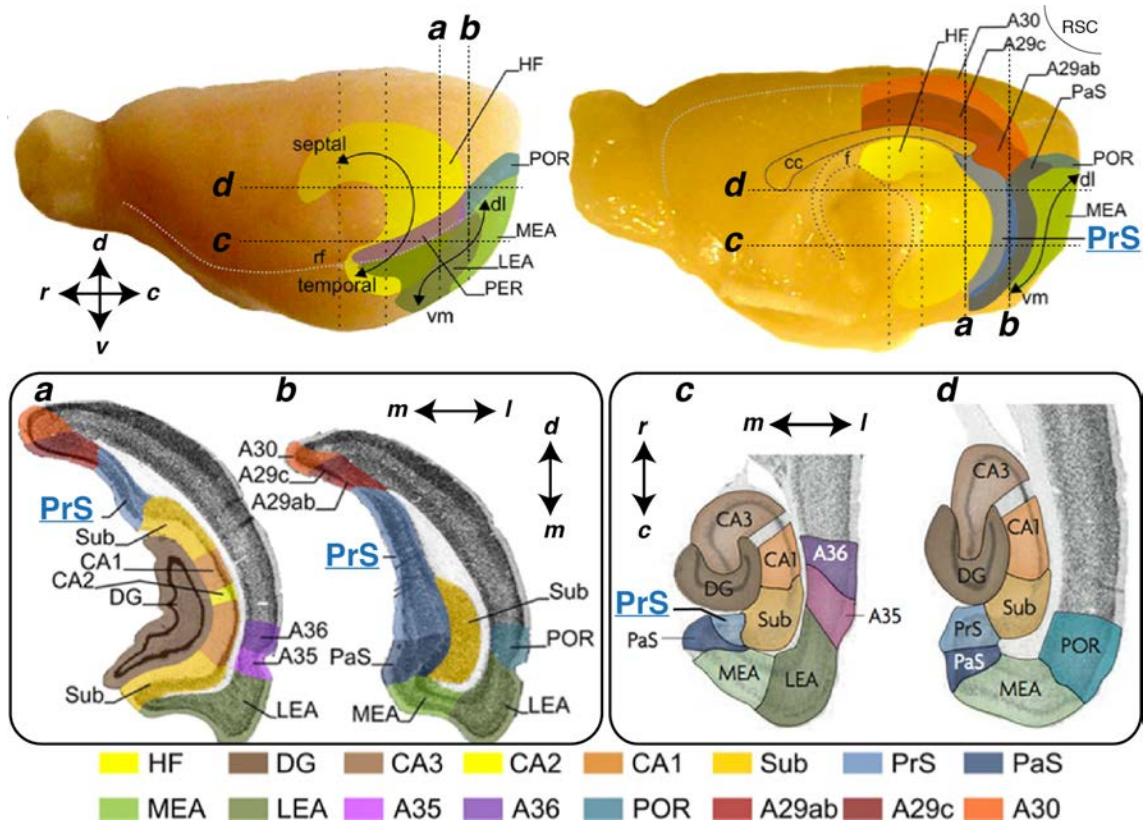


**Figure 1:** Representations of the hippocampal formation (HF), the parahippocampal region (PHR) and retrosplenial cortex (RSC) in rat brain. Lateral (A) and midsagittal (B) views of the rat brain. Hippocampus contains dentate gyrus (DG), Ammon's horn (CA1 to CA3) and subiculum (sub). Parahippocampal region is subdivided into pre-subiculum (PrS), parasubiculum (PaS), medial and lateral entorhinal areas (MEA and LEA) peri- and postrhinal cortices (PER and POR). Retrosplenial cortex is subdivided here in A29ab, A29c and A30 (Brodmann's nomenclature). Hippocampus, PrS and PaS follow a dorsoseptal-to-ventrotemporal axis; Entorhinal cortices follow a dorsolateral-to-ventromedial (dl, vm); PER and POR are defined along a rostro-caudal axis. The dashed vertical (a, b) and horizontal (c, d) lines indicate levels of coronal and horizontal sections depicted in C. rf: rhinal fissure; cc: corpus callosum; f: fibria. Adapted from Sugar et al. (2011) and van Strien et al. (2009)

approximately the same thickness as layer 1 and contains densely packed pyramidal and fusiform cells. In the most dorsal part of mouse presubiculum, layer 2 cell bodies tend to form clusters separated by fiber stripes (Slomianka and Geneser, 1991). Layer 3 is larger than layer 2 with a much lower neuronal density and is composed of pyramidal neurons. Layer 4 is also named "lamina dissecans" because it was described as a neuron free layer, containing only fibers and glial cells (Rose, 1926; Lorente De Nó, 1933). It is a convenient marker separating superficial layers (1, 2 and 3) from deep layers (5 and 6). Layer 5 is a layer with large to medium sized pyramidal cells whereas layer 6 contains smaller fusiform and pyramidal cells. In primate presubiculum, deep layers are separated in 3 sub-layers (5, 6, 7). This laminar organization has been observed with specific *in situ* hybridization stainings and is less clear in rodents (Ding, 2013).

The laminar organization of the presubiculum marks an abrupt transition with the adjacent subiculum, organized more like a cloud (even if subiculum may also be subdivided in different layers, O'Mara et al., 2001). An "extremely dense plexus formed by [ ] many afferent axons" in superficial layers of presubiculum distinguishes it from its neighbors, subiculum, parasubiculum and retrosplenial cortex (Ramon y Cajal, 1899; Blackstad, 1956). These terminals are more numerous in the dorsal part of presubiculum (area 48; Rose and Woolsey, 1948; Blackstad, 1956). The presubiculo-parasubiculum transition is marked by the absence of the densely packed layer 2 in parasubiculum, the cellular density of its superficial layers being more homogeneous. This transition is clearly visible with a specific marker of presubicular layer 2, calbindin (Boccarda et al., 2010).

The dense presubicular layer 2 is also remarkably avoided by the characteristic plexus targeting the presubiculum (Fig. 2A and B, Ramon y Cajal, 1899). These dense afferent fibers define very well the limits of presubiculum, especially dorsally, where their interruption marks the border of presubiculum with retrosplenial cortex (Ramon y Cajal, 1899; Blackstad, 1956).

### **1.1.2 What kind of cortex?**

During development, radial migration of neuronal progenitors from the ventricular zone shapes laminar compartments (Angevine and Sidman, 1961; Rakic, 1974). Then, subsequent change may occur to generate the adult cortical organization. Cortical areas may be classified according to the development of their laminar organization and their aspect in the adult stage (Lorente De Nó, 1933; Filimonoff, 1947). These historic classifications can be criticized because they are based only on anatomy, but they are still of interest for defining different parts of the cortex.

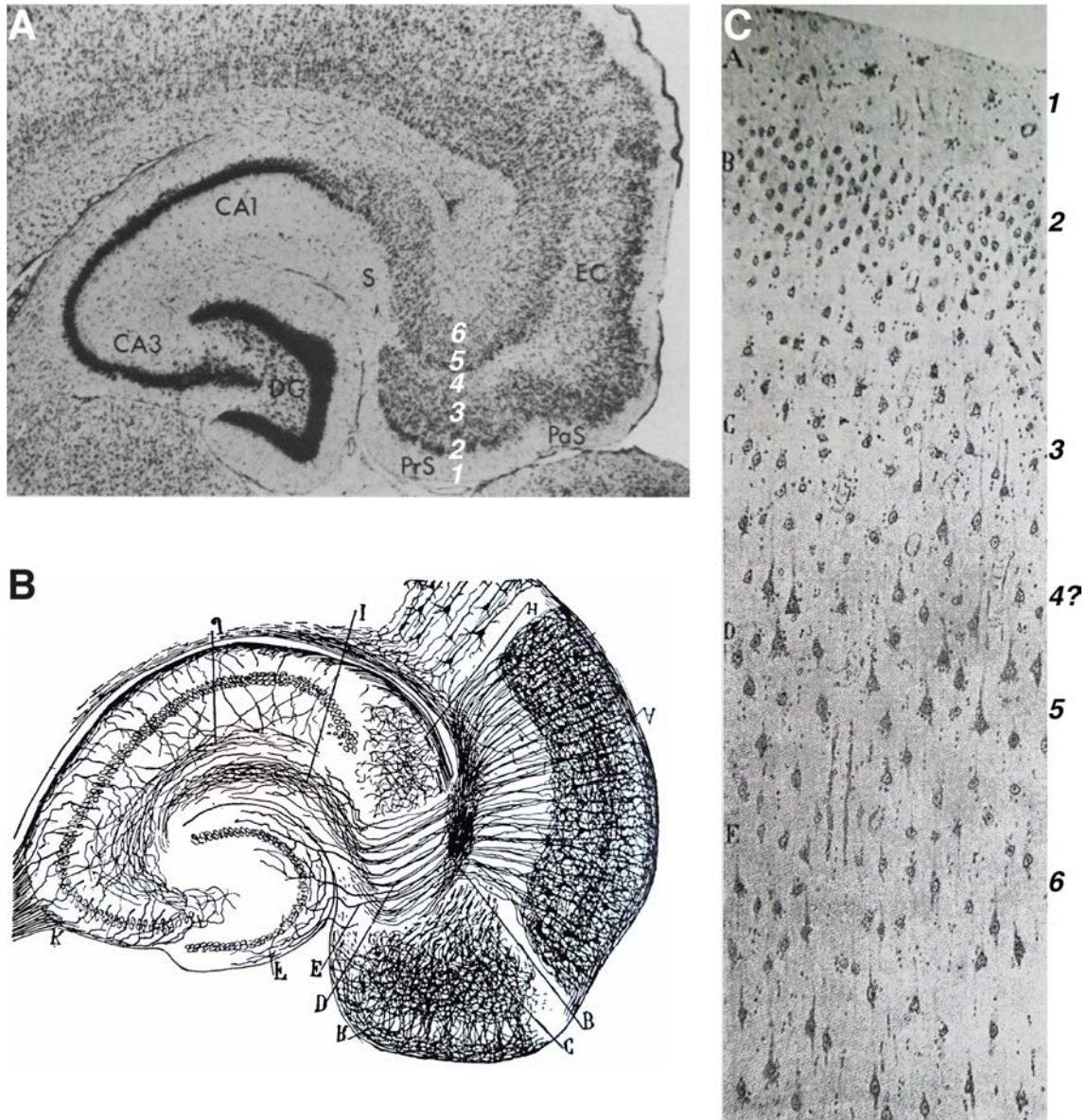


**Figure 2: Layers and afferent fibers in the presubiculum.** **A:** Tionin-stained horizontal section through the *rat* hippocampal formation. DG: dentate gyrus; S: subiculum; PrS: Presubiculum; PaS: Parasubiculum; EC : Entorhinal cortex; Note the obvious separation of superficial (1,2,3) and deep (5,6) layers by lamina dissecans (layer 4) in the presubiculum. Note that layer 2 is more dense than layer 3, and that presubicular deep layers appear as a continuation of the subiculum and entorhinal cortex deep layers. Adapted from Amaral and Witter, 1989. **B:** Drawing of a horizontal section corresponding to A, but using a 15 day old *mouse*, stained with the Golgi method. Adapted from Ramon y Cajal (1899). Note the dense "plexus" of afferent fibers in the presubiculum that partially avoid layer 2. **C:** Laminar organization of the human presubiculum. Nissl method, from Ramon y Cajal (1899). Cajal's nomenclature (my interpretation): A, plexiform layer (layer 1); B, small pyramidal and fusiform cell layer (layer 2); C, deep plexiform layer (layer 3); D, large to medium size pyramidal cell layer (layer 4 and 5); E, fusiform and triangular cell layer (layer 6).

The Isocortex (or Cortex Completus) comprise 6 layers whereas the Allocortex (or Cortex Incompletus) displays an incomplete structure (less than 6 layers) in developmental and adult stages. The Periallocortex (or Cortex Intermedius) physically lies between the two others and its structure changes between developmental and adult stage. Neocortex is Isocortex; hippocampus and subiculum constitute the Archicortex, which is part of the Allocortex; the presubiculum was lumped together with the entorhinal area and termed Periarhchicortex, which is part of the Periallocortex (Lorente De Nó, 1933; Filimonoff, 1947).

More recent findings (Bayer, 1980) have shown that embryogenesis is actually different between presubiculum and entorhinal cortex. First, neurogenesis occurs later in presubiculum. Second, deep layers are formed before superficial layers (like the classical cortical development) with a strong neurogenetic gradient. Indeed, deep layers appear at E15-18 whereas superficial layers appear at E17-20. A small gradient also exists in entorhinal cortex but it occurs a little earlier (finished at E17 in deep layers and E18 in superficial layers). Another intriguing fact is that neurogenesis timelines of presubiculum and subiculum are the same for deep layers but not for superficial layers. In the adult, it is interesting to look at the presubiculo-subiculum transition in horizontal slices (Fig 2A) to see that presubicular deep layers really appear to be a continuation of subiculum. From his studies on Marsupials, Brodmann (Brodmann, 1909) even described this transition as an "abrupt interruption of layer II-V at the beginning of the subiculum, with only layer I and VI continuing into Ammon's horn in greatly widened form".

All these developmental data showed that the six layers of presubiculum appear in a very specific and unique manner. However, functional consequences of this specific development, compared to neocortex or entorhinal cortex remain unknown.

## 1.2 Presubiculum and spatial orientation

To survive, mammals rely on their sense of orientation to get water, food, and mate, or to escape predators. This requires the innate ability to learn features of a novel environment as it is explored. This is spatial orientation and it uses two different cognitive processes: path integration and landmark navigation. Path integration uses a self derived representation of space using vestibular, proprioceptive and motor inputs; landmark navigation represents space using external cues such as visual, olfactory, auditory and somatosensory information. Among all the brain areas involved in these processes, the presubiculum encodes the head direction, one critical information for spatial cognition (Wiener and Taube, 2005; Taube, 2007).

### 1.2.1 Head direction cells of the presubiculum

Extracellular recordings in freely moving rats have shown that 50-60 % of neurons in dorsal presubiculum (postsubiculum) are discharging as a function of animal's directional heading (Ranck, 1984; Taube et al., 1990a; Taube, 2007; Boccara et al., 2010). These neurons are called Head Direction Cells. Each head direction cell is characterized by a specific tuning curve of its firing rate as a function of the animal's head direction (Fig. 3A). The cell's preferred direction is defined as the one leading to the maximum firing rate. Basal firing rate is close to zero and increases only for directional ranges varying from  $60^\circ$  to  $150^\circ$  (average  $90^\circ$ ) with a triangular or Gaussian distribution of frequencies around the preferred direction (Blair and Sharp, 1995; Taube, 1995). One cell is accurately tuned to only one head direction and the whole population allows a complete representation of orientation. Each neuron has a very stable tuning curve but the peak firing rate varies among presubicular neurons (from 5 to 115 Hz). Last, but not least, discharge persists without adaptation as long as the preferred direction is maintained (Taube et al., 1990a).

Head direction cells are not sensitive to the geomagnetic field but to environmental visual landmarks. Rotation of the major polarizing visual cue within the environment leads to a corresponding shift of the preferred direction (Fig. 3D). Head direction cell firing does not change in the absence of visual landmarks, but preferred direction can drift over time (Fig. 3E). Visual cues are used to control but not to generate the head direction signal. Furthermore, visual inputs exert a higher degree of control than other senses such as auditory or olfactory inputs (Goodridge et al., 1998). Motor activity seems to improve signal quality but is not necessary for its generation because preventing an animal from moving reduces peak firing rate but does not abolish head direction cell activity ((Fig. 3B), Taube et al., 1990b).

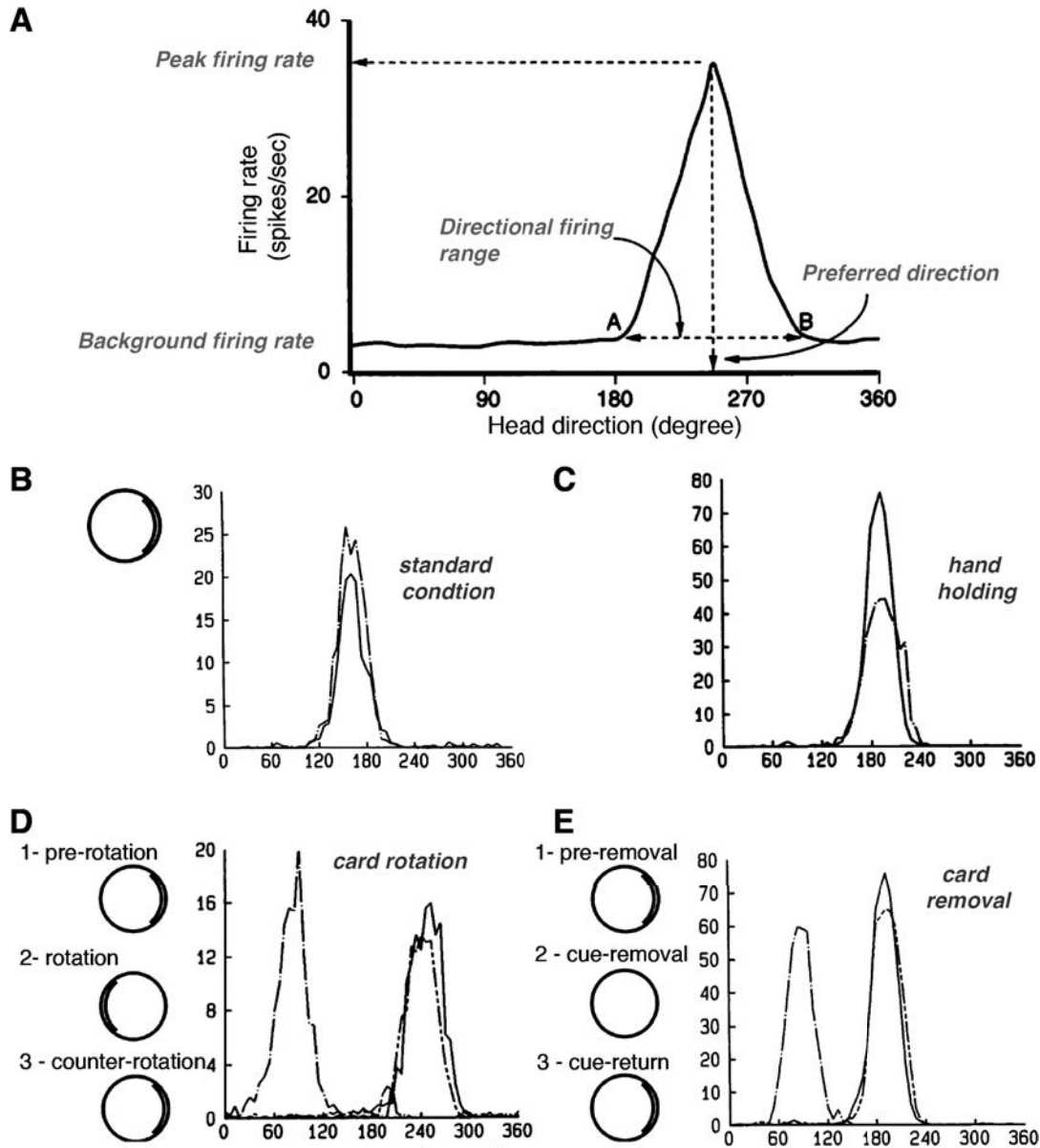


**Figure 3: Basic features of presubicular head direction cells.** **A.** Tuning curve features of head direction cells (adapted from Taube, 1995): background firing rate is close to zero but increases within the directional firing range to reach the peak firing rate for the preferred direction. **B.** Stability of head direction cell firing across two recording sessions, one (dashed line) recorded 15 days after the other (solid line). In standard condition, a prominent cue card is disposed as a polarizing cue on one side of the open field wall. **C.** Carrying the animal by hand and moving it around in the arena (dashed line) only decreased peak firing rate compared to standard condition (solid line). **D.** Cue card rotation causes a corresponding shift in preferred direction. Here, the same head direction was recorded in standard condition (1, solid line), after a 180° clockwise rotation of the cue card (2, dash-dot line) and after the equivalent counter rotation putting the card in its initial position (3, line with 2 short dashes). Animal has been returned to his home cage as environmental modifications were made. **E.** Drift of preferred direction following card removal. The same head direction was recorded in standard condition (1, solid line), after cue card removal (2, dash-dot line) and after cue card return to its initial position (3, line with 2 short dashes). Experimental results were adapted from Taube et al. (1990a,b).

Properties of presubicular head direction cells show that an animal primarily uses path integration to keep track of changes in head direction but also landmark navigation to stabilize and correct the signal. The sense of head direction is computed, not only in the presubiculum, but through a head direction macrocircuit containing several interconnected brain areas.

## 1.2.2 Head Direction Circuit

### Areas containing head direction cells

The head direction circuit that generates and maintains the directional heading signal includes the dorsal tegmental nucleus (DTN) (Sharp et al., 2001b), lateral mammillary nucleus (LMN) (Stackman and Taube, 1998), anterior dorsal thalamic nucleus (ADN) (Taube, 1995), lateral dorsal thalamus (LDN) (Mizumori and Williams, 1993), retrosplenial cortex (both granular and agranular regions) (Chen and Johnston, 2004; Cho and Sharp, 2001), entorhinal cortex (Sargolini et al., 2006) and the presubiculum. All these interconnected areas (Fig. 4; Table 1.1) contain head direction cells that differ in their specific tuning properties. One remarkable parameter is the directional range that is narrower for presubiculum and retrosplenial cortex compared to ADN, LMN and DTN (Tuning curves, Fig. 4). In addition, subcortical head direction cells anticipate future head direction, that is, ADN and LMN tuning curves slightly vary between clockwise and counterclockwise head rotations (Fig. 4). Cortical neurons appear to be the most accurate in signaling head direction. This is explained by the hierarchy in the head direction circuitry, which was established mainly by doing lesioning of one area and looking at the consequences in others (Clark and Taube, 2012 for review). These studies have drawn attention to a sub-cortical generator using self-movement information; cortical areas may bring sensory information to increase stability and precision.

### Subcortical origin of head direction signals

Head direction cell activity requires information generated by the vestibular labyrinth. The labyrinth is composed of the semicircular canal and the otolith organ that detect angular and linear acceleration respectively. Semicircular canal function is necessary for generating head direction cell activity in ADN (Muir et al., 2009) whereas the otolith organ is involved in signal robustness and stability (Yoder and Taube, 2009). The vestibular signal is carried by angular head velocity cells, that fire as a function of head rotation speed and direction. These neurons are found all along the integrative pathway, from the vestibular organ to the Dorsal Tegmental Nucleus (DTN)

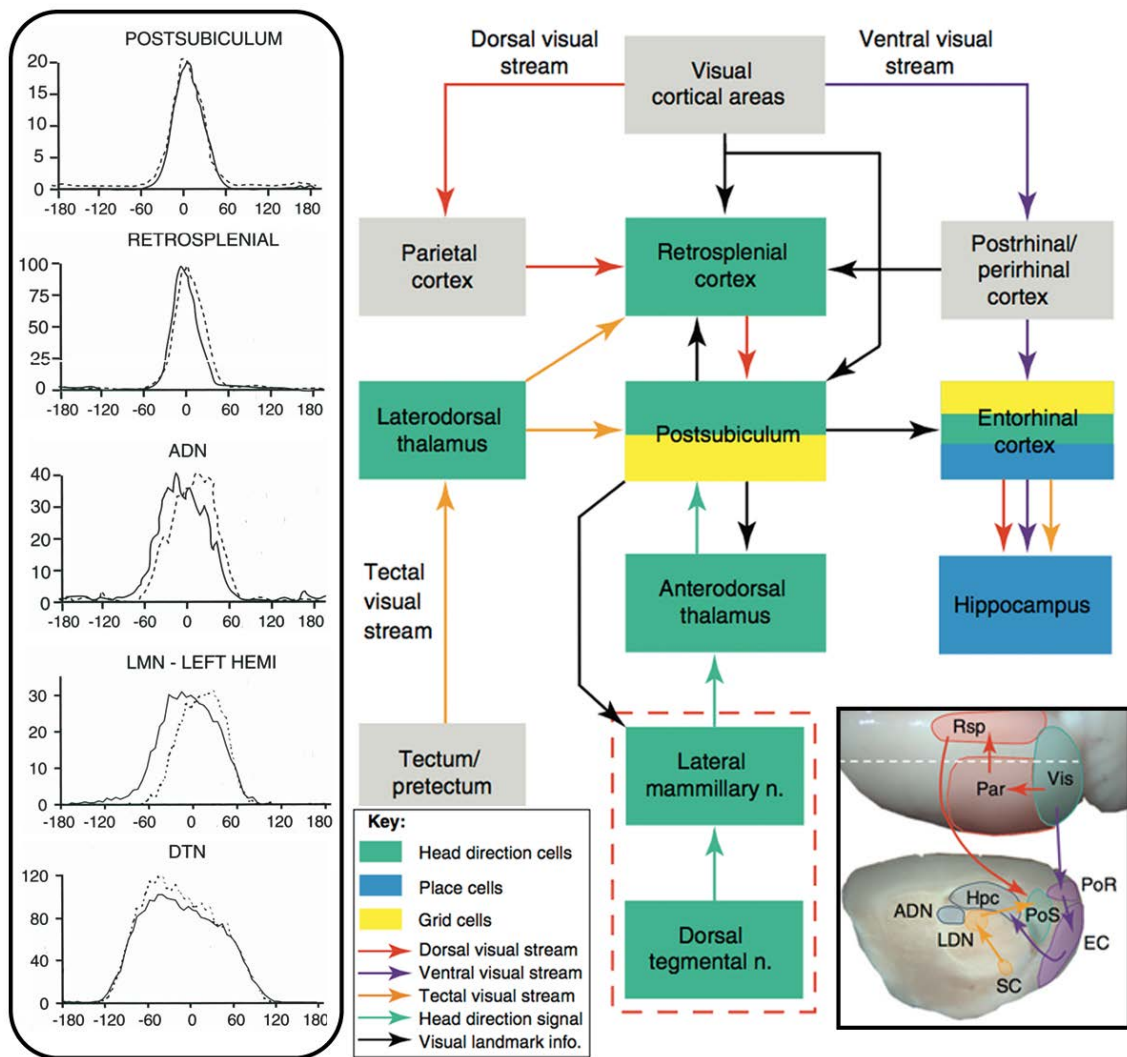


**Figure 4: The Head direction circuit.**

**Left.** Typical tuning curves showing firing rate (Hz) as a function of head direction (degree) are shown for presubiculum (postsubiculum), retrosplenial cortex, ADN, left LMN and DTN. Solid lines and dashed lines represent tuning curves during clockwise and counterclockwise head turns, respectively. Adapted from Wiener and Taube (2005).

**Right.** Hypothetical landmark-processing circuit in rodents adapted from Yoder et al. (2011). On the one hand, the head direction signal is being generated by the reciprocal connections between the DTN and the LMN (dashed red lines) and then sent from the LMN to ADN, which projects to presubiculum (here PoS). On the other hand, visual information is conveyed to the presubiculum through different routes, including a direct connection from visual cortex, dorsal (red), ventral (purple), and tectal (orange) visual streams. These pathways target retrosplenial cortex, which has reciprocal connections with presubiculum. The presubicular signal is then sent, as a feedback control to upstream areas of the head direction system, LMN and ADN. But is also drives entorhinal cortex and therefore hippocampus. Abbreviations: ADN, anterodorsal thalamus; EC, entorhinal cortex; Hpc, hippocampus; LDN, lateral dorsal thalamus; LMN, lateral mammillary nuclei; Par, parietal cortex; PoR, postrhinal cortex; PoS, dorsal presubiculum / postsubiculum; Rsp, retrosplenial cortex; SC, superior colliculus; Vis, visual cortex.

and Lateral Mammillary Nucleus (LMN). These two last areas also contain head direction cells. Many experimental and modeling studies suggest that the DTN-LMN interactions would constitute the head direction cell generative circuit, converting angular velocity information in head direction information (Bassett et al., 2007; Clark and Taube, 2012).

The head direction signal is thought to be generated according to continuous attractor dynamics (see Fig. 5 ; Skaggs et al., 1995; Redish et al., 1996; McNaughton et al., 2006) and different versions exist for the head direction circuit (e.g. Sharp et al., 2001a versus Boucheny et al., 2005). Recent experimental findings reinforce the validity of these models in the generation of stable activity states (Schmidt-Hieber and Häusser, 2013; Domnisoru et al., 2013), such as the head direction signal.

From LMN, the head direction signal is then relayed via the anterodorsal thalamus (ADN) (Fig. 4) that sends projections to cortical areas such as retrosplenial cortex (van Groen and Wyss, 1990a) and presubiculum (van Groen and Wyss, 1990c) driving cortical head direction cells. Functionally, ADN is a critical relay in the head direction circuit, its lesion disrupting head direction cells in cortical areas, including presubiculum (Goodridge and Taube, 1997), parasubiculum and entorhinal cortex (Clark and Taube, 2012).

If head direction signal in ADN is not abolished by lesions of presubiculum (Goodridge and Taube, 1997), this last one plays a significant feedback control in refining the signal with visual information.

### **Visual landmark control of the head direction signal by the presubiculum**

Presubiculum is one entry point of visual information into the head direction system (Fig. 4). It receives direct projections of primary and secondary visual cortices (Vogt and Miller, 1983) and projections from retrosplenial cortex, relaying information from visual cortex (Vogt and Miller, 1983; van Groen and Wyss, 1990a; Jones and Witter, 2007) and from associative visual cortical areas, such as posterior parietal and postrhinal cortices (Yoder et al., 2011). Visual information might also come from the laterodorsal thalamus (LDN) that sends direct projections to presubiculum (van Groen and Wyss, 1992b). LDN receives visual inputs from pretectal areas and superior colliculus but it has no functional impact onto visual landmark dependent activity in presubiculum (Golob et al., 1998). LDN seems also to be associated with somatosensory inputs (Bezdudnaya and Keller, 2008), but head direction signal dependence upon somatosensory inputs has never been shown. By its direct projections to ADN (van Groen and Wyss, 1990c; Ishizuka, 2001; Yoder and Taube, 2011) and LMN (Allen and Hopkins, 1989; Gonzalo-Ruiz et al., 1992;

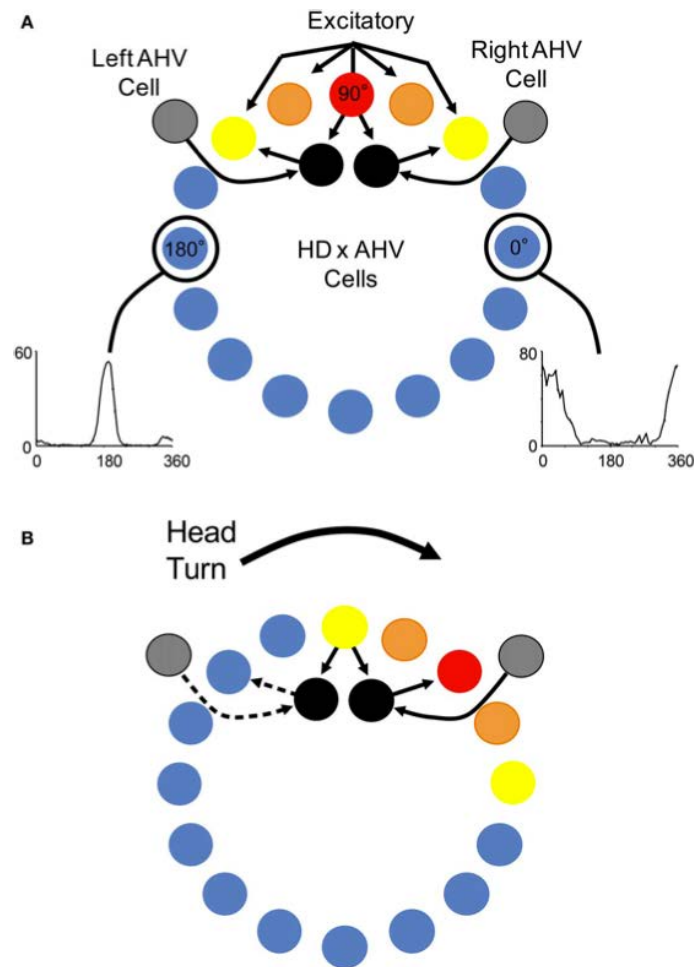


**Figure 5: A continuous attractor network model of Head Direction (HD) signal generation.** This network is graphically arranged in a ring with each HD cell (colored circles) positioned according to their corresponding preferred tuning direction. Each HD cell drives nearby neurons more strongly than more distant neurons and feedback inhibition limits the overall activity (not shown here); a "hill" of high activity (warm points) emerges from these elements. This equilibrium is stable until the animal's head turns, during which two additional signals are added to the circuit: an angular head velocity (AHV) (gray circle) and a conjunctive HD  $\times$  AHV (black circle). (B) Following a head turn, conjunctive HD  $\times$  AHV cells drive the activity hill in the appropriate HD. For example, a right head turn would engage HD  $\times$  AHV neurons that are specifically sensitive to clockwise head turns (solid arrows). These neurons would in turn activate HD cells to the right of the hill and drive activity to the animal's current HD. Adapted from Clark and Taube (2012); See also Sharp et al. (2001a) or McNaughton et al. (2006) for further information.

Yoder and Taube, 2011), the presubiculum appears like an ideal relay for carrying visual landmark information into subcortical generators of head direction signal. Indeed, presubiculum lesion impairs visual landmark control of a cell's preferred direction in ADN (Goodridge and Taube, 1997) and LMN (Yoder et al., 2011). In other words, without the presubiculum, Head direction cells' preferred directions in ADN and LMN are much less influenced by visual cues (Fig. 3D). This feedback visual control might be exerted in a larger extent in the whole head direction circuit, the presubiculum projecting also to the retrosplenial cortex (Wyss and van Groen, 1992), LDN (van Groen and Wyss, 1990b,c) or medial entorhinal cortex (Honda et al., 2008). Moreover, visual information transmitted via the presubiculum is also critical for the activity in the downstream hippocampus.

### **1.2.3 The presubiculum is a major contributor of spatial representation and memory**

The first evidence for the representation of space in the brain was the discovery of "place cells" in the hippocampus by O'Keefe and Dostrovsky (1971). Place cells fire as a function of the animal's position within space, and they are believed to be the neuronal substrate of a spatial cognitive map. Since, spatial information processing has been shown to occur at the level of the whole hippocampal-parahippocampal area, especially through dialogue between the hippocampus and the medial entorhinal cortex.

#### **Entorhinal-hippocampal connectivity**

Interconnectivity within the hippocampal, parahippocampal and entorhinal cortices is depicted in figure 6. Entorhinal cortex sends many different projections to the hippocampus. Layer 2 neurons project to the dentate gyrus and also directly to CA3 (perforant path). Dentate gyrus granule cells excite CA3 pyramidal cells, which then contact CA1 pyramidal cells (Amaral and Witter, 1989) and also other CA3 pyramidal cells (Le Duigou et al., 2014). Entorhinal layer 3 cells also make direct contacts onto CA1 (Amaral and Witter, 1989; Kohara et al., 2013), Subiculum, and CA2 receives strong inputs from superficial entorhinal neurons; the originating layer(s) being debated: layer 2/3 (Chevaleyre and Siegelbaum, 2010) or solely layer 2 (Kohara et al., 2013). CA1 projects to subiculum. Both close the loop by projecting back to entorhinal cortex (Amaral and Witter, 1989). Subiculum is also interconnected with pre- and parasubiculum (Amaral and Witter, 1989; Kim and Spruston, 2011), CA1 projections to the dorsal part of the presubiculum have been

described (van Groen and Wyss, 1990c), but contradicted thereafter by another study (Cenquizca and Swanson, 2007).

### **Spatial neurons in entorhinal-hippocampal circuit**

Hippocampus (CA1, CA3) contains place cells, that discharge for discrete locations (place fields) within the environment (O'Keefe and Dostrovsky, 1971). Grid cells were described in the entorhinal cortex (Fyhn et al., 2004) and in pre- and parasubiculum (Boccaro et al., 2010). A grid cell discharges for multiple place fields disposed in a hexagonal grid manner within the environment. Entorhinal cortex also possesses head direction cells (Sargolini et al., 2006). Border cells, which are active only close to the environmental borders, were identified in the entorhinal cortex (Solstad et al., 2008) and the presubiculum (Boccaro et al., 2010). Some cells encode a conjunctive representation of position, direction, and velocity in the entorhinal cortex (Sargolini et al., 2006) and presubiculum (Boccaro et al., 2010). At the neuronal level, space is coded by place, grid, border, or head direction signal in the whole hippocampal-parahippocampal circuit.

The emergence of all these spatial signals in the hippocampal and parahippocampal areas is poorly understood. Grid cells could be a path integration signal in response to incoming linear and angular velocity signals; place cells were thought to derive from grid cell signal (see McNaughton et al., 2006; Moser and Moser, 2013). A recent study, showing entorhinal grid cells projecting directly onto the hippocampus supports this theory showing a possible direct influence onto place cells (Zhang et al., 2013). However, generation of place cells by grid cells has become a very controversial idea, entorhinal grid cells being impaired following lesions of hippocampus (Bonnievie et al., 2013). Today, some researchers consider these two systems as complementary processes of spatial cognition (Bush et al., 2014).

Compared to grid and place signals, head direction signal maturation occurs earlier during development (Langston et al., 2010; Wills et al., 2010) and they are not altered by hippocampal lesions (Golob and Taube, 1997). Thus, presubicular head direction cells do not require place and grid cells of the hippocampal-entorhinal circuit. In contrast, presubiculum function may be required for the generation of grid and place cells.

### **The entorhinal-hippocampal circuit relies on the presubicular directional signal**

The presubiculum is an integrative relay for directional heading and visual information upstream to the entorhinal-hippocampal network (Yoder and Taube, 2011).

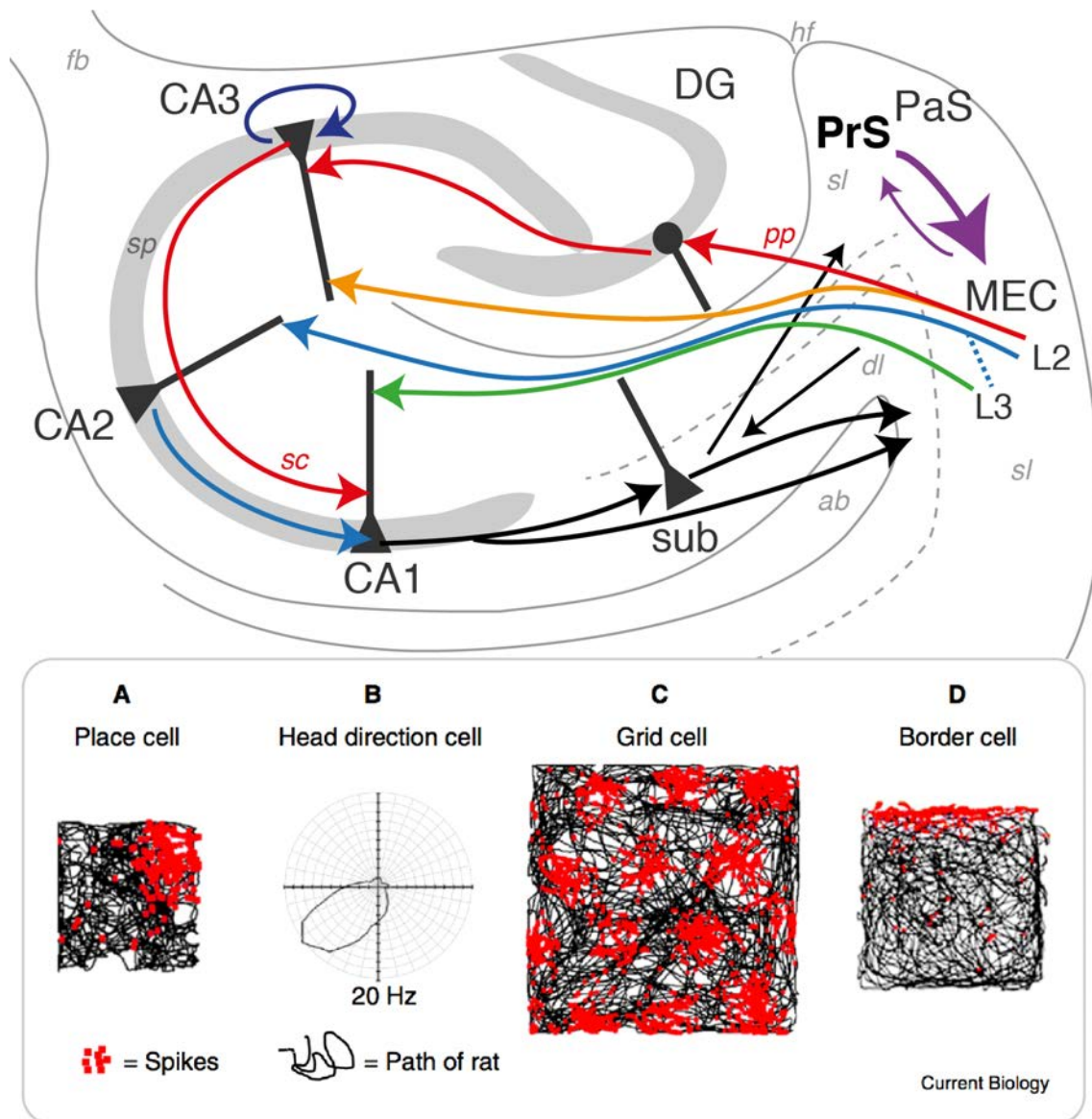


**Figure 6: Entorhinal-hippocampal circuit and function. Top.** Circuit of the main excitatory connections. Colors of arrows represent different pathways: In red, the classical tri-synaptic circuit; in green, the direct cortical projection to CA1; in light blue, the direct cortical projection to CA2; in dark blue, the recurrent excitation in CA3; In purple, the reciprocity between presubiculum (PrS) and medial entorhinal cortex (MEC), with more projections from PrS to MEC. See section text for more details. **Bottom.** Neurons that code spatial information in the entorhinal-hippocampal circuit. From Marozzi and Jeffery (2012). ab: angular bundle; fb: fimbria; dl: deep layers; hf: hippocampal fissure; pp: perforant path; sl: superficial layers; sc: Schaffer collaterals; sp: stratum pyramidale.

Inhibition of hippocampal place cell activity turns entorhinal grid cells into head direction cells (Bonnevie et al., 2013). This implies that the grid cell signal somehow contains a head direction signal. The only possible source of a directional signal for grid cells are the presubicular head direction cells (Fig 4). Ipsi- and contralateral projections from presubiculum reach layer 2/3 of entorhinal cortex (Honda et al., 2008), where grid cells are found.

Head direction cells, grid cells and place cells are equally influenced by visual landmarks. Rotation of a visual landmark produces an equivalent rotation of grid, place field and preferred direction (Fig. 7; Knierim et al., 1995; Sargolini et al., 2006). Lesions of anterior thalamus (ADN) and presubiculum degrade CA1 place fields (reduction of their spatial information content) and, interestingly, add them some directional information content (Calton et al., 2003). In addition, place fields of presubiculum-lesioned animals shift unpredictably and are barely controlled by visual landmarks. These results show that (1) without head direction signal - disrupted by ADN lesion - the presubiculum is still able to exert a visual landmark control over place cells; (2) without the contribution of presubiculum, the head direction signal is not sufficient to completely control the hippocampal function; finally, (3) without upstream directional information processing, the hippocampus hijacks place signal and transforms it into a conjunctive head-direction/place signal.

The integration of information about visual landmarks and head directions by the presubiculum is a crucial step for subsequent spatial processing by entorhinal cortex and hippocampus and might be important for memorizing the explored environment. The head direction information delivered by presubiculum is very stable over time (Fig. 3B) and therefore behaves as a long term process that could be used for memory retrieval. Direct implication of head direction cells in memory has never been directly demonstrated, but, performance in landmark navigation dependent memory task was impaired in rats with presubicular lesion (Taube et al., 1992). This result of the Morris water maze task - where the rat has to escape milky-water pool by finding a hidden platform using a landmark navigation - reproduces quite well the effect of hippocampal lesions (Morris et al., 1982).

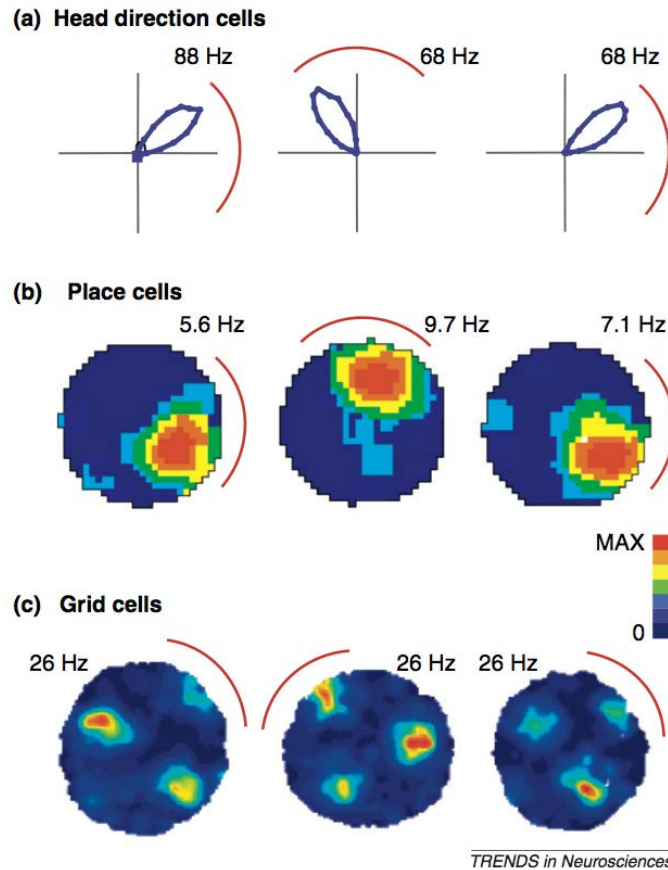


**Figure 7: Landmark control of spatial signals.** From Yoder and Taube (2011). Each panel displays the response of a different spatial cell type in rats to a 90° rotation of the salient visual landmark cue – a white sheet of cardboard attached along the inside wall of the enclosure (represented by a red arc in each panel). **(a)** The directional tuning curve of an anterior thalamic head direction cell, **(b)** the place field of a hippocampal place cell, and **(c)** the firing pattern of an entorhinal cortical grid cell show angular shifts of the spatial signal that approximate the amount of cue card rotation. Panel (a) is based on polar coordinates from Taube, 1995; (b) and (c) are based on data in Calton et al., 2003 and Sargolini et al., 2006, respectively. Data shown in plots (b) and (c) have been smoothed to improve presentation. Peak firing rates are indicated for each plot.

## 1.3 Information processing in the presubicular microcircuit

All spatial and non spatial information received by the presubiculum must be processed at the microcircuit level for building a local head direction signal. The continuous attractor network model (Fig. 5) has often been considered for larger scales than microanatomy (see Sharp et al., 2001a) and few experimental data are available to support or refute this model at the scale of the microcircuit (Taube, 2007). However, feedback inhibition (that might come from the local circuit) has been used in models to limit the overall neuronal activity (McNaughton et al., 2006). Furthermore, stellate cells in medial entorhinal cortex (putative grid cells) are mainly interconnected through disynaptic inhibition, which may constitute a recurrent inhibitory attractor network able to generate grid cells dynamics (Couey et al., 2013). However, a recent study has cast doubt on this model (Buetfering et al., 2014), and suggests that interneurons may just control the gain of grid cell output.

The fact that head direction cells have more precise tuning properties in presubiculum than in sub-cortical areas (Tuning curves on Fig. 4), may reflect the refinement of the signal being relayed many times. Of course, the specificity of local head direction signals may be due to the specific features of information processing within each area, and cortical complexity may generate a more precise signal than subcortical nuclei. Head directional tuning properties could therefore depend on some features of the presubiculum, including neuronal electrophysiological intrinsic properties and morphologies, intra- and inter-laminar information flows, or putative modular organization such as cortical columns.

### 1.3.1 Anatomy and intrinsic excitability of presubicular neurons

When I started my thesis work, little neuroanatomical data was available concerning the presubiculum. Funahashi and Stewart (1997a) partly characterized presubicular neurons physiology and morphology, however, without providing an extensive description of neuronal diversity across all 6 layers (Fig. 8A). Pyramidal cells were found in layer 3 and 5, as well as stellate cells in layer 2 and 5 and all these cells were regular spiking neurons (Funahashi and Stewart, 1997a). However, this study did not give a clear view of presubicular diversity, due to a low number of recorded neurons. Another more recent study reported that deep layer neurons had a higher sag ratio (showing the Ih expression level) and that they adapted more than superficial

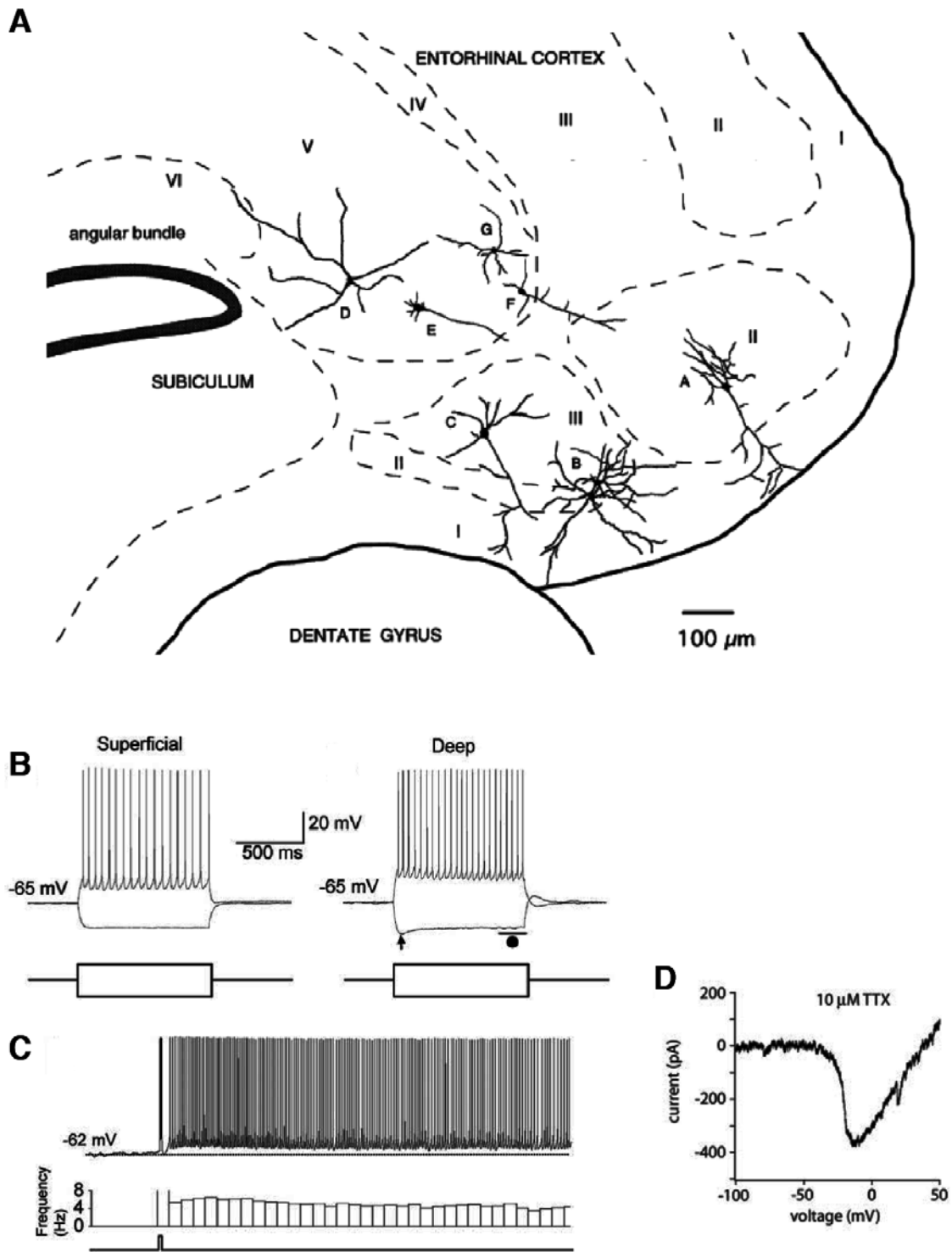


**Figure 8: Cellular properties in presubiculum.** **A.** Dendritic morphologies in pre- and parasubiculum, from Funahashi and Stewart (1997a). **B.** Intrinsic properties of deep and superficial layer neurons of dorsal presubiculum. These are regular spiking neurons; Ih expression seems higher in deep layer cells. **C.** Persistent activity can be induced in a presubicular neuron with an initial short depolarization that fires the cell, in the presence of a cholinergic agonist. B and C from Yoshida and Hasselmo (2009). **D.** A TTX-insensitive sodium current with slow activating and inactivating kinetics in presubicular principal neurons, from Fricker et al. (2009).

layer cells (Fig. 8B, Yoshida and Hasselmo, 2009).

Suprathreshold current pulses, in the presence of cholinergic receptor agonist carbachol (CCh; 10  $\mu$ M) that "mimics" waking, were able to trigger a persistent firing (less than 10 Hz) (Fig. 8C Yoshida and Hasselmo, 2009). The activation of  $I_{CAN}$  (calcium-activated nonselective cationic current), was found to underly this persisting firing in presubicular neurons. This study showed that head direction cell persistent firing may be supported at the cellular level, but its regulation should implicate an extrinsic inhibitory control, as the discharge persisted during tens of seconds.

Last, a TTX-insensitive sodium current with slow kinetics was revealed in superficial principal neurons, presumably expressed at distant sites from soma (Fig. 8D); Fricker et al., 2009). Such a current could support sustained firing in axon (Bean, 2007) and could amplify excitatory inputs in dendrites (Major et al., 2013).

### 1.3.2 Interlaminar, intralaminar and modular organization

Both interlaminar and intralaminar excitatory connection exist in the presubiculum (Funahashi and Stewart, 1997b). Recurrent excitation in deep layers (also in parasubiculum) can induce synaptic bursts in deep layers, but not in superficial layers, as few axonal collaterals are ascending (Funahashi and Stewart, 1997b, Fig. 9A, B). The lack of connectivity from deep to superficial layers was later confirmed with anterograde and retrograde tracings (Honda and Ishizuka, 2004, Fig. 9A, B). In contrast, many descending projections emerge from superficial layers and contact neurons in deep layers (Funahashi and Stewart, 1997b; Honda and Ishizuka, 2004, Fig. 9A, B, C). Axonal tracings of single layer 5 neurons showed that these cells had very diverse projection patterns including long septotemporal intrinsic projections (Honda et al., 2011, Fig. 9D). Different types of projections were highlighted: some of them were restricted to deep layers, hypothesized to send feedback information; other covered the whole presubicular plate and are thought to regulate the temporal dynamics within a widespread neuronal population in the presubiculum (Honda et al., 2011).

The presence of functional modules, such as cortical columns, was never demonstrated. Nevertheless, there are several peculiarities of the presubicular cortex indicating that this is a relevant question. Developmental cortical columns, clearly distinguishable during early post natal stage (Nishikawa et al., 2002), does not attest that functional units exists in the adult. Nonetheless, anatomical modules were revealed in the adult. In monkey, "patches" were identified in superficial layers of presubiculum by labeling with several markers, including acetylcholinesterase, cy-

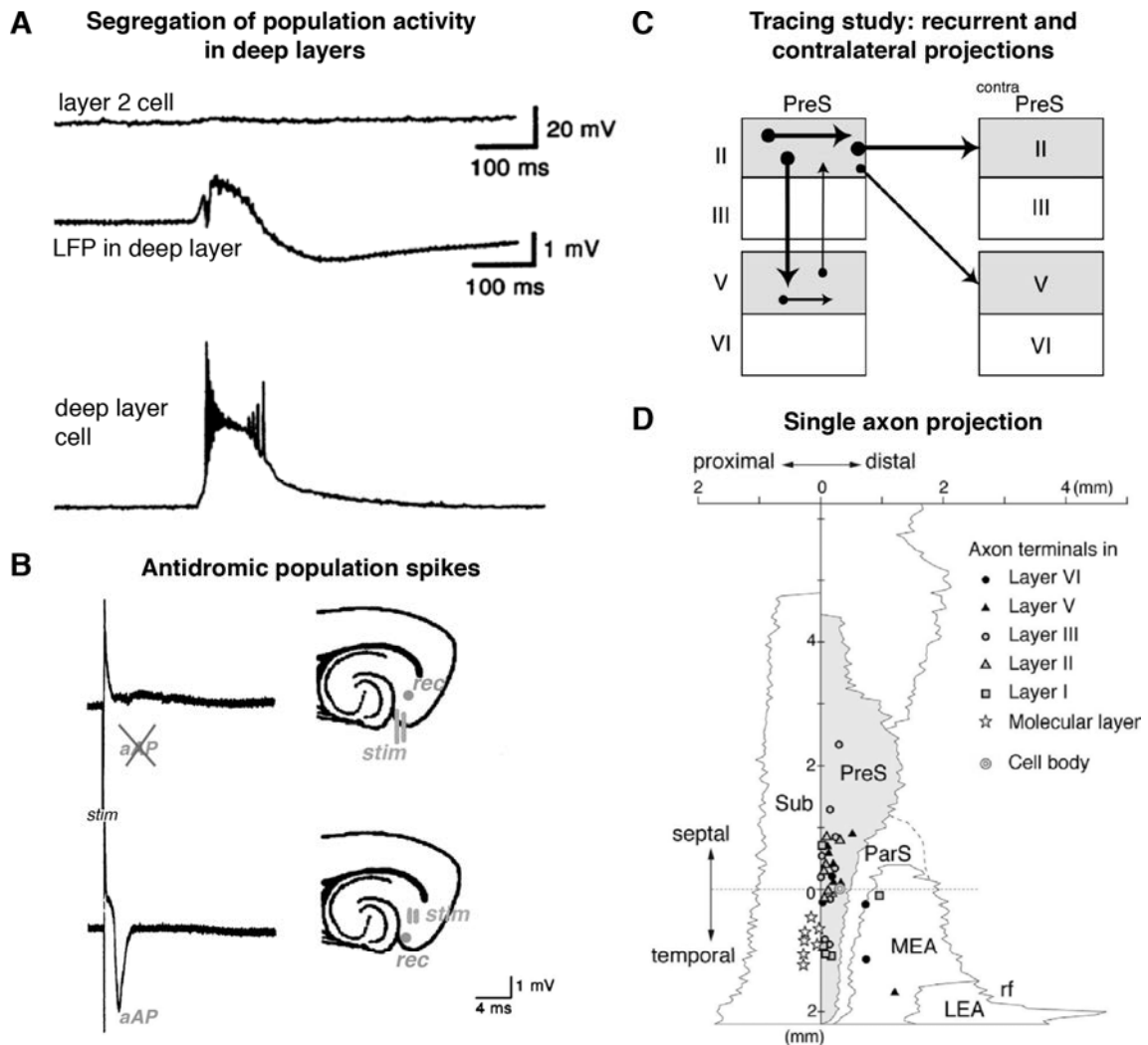


**Figure 9: Presubicular intrinsic connectivity.** **A.** Picrotoxin-induced burst revealed by Local Field Potential (LFP) recordings in deep layers of the presubiculum. During this burst, deep layer neurons fire, whereas layer 2 cells remain silent, showing the non-propagation of activity from deep to superficial layers **B.** Antidromic stimulations revealed projections from superficial layers to deep layers in the presubiculum, but not from deep to superficial layers. aAP: antidromic action potential; rec: recording site; stim: stimulation. A and B were adapted from Funahashi and Stewart (1997b). **C.** Summary of associative and contralateral projections unraveled by Honda and Ishizuka (2004) using retrograde and anterograde tracings. **D.** A unique layer 5 pyramidal cell projection area along the septo-temporal axis which covered all layers of presubiculum. Sub: subiculum; PreS: presubiculum; ParS: parasubiculum; MEA: medial entorhinal area; LEA: lateral entorhinal area. From Honda et al. (2011).

tochrome oxydase, myelin, calcium binding proteins parvalbumin, calbindin and calretinin (Ding and Rockland, 2001). The relevance of these patches is unclear, but they may be linked to some functional features. Indeed, a grid like arrangement of calbindin positive pyramidal cells exists in entorhinal cortex, and these neurons have been shown to be more theta modulated than the neighboring stellate, non-calbindin positive cells (Ray et al., 2014).

### **1.3.3 Input and output relays in the presubicular microcircuit**

The microcircuit organization makes more sense when incoming and outgoing information pathways are understood. The long range connectivity of the presubiculum is summarized in table 1.1 and its known laminar organization is depicted on figure 10. As the cellular neuroanatomy of the presubiculum has been unknown, it has been quite difficult to link the long range connectivity with the microcircuit elements. Some studies did identify input/output pathways in presubiculum. Only those identifying precise afferent targets or efferent populations will be presented here.

Presubicular superficial layer neurons constitute the major output toward ipsilateral and contralateral medial entorhinal cortices (MEC), mainly targeting their superficial layers (Köhler, 1985; Honda and Ishizuka, 2004). Ipsilateral and contralateral projection originated from different neurons in superficial layers, and 20-30% of ipsilaterally projecting neurons are GABAergic (van Haeften et al., 1997). In addition, some projections emerge from deep layer neurons of the presubiculum and target deep layers and layer 1 of the ipsilateral MEC (Honda and Ishizuka, 2004). In presubiculum, layer 3 neurons that project to the entorhinal cortex receive direct inputs from retrosplenial cortex on their proximal dendrites (Kononenko and Witter, 2011). Consequently, layer 3 neurons may relay the retrosplenial information directly to the entorhinal cortex.

Two non-overlapping pathways toward lateral mammillary nucleus (LMN) and toward anterodorsal thalamus (ADN) have been identified in dorsal presubiculum (Yoder and Taube, 2011). The presubiculum-to-LMN projection originates exclusively from a thin layer of large pyramidal cells in layer 4, whereas cells that project to ADN are a heterogeneous population in deep layers. These pathways could constitute the cellular basis of landmark control of head direction cells in subcortical areas (see section 1.2.2; Yoder and Taube, 2011).

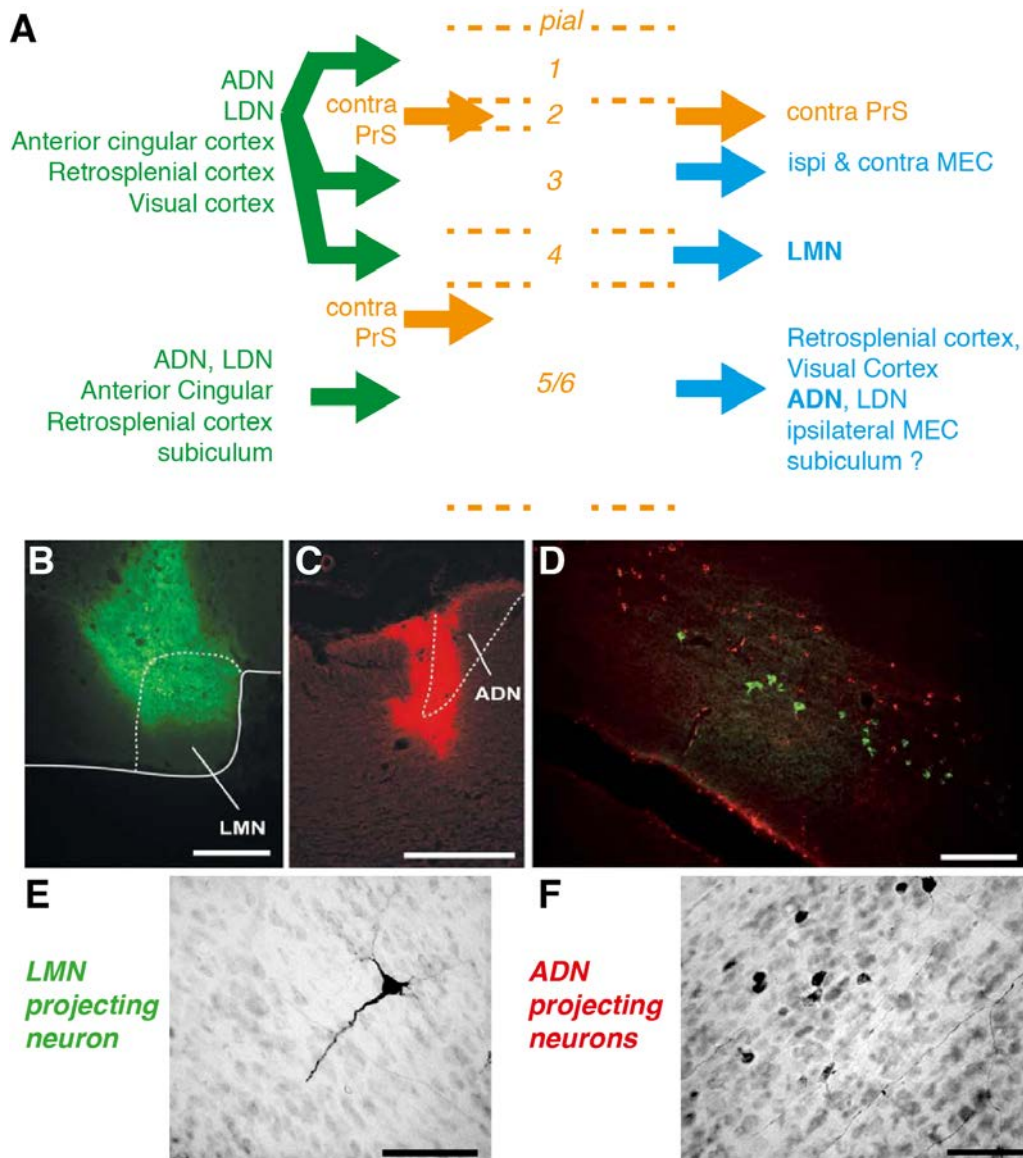


**Figure 10: Laminar specificity of afferences and efferences in presubiculum.** See table 1.1 for references. **B-F** from Yoder and Taube (2011). Cholera toxin fluorophore conjugates were injected into LMN (**B**, Alexa fluor 488) and ADN (**C**, Alexa fluor 594) (scale bars=500  $\mu\text{m}$ ), migrated retrogradely in non-overlapping neuronal populations in presubiculum (**D**, scale bar=300  $\mu\text{m}$ ). Biotinylate dextran amines were injected into LMN or ADN, and retrogradely stained neurons were revealed in slice counterstained for thionin (**E**, scale bar=75 $\mu\text{m}$  and **F**, scale bar=50 $\mu\text{m}$ ).

	<b>Does PrS receive from?</b>		<b>Does PrS project to?</b>	
LMN	<b>no</b>	otherwise it should have been shown by van Groen and Wyss (1990b,c)...	<b>yes</b>	Allen and Hopkins (1989); Gonzalo-Ruiz et al. (1992); Yoder and Taube (2011)
ADN	<b>yes</b>	van Groen and Wyss (1990b,c, 1995)	<b>yes</b>	van Groen and Wyss (1990b,c); Yoder and Taube (2011)
LDN	<b>yes</b>	van Groen and Wyss (1990b,c)	<b>yes</b>	van Groen and Wyss (1990b,c); Ishizuka (2001)
AV	<b>yes</b>	van Groen and Wyss (1990b, 1995)	<b>yes</b>	van Groen and Wyss (1990b); Ishizuka (2001)
AM	<b>yes</b>		<b>no</b>	van Groen and Wyss (1990b); Ishizuka (2001)
AC cx	<b>yes</b>	Vogt and Miller (1983); Jones and Witter (2007)	<b>no</b>	Jones and Witter (2007)
RS cx	<b>yes</b>	Vogt and Miller (1983); van Groen and Wyss (1990a,c); Jones and Witter (2007)	<b>yes</b>	Vogt and Miller (1983); van Groen and Wyss (1990c, 1992a); Wyss and van Groen (1992)
vis cx	<b>yes</b>	Vogt and Miller (1983)	<b>yes</b>	Vogt and Miller (1983)
hip	<b>?</b>	van Groen and Wyss (1990c); Cenquizca and Swanson (2007)	<b>no</b>	Rowland et al. (2013)
sub	<b>yes</b>	van Groen and Wyss (1990b,c); Funahashi et al. (1999); Kim and Spruston (2011)	<b>yes</b>	Funahashi et al. (1999)
cPrS	<b>yes</b>	Honda et al. (2008)		
PaS	<b>yes</b>	van Groen and Wyss (1990b); Ding (2013)	<b>yes</b>	van Groen and Wyss (1990b); Ding (2013)
MEC	<b>yes</b>	Michael Wyss (1981); Funahashi and Stewart (1997a); van Groen and Wyss (1990b,c)	<b>yes</b>	Swanson and Cowan (1977); Beckstead (1978); Köhler (1985, 1984); Bartesaghi and Gessi (1990); van Groen and Wyss (1990b,c); Honda and Ishizuka (2004); Kononenko and Witter (2011); Canto et al. (2012); Rowland et al. (2013)
LEC	<b>?</b>	Michael Wyss (1981) but never reproduced	<b>no</b>	Shiple (1975)
Rh cx	<b>no</b>	Kosel et al. (1983)	<b>no</b>	van Groen and Wyss (1990c)

**Table 1.1:** Long range connectivity of the presubiculum (main connections). LMN: lateral mammillary nucleus; ADN: anterodorsal thalamus; LDN: laterodorsal thalamus; AV: anteroventral thalamus ; AM: anteromedial thalamus; AC cx: anterior cingular cortex; RS: retrosplenial; vis: visual; hip: hippocampus; sub; subiculum; cPrS: contralateral pre-subiculum; PaS: parasubiculum; MEC: medial entorhinal cortex; LEC: lateral entorhinal cortex; Rh cx: perirhinal and postrhinal cortices.



## 2 | How does a microcircuit work?

In the context of my PhD, this question would rather be “How does the presubicular microcircuit work?” Indeed, the network of the presubiculum has not been very well described so far. To understand how a network generates information, it is important to understand how the different elements of a given network participate to information processing. The present chapter mainly focused on the current understanding of neuronal network physiology in a more general context.

My 3 first studies deal with neuronal properties: the morphology and intrinsic electrophysiology. I therefore go over the basis of neuronal excitability, explaining the biophysics behind the different parameters that I described in presubicular neurons (resistance, membrane time constant, the action potential shape. . .) and why this is important for neuronal function.

In my last work, I am showing that the short-term dynamics of information transfer from pyramidal cells to Martinotti cells is uncommon. The synaptic transfer seems muted initially, but becomes efficient with repetitive high frequency stimuli. This may involve a presynaptic form of plasticity in the axon and/or at the presynaptic terminals. I therefore reviewed the molecular mechanisms of plasticity present in the axons and at the presynaptic terminal in order to better discuss my results.

### 2.1 Many integrative levels in neuronal networks

The principle of a neuronal network was introduced for decades by Santiago Ramon y Cajal, who was the first to understand that neurons were anatomically and functionally distinct cellular units (Ramon y Cajal, 1899; Bullock, 2005; García-López et al., 2007). Drawings of Golgi stained neurons perfectly depicted the complexity of neuronal network anatomy, suggesting the direction of information flows between neurons and therefore providing a cartography of neuronal networks (Fig. 11, Ramon y Cajal, 1899; Lorente de Nó, 1934). However, knowing the diversity of neuronal morphologies, the location of neurons, and the anatomical pathway of information

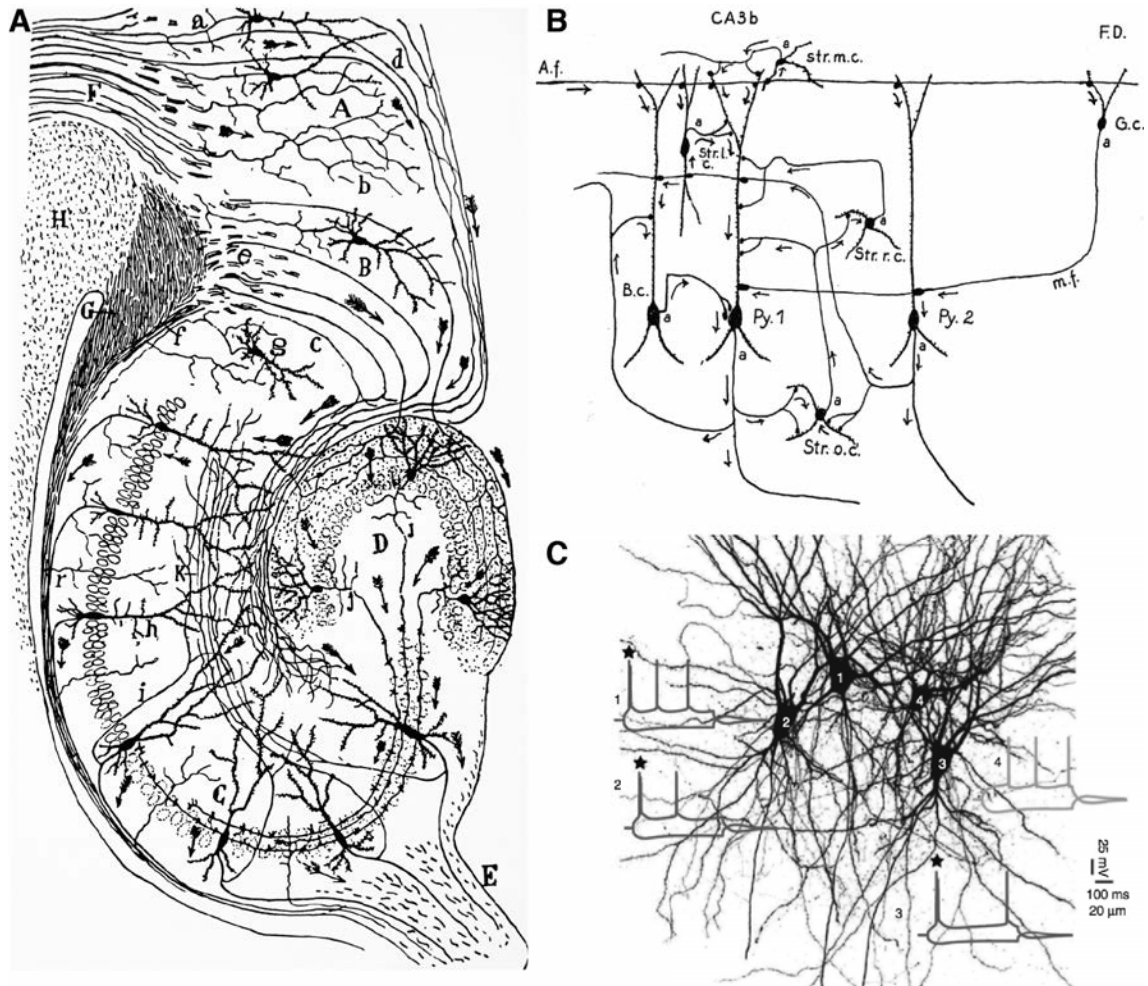


**Figure 11: Studying the network. Same neurons, different methods.** **A.** Drawing made by Ramon y Cajal of the hippocampal and parahippocampal network. (Ramon y Cajal, 1899). **B.** Lorente de No's drawing of CA3 recurrent network (Lorente de No, 1934). The two authors deduced physiological pathways from their drawing, suggested with arrows. **C.** A way to address microcircuit connectivity through multiple patch clamp recordings, linking structure and physiology, from Couey et al. (2013).

is only the first step to understand information processing in neuronal networks. These pathways are routes for information. As all the elements of the network possess properties that can modulate the information, the nervous signal is not only passively transferred from one neuron to another.

Let's take the example of sensory thalamo-neocortical projections. Excitatory information from the ventrobasal thalamus principally targets layer 4 (L4) neurons, which subsequently distribute intra-laminar (within L4) and inter-laminar (in layer 3 and 5) excitation (Lübke and Feldmeyer, 2007). Ventrobasal thalamus neurons directly project onto layer 4 fast spiking (FS) interneurons, which fire with very short latency due to the high amplitude of the synaptic responses and their fast integrative properties (Gabernet et al., 2005; Cruikshank et al., 2007, 2010); FS cells therefore provide feedforward inhibition onto L4 cells and enhance their temporal precision by defining an early and short window for excitation (Swadlow and Gusev, 2002; Cruikshank et al., 2007; Gabernet et al., 2005). In contrast, low-threshold spiking interneurons (LTS), putative dendrite-targeting interneurons, are not recruited by ventrobasal thalamic projections (Cruikshank et al., 2010), so they do not provide feedforward inhibition in L4, at least for the thalamic pathway. L4 excitatory neurons are able to activate LTS and PV cells, as a feedback inhibitory control (Beierlein et al., 2003), however their synaptic recruitment has very distinct dynamics. FS cells provide an initial feedback control that attenuates with time, whereas LTS are recruited later during high frequency stimuli (Beierlein et al., 2003). Moreover, as they target specific subcellular compartments they do not have the same impact, as somata targeting PV cells may directly regulate outputs whereas dendrite-targeting LTS neurons modulate inputs.

Even this oversimplified view of layer 4 activation by thalamic axons gives an idea of the complexity of computation in a microcircuit, depending on the targets of afferent axons, the intrinsic connectivity of local networks, the strength and dynamics at a given synapse or the integrative properties of excitatory and inhibitory neurons.

## 2.2 Neuronal intrinsic excitability

Excitability properties allow neurons to continuously make decisions as they receive information. All neurons are not alike and can be defined by their intrinsic excitability that reflects their responsiveness to incoming information. Knowledge of neuronal intrinsic excitability is, thus, essential for a better understanding of microcircuit information processing (Toledo-Rodriguez et al., 2005).

### 2.2.1 Resting membrane potential

Resting membrane potential ( $V_{rest}$ ) is the neuronal membrane potential when the neuron does not receive any information from afferences.  $V_{rest}$  is determined by plasma membrane total conductance that mainly depends on  $K^+$ ,  $Na^+$  and  $Cl^-$  ion movements. The membrane basal conductance is called leak conductance  $G_L$ ;  $V_{rest}$  value can be expressed by the Goldman-Hodgkin-Katz equation:

$$V_{rest} = 58 \log_{10} \frac{p_K [K^+]_e + p_{Na} [Na^+]_e + p_{Cl} [Cl^-]_i}{p_K [K^+]_i + p_{Na} [Na^+]_i + p_{Cl} [Cl^-]_e}$$

This value is negative, generally close to -70 mV, and is mainly due to the high conductance of potassium ions, that brings the membrane potential close to  $E_{K^+}$ ;  $Na^+$  and  $Cl^-$  ions also participate but their impact is more limited due to their lower permeability at this potential.

### 2.2.2 Neuronal passive properties

The elements of the neuronal plasma membrane can be seen as elements of an electrical circuit. The lipid bilayer is an insulator, separating external and internal conductive media; it is also a capacitor, its capacitance  $C$  being proportional to membrane surface. Currents can cross through the opened ionic channels: those are resistors and the total resistance equals the reciprocal of the sum of all specific conductances. At rest, membrane electrical properties can be modeled by a resistor (membrane resistance  $R_m$ ) and capacitor (membrane capacitance  $C_m$ ) put in parallel and under the electromotive force  $V_{rest}$ . When a constant current  $I_{stim}$  is applied to the circuit, the parallel RC circuit passively reacts according to  $R_m$  and  $C_m$  values.

$$I_{stim} = I_{C_m} + I_{R_m} ; \text{ with } I_{C_m} = C_m \frac{dV}{dt} \text{ and } I_{R_m} = \frac{V}{R_m}$$

$$\text{Then, } I_{stim} = C_m \frac{dV}{dt} + \frac{V}{R_m}$$

Where  $V$  is the relative variation of  $V_m$ . The exponential resolution of this differential equation predicts membrane potential dynamics:

$$V = V_S(1 - e^{-t/R_m C_m})$$

$t$  is the latency from the beginning of current application. At stationary state,  $I_{C_m}$  is null and  $V$  equals  $V_S$ , as predicted by Ohm's law.

$$V_S = R_m I_{stim}$$

During non-stationary states, potential variation depends on the exponential time constant  $\tau$ :

$$\tau = R_m C_m$$

From an initial value (e.g.  $V_{rest}$ ) and given the passive properties  $R_m$  and  $C_m$ , the membrane potential value  $V_m$  resulting from a constant current application  $I_{stim}$  can then be deduced:

$$V_m = V_{rest} + R_m I_{stim}(1 - e^{-t/\tau})$$

These equations describe how passive properties influence neuronal excitability. To summarize, the amplitude of the steady state response is determined by membrane resistance, and the time necessary to reach the steady state depends on the capacitance and resistance. Small neurons with a small membrane surface and a low amount of leak current would have small capacitance and high resistance, and should be very excitable. In addition to these passive properties, many active conductances are present in neurons.

### 2.2.3 Action potentials

The action potential constitutes the most characteristic neuronal active property. Their molecular basis, ion channels, were still unknown when the ionic basis underlying its generation was elucidated (Hodgkin and Huxley, 1952). Nonetheless, the Hodgkin-Huxley model described dynamics of ionic exchanges, in the giant squid axon, that predicted the channel dynamics during these transient impulses. The action potential is generated by the interaction of voltage-gated sodium and potassium channels. It starts when membrane potential reaches a threshold, where the opening of voltage gated sodium channels produces a regenerative depolarizing sodium influx. Consecutive sodium channel inactivation and voltage gated potassium channel opening underlie the repolarization phase, followed by the afterhyperpolarization (AHP) when sodium channels are closed. The slow inactivation of the outward

conductances eventually lets membrane potential return to its initial value. Action potentials are followed by an "absolute refractory period", during which the inactivation of sodium channels makes impossible the initiation of another action potential. During the following "relative refractory period", sodium channels start to recover from inactivation and action potentials of lower amplitude can be generated (Hodgkin and Huxley, 1952).

Compared to the giant squid axon, mammalian neurons express much more voltage dependent ion channels that can influence action potential shape (Bean, 2007). Furthermore, channel expression may differ between neuron subtypes, so action potential shape can be very different from one cell to another (Bean, 2007). First, sodium and potassium currents that are required for action potentials are not necessarily carried by the same channels in different neuronal populations, as it was shown in fast spiking (FS) interneurons of dentate gyrus. Their  $K_V3$  channels have fast kinetics of activation and inactivation and thus enhance a fast repolarization (Martina et al., 1998), responsible for the short duration and the deep AHP of these action potentials. Second, many other conductances can be triggered by the action potential waveform ( $Ca^{2+}$ :  $I_L$ ;  $K^+$ :  $I_{KCa}$ ;  $Na^+$ :  $I_{Na}$ ...) (Toledo-Rodriguez et al., 2005; Bean, 2007). For example, midbrain dopaminergic neurons of mouse have very wide action potentials due to the activation of large calcium conductances (Puopolo et al., 2007). Action potentials of different neurons may have very different shapes and these can be considered as signatures typically reflecting plasma membrane channel composition. Last, it is worth noting that the action potential waveform can change according to the activity-dependent activation or inactivation of specific conductances, especially in the axon (see section 2.3.2).

## 2.2.4 Firing properties

Active conductances of the neuronal plasma membrane operate either in subthreshold ranges, suprathreshold ranges, or in both. Subthreshold dynamics of membrane potential will determine firing onset (Toledo-Rodriguez et al., 2005). For example, subthreshold potassium conductances (such as the  $I_D$ -like current; see section 2.3.2) can delay firing onset by opposing the initial depolarization (Goldberg et al., 2008; Campanac et al., 2013). Both suprathreshold and subthreshold conductances determine the firing pattern (Toledo-Rodriguez et al., 2005).

Different populations of cortical neurons can be distinguished by their firing patterns in response to direct current (DC) injections (Connors and Gutnick, 1990). Initially, cortical neurons were grouped into 3 categories: regular spiking and intrinsically bursting patterns for excitatory neurons and fast spiking interneurons

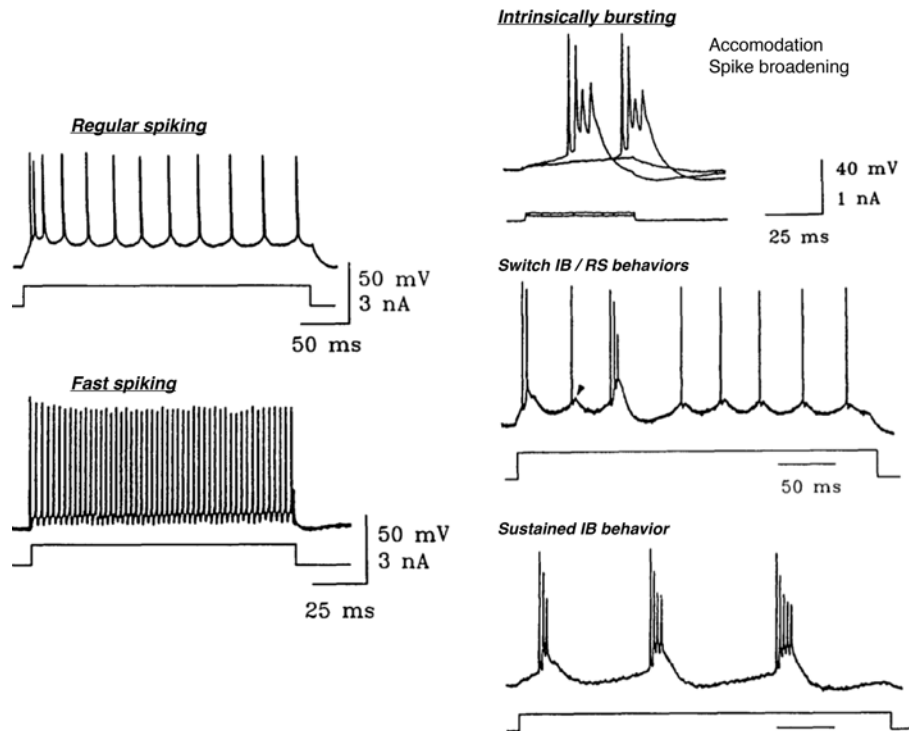


**Figure 12: Firing patterns of neocortical neurons.** Three distinct firing patterns had been identified initially: Regular Spiking (RS), Intrinsically Bursting (IB) and Fast Spiking (FS). Adapted from Connors and Gutnick (1990)

(Connors and Gutnick, 1990).

Regular spiking (RS) cells are the most common cells encountered in cerebral cortex. In response to depolarizing currents, they fire action potentials regularly, their frequency increases with the injected current and they exhibit a pronounced initial adaptation, meaning that firing frequency dramatically decreases over the initial period (few tens of ms). Intrinsically bursting (IB) cells have stereotyped clustered patterns of high frequency discharge (150-250 Hz), the burst, rhythmically initiated at 5-15 Hz. The bursts are initiated by depolarizing waves, which typically lead to a decrease in amplitude of successive spikes (accommodation, due to sodium channel inactivation) as well as their broadening (Fig. 12). Increasing the DC injection may eventually turn IB to RS behavior, but keeping the typical spike shape of an IB cell, with the underlying depolarization. Fast spiking interneurons can initiate spikes at high frequency (400-600 Hz) without adaptation or accommodation.

Since Connors and Gutnick (1990), the investigations of neuronal properties in many cortical areas have shown a greater diversity of firing patterns, especially for interneurons (Fig. Ascoli et al., 2008). Interneuron firing patterns can be defined according to their steady state firing pattern, including adapting or non-adapting regular spiking, irregular spiking, fast spiking, intrinsically burst spiking; or ac-

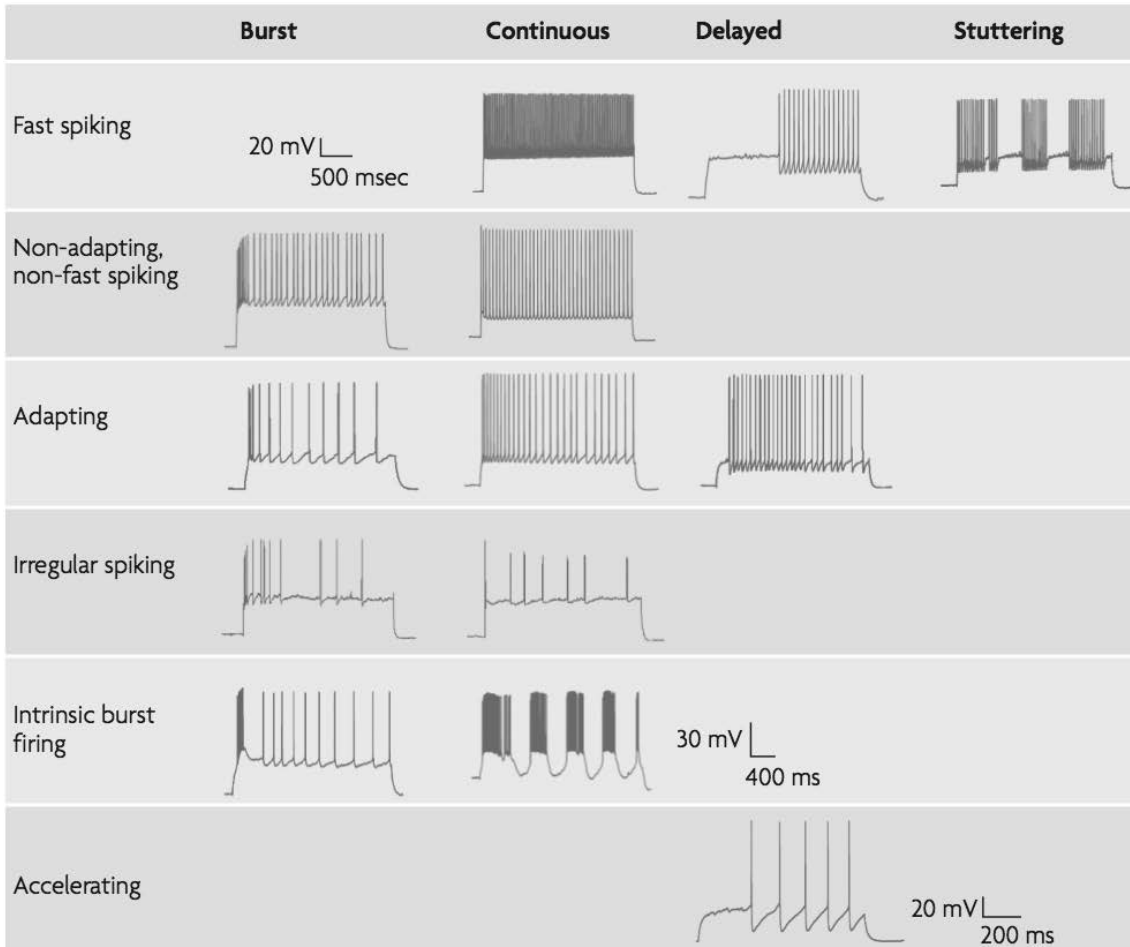


**Figure 13: Firing patterns of cortical interneurons.**

according to the response for the step onset, including burst, continuous, delayed or stuttering firing (Fig. 13).

The sequence of individual action potentials emitted by a neuron constitutes one basic feature describing its responsiveness, that is, how it is able to transform input into output (Connors and Gutnick, 1990). Specific firing patterns may be linked to specific functions. A burst is thought to be more efficient than a regular spiking train in the initiation of synchronized cortical activities (Chagnac-Amitai and Connors, 1989). Intrinsic firing patterns were correlated to function in hippocampal neurons *in vivo*; place cells were intrinsically bursting neurons, whereas silent cells were regular spiking (Epsztein et al., 2011). Last, it is worth noting that a regular spiking neuron can experience a synaptically triggered bursting behavior, but in this case it is not an intrinsic mechanism of bursting because it needs synaptic activation first (Larkum et al., 1999; Gullledge et al., 2005).

The information content given by a firing pattern could be easily deduced if all single spikes carried the same information. However, the final purpose of an action

potential is the synaptic activation, and it highly depends on activity dependent regulatory mechanisms occurring in the axon (Debanne et al., 2011), or in the synaptic terminals (Abbott and Regehr, 2004).

## 2.3 Wiring a network: axonal conduction and regulation of information

Action potentials are generated in the axon initial segment (AIS), a discrete axonal domain of 10-60  $\mu\text{m}$  length, located near the soma (Kole and Stuart, 2012). They are actively conducted to the remote axonal terminals, where they activate the synapses. Action potential conduction is blocked by tetrodotoxin (TTX, a selective blocker of voltage gated sodium channel) or by changing sodium gradient (Hodgkin and Katz, 1949), the regenerative sodium influx is therefore the motor of axonal conduction. The AIS action potential depolarizes the proximal axon to the action potential threshold; an axonal action potential is then generated and actively transmitted to the downstream axon, this conduction being unidirectional because of sodium channel refractory period and the high conductance state generated by potassium channel activation.

### 2.3.1 Axonal conduction velocity

The synaptic activation delay from the AIS discharge is set by axonal conduction velocity, which depends on passive axonal conduction properties, defined by length and time constant, as well as on the density of voltage gated ion channels (Bucher and Goaillard, 2011). The signal propagates faster if the axon diameter is high (reduced axial resistance) or if its membrane capacitance is low (faster to load). Higher sodium channel density would increase the speed of the regenerative wave propagation (Manor et al., 1991). Geometrical irregularities - such as bifurcations, swellings or synaptic boutons - constitute abrupt changes in biophysical properties that tend to slow down conduction velocity (Goldstein and Rall, 1974; Lüscher and Shiner, 1990; Manor et al., 1991).

Conduction velocity is highly dependent on recent activity history and linked to the recovery cycle of axon excitability (Bucher and Goaillard, 2011). Early studies on frog's sciatic-gastrocnemius preparation have shown that, compared to resting state, conduction velocity is higher after a first neural impulse (Adrian, 1920). This modulation induced by repetitive stimuli depended on the inter-stimulus-interval. Very short intervals ( $\leq 2$  ms) led to a depression of conduction velocity whereas higher intervals (up to 100 ms) induced its facilitation (Bullock, 1951). Moreover, this facilitating period, called the "supernormal period", could be extended as much as the number of conditioning stimuli increased.

Activity-dependent conduction velocity is indeed correlated to axonal excitabil-

ity and depends on axonal ion channel dynamics. The depression occurring for very short inter-stimulus-intervals is linked to the relative refractory period following an action potential (Hodgkin and Huxley, 1952), during which a higher action potential threshold slows conduction velocity. Many underlying mechanisms have been proposed to explain the facilitating period and all imply an activity-dependent increase of excitability such as activation of persistent sodium currents or increased extracellular potassium concentration (Bucher and Goaillard, 2011).

Myelination enables a saltatory conduction that causes a dramatic acceleration of conduction (Lillie, 1925; Huxley and Stämpfli, 1949; Tasaki, 1939), and therefore allows a faster synaptic activation (Bucher and Goaillard, 2011). Velocity was reported to be 0.25 - 0.4 m.s<sup>-1</sup> in hippocampal un-myelinated thin axons, 2.9 m.s<sup>-1</sup> in myelinated layer 5 pyramidal cells, and it can reach several tens of m.s<sup>-1</sup> in motoneuron myelinated fibers (Debanne et al., 2011). Myelinated axons are composed of two kinds of specialized domains: nodes of Ranvier and myelin sheath. Nodes of Ranvier contains a high density of sodium channels and they are separated by internodes, axons encapsulated by an isolating myelin sheath. Myelin reduces membrane capacitance and increases membrane resistance (acts like the insulation of a cable), and therefore increases length constant. Consequently, depolarization generated at nodes of Ranvier is transferred almost instantaneously toward the following node (Debanne et al., 2011).

### 2.3.2 Analog information encoding in the axon

All along their axonal conduction, action potentials undergo modulations that change their impact onto presynaptic terminals and therefore refine the primitive neuronal information given by firing patterns. The change of axonal membrane properties during sustained discharges can oppose or enhance propagation of action potentials. The presence of specific conductances coupled to membrane potential changes in the axon can alter action potential shape (height, duration), which is a crucial parameter for synaptic activation. Analog signalling (Alle and Geiger, 2008; Debanne et al., 2013) adds some information to the digital, all-or-none, neuronal code and plays a significant role in synaptic transfer reliability (Debanne, 2004; Alle and Geiger, 2008; Debanne et al., 2011; Bucher and Goaillard, 2011; Kole and Stuart, 2012; Debanne et al., 2013).

## Action potential propagation failure

In an extreme case of such modulation, the action potential conduction can be totally stopped. Impedance mismatches caused by bifurcations or swelling can induce propagation failures (Grossman et al., 1979; Lüscher and Shiner, 1990; Baginskas et al., 2009; Bucher and Goillaud, 2011). Conduction failures occur more often during high frequency ( $\geq 1$  Hz) stimulation (Grossman et al., 1979; Krnjevic and Miledi, 1959) but not only because of geometrical parameters (Debanne, 2004).

Repetitive firing increases extracellular potassium concentration that depolarizes the membrane and therefore induces sodium channel inactivation (Debanne, 2004). Alternatively, the activation of a BK conductance (large-conductance  $\text{Ca}^{2+}$ -activated  $\text{K}^+$  channels) or the  $\text{Na}^+/\text{K}^+$  pump (activated by accumulation of intracellular sodium) induces outward currents that keep membrane potential away from threshold and can lead to conduction block (Debanne, 2004). Interestingly, the hyperpolarization-induced cationic current ( $I_H$ ) has been shown to counteract hyperpolarization in terminals so as to limit propagation failures during repetitive stimulation in hippocampus (Soleng et al., 2003) and cerebellar cortex (Baginskas et al., 2009).

In contrast, propagation failures can occur during sparse activity and are less likely during sustained activity. In hippocampal axons, propagation failures were linked to an  $I_A$  conductance (Debanne et al., 1997). The fast activating and inactivating kinetics of this current imply that failures occur only when action potentials are initiated with very short latency after depolarization onset. When firing is delayed from the depolarization onset, or if the action potential occurs during a train of action potentials,  $I_A$  inactivation increases conduction reliability (Debanne et al., 1997).

## Action potential shape and synaptic efficiency

In cortical neurons, the modification of action potential waveform leads to changes in synaptic strength (Boudkkazi et al., 2011), as it controls voltage-gated calcium channel opening at the synapse (e.g. Sabatini and Regehr, 1997; Geiger and Jonas, 2000; see section 2.4). Several mechanisms of synaptic analog-digital facilitation by spike-shape modification have been reported in central axon (Debanne et al., 2013), mostly involving potassium channels.

**$I_D$  and  $I_A$  potassium conductances.** Action potential waveform highly depends on the activity dependent modulation of A- and D-type potassium conductances (Debanne et al., 2011).  $I_D$  conductances, carried by dendrotoxin-sensitive  $\text{K}_V1$  channels,

are characterized by fast activation (ms) and slow inactivation (seconds) below the spike threshold, as well as a slow recovery from inactivation (seconds) (Storm, 1990).

The axon initial segment is able to perform advanced signal processing as it can express many voltage-gated sodium and potassium channels, including  $K_V1$  channels (Kole and Stuart, 2012). In neocortical layer 5 pyramidal neurons,  $K_V1$  expression in the axon initial segment strongly controls action potential width ahead from its initiation site (Kole et al., 2007). This is further improved by  $K_V1$  expression in axonal collaterals and synaptic terminals (Foust et al., 2011). A long somatic depolarization of layer 5 pyramidal neurons is transmitted along the axon, and increases spike width and synaptic efficiency (Shu et al., 2006) by the inactivation of  $K_V1$  (Shu et al., 2007; Kole et al., 2007). This provides a mechanism for a cortical state-dependent modulation of information transfer, favoring communication during wakefulness (Shu et al., 2006; Kole et al., 2007). The transmission of somatic depolarization along the axon diminishes with the distance from soma, due to attenuation by axonal passive integration (Sasaki et al., 2012; Debanne et al., 2011). Consequently, steady state depolarization may facilitate the transfer of information to nearby neurons and may promote the creation of localized functional modules.

In CA3, an D-type potassium conductance, expressed at least in the proximal axon (Axonal Kv1 Channels determine pyramidal cell excitability, S. Rama et al. 9th FENS forum of Neurosciences, 2014), was involved in the strength of recurrent excitatory synapses (Saviane et al., 2003). Contrary to neocortical layer 5 pyramidal cells (Kole et al., 2007),  $I_D$  in CA3 influences somatic spike repolarization and cell excitability, causing a typical depolarizing ramp prior to discharge, abolished with specific blockers of  $I_D$  (DTX).

In mossy fiber boutons, the heteromultimeric assemblies of  $K_V1.2$  ( $I_D$ ) and  $K_V1.4$  ( $I_A$ ) subunits (Sheng et al., 1993) generate a A-type potassium with unique properties: fast activation (ms), fast inactivation (tens of ms) and slow recovery from inactivation (hundreds of ms) (Po et al., 1993; Geiger and Jonas, 2000). This potassium conductance efficiently participates to action potential repolarization at low frequency stimulation ( $>1$  Hz, Geiger and Jonas, 2000). Its cumulative inactivation and slow recovery during trains of action potentials at high frequencies (10 to 100 Hz) induces spike broadening in synaptic terminals, but not in the soma. Spike broadening enhances the calcium influx and therefore the synaptic activation, even few seconds after the end of the stimulus (Fig. 14; Geiger and Jonas, 2000).

**$K_V7$  potassium channels -  $I_M$  conductance.** The M-current ( $I_M$ ) is a slowly activating (tens of ms) and non-inactivating potassium current. It is suppressed

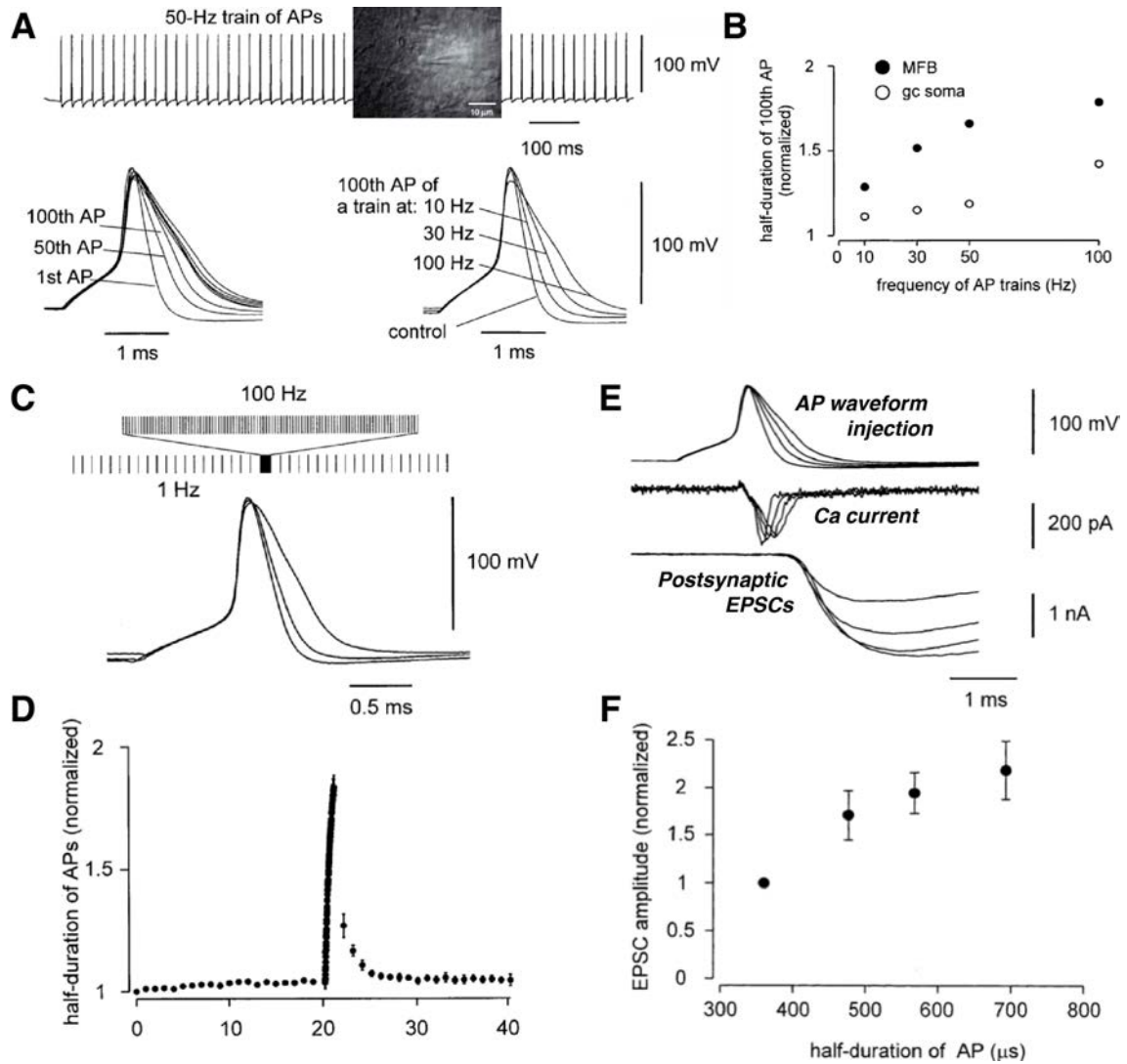


**Figure 14: Action potential broadening enhances synaptic efficiency in mossy fiber boutons (MFB).** **A.** Broadening during a train of action potentials (APs) recorded from a MFB (inset). Spike width increased with the number and frequency of APs, more at the MFB than at the soma (**B**). **C.** Slow recovery of AP width after a high stimulus train. **E.** Recorded AP waveforms were injected as a command in voltage clamp mode (action potential clamp) at the MFB. It revealed an increase of calcium influx with AP broadening, which enhanced synaptic strength (**F**). Adapted from Geiger and Jonas (2000), inset in (**A**) from Bischofberger et al. (2006).

by activation of muscarinic receptors by acetylcholine and may be enhanced by somatostatin (Storm, 1990).  $K_V7$  potassium channels are responsible for the M-current and they are specifically co-expressed with sodium channels in the AIS and in nodes of Ranvier in central neurons (Devaux et al., 2004; Rasmussen et al., 2007). This current influences neuronal excitability parameters (Peters et al., 2004), such as spontaneous firing (Shah et al., 2008). The M-current may also improve neurotransmitter release efficiency at Schaffer collateral synapses by preventing sodium channel inactivation, thereby preserving action potential amplitude (Vervaeke et al., 2006).  $K_V7.2/7.3$  channels may increase  $Na_V$  channel availability in nodal domains in myelinated central nervous system axons, and so enhance action potential conduction (Battefeld et al., 2014).

**Large-conductance calcium-activated potassium channels (BK or  $K_{Ca}1.1$  channels).** The BK conductance, with slower kinetics than the M-current, is typically activated by the calcium entry triggered by discharge, and participates in frequency adaptation and long-lasting hyperpolarization (Storm, 1990). A BK conductance was identified in the presynaptic terminals of CA3 pyramidal cells and contributes to spike repolarization in the axon (Raffaelli et al., 2004; Hu et al., 2001). The activity-dependent inactivation of axonal BK produces spike broadening and therefore increases release probability at the CA3 recurrent synapses (Raffaelli et al., 2004) and the CA3-to-CA1 synapses (Hu et al., 2001).

**Extrinsic modulation of action potential shape.** The action potential waveform can be modified through the activation of specific receptors on the axonal plasma membrane (Sasaki, 2013). In CA3 neurons in organotypic culture, astrocytic glutamate release was shown to broaden action potentials by activation of AMPA receptors (Sasaki et al., 2011) - astrocytic release of neurotransmitter being quite controversial as it was never clearly demonstrated *in vivo* (Hamilton and Attwell, 2010).

Endogenous adenosine is thought to be a very important factor for homeostatic plasticity (Dias et al., 2013). This purine nucleoside is known to regulate the general state of arousal and its increasing level during wakefulness eventually promotes sleep at the end of the day (Dunwiddie and Masino, 2001). The basal extracellular level (25-250 nM) continuously activates axonal  $G_{I/O}$ -coupled  $A_1$  adenosine receptors (Dias et al., 2013) that shorten action potentials, certainly via the activation of axonal  $K_V1$  channels (Sasaki et al., 2011).

## 2.4 Synaptic transfer and modulation of information in the presynaptic terminal

A synapse is the communication tool used by axons to transfer information onto effector cells such as muscles, glandular cells and other neurons. There are different types of synapses including chemical, electrical and mixed synapses. In the mammalian nervous system, most of them are chemical synapses, where the information is carried by the presynaptic secretion of neurotransmitter onto the postsynaptic neuron. Chemical synapses are divided into three parts that can be identified with electron microscopy (Fig. 15): the presynaptic element, the postsynaptic element and the synaptic cleft. Presynaptic elements, the synaptic boutons, are axonal swelling characterized by numerous mitochondria and synaptic vesicles that contain neurotransmitter (Fig. 15, Harris and Weinberg, 2012). The active zone is the functional area of the presynaptic terminal membrane where vesicles are docked and primed for release (Harris and Weinberg, 2012). The postsynaptic density (Fig. 15) is a submembranous electron-dense zone reflecting the presence of postsynaptic receptors and scaffolding molecules that are aligned with the presynaptic active zone (Harris and Weinberg, 2012; Sheng and Kim, 2011). The neurotransmitter is released into the synaptic cleft, which consists of a widening of extracellular space between pre- and postsynaptic compartments and contains electron-dense material corresponding to extracellular matrix and specialized synaptic proteins (Fig. 15; Harris and Weinberg, 2012; Sheng and Kim, 2011).

### 2.4.1 Basic mechanism of neurotransmitter release

An action potential that invades the presynapse is able to trigger neurotransmission with a high temporal precision (Kaeser and Regehr, 2014). The two requirements for neurotransmitter release are: (1) the availability of releasable vesicles at the active zone and (2) an increase of  $\text{Ca}^{2+}$  level at the active zone.

Even if hundreds of vesicles are associated with each active zones (Rizzoli and Betz, 2005), only few of them are able to be released: the readily releasable pool (RRP,  $< 5\%$ , e.i. 5-10 vesicles) and the recycling pool (RP, 10-20%). The remaining non-recycling pool (NRP; also named Reserve Pool) would not be released (but see Ikeda and Bekkers, 2009) but rather provide a store for the RP (Rizzoli and Betz, 2005). The RP can be released only during sustained and high frequency activation but the RRP is released instantaneously when terminals are activated. RRP vesicles are primed in a dedicated molecular framework that promotes the  $\text{Ca}^{2+}$ -dependent

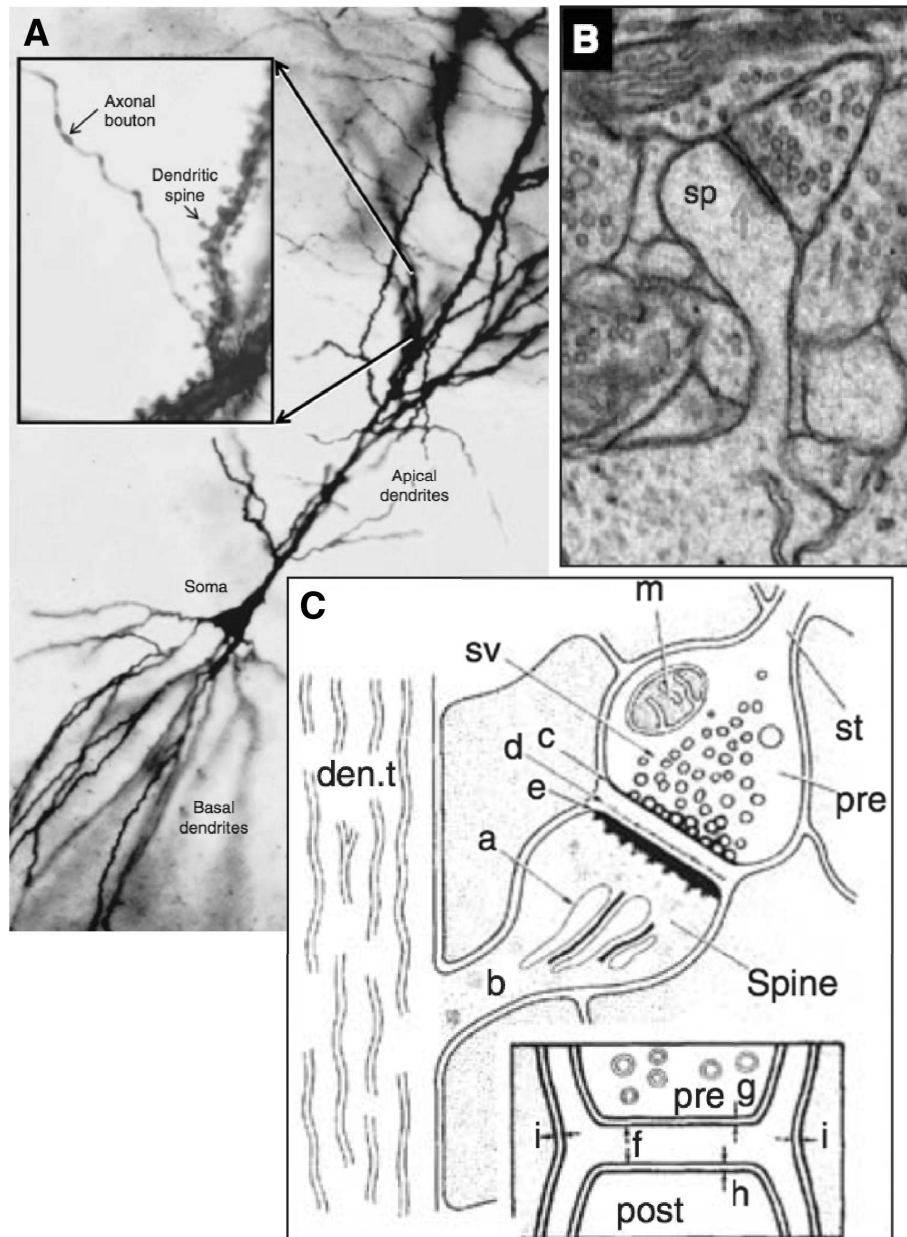


**Figure 15: Cortical chemical synapse.** **A.** Golgi-impregnated pyramidal cell in hippocampal area CA1, showing the soma and apical and basal dendrites. **Inset, left.** Higher magnification shows an axon passing by dendritic spines protruding from the apical dendritic shaft. **B.** Chemical asymmetrical synapse (glutamatergic) on a CA1 pyramidal cell spine revealed with electron microscopy. The postsynaptic density (green arrow) highlights the synaptic contact. Note the presence of vesicles in presynaptic terminals (bar =  $1\mu\text{m}$ ) **C.** Drawing of dendritic spine synapse: (a) spine apparatus; (b) spine neck; (c) presynaptic membrane; (den.t.) dendritic microtubules; (d) dense material in synaptic cleft; (e) postsynaptic membrane; (f) synaptic cleft; (g,h,i) plasma membranes of pre-, post-, and neighboring processes; (m) mitochondrion; (pre) presynaptic axons; (st) “stalk” of axon; (sv) synaptic vesicles. Adapted from Harris and Weinberg (2012).

fusion by coupling vesicles to voltage gated calcium channels (Fig. 16A). Calcium channel opening following an action potential induces a sharp calcium increase (from  $0.1 \mu\text{M}$  to  $30\text{-}100 \mu\text{M}$ ). The  $\text{Ca}^{2+}$  transient ( $\text{Ca}_{local}$ ) is very short ( $\sim 200 \mu\text{s}$ ) due to the fast inactivation of channels with action potential repolarization and a subsequent diffusion and buffering by calcium binding proteins (Roberts, 1993). The activation of the release machinery is enhanced by calcium fixation on low affinity domains of synaptotagmin (Fig 16, Südhof, 2013) and therefore requires high  $\text{Ca}^{2+}$  levels. Taken together, these elements ensure the temporal precision of neurotransmitter release. The RRP can be divided into fast and slow releasing subpools (Wu and Borst, 1999; Sakaba and Neher, 2001), and the more easily released pool has the lower replenishment rate. This heterogeneity of RRP vesicle release might reflect their accessibility to calcium and therefore their proximity to calcium channels.

The basic organization of the synaptic active zone determines the synaptic strength. In a recent study on CA3 recurrent synapses, Holderith et al. (2012) has shown that the size of the active zone determines the number of docked vesicles, the calcium entry and therefore the release probability.

## 2.4.2 Synchronous versus asynchronous release of neurotransmitter

Synchronous release - when synchronized with the arrival of an action potential in the presynaptic terminal - constitutes the major mode of neurotransmitter release at most synapses, especially for low frequency stimuli (Kaesler and Regehr, 2014). Neurotransmitter release can be asynchronous, that is, vesicle fusion is not time locked with the action potential. An extreme case is the deep cerebellar nuclei to inferior olive synapses that operate mainly with this transfer mode (Best and Regehr, 2009).

Delayed release depends on the accumulation of intracellular  $\text{Ca}^{2+}$ , occurring especially during rapid and sustained firing. The high level of residual  $\text{Ca}^{2+}$  ( $\text{Ca}_{res}$ ) might enhance the exocytosis of the subset of RRP vesicles that releases slowly and recovers rapidly (Wu and Borst, 1999; Sakaba and Neher, 2001; Otsu et al., 2004; Kaesler and Regehr, 2014). Indeed, the introduction of the slow calcium chelator EGTA in the presynaptic compartment suppresses asynchronous but not synchronous release (Cummings et al., 1996; Atluri and Regehr, 1998; Manseau et al., 2010, but see Vyleta and Jonas, 2014). Delayed release seems to depend on  $\text{Ca}^{2+}$  sensors that have lower affinity than those involved in synchronous release (Kaesler and Regehr, 2014). An increased  $\text{Ca}_{res}$  may depend on the asynchronous activation of  $\text{Ca}^{2+}$  channels (Few et al., 2012), the activation of  $\text{Ca}^{2+}$  permeable receptors

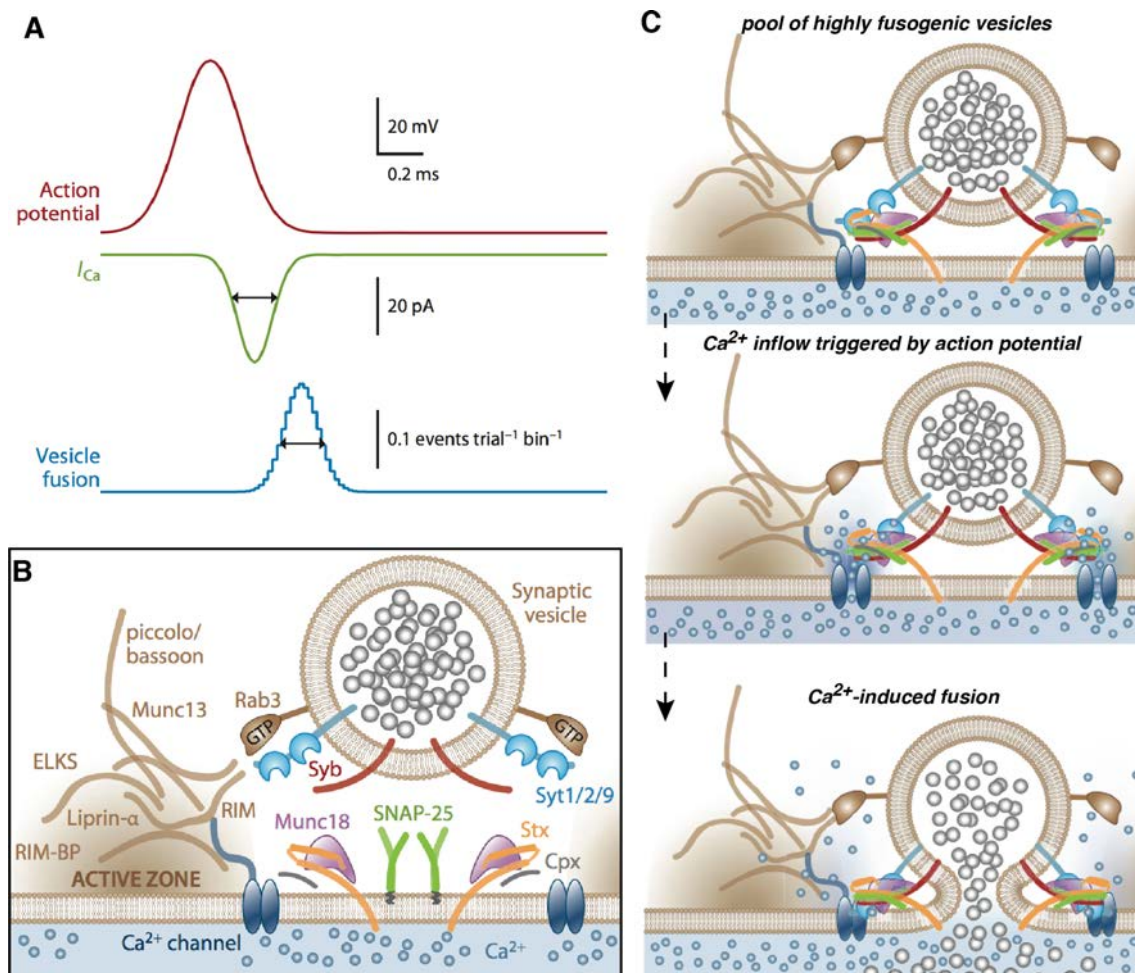


**Figure 16: Schematic of neurotransmitter release.** **A.** Action potential induces voltage dependent  $Ca^{2+}$  influx leading to fusion of vesicles. **B.** Molecular components of release machinery. **C.** Molecular mechanism of release. Priming consists of the liaison of membrane and vesicles thanks to SNAREs (soluble N-ethylmaleimide-sensitive factor-attachment protein receptors) and SM proteins (for Sec1/Munc18-like proteins). SNAREs are syntaxin-1 (Stx) and SNAP-25 on the membrane ; Synaptobrevin (Syb) on the vesicle. Munc18-1 is the main SM protein. Synaptotagmin (Syt1/2/9) is the calcium sensor that enhances the SNARE/SM protein fusion mechanism. Coupling with voltage gated calcium channels is operated by proteins of the active zone: Rab3, RIM (Rab3 interacting molecules), RIM-BP (RIM binding proteins), liprin- $\alpha$ , ELKS and piccolo/bassoon. Adapted from Kaeser and Regehr (2014)

(P2X2, TRPV1), a  $\text{Ca}^{2+}$  dependent enhancement of voltage gated  $\text{Ca}^{2+}$  channel permeability or a  $\text{Ca}^{2+}$ -induced  $\text{Ca}^{2+}$  release from intracellular stores (Kaeser and Regehr, 2014). The last mechanism does seem universal (Carter et al., 2002) and mitochondria could limit asynchronous release by an uptake of cytosolic  $\text{Ca}^{2+}$  during high rate stimuli (David and Barrett, 2003; Talbot, 2003; see section 2.4.3). This limitation of delayed release would ensure longer lasting synchronous release by preventing vesicular depletion (David and Barrett, 2003; Talbot, 2003).

Cortical  $\text{PV}^+$  interneurons provide dense inhibition that cover neighboring principal neurons like a blanket (Packer and Yuste, 2011). They are crucial in oscillating neuronal networks and enable ensemble coding of information by improving spike timing precision of pyramidal neurons (Fig. 17A, B; McBain and Fisahn, 2001). Asynchronous release of neurotransmitter occurs for high frequency stimuli at autaptic and synaptic connections of  $\text{PV}^+$ /fast spiking interneurons in neocortex (Manseau et al., 2010). At these synapses, asynchronous release rises as time and frequency of discharge increase, providing a prolonged and desynchronizing inhibition, thought to disrupt cortical information processing (Manseau et al., 2010, Fig. 17C, D). Release synchrony modulation enables the same fast spiking interneurons to enhance either synchronization or desynchronization and therefore appears to be a key regulator for network information processing.

Asynchronous release has also been described at cortical excitatory synapses. It occurs for high frequency stimuli (40 Hz) at synapses made by excitatory neurons onto low threshold spiking interneurons in somatosensory cortex layer 4 (Beierlein et al., 2003). The functional role of asynchronous release at this glutamatergic synapse is unknown (Beierlein et al., 2003) but it could constitute a short term synaptic memory, facilitating summation of synaptic events and therefore firing.

### 2.4.3 Short term presynaptic plasticity

An initial synaptic activation typically produces a transient alteration of synaptic efficiency, known as short term presynaptic plasticity. Different types have been identified: short-lived depression, facilitation, long-lived depression, augmentation and posttetanic potentiation (PTP) (Regehr, 2012, Fig. 18). These adaptive changes of functional connectivity determine the dynamics of information flow and therefore constitute key processes for microcircuit computation (Fisher et al., 1997; Zucker and Regehr, 2002; Abbott and Regehr, 2004; Regehr, 2012).

Short-lived depression and facilitation are typically observed by looking at the postsynaptic amplitudes for two closely spaced stimuli (paired-pulse). Paired-pulse depression corresponds to a decreasing amplitude; Paired-pulse facilitation is defined

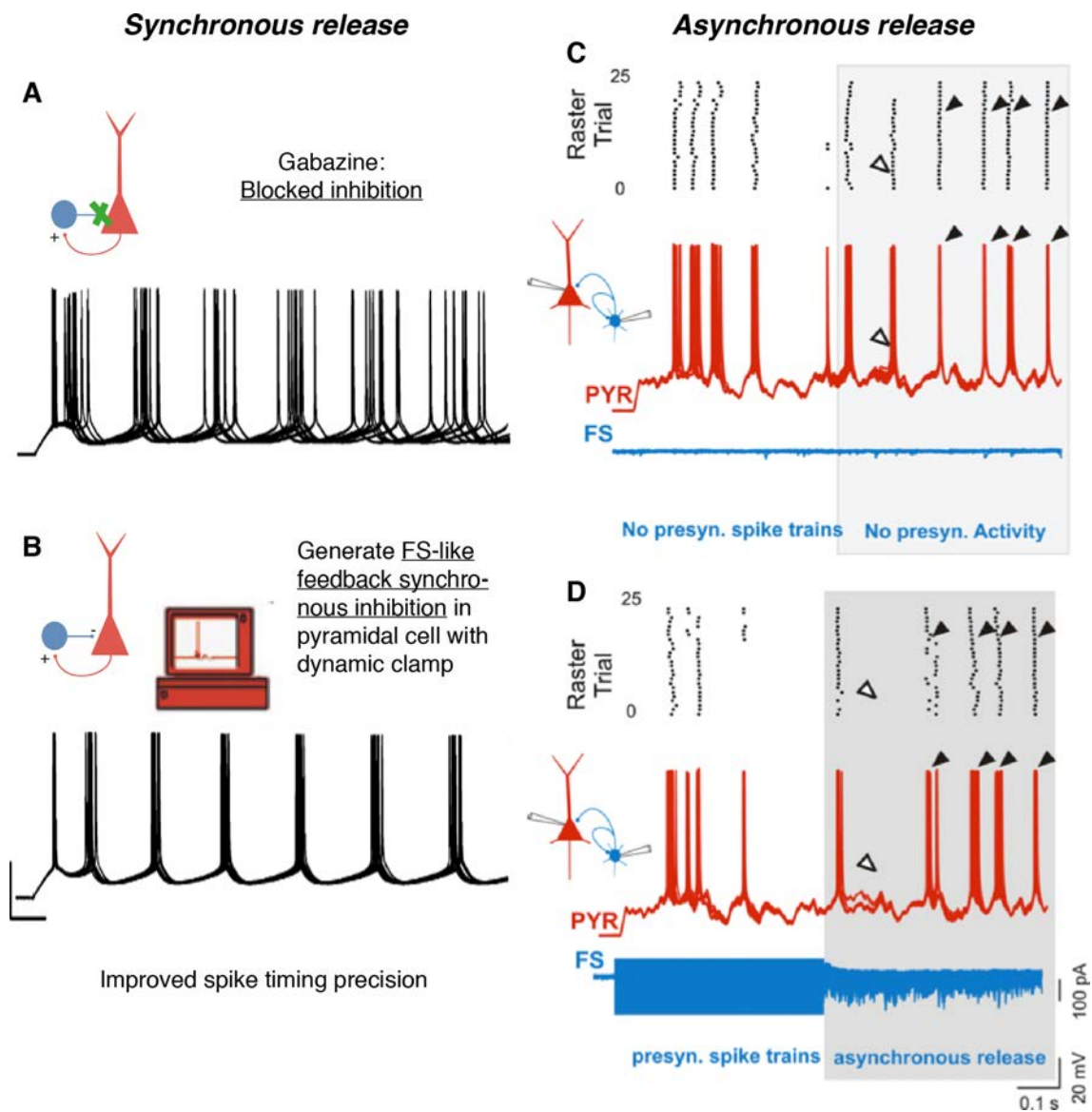


**Figure 17: Impact of fast spiking interneuron-mediated synchronous and asynchronous GABA release onto neocortical pyramidal cell firing.** **A, B.** Adapted from Bacci and Huguenard (2006); Deleuze et al. (2014). Pyramidal cell spike timing precision is improved by fast-spiking interneuron-like synchronous feedback inhibition. Scale bars: 40 mV, 50ms. **C, D.** Adapted from Manseau et al. (2010). Asynchronous synaptic release of GABA deteriorates the overall precision and reliability of APs in pyramidal neurons. The scheme on the left refers to the paired-recording configuration where one presynaptic fast-spiking (FS) interneuron is synaptically connected to itself and to a postsynaptic pyramidal neuron (PYR). Current-clamp superimposed traces recorded from a pyramidal cell (red traces) stimulated with frozen noise current injections in the absence (**C**) and presence (**D**) of a spike train (300 Hz, 500 ms) elicited in a presynaptic FS interneuron. Spike trains in the FS interneuron (blue trace) induced asynchronous release (**D**). Pyramidal neuron spike precision and reliability deteriorates both during and over 500 ms after the train (gray box) during asynchronous synaptic release (raster plots). Note the spike disappearance (white arrowheads) and the increased jitter after the presynaptic stimulus train.

by an increasing amplitude (Regehr, 2012, Fig 18A, C). The amplitude difference tends to disappear as the time between the two stimuli increases; depression may persist longer (decay time constant  $\approx 1$  sec, Fig 18A) than facilitation (decay time constant of tens or few hundreds of ms, Fig 18C). Long-lived depression, augmentation and PTP are longer lasting, but still transient changes that occur after an intense stimulus (decay time constant of seconds to minutes; Regehr, 2012, Fig 18B, D). Such alterations of synaptic efficiency can be due to different mechanisms (not all present at the same synapse) involving vesicular pool dynamics and/or calcium signalling (Fig. 18). Different kinds of plasticity often coexist in the same terminal, so the level of their relative expression determines the overall synapse dynamics (Regehr, 2012).

## Depression

Decrease of synaptic strength may be due to vesicular depletion. If a large fraction of vesicles is released by an action potential or a train of action potentials, less will be available for subsequent activation (Betz, 1970; Regehr, 2012; Zucker and Regehr, 2002). Depletion and the resulting depression depend on several factors including the availability of releasable vesicles, their release probability and replenishment rate (Regehr, 2012). The depletion model predicts that a lower release probability should decrease depression (Regehr, 2012). This is true in cortical synapses where depression may be turned into facilitation by a decrease of release probability (Debanne et al., 1996; Angulo et al., 1999). However, not all the predictions of this model were always confirmed (Sullivan, 2007; Waldeck et al., 2000), thus depletion cannot account for all depressing synapses (Regehr, 2012).

Another model explaining depression considers the inactivation of release sites by fused vesicle material (Regehr, 2012). Blocking endocytosis, which is involved in clearance of fusion proteins at the active zone, enhances depression in the Calyx of Held (Hosoi et al., 2009). The accessibility of the active zone would be a very limiting parameter at these synapses that possess only 2 release ready vesicles per active zone (1100 docked vesicles for 554 active zones, Sätzler et al., 2002). At synapses with a large releasable pool of vesicles (Saviane and Silver, 2006), the presence of this mechanism is unknown but it might be less critical given the greater number of docked vesicles (10-30, Schikorski and Stevens, 1999, 2001).

Other proposed mechanisms for depression imply the change of release probability (Sullivan, 2007; Regehr, 2012), such as the use-dependent inhibition of the release machinery (Hsu et al., 1996; Waldeck et al., 2000) or the calcium-induced inhibition of calcium currents (Xu and Wu, 2005; Xu et al., 2007; Sullivan, 2007).

These and other mechanisms can account not only for short-lived but also for long-lived depression. The depletion model for long-lived depression refers to vesicular depletion of the entire RP, and not only the RRP, resulting in a longer delay for a full replenishment (Regehr, 2012). A transient decrease of release probability can also explain long-lived depression (Regehr, 2012); for instance, the slow recovery after inactivation of presynaptic voltage gated calcium channels is involved in a reduced synaptic strength at the calyx of Held (Forsythe et al., 1998).

### **Short term facilitation**

All mechanisms that were proposed to explain facilitation involve calcium signalling (Fig. 18).

One of the most popular theories is the residual calcium hypothesis, in which calcium would be directly responsible for facilitation (Katz and Miledi, 1968). The calcium signal that triggers release ( $Ca_{local}$ ) is quickly cleared from presynaptic terminals. However, a residual "active calcium" level ( $Ca_{res}$ ) can persist and enhance  $Ca_{local}$  evoked by a subsequent action potential, leading to a higher vesicular release, thus causing facilitation. This hypothesis is controversial as  $Ca_{res}$  level is very low ( $\sim 1\%$  of  $Ca_{local}$ ) and the summation of  $Ca_{res}$  and  $Ca_{local}$  would therefore not be able to cause a significant facilitation (Regehr, 2012). However,  $Ca_{res}$  may act on high affinity calcium sensors involved in vesicular fusion enhancement (Regehr, 2012).

Different calcium buffers are found among different neuronal populations, and they are often used as descriptive tools (Ray et al., 2014) rather than for their function. Artificial calcium buffers are known to influence synaptic strength, especially BAPTA, with its fast kinetics, reduces  $Ca_{local}$  as it enters the synapse (Adler et al., 1991). Endogenous buffers with similar kinetics, such as calbindin or calretinin, would be able to capture  $Ca_{local}$  and diminish the initial synaptic activation; its progressive saturation would result in facilitation (Regehr, 2012; Faas et al., 2007). EGTA, a slower calcium buffer, does not affect synchronous release (Adams et al., 1985; Adler et al., 1991) but abolishes asynchronous release (see section 2.4.2), suggesting a capture of  $Ca_{res}$ . Parvalbumin (PV) is a neuronal marker of fast-spiking interneurons and also a  $Ca^{2+}$  binding protein similar to EGTA. PV downregulates facilitation by accelerating the decay of  $Ca_{res}$ , thus preventing  $Ca_{res}$  increase during repetitive stimuli (Caillard et al., 2000; Regehr, 2012).

### **Augmentation - Posttetanic potentiation (PTP)**

Augmentation and PTP describe transient increases of synaptic strength (enhancement) triggered by an intense ("tetanic") conditioning stimulus (Regehr, 2012). This

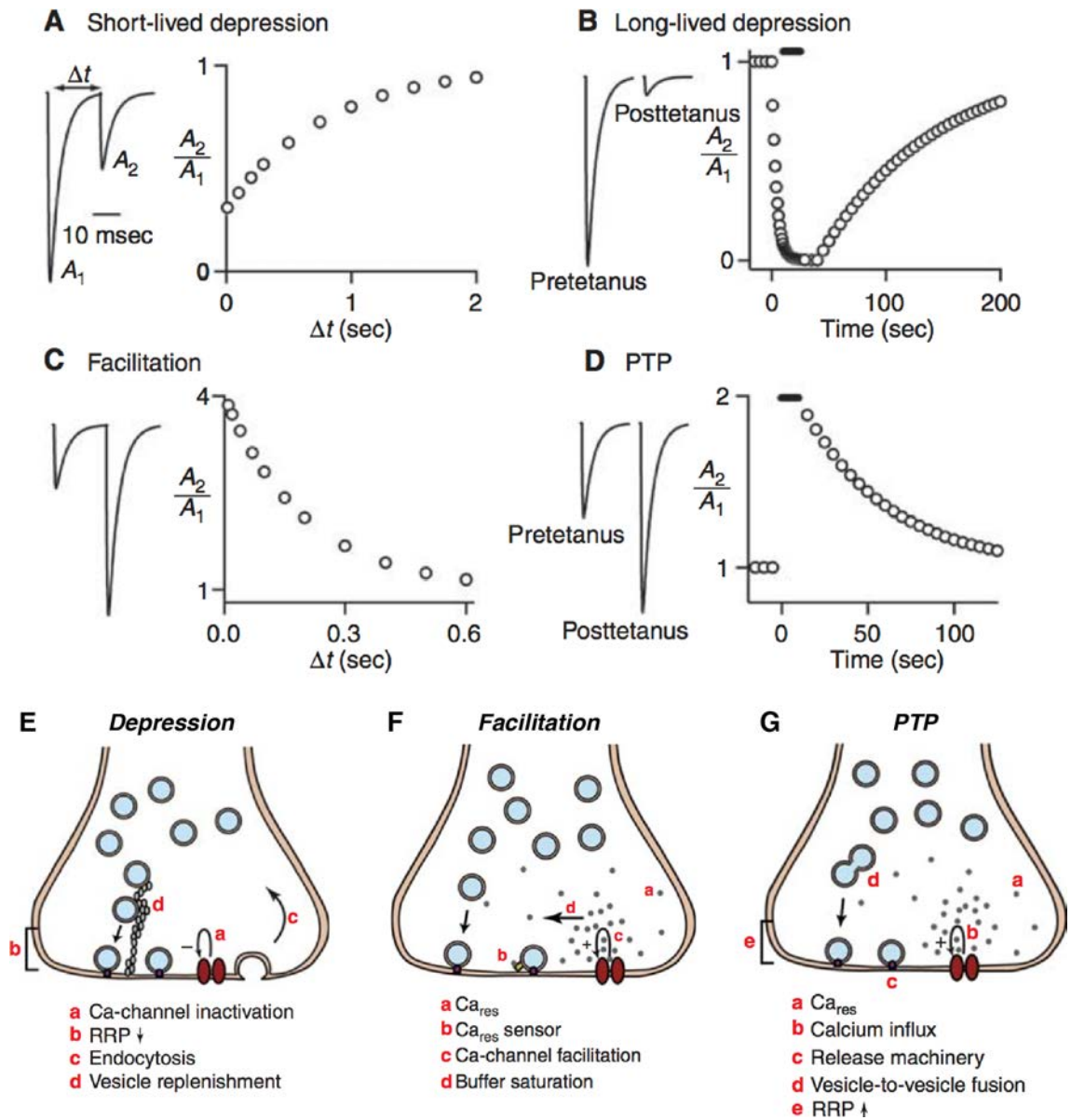


**Figure 18: Short term presynaptic plasticity. A-D.** Different forms of plasticity (see text). **E-G.** Mechanisms of use-dependent plasticity (see text) Adapted from Regehr (2012)

kind of enhancement was reported in the neuromuscular junction (Magleby and Zengel, 1975, 1976) and in central synapses, such as the Calyx of Held (Habets and Borst, 2005; Korogod et al., 2005), mossy fiber boutons (Lee et al., 2007) and hippocampal Schaffer collaterals (Brager et al., 2003).

**Augmentation or PTP?** Augmentation decays faster (seconds or a few tens of seconds) than PTP (tens of seconds or minutes) and may be theoretically triggered by shorter stimuli of lower frequency (Regehr, 2012). In their study, Mochida et al. (2008) induced augmentation with a 10 Hz stimulus lasting 10 seconds and PTP with a 10 Hz stimulus lasting 60 seconds. However, conditioning stimuli may be very different according to different studies. At the Calyx of Held of young animals, Korogod et al. (2005, 2007) stimulated 4 to 8 seconds at 100 Hz whereas Habets and Borst (2005) stimulated during 5 min at 20 Hz; both triggered what they called PTP and reported very different decays (20-60 sec versus 9 min), suggesting different mechanisms, the shorter forms being "similar to augmentation in hippocampal synapses", according to the authors (Korogod et al., 2005). This illustrates that the distinction between PTP and augmentation is not always obvious (Regehr, 2012). A feature that suggests two distinct mechanisms was described at the frog neuromuscular junction: augmentation time course is relatively insensitive to the duration of tetanic stimulation (Magleby and Zengel, 1976), whereas the magnitude and decay of PTP increase with the duration of the conditioning stimulus (Magleby and Zengel, 1975). Last, it is worth noticing that the total enhancement at a synapse results from the sum of facilitation, augmentation and PTP (Fisher et al., 1997; Zucker and Regehr, 2002).

**Calcium is responsible for the time course of enhancement.** Similar time courses were reported for amplitudes of  $Ca_{local}$  transients,  $Ca_{res}$  level, frequency of miniature events and synaptic enhancement following tetanic stimuli at the Calyx of Held (Korogod et al., 2005, 2007; Habets and Borst, 2005, 2006); action potential waveform was not involved in these processes, as shown by direct recording from Calyx of Held (Korogod et al., 2007) (see section 2.3.2). The long lasting  $Ca^{2+}$  elevation in the presynaptic terminal is pretty often responsible for enhancement (Regehr, 2012). Two presynaptic actors were involved in persistent  $Ca_{res}$ :  $Na^+/Ca^{2+}$  exchanger and mitochondria. During an intense stimulus,  $Ca^{2+}$  was shown to enter the mitochondria, which slows and reduces its cytosolic elevation; after the stimulation, mitochondrial  $Ca^{2+}$  release further maintains the cytosolic  $Ca^{2+}$  level and contributes to the slow decay of  $Ca_{res}$  (Regehr, 2012). This may not be the case in all synaptic terminals, especially not in those without mitochondria, such as ~50%

of hippocampal Schaffer collateral synapses (Shepherd and Harris, 1998). Known processes of  $\text{Ca}^{2+}$  extrusion are the  $\text{Ca}^{2+}$  ATPase and the  $\text{Na}^+/\text{Ca}^{2+}$  exchanger in plasma membrane. During intense stimuli,  $\text{Na}^+$  becomes elevated in the terminal and the  $\text{Na}^+/\text{Ca}^{2+}$  exchanger is therefore not able to eliminate  $\text{Ca}^{2+}$  until  $\text{Na}^+$  returns to its initial level, which slows  $\text{Ca}^{2+}$  elimination (Regehr, 2012).

**Calcium dependent mechanisms.** Many  $\text{Ca}_{res}$ -dependent mechanisms that improve release probability and quantal size have been suggested to be involved in enhancement (Regehr, 2012).  $\text{Ca}_{res}$ -dependent activation of protein kinase C (PKC) has been proposed to mediate functional regulation of release machinery proteins (Regehr, 2012) such as Munc18-1 (Fig. 16, Genc et al., 2014). It may also facilitate  $\text{Ca}^{2+}$  influx (increase of  $\approx 15\%$ ) through presynaptic voltage gated channels (Korogod et al., 2007; Habets and Borst, 2006) that would account for augmentation but not PTP (Mochida et al., 2008). Synapsin (Fig. 16) phosphorylation by  $\text{Ca}^{2+}$ /calmodulin (and cAMP-dependent protein kinases) will reinforce its interaction with vesicles, speed up trafficking and therefore promote PTP, but not augmentation (Fiumara et al., 2007). PTP was shown to increase the RRP by 30% (Habets and Borst, 2005); nevertheless, this may rather be due to a  $\text{Ca}^{2+}$ -dependent change of cytoskeleton dynamics that moves RRP closer to the presynaptic  $\text{Ca}^{2+}$  sources (Lee et al., 2010) and therefore increases the proportion of the fast RRP subpool (section 2.4.1). He et al. (2009) and Xue and Wu (2010) described a PTP associated with an increased amplitude of miniature events, albeit previous studies reported PTPs that were not associated with amplitude changes (Korogod et al., 2005; Habets and Borst, 2005). This improved PTP was triggered using more intense stimuli compared to those used in earlier studies, and was linked to an increased vesicular size resulting from the activation of PKC (He et al., 2009; Xue and Wu, 2010).

### **Microcircuit information processing depends on short term presynaptic plasticity**

Microcircuit function depends on the anatomy and dynamics of synaptic pathways that functionally binds neuron in assemblies (Abbott and Regehr, 2004; Silberberg et al., 2005). Synaptic dynamics depends on the initial release probability and therefore act as a filter. Synaptic depression, occurring at synapses with a high initial release probability, is able to convert an apparent presynaptic spike rate code into a spike timing code (Shadlen and Newsome, 1995) as it better encodes the stimulus onset or the percentage changes in the stimulus intensity (Abbott and

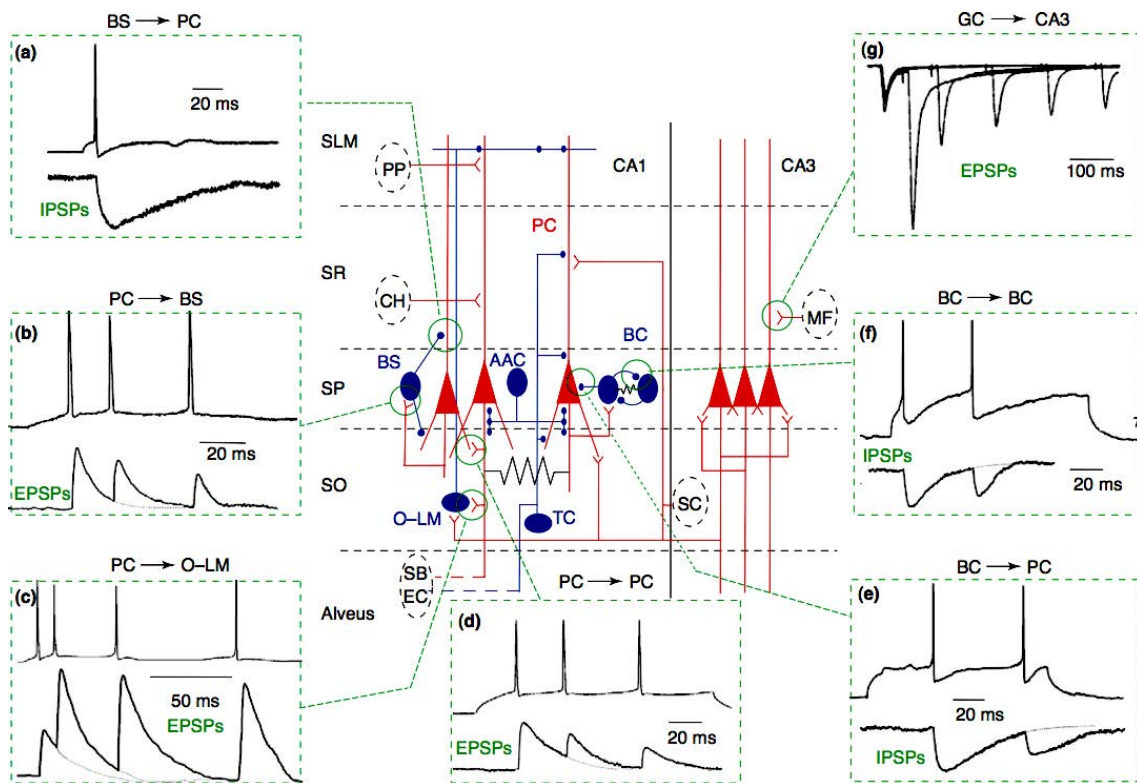


**Figure 19: Synaptic transmission in the mammalian hippocampus.** The central scheme represents the main neuron types and synaptic connections in hippocampal area CA1. Excitatory glutamatergic neurons are in red, and inhibitory GABAergic neurons are in blue. The different types of connections are depicted in the inserts. (a) An inhibitory connection between a bistratified cell (BS) and a pyramidal cell (PC). (b) A depressing excitatory connection between a PC and a BS. (c) A facilitating excitatory connection between a PC and an oriens–lacunosum moleculare cell (O–LM). (d) A depressing excitatory connection between PCs in CA1. (e) A depressing inhibitory connection between a basket cell (BC) and a PC. (f) A depressing inhibitory connection between BCs. (g) A facilitating excitatory connection between a granule cell (GC) and a CA3 PC. Additional abbreviations: AAC, axo-axonic cell; CH, contralateral hemisphere; EC, entorhinal cortex; MF, mossy fibre; PP, perforant pathway; SB, subiculum; SC, Schaffer collateral; SLM, stratum lacunosum moleculare; SO, stratum oriens; SP, stratum pyramidale; SR, stratum radiatum; TC, trilaminar cell. From Silberberg et al. (2005).

Regehr, 2004; Regehr, 2012). In contrast, facilitation, occurring at synapses with a low initial release probability, is better to encode sustained and fast activity (Abbott and Regehr, 2004; Regehr, 2012).

In cortical areas, the strength and plasticity of synapses made by an individual neuron of the circuit depends on presynaptic properties but also on the postsynaptic target (Scanziani et al., 1998; Markram et al., 1998; Koester, 2005; Ali and Thomson, 1998; Ali et al., 1998; Abbott and Regehr, 2004; Silberberg et al., 2005, Fig. 19). This is particularly true regarding interactions between excitatory neurons and the different subtypes of interneurons (Silberberg et al., 2005), as depicted on figure 19. In hippocampus (Fig. 19) and neocortex, the pyramidal to basket cell connection tends to depress (Beierlein et al., 2003; Ali et al., 1998) whereas the pyramidal-to-dendrite targeting interneuron synapse is facilitating (Beierlein et al., 2003; Fanselow et al., 2008; Ali and Thomson, 1998). This is an interesting tool used by the microcircuit to perform a temporal separation of perisomatic and dendritic inhibition. Indeed, the nature of recurrent inhibition onto hippocampal pyramidal cells shifts during a persistent stimulation, from an onset transient perisomatic inhibition to a late persistent dendritic inhibition (Pouille and Scanziani, 2004). This spatio-temporal shift in inhibition relies on synapse dynamics, but also on synaptic event kinetics, membrane time constant and dynamics of dis-inhibition (Pouille and Scanziani, 2004).

#### 2.4.4 Voltage dependent regulation of synaptic activation

As described above,  $\text{Ca}^{2+}$  is a core component of neurotransmitter release as it takes part in many, if not all, processes that lead to and regulate vesicular fusion at the presynaptic terminal. However, synaptic activation may also be modulated in a  $\text{Ca}^{2+}$ -independent way (Debanne et al., 2013). In hippocampal mossy fiber terminals, subthreshold depolarization enhanced synaptic activation, independently of action potential waveform or calcium entry modulation (Alle, 2006; Scott et al., 2008) and with a very short latency. Earlier studies have shown that depolarization of the presynaptic terminal could enhance release, independently of its role on calcium channel opening (Hochner et al., 1989). Membrane potential is therefore believed to be a key regulator of release probability (Parnas and Parnas, 2010; Debanne et al., 2013).

Independently of calcium entry, presynaptic  $\text{Ca}^{2+}$  channels could serve as a voltage sensor enhancing release of synaptic vesicles thanks to the physical interaction of channels and release machinery (Dekel et al., 2012). Another class of molecules

involved in voltage dependent release of neurotransmitter are G protein-coupled receptors (GPCR) (Parnas and Parnas, 2010). Many GPCRs can exert a tonic inhibition of synaptic activation by inhibition of calcium channels or the increase of  $K^+$  conductances; others, such as muscarinic  $M_2$  receptors ( $M_2R$ ) are tightly coupled to the release machinery and are able to exert a tonic block of fusion (Parnas and Parnas, 2010). At resting membrane potential,  $M_2R$  affinity is high and its activation inhibits release. During synaptic activation, depolarization decreases  $M_2R$  affinity, which unbinds neurotransmitter and inactivates the tonic block of the release machinery (Parnas and Parnas, 2010) - a nice example of information encoding by the direct interaction between intrinsic and extrinsic signals. This kind of regulation is likely to occur in cortical synapses, such as the mossy fibers terminals that contain many GPCRs, such as GABA-B receptors, metabotropic glutamate receptors or adenosine receptors (Debanne et al., 2013).

#### 2.4.5 Regulation of presynaptic function by extrinsic factors

Extrinsic molecules, present in the extracellular medium may bind to their receptors on the presynaptic membrane and regulate synaptic transfer of information. Among all systems that can interact with presynaptic terminals, adenosine and endocannabinoid signalling offer interesting regulatory mechanisms of information.

**Adenosine.** Adenosine regulates synaptic efficiency by modulation of the action potential waveform (2.3.2) but also acts directly on synaptic terminals (Dias et al., 2013). The diversity of adenosine receptors and their coupling to intracellular signalling is likely to induce different levels of plasticity, from depression to potentiation, also depending on adenosine levels (Dias et al., 2013). For example, in response to synaptic activation, adenosine may be released by astrocytes and enhance neurotransmitter release via presynaptic  $G_S$ -coupled  $A_{2A}$  receptor activation (Panatier et al., 2011). This neuroglial collaboration seems essential as blocking astrocyte signalling disrupts basal synaptic transmission (Panatier et al., 2011). Alternatively, astrocytic release of adenosine can mediate depression of synaptic activity via a  $G_{I/O}$ -coupled  $A_1$  receptor (Pascual, 2005) .

**Endocannabinoids.** Endocannabinoids are powerful regulators of synaptic function, able to suppress neurotransmitter release in a transient or long-lasting manner, at both excitatory and inhibitory synapses (Castillo et al., 2012). They are phospholipid derivatives, including N-arachidonoyl-ethanolamide (anandamide) and 2-arachidonoyl glycerol (2-AG), mainly binding type 1 cannabinoid receptor  $CB_1R$  -

a GPCR - in nerve terminals (Alger and Kim, 2011).

Endocannabinoids may act via retrograde signalling. Endocannabinoids are synthesized as a response to postsynaptic  $\text{Ca}^{2+}$  elevation, generally induced by a sustained (seconds) depolarization. Their lipophilic properties allow their diffusion to the presynaptic compartment, where they bind to presynaptic  $\text{CB}_1\text{Rs}$ , suppressing neurotransmitter release (Castillo et al., 2012).  $\text{CB}_1\text{R}$ -induced short-term synaptic depression is mediated by a  $G_{I/O}$  protein that may inhibit voltage gated  $\text{Ca}^{2+}$  channel influx or increase  $\text{K}^+$  conductances, whereas long term depression requires adenylate-cyclase inhibition and inactivation of PKA pathway (Castillo et al., 2012; Alger and Kim, 2011).

Endocannabinoids mediate a form of metaplasticity, a plasticity that serves subsequent synaptic plasticity; retrograde signaling from dendrites of CA1 pyramidal neurons was shown to depress inhibitory synapses locally and therefore favor the potentiation of nearby excitatory synapses (Chevaleyre and Castillo, 2004).

Tonic activation of presynaptic  $\text{CB}_1\text{Rs}$  was shown to mute a subpopulation of CCK-containing neurons in CA3 of the hippocampus (Losonczy et al., 2004). Information transfer at these neurons was enabled by sustained high firing frequencies ( $>> 100$  action potentials at 25 Hz) and endocannabinoid signalling could constitute a high pass filter for information coming from CCK-interneurons to pyramidal cells.

# Methods



## Animals

The choice of the animal model is always conditioned by the question.

Sprague-Dawley rats of 21 – 35 days of age (CERJ Janvier, Le Genest Saint Isle, France) were used to study principal neurons. Principal neurons constitute the majority of cells ( $\approx 80\%$ ) so their identification in the slice preparation does not require specific markers. Moreover, slices from rats are often of better quality compared to those from mice.

The other studies needed the identification of interneurons. I therefore had to use specific mouse strains expressing fluorescent proteins in interneuron populations. It is worth noting that using 2 different species (mouse and rat) did not ease the comparison between principal cells and interneurons, due to possible inter-species variability.

The GAD67-GFP knock-in mouse reveals most of the interneurons (Tamamaki et al., 2003; Suzuki and Bekkers, 2010). It has been generated by the insertion of an enhanced green fluorescent protein (eGFP) to the locus encoding GAD67 (glutamic acid decarboxylase-67) using homologous recombination (Tamamaki et al., 2003). The GAD67 is the main enzyme that synthesizes GABA from glutamate. Consequently, the genetic construct might diminish the amount of GABA in these neurons. Indeed, 10-20 % of what were found to be negative for GABA with immunohistochemistry, a result that has been attributed to a possibly diminished amount of GABA in these cells (Tamamaki et al., 2003; Suzuki and Bekkers, 2010). However, it can be due to sensitivity issues with immunochemistry, non related to a reduced production of GABA, but rather to a natural low amount of GABA in some interneurons. For the maintaining of this strain, I have been crossing knock-in males with C57Bl/6J females (CERJ Janvier, Le Genest Saint Isle, France). Other models were used to identify more specific population of interneurons.

Pvalb-Cre mice (Jax 008069; Hippenmeyer et al., 2005) or Sst-IRES-Cre mice (Jax n°013044; Taniguchi et al., 2011) were crossed with the Ai14 Cre reporter line (Jax n°007914; Madisen et al., 2010). Cre-mediated recombination resulted in the expression of red fluorescent tdTomato (RFP) labeling in subsets of GABAergic neurons. Pvalb-Cre x Ai14 labels neurons expressing the calcium binding protein parvalbumin (PV). These interneurons are typically fast spiking and provide perisomatic inhibition in cortical areas (Ascoli et al., 2008). Sst-IRES-Cre x Ai14 stains neurons expressing the neuropeptide somatostatin (SOM). These interneurons are rather regular spiking and target the dendrites of principal cortical neurons (Ascoli et al., 2008). It is worth noting that somatostatin can be expressed by other neurons

than dendrite-targeting interneurons, especially during developmental states; these transient expression of somatostatin may induce the expression of the RFP for life (Hu et al., 2013).

I also used the transgenic mouse line X98-SST (Jax n°006340), in which GFP expression is driven by the GAD67 promoter. For this mouse line, the random insertion of the transgene in the genome has led to the labeling of a subset of somatostatin positive neurons with axonal arborizations in layer I (Martinotti-type morphology in neocortex; Ma et al., 2006). For the maintaining of this strain, I have been crossing transgenic males with C57Bl/6J females (CERJ Janvier, Le Genest Saint Isle, France).

## Slices

The success of slice electrophysiology mainly depends on the good quality of slices. This is really a critical point that I have been trying to improve during my PhD. The methodology should be modified according to the age of the animal and many recipes and experimental procedures exist in the literature (many references and tricks can be found on [BrainSliceMethods.com](http://BrainSliceMethods.com), for example). The common idea with slice preparation is that nothing should be left to chance. All the steps that can be under control have to be done meticulously, from the preparation of solutions to the dissection and slicing. More subtle parameters, such as water quality or the stress of the animals, should alter the slice quality and must therefore be controlled as much as possible. Following these general principles, slice quality has been good most of time, even with the oldest animals (> P60) that I used.

After anesthesia with ketamine hydrochloride and xylazine (for rat: 80 and 12 mg/kg; for mouse: 100 and 25 mg/kg, respectively), animals were perfused via the heart with a the cutting solution cooled to 2–6 °C and equilibrated with 5% CO<sub>2</sub> in O<sub>2</sub>. The success of the perfusion significantly improves the slice quality with animals older than 25 days. I have been using 2 different cutting solutions: one based on choline chloride, the other on sucrose. The choline chloride solution contained (in mM): 110 choline Cl, 2.5 KCl, 25 NaHCO<sub>3</sub>, 1.25 NaH<sub>2</sub>PO<sub>4</sub>, 7 D-glucose, 0.5 CaCl<sub>2</sub> and 7 MgCl<sub>2</sub>. The sucrose solution contained (in mM): 125 NaCl, 25 sucrose, 2.5 KCl, 25 NaHCO<sub>3</sub>, 1.25 NaH<sub>2</sub>PO<sub>4</sub>, 2.5 D-glucose, 0.1 CaCl<sub>2</sub>, 7 MgCl<sub>2</sub> (in mM).

The forebrain was dissected, and slices of 250-350  $\mu$ m were cut. Two different angles have been used for making slices containing the presubiculum. The simpler was the "horizontal" angle: the dorsal part of the brain was glued on the slicer platform. For the "oblique" angle, the brain was split in two with a knife cut sep-

arating the two hemispheres; then an additional cut was performed starting from the ventral side, with a 30° angle with respect to the sagittal plane. This angle is supposed to better preserve the integrity of the hippocampal network. More possibilities exist and should be tested in the future. I have tested "parasagittal" slices, but they did not seem ideal because this angle does not allow to distinguish easily the limit between presubiculum and retrosplenial cortex. For "horizontal", "oblique" and "parasagittal" slices, the vibratome slicing was operated following the caudo-rostral direction. I tried coronal slices once, however the angle seemed really not appropriate for physiology: neurons were dead.

Before recording, slices were being stored for at least 1 h at 22–25°C in a chamber containing artificial cerebrospinal fluid (ACSF). ACSF contained (in mM) 124 NaCl, 2.5 KCl, 26 NaHCO<sub>3</sub>, 1 NaH<sub>2</sub>PO<sub>4</sub>, 2 CaCl<sub>2</sub>, 2 MgCl<sub>2</sub>, and 11 D-glucose and was gently bubbled with 5% CO<sub>2</sub> in O<sub>2</sub> (pH 7.3, 305–315 mOsm/L).

## Recordings

For recordings, slices were transferred to a chamber (volume ≈ 2 mL), heated to 32–35 °C, on the stage of an Axioskop 2 FS plus microscope (Zeiss, France). Neurons were visualized with an EMCCD Luca-S camera (658 x 496 pixels, 10 x 10 μm; Andor) using infrared differential interference contrast. Fluorescent neurons were visualised using a white LED mounted on the epifluorescent port of the microscope, coupled to an excitation/emission filter system.

Recordings were made with glass pipettes pulled using a Brown–Flaming electrode puller (Sutter Instruments) from borosilicate glass of external and internal diameter of 1.5 mm and 0.86, respectively (Harvard Apparatus, UK; reference: GC150F-10). The electrode resistance, when filled with the internal solution was 3–6 MΩ.

I used different kinds of internal solutions, depending on the study. The potassium-gluconate solution 1.0 contained (in mM) 130 K-gluconate, 5 KCl, 10 HEPES, 10 ethylene glycol tetra-acetic acid (EGTA), 2 MgCl<sub>2</sub>, 4 MgATP, 0.4 Tris-GTP, 10 Na<sub>2</sub>-phosphocreatine. The high amount of EGTA in this solution certainly allowed a good stability of recordings. However, with perspective I consider 10 mM as a concentration that may have a huge effect on calcium signaling and therefore on physiology; 1 mM could have been enough. I performed few recordings using a solution with the same compounds except EGTA, firing patterns were not changed, but action potential shapes were altered. Thus, EGTA is a compound that has to be carefully used, because it can influence cell physiology.

I then modified the potassium gluconate 1.0, diminishing the amount of chloride to better see the inhibition and eliminating the EGTA, to not counteract calcium signaling. This was particularly important for the study of synapse dynamics with paired recordings. The potassium-gluconate 2.0 contained (in mM) 150 K-gluconate, 1 KCl, 10 HEPES, 2 MgCl<sub>2</sub>, 4 MgATP, 0.4 Tris-GTP, 10 Na<sub>2</sub>-phosphocreatine.

To reveal the morphology, I added 1-3 mg/ml of biocytin in these solution. One might think that having a lot of biocytin could be better. It seems to be true. However, the background staining increases with the time spent with the pipette in the slice before patching. In conclusion, with high amount of biocytin, patching has to be very fast (few seconds after penetration of the pipette in slice).

## Analysis of the electrophysiology

Electrophysiological parameters were analysed with dedicated softwares: AxoGraph X (<http://www.axograph.com/>) for manual analysis, Spikoscope (a Labview based software developed by Ivan Cohen) and routines that I developed with Matlab (the Mathworks) for automated analysis. Details will not be extensively described here, as they are specifically provided in the methods of the different studies.

## Morphology

Neurons were filled with biocytin, included in the recording pipette (1-3 mg/mL), so that their anatomy could be examined. Slices containing filled cells were fixed in 4% paraformaldehyde (PFA) in 0.12 M phosphate buffer (PB) at least overnight at 4 °C. PB contained (in mM) 0.14 NaH<sub>2</sub>PO<sub>4</sub>H<sub>2</sub>O and 0.1 NaOH and was adjusted at pH 7.3. Slices were then rinsed 3 times in PB, and put in 30% sucrose (for cryoprotection) at 4°C at least overnight. Slices could be kept in 30% sucrose for several weeks.

Membranes were permeabilized by three cycles of freezing/thawing over dry ice. To do so, slices are disposed on a slide, in a small drop of sucrose. The slide is then put on dry ice until sucrose is frozen. The slide is then put on a warm surface, such as the experimenter palm, until full thawing. The process has to be done three times.

Slices were then washed 3 times in 0.02 M Potassium Phosphate buffered saline (KPBS). KPBS contained (in mM) 0.0035 KH<sub>2</sub>PO<sub>4</sub>H<sub>2</sub>O, 0.0165 K<sub>2</sub>HPO<sub>4</sub>H<sub>2</sub>O and 0.9% NaCl, was adjusted at pH 7.3 and then filtered. The aim of this step is to eliminate the remaining sucrose. The first washing can be fast, the two following

should be longer (10-20 min).

Slices were then pre-incubated 2-4 hours in a solution composed of KPBS, Triton 0.3 %, Milk 2%. The Triton starts the permeabilization for the subsequent incubation, proteins of the Milk saturate the non-specific fixation sites (e.g. charges) to limit the background staining.

To reveal the biocytin, slices were then incubated overnight at 4°C with a fluorescent streptavidin (Alexa 488, cy3 or cy5 conjugate, Invitrogen, Eugene, OR, USA) diluted at 1:200 to 1:500 in 0.02 M KPBS, Milk 2 %, Triton 1 %. 4',6'-diamidino-2-phenylindole (DAPI) was added for staining of the tissue structure. Note that a high concentration of Triton was used because of the slice thickness: it improves permeabilization without degrading the staining, streptavidin not being sensitive to high Triton concentration (not the case with some antibodies).

Slices were then washed 3 x 20 min before mounting (mounting medium: Pro-Long Gold, life technology). Before mounting, the location of the revealed cell was checked to adjust the orientation of the slice on the slide.

Slides were visualized with a QImaging Retiga EXI camera (Qimaging Surrey, BC, Canada), and scanned with an Optigrad II (Thales Optem, Qioptik, Rochester, NY, USA) mounted on an inverted Olympus IX81 microscope. The Optigrad system permitted the acquisition of structured images and the subsequent three-dimensional reconstruction of filled neurons with the software Volocity (Improvision, Perkin-Elmer, Coventry, UK). Stacks of 75–250 images were acquired using a X20 NA 0.85 oil immersion objective (steps of maximum 0.7  $\mu\text{m}$  between images). Overview images were acquired with a X4 NA 0.16 objective.

After the acquisition, neurons were reconstructed using the NeuroLucida software (MicroBrightfield, Williston, VT, USA). RGB stacks were exported from Volocity as a RGB tif stacks, converted into 8 bit tif stacks using ImageJ and then imported into NeuroLucida. Manual 3D reconstructions were executed in NeuroLucida by discriminating axons from dendrites, as well as apical and basal dendrites for pyramidal neurons. Dendrite diameters were typically bigger than axon's and the presence of spines on dendrites and varicosities on axons helped the discrimination.

The orientation of dendritic arbors were described using the "wedge analysis". From the soma of each cell, 12 segments each occupying 30° of arc were created, starting with a 15° segment centered on the vertical. The cortical surface was set as 0°, the subiculum was situated to the left and the parasubiculum to the right. The total dendritic length in each segment was measured. Twelve-segment wedges were converted to six-segment wedges for some analyses by summing pairs of adjacent segments, starting with that centered on 0°.

The `neurolucida` function "layer length analysis" was used to determine dendritic length in each presubicular layer, and also in the neighboring areas.

Axonal projections within the presubiculum were defined for projections that could be followed for 500  $\mu\text{m}$  or more.

No correction for tissue shrinkage was applied.

All the results were exported in excel format and imported in Matlab (The Mathworks) for compiling results and making figures.

## **A rather objective method to describe neuronal populations: unsupervised clustering**

Describing neuronal properties could appear as a quite easy task as it solely needs to highlight the similarities and differences between distinct populations. However, the identification of populations can be difficult, especially because there are many ways to describe and classify neurons. They can be described according to the expression of specific molecular markers, morphology, intrinsic electrophysiological properties, their recruitment by specific inputs or their target as well as their activity related to a specific behavior (Ascoli et al., 2008).

Neuronal populations can be distinguished by two opposed methods. Groups can be defined arbitrarily in a first place (e.g. neurons of different layers, with different shapes), and then their properties can be compared in a subsequent step. In contrast, populations can be defined as results of their description, neuronal properties being used to defined groups in an objective manner. The second method is called unsupervised clustering, because the groups of neurons are not defined in an initial step. Neuronal features therefore define groups objectively, even though the choice of the descriptive parameters can influence the results. Indeed, if different kind of parameters are used, the resulting classification has quasi no chance to be the same (Cauli et al., 2000). Moreover, using different sets of one kind of parameters (e.g. molecular markers) is likely to provide a different classification.

When establishing groups of neurons is done arbitrary, only few parameters can be used. For example, one can decide to group neurons according to their position in a tissue, or according to their firing pattern (regular spiking, fast spiking, intrinsic burst firing). However, this initial choice is not necessarily the best, as it might hide the intrinsic diversity of each population. It is extremely difficult to take into account a lot of features to manually define different populations, especially because we are compelled to define groups looking at each parameter, one after the other. In contrast, unsupervised clustering classifies objects by attributing the same weight

to each parameter; and this can include many parameters.

Each neuron is thus represented by one point in a multidimensional space (the number of dimension equals the number of parameters) and the closest neurons in this space are then grouped together. Our clustering was based on Ward's method (Ward Jr, 1963), as previously used to classify neuronal subpopulations (Cauli et al., 2000). It was implemented using Matlab (The Mathwork) and its statistical toolbox. Data were first standardized by centering and reducing all values. For each step of this agglomerative method, the two closest points (neurons) were grouped together using the matrix of their Euclidean distances. The centroid of the newly created population substituted the two previous values, updating the matrix of Euclidean distance then used for the subsequent step. For each step, the mean individual-to-centroid distance (or mean within-cluster distance) was calculated. This value typically decreased as the number of clusters increased. The maximum reduction (breaking point) defined a statistically optimal number of clusters (Thorndike procedure, Thorndike, 1953). For each number of clusters, different parameters were described statistically to provide a 'biological signature' for each cluster. Final clusters were defined from statistical and biological parameters as described in the Results.

This methodology really eases the process of classification and remains quite objective. One bias still remains: the choice of parameters. Different statistical methods exists to check the influence of parameters on the final classification. For example, one can perform a factor analysis using the principal component analysis (Dumitriu et al., 2007), which determines what are the parameters that are the most related to the first component; in other words, those responsible for the highest part of the variability. Another method consists in the scrambling of the values of one parameter in the dataset, which disrupts its correlation with others, but not its distribution (Karagiannis et al., 2009; Perrenoud et al., 2013). Classification is more affected when randomization is performed on important parameters.



# Results



# ARTICLE 1

## Cellular neuroanatomy of rat presubiculum

The presubiculum is involved in spatial orientation signaling as it contains head direction cells, neurons that discharge as a function of the animal's directional heading. The generation of the presubicular head direction signal seems to result from the integration of vestibular and visual information in this six-layered cortex. How presubiculum processes this information is still unresolved, and its microcircuit has not been studied in detail. In particular, the neuronal basis of presubicular information processing has been unknown.

What are the morphologies and firing patterns of neurons composing the presubicular cortex? Are there different kinds of neurons in the different layers of the presubiculum? The first part of my PhD work was to shed light on the presubicular neuronal properties in the different layers of the presubiculum. I studied electrophysiology and morphology using the whole cell patch clamp technique in the slice preparation of the young adult rat.

I have shown that the presubiculum possesses a laminar specificity of neuronal integrative properties: neurons are different in different layers. Neurons in superficial layers were all regular spiking, very hyperpolarized from firing threshold and mainly pyramidal cells. I found a group of intrinsic burst firing pyramidal neurons in layer 4. Neurons in deep layers were rather heterogeneous in terms of morphologies and excitable properties, but all were regular spiking cells, even though they differed from those in superficial layers. The cellular diversity in deep layers suggests that computation may be more diverse there than in superficial layers.

In addition, I confirmed that presubicular regular spiking cells were intrinsically able to sustain firing in response to long depolarizations, similar to presubicular head direction cells *in vivo*.

These results are essential to understand the presubicular physiology and suggest that information processing in this area might be based on a cortical model. Specific hypotheses about information flow in the presubiculum remain to be tested.

## Cellular neuroanatomy of rat presubiculum

Jean Simonnet, Emmanuel Eugène, Ivan Cohen, Richard Miles and Desdemona Fricker

Centre de Recherche de l'Institut du Cerveau et de la Moelle Epinière CRICM, UPMC/INSERM UMR S975/CNRS UMR 7225, CHU Pitié-Salpêtrière, 47 Boulevard de l'Hôpital, 75013, Paris, France

**Keywords:** adaptation, excitability, head direction, morphology, postsubiculum

### Abstract

The presubiculum, at the transition from the hippocampus to the cortex, is a key area for spatial information coding but the anatomical and physiological basis of presubicular function remains unclear. Here we correlated the structural and physiological properties of single neurons of the presubiculum *in vitro*. Unsupervised cluster analysis based on dendritic length and form, soma location, firing pattern and action potential properties allowed us to classify principal neurons into three major cell types. Cluster 1 consisted of a population of small regular spiking principal cells in layers II/III. Cluster 2 contained intrinsically burst firing pyramidal cells of layer IV, with a resting potential close to threshold. Cluster 3 included regular spiking cells of layers V and VI, and could be divided into subgroups 3.1 and 3.2. Cells of cluster 3.1 included pyramidal, multiform and inverted pyramidal cells. Cells of cluster 3.2 contained high-resistance pyramidal neurons that fired readily in response to somatic current injection. These data show that presubicular principal cells generally conform to neurons of the periarchicortex. However, the presence of intrinsic bursting cells in layer IV distinguishes the presubicular cortex from the neighbouring entorhinal cortex. The firing frequency adaptation was very low for principal cells of clusters 1 and 3, a property that should assist the generation of maintained head direction signals *in vivo*.

The presubiculum lies at the transition between the hippocampal archicortex and the six-layered neocortex. Principal cells in the CA1 and CA3 areas of the hippocampus proper are tightly packed in a single layer and neighbouring cells have similar electrical properties and shape (Jarsky *et al.*, 2008). In contrast, excitatory neurons of the canonical neocortex are organized in vertical columns and six horizontal layers with differing properties (Mountcastle, 1997; Douglas & Martin, 2007; Lübke & Feldmeyer, 2007). The organization of the presubiculum is suggested to lie between these patterns with elements of horizontal and vertical stratification.

The superficial layers I–III of the presubiculum are separated by a plexiform layer IV (lamina dissecans) from the deep layers, V and VI (Canto *et al.*, 2008). The deep layers are in continuity with those of the entorhinal cortex (Lorente de No, 1934; Witter *et al.*, 1989; Van Strien *et al.*, 2009). Evidence for a vertical, columnar organization is more controversial. Vertical structures appear transiently during early postnatal development in mice (Nishikawa *et al.*, 2002). The monkey presubiculum exhibits a vertical neurochemical modularity, for calbindin and cytochrome oxidase, in layers I and II (Ding & Rockland, 2001), which may correspond to a patchy afferent innervation (Goldman-Rakic *et al.*, 1984) also evident in the Nissl-stained human presubiculum (Longson *et al.*, 1997).

The presubiculum may have a specific role in the representation of space by the hippocampal formation (Rolls, 2006). Some presubicular cells signal head direction persistently (Ranck, 1984; Taube *et al.*, 1990), and some are sensitive to location (Cacucci *et al.*, 2004; Boccara *et al.*, 2010). Head direction signalling in the presubiculum probably depends on specific afferent information. Afferents include polymodal inputs to layers I and III from the visual and retrosplenial cortex (Vogt & Miller, 1983; Kononenko & Witter, 2012) and to layers I and III–VI from the anterior thalamus (Shiple & Sorensen, 1975; van Groen & Wyss, 1990; Yoder *et al.*, 2011; Shibata & Honda, 2012). The presubiculum is also innervated by fibres from the anteroventral and lateral dorsal thalamus, hippocampus and subiculum (van Groen & Wyss, 1990; O'Mara *et al.*, 2001). Outputs from the presubiculum project to the entorhinal cortex (layers II/III) and lateral mammillary nucleus (layer IV), whereas principal cells of layers V and VI excite the anterodorsal nucleus of the thalamus (Yoder & Taube, 2011). However, less is known about the cellular and anatomical substrates of information processing within the presubiculum (Funahashi & Stewart, 1997a,b). How many cell types exist? What are their firing patterns? Do cells of different layers possess specific and distinct properties? How do principal cell dendritic processes and axonal projections underlie the spread of activity within the presubiculum?

To answer these questions, we correlated the anatomy with the electrophysiology of rat presubicular neurons recorded *in vitro*. We examined different morphological properties, action potential (AP) shapes and firing patterns of pyramidal and non-pyramidal cells, situated throughout the presubiculum. Presubicular cells of different layers differed in excitability and anatomy. Most principal cells showed

Correspondence: D. Fricker, as above.  
E-mail: desdemona.fricker@upmc.fr

Received 6 August 2012, revised 1 October 2012, accepted 24 October 2012

little spike frequency adaptation *in vitro*, consistent with their maintained signalling of head direction *in vivo* (Taube & Muller, 1998).

## Materials and methods

### *Electrophysiology: whole-cell records in a submerged chamber*

Slices containing the hippocampus, subicular complex and entorhinal cortex were prepared from 71 male Sprague-Dawley rats aged 21–35 days (CERJ Janvier, Le Genest Saint Isle, France), for electrophysiological and subsequent immunohistochemical experiments. Our care and use of the rats conformed to the European Communities Council Directive 86/609/EEC and institutional policies and guidelines. Our study was approved by local ethical committees (Université Pierre et Marie Curie and INSERM). After anaesthesia with ketamine hydrochloride and xylazine (80 and 12 mg/kg, respectively), animals were perfused via the heart with a solution containing (in mM): 110 choline Cl, 2.5 KCl, 25 NaHCO<sub>3</sub>, 1.25 NaH<sub>2</sub>PO<sub>4</sub>, 7 D-glucose, 0.5 CaCl<sub>2</sub> and 7 MgCl<sub>2</sub>, cooled to 2–6 °C and equilibrated with 5% CO<sub>2</sub> in O<sub>2</sub>. The forebrain was dissected, and slices (300 µm thick) were cut (Microm HM 650V, Walldorf, Germany). Horizontal brain sections were made in a 3.9–5.7 mm vertical range with respect to the ear bar horizontal plane (Kruger *et al.*, 1995), with 80% of slices between levels 4.2 and 5.2 mm. This standardized plane allowed for a description of the properties of neurons from a similar dorsoventral level. Before recording, slices were stored for at least 1 h at 22–25 °C in a chamber containing a solution of (in mM): 124 NaCl, 2.5 KCl, 26 NaHCO<sub>3</sub>, 1 NaH<sub>2</sub>PO<sub>4</sub>, 2 CaCl<sub>2</sub>, 2 MgCl<sub>2</sub>, and 11 D-glucose, gently bubbled with 5% CO<sub>2</sub> in O<sub>2</sub> (pH 7.3, 305–315 mOsm/L). Salts were obtained from Sigma (Lyon, France).

Slices were transferred to a chamber (volume 2 mL), heated to 32–34 °C, on the stage of an Axioskop 2 FS plus microscope (Zeiss, France) for recordings. Neurons were visualized with an EMCCD Luca-S camera (658 × 496 pixels, 10 × 10 µm; Andor) using infrared differential interference contrast.

Recordings were made with glass pipettes pulled using a Brown-Flaming electrode puller (Sutter Instruments) from borosilicate glass of external diameter 1.5 mm (Hilgenberg, Germany). The electrode resistance, when filled with a solution containing (in mM): 130 K-gluconate, 5 KCl, 10 HEPES, 10 ethylene glycol tetra-acetic acid, 2 MgCl<sub>2</sub>, 4 MgATP, 0.4 Tris-GTP, 10 Na<sub>2</sub>-phosphocreatine and 2.7 biocytin, was 3–6 MΩ. Whole-cell current-clamp records were made with an Axopatch 200A amplifier (Molecular Devices, Sunnyvale, CA, USA) operated in fast mode and low-pass filtered at 5 kHz. A chlorided silver wire contacted the pipette solution and a 3 M KCl agar bridge contacted the bath solution, yielding an estimated junction potential of 15 mV, which was not corrected. Fifteen of 133 presubicular neurons were recorded without ethylene glycol tetra-acetic acid in the pipette solution to determine how calcium buffering influenced firing frequency adaptation. The hyperpolarization-activated cyclic nucleotide-gated channel blocker ZD7288 (20 µM; Tocris, Bristol, UK) was bath applied in some experiments to evaluate the presence of the hyperpolarization-activated current (*I<sub>h</sub>*) pharmacologically.

### *Electrophysiological intrinsic properties*

The recorded signals were analysed with AxoGraph X or software written in Labview (National Instruments). We waited for 3–5 min after whole-cell recordings began, before measuring cellular parameters as the neuronal membrane potential typically decreased by about 10 mV over this period, presumably due to the equilibration of a

Donnan potential. The resting membrane potential was the mean potential over at least 10 s. Most electrophysiological parameters were measured from responses to step current injections of 800 ms duration applied from a fixed membrane potential of –65 mV. Injected currents increased in increments of 5 pA from negative to positive values. The range of current amplitudes was adjusted to induce voltage deflections that ranged between a hyperpolarization to about –100 mV during the first step and a depolarization to maximum firing frequency. Exceptions to this protocol are specified in the text.

The neuronal input resistance (*R<sub>in</sub>*) was determined as the slope of the current–voltage relationship from –10 to 10 pA of injected current. Membrane time constants ( $\tau$ ) were obtained by fitting single or double exponentials (Axograph, Simplex algorithm) to potential changes induced by step hyperpolarizing current injections. The membrane capacitance (*C*) was calculated using the following relation:  $C = \tau/R_{in}$ . A 'sag index', reflecting the presence of the h-current, was calculated as the ratio of the maximal negative potential (sag, reached typically between 0 and 200 ms), divided by the mean steady-state voltage deflection (typically between 400 and 800 ms).

Action potentials were detected from continuous periods of rising membrane potential with an amplitude threshold typically set at 30 mV (Cohen & Miles, 2000). The threshold current for firing (rheobase) was defined as the minimum depolarizing current that initiated an AP. Input–output curves plot the mean firing frequency as a function of the injected current. The firing frequency (Hz) was deduced either by counting the number of APs over time (normalized AP count) or by averaging all instantaneous frequencies. The initial slope (I–O slope) was determined using the normalized AP count from the first five current steps beyond rheobase. A bursting index (BI) and indices to describe the initial and late firing frequency adaptation [initial adaptation index (IAI) and late adaptation index (LAI), respectively] were calculated. The BI was calculated as  $1 - (ISI_{min}/ISI_{av})$ , where *ISI<sub>min</sub>* was the minimum interspike interval and *ISI<sub>av</sub>* was the mean interspike interval. The BI was thus close to 0 for regular spiking (RS) cells and close to 1 for burst firing cells. The IAI measured the percentage change in firing frequency from the first to the fifth AP and the LAI measured frequency changes between the fifth and the last AP. Both indices were calculated from five consecutive depolarizing pulses ( $\Delta I$  5 pA), with evoked repetitive firing at frequencies close to 20 Hz, and then averaged. The adaptation indices were not calculated for intrinsic bursting neurons. We measured the highest sustained firing frequency ('maximum frequency') from depolarizing pulses of increasing amplitude, and duration of 2 s. At high-amplitude current injections, the total number of APs could fall, even as the mean instantaneous frequency continued to rise or remained stable. This point was considered as the maximal sustainable frequency.

The AP threshold was measured from the first evoked AP, as the potential where  $dV/dt > 10$  V/s (Fricker *et al.*, 1999). The AP peak was its maximum potential. The AP height was measured as the difference between the AP peak and maximal afterhyperpolarization (AHP), during the next 20 ms. The AHP amplitude denotes the voltage difference between AHP and threshold. The AHP trajectories were sometimes complex, with a first AHP followed by an afterdepolarization and then a second AHP. For simple AHP trajectories, the first AHP equalled AHP. The AP rising amplitude was the difference between the threshold and the peak AP voltage. The AP width was measured from the first AP, at the midpoint of the AP rising phase.  $dV/dt$  was monitored during the evolution of the AP. The maximum and minimum  $dV/dt$ , occurring during the rising phase and falling phase respectively, are given as the maximum depolarization rate and the maximum repolarization rate.

### Anatomy and immunohistochemistry

Neurons were filled with biocytin, included in the recording pipette (1 mg/mL), so that their anatomy could be examined. Slices containing filled cells were fixed overnight at 4 °C in 4% paraformaldehyde in 0.12 M phosphate buffer (pH 7.4), rinsed in phosphate buffer, and cryoprotected in 30% sucrose. Membranes were permeabilized by three cycles of freezing/thawing over dry ice. The morphology was revealed using a streptavidin–Cy3 conjugate (1 : 500, Invitrogen, Eugene, OR, USA). Filled cells were visualized with a QImaging Retiga EXI camera (Qimaging Surrey, BC, Canada), and scanned with an Optigrid II (Thales Optem, Qioptik, Rochester, NY, USA) mounted on an inverted Olympus IX81 microscope. The Optigrid system permitted the acquisition of structured images and the subsequent three-dimensional reconstruction of filled neurons with the software Volocity (Improvision, Perkin-Elmer, Coventry, UK). Stacks of 75–250 images were acquired using a  $\times 20$  NA 0.85 oil immersion objective (steps of 0.5  $\mu\text{m}$  between images). Overview images were acquired with a  $\times 4$  objective of NA 0.16. All principal cells had dendritic spines. Pyramidal neurons possessed one or two main (apical) dendrites oriented radially toward the pial surface. The main dendrite of inverted pyramidal cells was oriented away from the pial surface. Multiform cells did not have an obvious main dendrite.

### Biocytin reconstruction of neurons

NeuroLucida software (MicroBrightfield, Williston, VT, USA) was used to reconstruct the neuronal form in three dimensions from

stacks of acquired images (Fig. 1A). Dendritic arbors were described by wedge analysis. From the soma of each cell, 12 segments each occupying 30° of arc were created, starting with a  $\pm 15^\circ$  segment centred on the vertical. The cortical surface was set as 0°, the subiculum was situated to the left and the parasubiculum to the right. The total dendritic length in each segment was measured. Twelve-segment wedges were converted to six-segment wedges for some analyses by summing pairs of adjacent segments, starting with that centred on 0°. The NeuroLucida function ‘layer length analysis’ was used to determine dendritic length in each presubicular layer. Axonal projections within the presubiculum were defined for projections that could be followed within axons for 500  $\mu\text{m}$  or more. No correction for tissue shrinkage was applied.

### Projection onto a standardized presubiculum map

We wished to compare the form of neurons from different slices. We therefore projected the somatic location of each recorded cell onto a standardized map of the presubiculum. One axis of this map followed the cortical surface from the border between the subiculum and presubiculum to that between the presubiculum and parasubiculum. The other axis corresponded to the apical–basilar dendritic axis of pyramidal cells. This axis closely followed the orientation of blood vessels penetrating the presubiculum from the pia (Fig. 1C). Each recorded neuron was assigned normalized  $x/y$  coordinates (between 0 and 1) according to the location of its soma in the presubiculum (Fig. 1D).

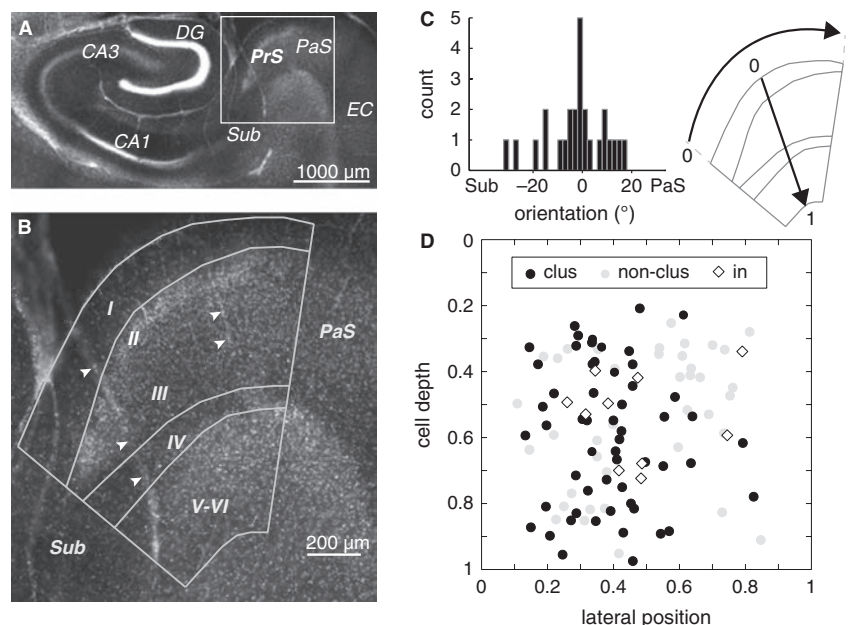


FIG. 1. Situation and anatomy of the rat presubiculum. (A) Horizontal section (300  $\mu\text{m}$ ) stained with 4',6-diamidino-2-phenylindole to reveal nuclei in the hippocampus and parahippocampal regions. The presubiculum (PrS) and parasubiculum (PaS) are indicated as well as the subiculum (Sub), entorhinal cortex (EC), dentate gyrus (DG) and CA3 and CA1 regions. (B) Enlargement of the presubiculum from the inset in A showing differences in cell density in different cytoarchitectonic layers I–VI. Blood vessels (arrowheads) project from the pia to the deep presubiculum. (C) Left panel: the major axis of pyramidal cell dendrites ( $n = 26$ ) is closely aligned with blood vessel orientation. Right panel:  $x$ – $y$  coordinates for somatic location on a standardized map.  $x$  coordinates give the lateral position of the cell body, ranging from 0 (next to the subiculum) to 1 (next to the parasubiculum).  $y$  coordinates indicate cell depth (0, cortical surface; 1, below layer VI). (D)  $x$ – $y$  coordinates of  $n = 101$  identified presubicular neurons plotted on the standardized map. Filled circles, cells with a complete dataset of morphological and electrophysiological parameters included in cluster analysis (clus). Grey circles, cells with partial datasets, not included in cluster analysis (non-clus). Diamonds, interneurons (in), not included in cluster analysis.

### Interneurons

Putative interneurons were identified according to several criteria. Fast spiking neurons were classified as interneurons, when firing in response to current injection was sustained at maximum instantaneous firing frequencies  $\gg 100$  Hz ( $n = 8$ ). Other cells were classified as stuttering interneurons, if they discharged with an instantaneous firing frequency  $\gg 100$  Hz, and firing was not continuous but interrupted by silent intervals ( $n = 2$ ; Petilla Interneuron Nomenclature Group *et al.*, 2008). For these and other cells, interneuron identity was confirmed if the AP halfwidth was short ( $< 0.7$  ms) and spikes were followed by a deep AHP of amplitude at least 15 mV. Anatomical evidence was also used to confirm interneuron identity. The criteria applied to well-filled cells included a non-pyramidal morphology, dendrites with few or no dendritic spines and a dense, local axonal arborization. A very high firing frequency was the single most reliable criterion for classification. Typically, identified interneurons fulfilled most of the criteria that we used. However, in the absence of immunohistochemistry, we cannot exclude that some cells may have falsely been classified as principal neurons.

### Cluster analysis

The neuronal form, position and electrical properties were used to make a bias-free classification of principal cells based on unsupervised clustering. Neurons classified as interneurons on the basis of anatomical and physiological criteria were excluded. Clustering was based on 14 electrophysiological, 13 morphological and two positional parameters. The electrophysiological parameters were: passive and active properties (resting membrane potential,  $R_{in}$ , tau, sag ratio, rheobase, I–O slope, mean instantaneous frequencies for a 100 pA current step injection, mean of BI for the five first steps with at least five APs), and AP properties (width, AHP, first AHP, amplitude, maximum depolarization rate and maximum repolarization rate). The morphological properties were dendrite count, dendritic length, six-segment wedge-analysis results (six values) and layer-length-analysis results (five values). The positional parameters were standardized coordinates. Each neuron was thus represented by one point in a multidimensional space (29 dimensions). Our clustering was based on Ward's method (Ward, 1963), as previously used to classify neuronal subpopulations (Cauli *et al.*, 2000). It was implemented using MATLAB (The Mathwork) and its statistical toolbox. Data were first standardized by centring and reducing all values. For each step of this agglomerative method, the two closest points (neurons) were grouped together using the matrix of their Euclidean distances. The centroid of the newly created population substituted the two previous values, updating the matrix of Euclidean distance then used for the subsequent step. For each step, the mean individual-to-centroid distance (or mean within-cluster distance) was calculated. This value typically decreased as the number of clusters increased. The maximum reduction (breaking point) defined a statistically optimal number of clusters (Thorndike procedure) (Thorndike, 1953). For each number of clusters, different parameters were described statistically to provide a 'biological signature' for each cluster. Final clusters were defined from statistical and biological parameters as described in the Results.

### Statistics

Results are given as mean  $\pm$  SEM. 25%, 50% and 75% quantiles are indicated in Supporting Information Table S2. Statistical analysis

was performed with Prism (GraphPad Software, Inc.). We calculated Pearson's  $r$  correlation index to reveal the association of two variables. Statistical comparison between different cell clusters used unpaired one-way ANOVA combined with a *post hoc* Tukey's test, in the case of normal distribution of data points, and if variances did not differ significantly. If the normality test was not passed, or if variances differed significantly, we applied the non-parametric Kruskal–Wallis test followed by Dunn's multiple comparison test (Supporting Information Table S1). When comparing a value of one cluster with all of the other clusters, the highest  $P$ -values are given in the text.

## Results

### Presubicular anatomy and distribution of presubicular neurons

The rat presubiculum is shown in the context of the hippocampal formation in Fig. 1A and in greater detail in Fig. 1B. In our slice preparation, it was a curved, rather trapezoid region (Fig. 1B and C). The thickness of the layers and particularly that of layers II/III increased between the proximal presubiculum, next to the subiculum, and the distal part next to the parasubiculum. Apical dendrites of pyramidal neurons ran towards the cortical surface. Blood vessels of this strongly vascularized region followed the same radial axis (Fig. 1B, arrowheads). The orientation of the blood vessels and apical dendrites of nearby pyramidal cells were typically close, within 10% ( $n = 30$  slices, Fig. 1C). Thus, the blood vessel orientation was closely aligned with the somatodendritic axis of principal cells in this region.

The neuronal somatic depth was therefore situated on a standardized map with respect to the axis defined by presubicular blood vessels. Laterally, the somatic position could vary between 0 at the most proximal region of the presubiculum bordering the subiculum, and 1 at the most distal limit at the border to the parasubiculum (Fig. 1C). The vertical coordinates varied between 0 at the pial surface, and 1 at the lower limit of the presubiculum (Fig. 1C).

We recorded from 133 neurons distributed throughout the presubiculum. The somatodendritic anatomy was recovered for 101 biocytin-filled neurons with somata in all layers of the presubiculum as shown in Fig. 1D. We performed cluster analysis on a subset of 58 principal cells (Fig. 1D, black dots) with complete data for all morphological and electrophysiological parameters (Table 1). Putative interneurons were not included in this analysis. Ten recorded cells with somata in superficial or deep layers were identified as interneurons (Fig. 1D, diamonds), according to their firing pattern, short AP width, maximum firing frequency higher than 100 Hz, non-pyramidal dendritic and axonal form, and the absence of dendritic spines.

### Cluster analysis reveals four main groups of presubicular neurons

An unsupervised cluster analysis was used to classify presubicular neurons based on the electrophysiological, morphological and positional parameters of Table 1 ( $n = 58$ , see Materials and methods). Figure 2A shows the hierarchical tree diagram of clusters that emerged. Small distances indicate close cells or groups of cells. Clusters were cell groups with a separating Euclidean distance higher than a defined cutoff. The Thorndike procedure first separated two clusters (within-cluster distance drop from 5.03 to 4.23) of neurons with somata located in superficial and deeper layers. The within-cluster distance was more than 1.5  $\times$  higher (5.14 vs. 3.32)

TABLE 1. Electrophysiological and dendritic properties of presubicular neuron clusters

Clusters	1 – RS sup			2 – IB			3.1 – RS deep 1			3.2 – RS deep 2		
	Mean	SEM	<i>n</i>	Mean	SEM	<i>n</i>	Mean	SEM	<i>n</i>	Mean	SEM	<i>n</i>
Lateral position (normalized coordinates)	0.40	0.03	24	0.36	0.04	6	0.39	0.03	17	0.39	0.06	11
Cell depth (normalized coordinates)	0.39	0.02	24	0.59	0.02	6	0.82	0.02	17	0.72	0.04	11
Resting membrane potential (mV)	-77.5	0.8	24	-62.1	1.4	6	-71.1	1.3	17	-67.9	1.6	11
Neuronal input resistance (MΩ)	360	24	24	216	28	6	415	32	17	819	67	11
Tau (ms)	22	1	24	18	2	6	26	3	17	52	7	11
Sag ratio	1.06	0.01	24	1.23	0.03	6	1.18	0.03	17	1.10	0.02	11
Rheobase (pA)	37	2	24	43	8	6	36	4	17	15	1	11
Firing rate at 100 pA (Hz)	27	1	24	68	22	6	24	2	17	33	1	11
Input-output slope (Hz/nA)	463	24	24	346	196	6	371	23	17	514	27	11
Bursting Index	0.18	0.02	24	0.88	0.04	6	0.32	0.06	17	0.19	0.05	11
AP width (ms)	0.80	0.03	24	0.89	0.05	6	0.95	0.05	17	1.24	0.10	11
AP AHP (mV)	-12.7	0.4	24	-14.8	1.7	6	-14.6	0.8	17	-14.2	0.8	11
AP rise amplitude (mV)	98.1	1.0	24	89.8	3.5	6	92.7	1.5	17	94.4	1.7	11
AP maximum depolarization rate (V/s)	506	19	24	359	26	6	367	16	17	340	24	11
AP maximum repolarization rate (V/s)	-122	5	24	-91	7	6	-97	5	17	-80	6	11
AP first AHP (mV)	-11.6	0.5	24	2.8	1.2	6	-13.7	0.9	17	-13.8	0.8	11
Dendritic count	4.5	0.3	24	5.3	0.6	6	5.4	0.4	17	3.9	0.4	11
Dendritic length (μm)	3175	171	24	3357	416	6	3861	263	17	3166	295	11
Layer I dendritic length (μm)	1340	108	24	1056	311	6	239	151	17	510	106	11
Layer II dendritic length (μm)	254	48	24	258	28	6	102	63	17	161	34	11
Layer III dendritic length (μm)	1481	139	24	558	171	6	224	63	17	602	133	11
Layer IV dendritic length (μm)	87	30	24	1167	100	6	239	80	17	355	117	11
Layer V/VI dendritic length (μm)	0	0	24	266	109	6	2631	208	17	1775	227	11
0° wedge dendritic length (μm)	1532	107	24	1762	267	6	748	132	17	1208	242	11
60° wedge dendritic length (μm)	276	59	24	383	171	6	695	200	17	396	150	11
120° wedge dendritic length (μm)	216	32	24	309	73	6	525	132	17	302	91	11
180° wedge dendritic length (μm)	442	59	24	327	66	6	906	115	17	428	72	11
240° wedge dendritic length (μm)	451	60	24	311	40	6	484	90	17	564	129	11
300° wedge dendritic length (μm)	281	58	24	292	42	6	535	52	17	283	76	11

Cluster 1 corresponds to RS cells in layers II/III (RS sup); cluster 2 corresponds to intrinsic bursting neurons (IB) with soma location in layer IV; clusters 3.1 and 3.2 correspond to subpopulations of RS neurons in layer V/VI (RS deep-1 and RS deep-2). Electrophysiological and morphological parameters used for cluster analysis are given for each of the four main clusters.

in the second than in the first cluster, corresponding to a higher variability in the second cluster. Decreasing the cutoff value further separated the second cluster into a group of deep layer neurons, and a distinct neuronal population in layer IV (Fig. 2B).

The emerging clusters thus corresponded quite closely to the principal cell somatic location on an axis between layers II and VI. Cluster 1 comprised RS cells of superficial layers II and III ( $n = 24$ ; RS sup cells). Cluster 2 contained intrinsically burst firing cells of layer IV ( $n = 6$ ; IB cells). Cluster 3 was composed of mostly RS cells of layers V and VI ( $n = 28$ ; RS deep cells). This cluster was subdivided into two further subgroups: cluster 3.1 of regularly spiking neurons with diverse morphologies ( $n = 17$ ; RS deep-1) and cluster 3.2 of more excitable regularly spiking, pyramidal-shaped cells ( $n = 11$ ; RS deep-2). We now describe each of these four groups of presubicular principal cells in detail.

#### *Principal cells of cluster 1: regular firing neurons with somata in layers II and III*

Figure 3A shows the reconstructed, two-dimensional dendritic form for seven neurons with somata located in superficial layers of the presubiculum. Layer I was relatively cell-free, with sparse, possibly inhibitory neurons. We recorded 44 cells, mostly with a pyramidal dendritic form, from layers II or III. Twenty-four of these neurons, with data on all parameters, were included in the cluster analysis and were grouped together in cluster 1.

The presubicular pyramidal cells of layers II and III typically had rather small somata with a cross-sectional area of  $94 \pm 6 \mu\text{m}^2$  ( $n = 20$ , Supporting Information Fig. S1). They extended a single major apical dendrite that ramified with terminal apical tuft dendrites in layer I as it approached the cortical surface (Fig. 3A). The apical dendrites of some cells bifurcated at several tens of  $\mu\text{m}$  from the soma to form twin dendrites that usually branched symmetrically. Layer II/III neurons extended up to seven basal dendrites ( $4.5 \pm 0.3$ ,  $n = 24$ ) and some cells possessed sparse oblique dendrites. The apical dendrites of these cells were radially oriented, whereas the basal dendrites extended in all directions from the soma (Fig. 7A, RS sup, blue). Three layer II neurons were atypical with less well-defined apical and basilar dendrites (e.g. cell No. 174 in Fig. 3A). The mean total dendritic length of superficial pyramidal cells was  $3175 \pm 171 \mu\text{m}$  ( $n = 24$ ; for  $n = 21$  neurons, apical  $1741 \pm 126 \mu\text{m}$ ; basal  $1496 \pm 114 \mu\text{m}$ ). The greatest mean dendritic length was found in segments oriented towards the cortical surface (Fig. 7A) with a high density of distal apical tuft dendrites in layer I. The basal dendrites of layer II/III neurons did not penetrate deep layers, but rather extended horizontally on approaching the border with layer IV (Fig. 7B and C).

Neurons of all clusters possessed a high density of dendritic spines. Well-filled cells projected profuse local axon collaterals, thinner than dendrites with varicosities. The axons of the superficial cells in cluster 1 tended to project to deeper layers of the presubiculum.

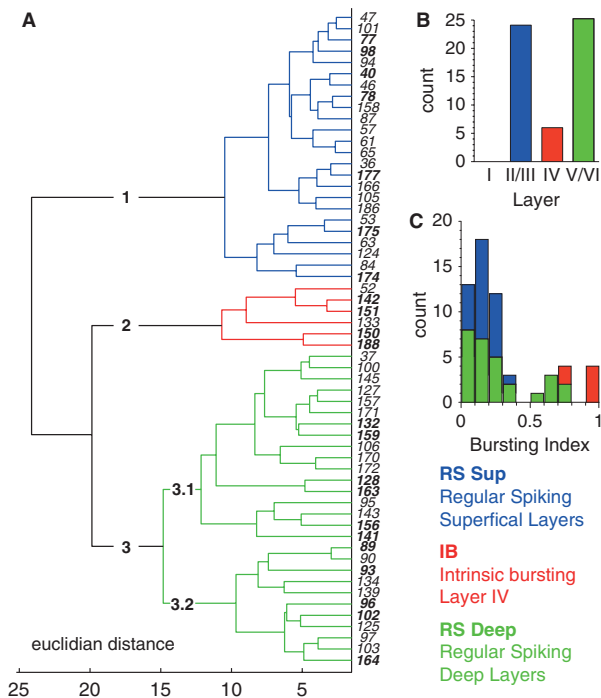


FIG. 2. Classification of presubicular cell types by cluster analysis. Fifty-eight neurons with complete anatomical and physiological data (cell identification number, right) were included in the analysis based on the parameters given in Table 1. (A) Dendrogram reveals three main clusters: 1, 2 and 3. Cluster 3 may be separated into 3.1 and 3.2 with Euclidean distance  $> 14$  between the two subgroups. (B) The three main clusters correspond to neurons located in superficial layers II/III (blue), layer IV neurons (red), and neurons in deep layers V/VI (green). (C) Cluster 2 neurons [red, intrinsic bursting (IB)] fire in bursts. The BI shows a gradient. Most cells from clusters 1 and 3 fire regularly (blue, RS sup, Regular Spiking cells of layers II/III; green, RS deep, Regular Spiking cells of layers V/VI).

lum (six out of 10 well-filled axons, cf. Fig. 7D and E). Possible longer range axonal projections were typically cut in the slice preparation.

The layer II/III neurons of cluster 1 did not discharge spontaneously in either cell-attached or whole-cell recording modes. The membrane voltage measured several minutes after break-in was  $-77.5 \pm 0.8$  mV, more negative than in other clusters (ANOVA and Tukey's *post hoc* test,  $P < 0.001$ ). Their mean firing threshold was  $-39.8 \pm 0.5$  mV ( $n = 24$ ). An  $R_{in}$  of  $360 \pm 24$  M $\Omega$  and a membrane time constant,  $\tau$ , of  $22 \pm 1$  ms were measured from step current injections made from a holding voltage of  $-65$  mV. All layer II/III neurons discharged regularly in response to maintained or step current injections (Table 1; Fig. 3B and C).

The potential difference between the resting and threshold potential in layer II/III neurons was  $37.7 \pm 0.9$  mV (cf. Fig. 8A, blue circles). The mean rheobase, the minimum current needed to elicit an AP, at a latency  $< 800$  ms was  $37 \pm 2$  pA. Figure 3B shows the responses of three principal neurons located in layer II or III to step current injections. The input-output curves (Fig. 8), constructed by plotting the number of APs ( $E$ ) or their frequency ( $F$ ) against the injected current, had a mean initial slope of  $463 \pm 24$  Hz/nA. At larger currents, the total number of APs could fall, even as the peak instantaneous frequency continued to rise or remained stable. This point was considered as the maximal sustainable frequency ( $48 \pm 3$  Hz,  $n = 14$ ).

The AP peak and amplitude in neurons of layers II/III were  $58.2 \pm 0.8$  and  $98.1 \pm 1.0$  mV, respectively. The mean duration at half amplitude of evoked APs was rather short,  $0.80 \pm 0.03$  ms, shorter than for other clusters (Fig. 8G). The maximum AP depolarization and repolarization rates were fast ( $506 \pm 19$  and  $-122 \pm 5$  V/s, respectively) (Fig. 8H). The spike AHP was typically complex or biphasic (Fig. 3D), with a mean maximal amplitude of  $-12.7 \pm 0.4$  mV.

The  $I_h$  inferred by a 'sag' in responses to step hyperpolarizations, was small or absent in layer II/III cells (Figs 3B and 8C). The addition of ZD7288, an  $I_h$  blocker, caused little change in membrane resistance at rest ( $20 \mu\text{M}$ ,  $n = 3$ ,  $< 10\%$ ).

#### Pyramidal cells of cluster 2: burst firing neurons with somata in layer IV

Figure 4A shows the reconstructed somatodendritic form of four neurons with somata located in the less densely populated layer IV (lamina dissecans). We recorded nine cells from this region and six of them included in the cluster analysis formed a distinct group (cluster 2).

Layer IV may represent a continuation of the subiculum (Fig. 1B) with large pyramidal cells of this region projecting to the lateral mammillary nuclei (Yoder & Taube, 2011). The mean cross-sectional area of the somata was  $159 \pm 8 \mu\text{m}^2$  ( $n = 6$ , Supporting Information Fig. S1). The cells shown in Fig. 4A possess prominent apical dendrites extending towards the pia, with a more or less elaborate tuft, and three to five basal dendrites. The mean total dendritic length was  $3357 \pm 416 \mu\text{m}$  ( $n = 6$ ). Dendrites of layer IV cells ramified largely in layers I-IV, with lesser projections to layer V/VI (Fig. 7, intrinsic bursting cells, red). The dendrites of some cells deviated asymmetrically from the main tissue axis. Those of neurons close to the subiculum, in particular, were often oriented towards the subiculum (cf. Fig. 4A, No. 151 and 188). Axons of well-filled layer IV pyramidal cells ramified in all layers, except layer I (Fig. 7D and E).

The pyramidal cells of layer IV discharged in single or repeated bursts in response to suprathreshold current steps ( $n = 6$ ; BI  $0.88 \pm 0.04$ , Fig. 4B and C). Their mean resting membrane potential was  $-62.1 \pm 1.4$  mV, less negative than the pyramidal cells of layers II and III, and the mean voltage threshold was  $-44.1 \pm 2.0$  mV ( $n = 6$ ). The mean membrane resistance was  $216 \pm 28$  M $\Omega$ , lower than for cells of other clusters, and the time constant was short ( $18 \pm 2$  ms). We distinguished weakly burst firing cells (two of six cells; Fig. 4, No. 142) where current injection induced an initial burst of two to five APs (at intervals of 3–10 ms) followed by regular firing at 10–50 Hz, from more strongly bursting neurons where repetitive bursting was elicited (four of six cells; Fig. 4, No. 150) (cf. Williams & Stuart, 1999).

The potential difference between the resting and threshold potential in burst firing neurons was  $18.0 \pm 2.4$  mV, smaller than for cells of other clusters (Fig. 8A, red squares). Nevertheless, the mean rheobase was higher than in other clusters ( $43 \pm 8$  pA). Rebound spikes were sometimes observed after the offset of a hyperpolarizing pulse (not shown). Bursting neurons had a high sag index ( $1.23 \pm 0.03$ ) (Fig. 8C). The sag was suppressed by the  $I_h$  blocker ZD7288 ( $20 \mu\text{M}$ ,  $n = 2$ ) but burst firing was maintained (not shown).

The AP peak and amplitude were  $45.6 \pm 2.7$  and  $89.8 \pm 3.5$  mV, respectively, with a mean halfwidth of  $0.89 \pm 0.05$  ms (Figs 4D and 8G). The first AP of a burst repolarized to a potential of  $+2.8 \pm 1.2$  mV before a second AP was initiated ('first AHP';

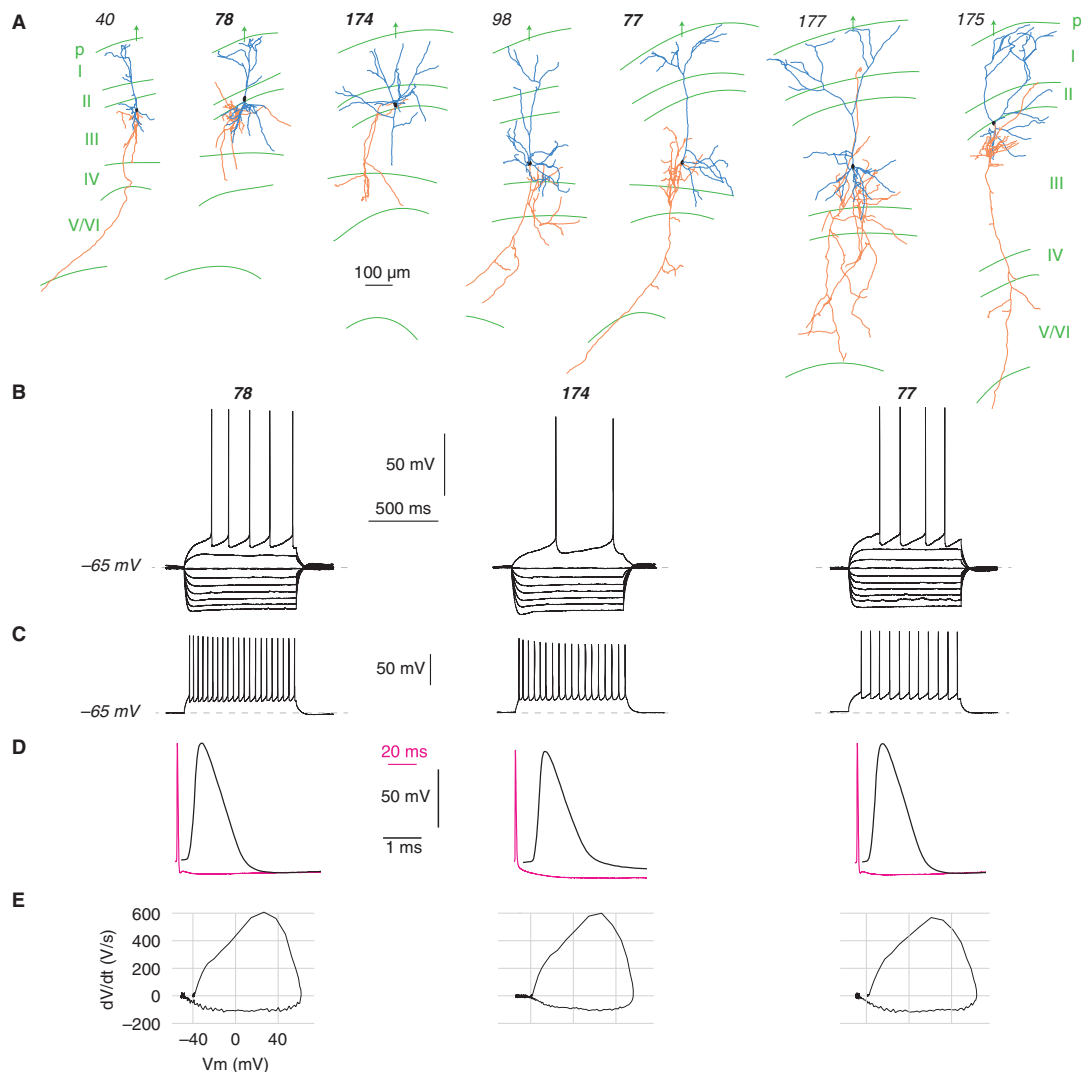


FIG. 3. Cluster 1 neurons with somata in presubicular layers II and III (RS sup cells). (A) Reconstructions of seven biocytin-filled neurons in superficial layers of the presubiculum. Most cells in cluster 1 are small pyramidal-shaped neurons. Neurons are rotated to present the radial axis as vertical. Axons are red, dendrites blue, with layer limits and the pial surface in green. Cell identification numbers are indicated above each reconstruction. (B) Current-clamp records of responses to 800 ms hyperpolarizing and depolarizing current steps ( $\Delta 25$  pA). Identification numbers are given. (C) RS firing patterns of three layer II and II cells in response to a +150 pA step current injection. (D) AP waveforms show a rather short AP halfwidth. (E) AP phase plots reveal high rising  $dV/dt$  in cluster 1 cells.  $V_m$ , membrane potential.

Fig. 4D). Following a burst, a mean AHP of amplitude of  $-14.8 \pm 1.7$  mV was reached after  $60 \pm 17$  ms.

#### Cells of clusters 3.1 and 3.2: regular firing neurons with diverse anatomy and somata in layers V/VI

The morphologies of neurons with somata located in deep layers V and VI were more diverse than those of superficial cells of cluster 1. They possessed pyramidal, polymorphic or multiform dendritic shapes (Figs 5A and 6A) (Lorente de No, 1934). Thirty-eight cells were recorded from layers V and VI, and 28 of them with complete data formed a third cluster. This cluster was in turn separated (Fig. 2A) into cluster 3.1 ( $n = 17$ ) and cluster 3.2 ( $n = 11$ ). The APs of neurons from clusters 3.1 and 3.2 tended to be larger and slower than those of the superficial layer cells of cluster 1. The

mean halfwidth for APs of cluster 3.2 cells was longer than for all other clusters.

Figure 5A shows the somatodendritic anatomy for five layer V/VI neurons of cluster 3.1. Their cross-sectional soma area was  $143 \pm 11 \mu\text{m}^2$  ( $n = 14$ , Supporting Information Fig. S1). The apical dendrites of cells in this cluster either extended to layer I forming a sparse tuft (No. 159) or terminated abruptly in layer II/III (No. 163). They possessed one to six basal dendrites. Multiform cells did not have a single, major dendrite, but rather three to six primary dendrites oriented in different directions within the deep layers or towards layer III (No. 128). Inverted pyramidal cells possessed one major dendrite extended laterally or downward, and another three to four first-order dendrites (No. 132). The mean total dendritic length of cluster 3.1 cells was  $3861 \pm 263 \mu\text{m}$  ( $n = 17$ ), higher than in all other clusters. The dendritic distribution for all deep layer cell types was maximal in layer V/VI with little spread to superficial layers

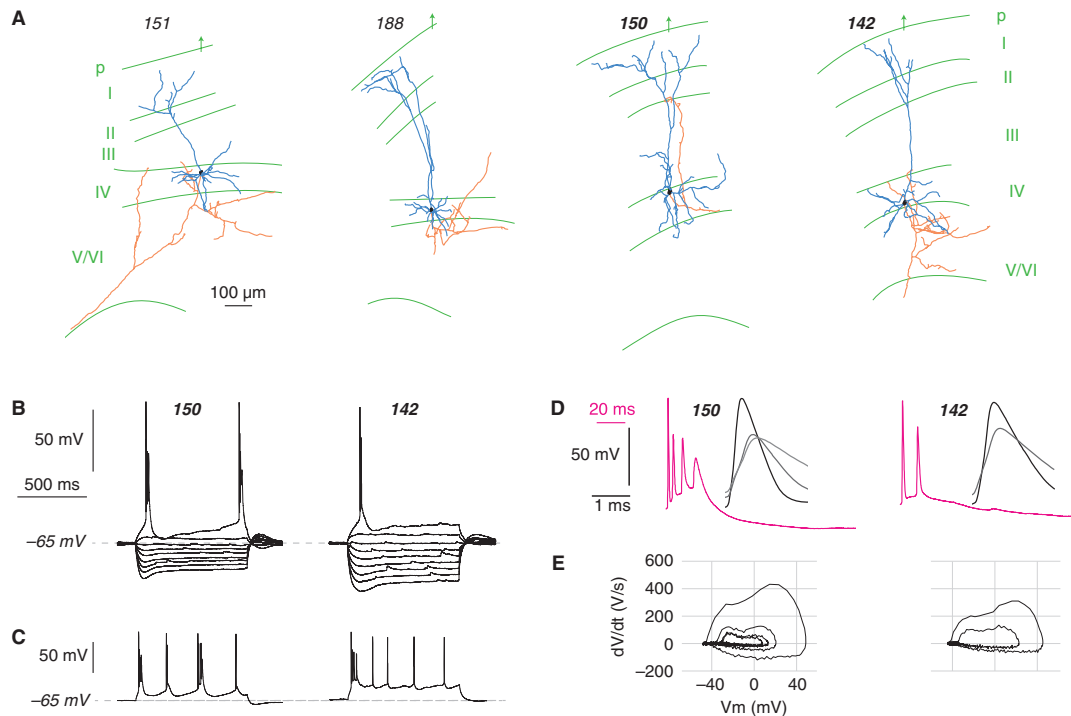


FIG. 4. Cluster 2 neurons are intrinsic bursting neurons of layer IV (intrinsic bursting cells). (A) Biocytin reconstructions of four cells with somata in layer IV. They are large pyramidal neurons with apical dendrites projecting to the pial surface. Neurons are rotated to present the radial axis as vertical. Axons are red, dendrites blue, and the layer limits and pial surface are shown in green. Cell identification numbers are indicated above each reconstruction. (B) Responses of two layer IV cells to 800 ms hyperpolarizing and depolarizing current steps ( $\Delta 25$  pA). (C) Burst firing induced by +100 pA step current injection. (D) Two to four APs occur within a burst. (E) Phase plot of AP bursts.  $V_m$ , membrane potential.

(Fig. 7A–C). Well-filled local axons of deep layer cells projected into the superficial layers ( $n = 6/12$ ) (Honda *et al.*, 2008, 2011) and projecting axons were cut as they entered the white matter.

The mean resting potential of neurons of cluster 3.1 in layers V/VI was  $-71.1 \pm 1.3$  mV ( $n = 17$ ), more depolarized than the superficial cells. The mean voltage threshold was  $-38.8 \pm 0.7$  mV. The mean membrane resistance was  $415 \pm 32$  M $\Omega$ , which was rather high, and the mean membrane time constant,  $\tau$ , was  $26 \pm 3$  ms, longer than in the superficial layer neurons. These cells tended to fire repetitively in response to step current injections. The difference between the resting and threshold potential in cluster 3.1 cells was  $32 \pm 2$  mV. The mean rheobase was  $36 \pm 4$  pA. Figure 5B and C shows repetitive discharges induced by step current injections in different deep layer pyramidal cells and a multiform cell. The input–output curves (Fig. 8E and F) for cells of this cluster were similar to those of cluster 1, with a mean initial slope of  $371 \pm 23$  Hz/nA. The maximal sustained firing frequency was  $35 \pm 3$  Hz ( $n = 9$ ).

The mean sag index for cells of cluster 3.1 was  $1.18 \pm 0.03$  (Fig. 8C). The sag was suppressed by ZD7288 (10  $\mu$ M;  $n = 3$ ), and the resting membrane potential hyperpolarized by  $-10$  mV (not shown). Thus, in the absence of  $I_h$ , the membrane potential of these neurons approached that of layer II/III cells.

The AP peak and amplitude for cells of cluster 3.1 were  $53.9 \pm 1.1$  and  $92.7 \pm 1.5$  mV, respectively, and the AP width was  $0.95 \pm 0.05$  ms (Fig. 8G). The maximum rates of AP depolarization and repolarization were  $367 \pm 16$  and  $-97 \pm 5$  V/s, respectively. This was lower than in superficial RS cells (depolarization rate: Kruskal–Wallis with Dunn's multiple comparisons test,  $P < 0.001$ ;

repolarization rate, normal distribution: ANOVA and Tukey's *post hoc* test,  $P < 0.01$ ), as revealed by phase plots of APs (Figs 5E and 8H). The APs in some cells repolarized with a shoulder (Fig. 5D) unlike RS superficial layer cells. The amplitude of the AHP was  $-14.6 \pm 0.8$  mV.

Figure 6A shows the somatodendritic form of five neurons with somata located in layer V/VI that were grouped in cluster 3.2 (soma cross-sectional area,  $136 \pm 8$   $\mu$ m<sup>2</sup>;  $n = 11$ ). The dendrites of these cells were pyramidal shaped, largely oriented in segments directed towards or away from the pial surface and often with a slender horizontal spread (Fig. 7A). The mean total dendritic length for cluster 3.2 cells was  $3166 \pm 295$   $\mu$ m ( $n = 11$ ). Dendrites were largely confined to deep layers V and VI, even though proportionally more dendrites of cluster 3.2 cells projected to layers I–III compared with those of neurons from cluster 3.1 (Fig. 7B and C). Well-filled axons of cluster 3.2 cells tended to ramify locally in deep layers and typically also projected into superficial layers, as for those of cluster 3.1 cells.

The neurons of cluster 3.2 had a mean resting potential of  $-67.9 \pm 1.6$  mV ( $n = 11$ ), more depolarized than superficial cells, and their mean voltage threshold was  $-40.1 \pm 0.6$  mV. The mean membrane resistance was  $819 \pm 67$  M $\Omega$ , higher than in all other clusters (Kruskal–Wallis with Dunn's multiple comparisons test,  $P < 0.01$ ), and the mean membrane time constant,  $\tau$ , was  $52 \pm 7$  ms, which was also high (Kruskal–Wallis with Dunn's multiple comparisons test,  $P < 0.01$ ). The difference between the resting and threshold potential in these pyramidal cells of layers V and VI was  $27.9 \pm 1.9$  mV. The mean rheobase was  $15 \pm 1$  pA, significantly lower than in other clusters (Kruskal–Wallis with Dunn's

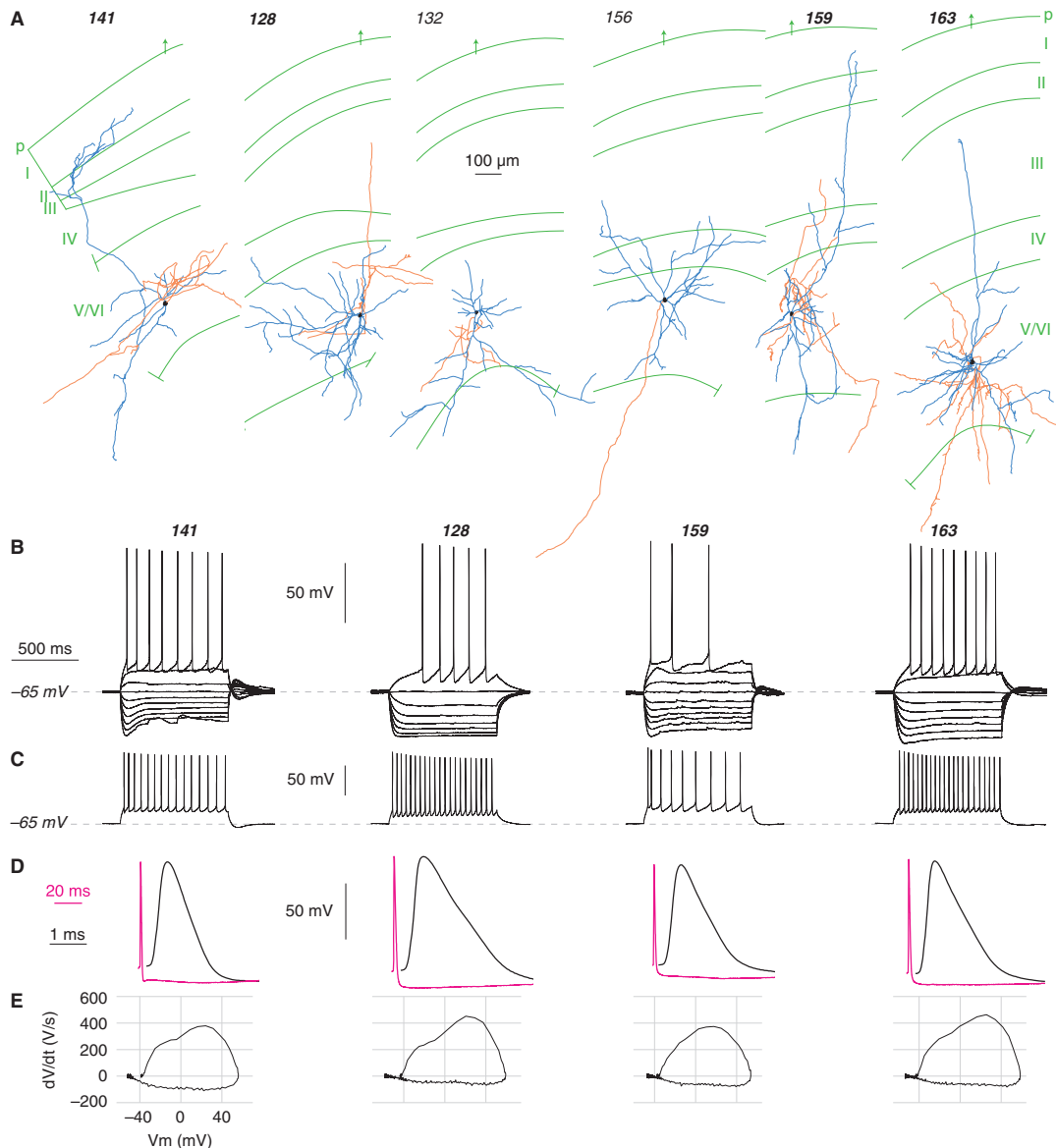


FIG. 5. Cluster 3.1 neurons of presubicular layers V and VI (RS deep-1 cells). (A) Biocytin reconstructions of six neurons of cluster 3.1. This subgroup includes pyramidal-shaped neurons, inverted pyramids and multiform neurons. Neurons are rotated to present the radial axis as vertical. Axons are red, dendrites blue, and the layer limits and the pial surface are shown in green. Cell identification numbers are indicated above each reconstruction. (B) Responses of four layer V/VI cells of cluster 3.1 to 800 ms hyperpolarizing and depolarizing current steps ( $\Delta$  25 pA). Some cluster 3.1 neurons display a prominent sag, indicating expression of  $I_h$ . (C) Regular firing induced by +100 pA step current injections. Sometimes the first two spikes occur at a short interspike interval (No. 159). (D) AP waveform and, below in E, AP phase plots showing lower rise  $dV/dt$  compared with RS sup neurons of cluster 1.  $V_m$ , membrane potential.

multiple comparisons test,  $P < 0.01$ ). Figure 6B and C shows regular, repetitive firing induced by step current injections for three deep layer pyramidal cells. The input–output curves (Fig. 8E and F) for cluster 3.2 cells had the steepest mean initial slope of  $514 \pm 27$  Hz/nA. The maximal sustained firing frequency was  $31 \pm 7$  Hz ( $n = 4$ ).

The mean sag index for RS deep layer cells of cluster 3.2 was  $1.10 \pm 0.02$  (Fig. 8C). The peak and amplitude voltage of the first AP were  $54.4 \pm 1.5$  and  $94.4 \pm 1.7$  mV, respectively. The mean AP width was  $1.24 \pm 0.1$  ms, larger than other clusters (Fig. 8G). The APs of cluster 3.2 possessed a ‘shoulder’ upon repolarization similar to neurons of cluster 3.1. The maximum rates of AP

depolarization and repolarization were  $340 \pm 24$  and  $-80 \pm 6$  V/s, respectively (Fig. 8H). The amplitude of the AHP was  $-14.2 \pm 0.8$  mV.

#### Repetitive firing: frequency, regularity and adaptation

Many presubicular neurons signal head direction (Taube *et al.*, 1990). While an animal’s head is oriented in its preferred direction, a given presubicular cell discharges APs in sustained fashion over periods of several minutes. We found that small positive current injections (40–120 pA) induced maintained firing in both deep and superficial layer cells *in vitro*. In records from 14 neurons, a

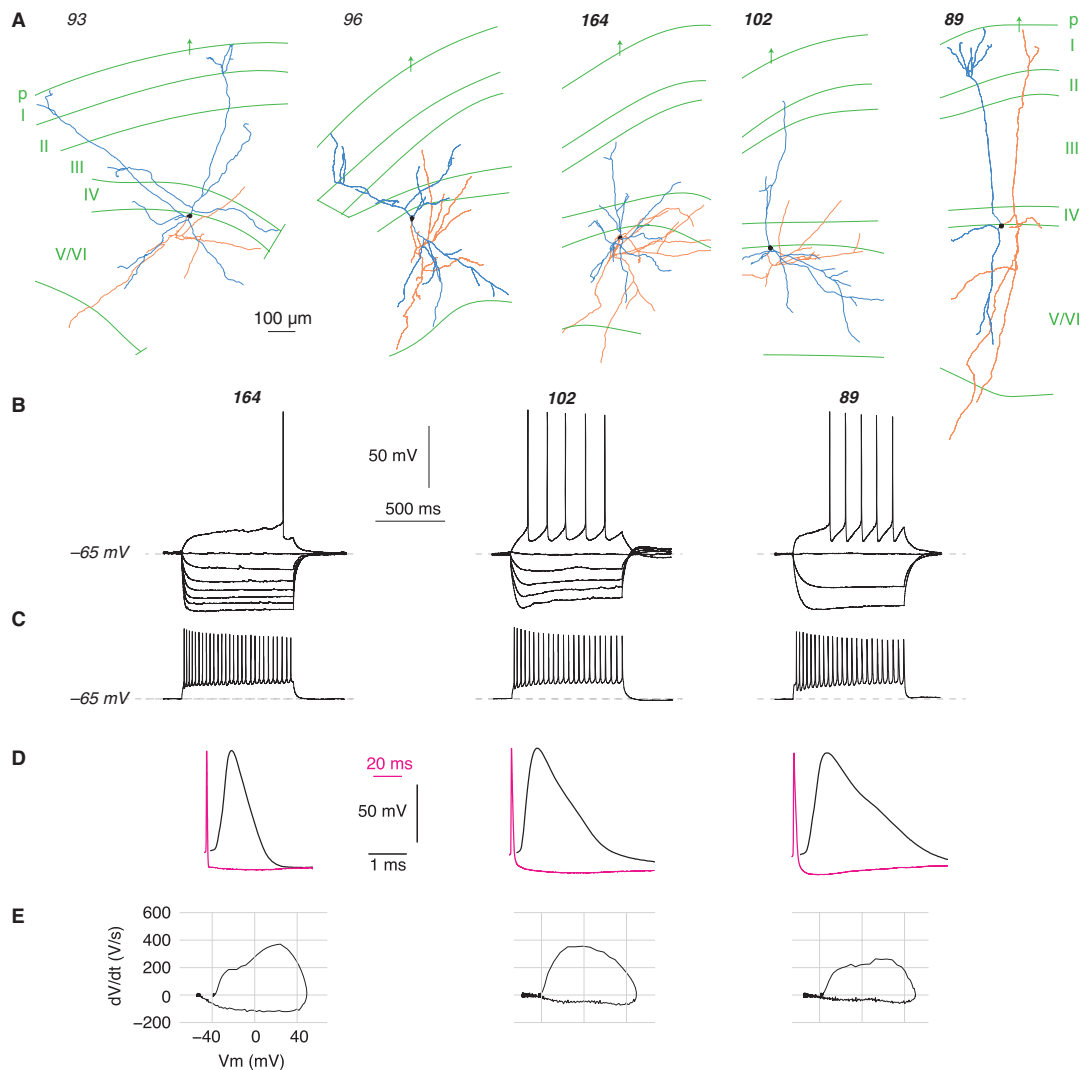


FIG. 6. Cluster 3.2 neurons of presubicular layers V and VI (RS deep-2 cells). (A) Biocytin reconstructions of five neurons from cluster 3.2, which comprises deep layer neurons with diverse dendritic shapes, including polymorphic neurons, and slender pyramidal-shaped neurons. Neurons are rotated to present the radial axis as vertical. Axons are red, dendrites blue, and the layer limits and pial surface are shown in green. Cell identification numbers are indicated above each reconstruction. (B) Responses of three cells from cluster 3.2 to 800 ms hyperpolarizing and depolarizing current steps ( $\Delta 25$  pA) show high  $R_{in}$  and low current threshold in these cells. (C) RS in response to +100 pA step current injection. (D) APs of most cells in this cluster possessed a rather large halfwidth, and phase plots (E) show a low depolarization rate.  $V_m$ , membrane potential.

maintained current was applied for at least 60 s to induce an initial firing at 15–25 Hz, which is similar to physiological firing rates *in vivo* (Taube *et al.*, 1990). Even though the firing frequency tended to decline over time, all 14 cells tested fired repetitively in a maintained fashion while the current was applied (Fig. 9A). The firing frequency after 60 s was between 5 and 20 Hz.

To better define the firing frequency adaptation from cells of cluster 1 and 3, we analysed responses to a standard 800 ms depolarizing pulse (Fig. 9C). As early firing frequency adaptation was usually more pronounced than late adaptation, we calculated two indices: the IAI and LAI, showing the evolution of firing frequency before and after the fifth AP, respectively. The mean IAI was  $-23 \pm 4\%$  ( $n = 52$ ). Strong initial adaptation was correlated with a high BI, as was the case for some cluster 3 neurons with a narrow first interspike interval (Pearson's  $r = 0.8$ ,  $P < 0.0001$ , Fig. 9D). Late adaptation was smaller than initial adaptation, with a mean LAI

of  $-9 \pm 1\%$  at 20 Hz ( $n = 52$ , Fig. 9E), and this adaptation index varied little for physiological firing frequencies.

As neurons discharge repetitively, calcium enters and activates several potassium channels with different kinetics that could contribute to distinct time scales of adaptation. We thus asked how adaptation was affected by omitting the calcium buffer ethylene glycol tetra-acetic acid from the recording solution. The current and voltage thresholds were reduced in the absence of the Ca buffer, so smaller currents could induce similar frequencies of firing. Both early and late adaptation were significantly reduced. In the absence of ethylene glycol tetra-acetic acid, the IAI was  $-11 \pm 4\%$  and the LAI was as small as  $-2 \pm 3\%$  (for mean firing frequencies of 20 Hz;  $n = 15$ ).

Overall, these data show that RS presubicular cells fire in sustained fashion with only a minor degree of adaptation that is due in part to currents resulting from Ca entry.

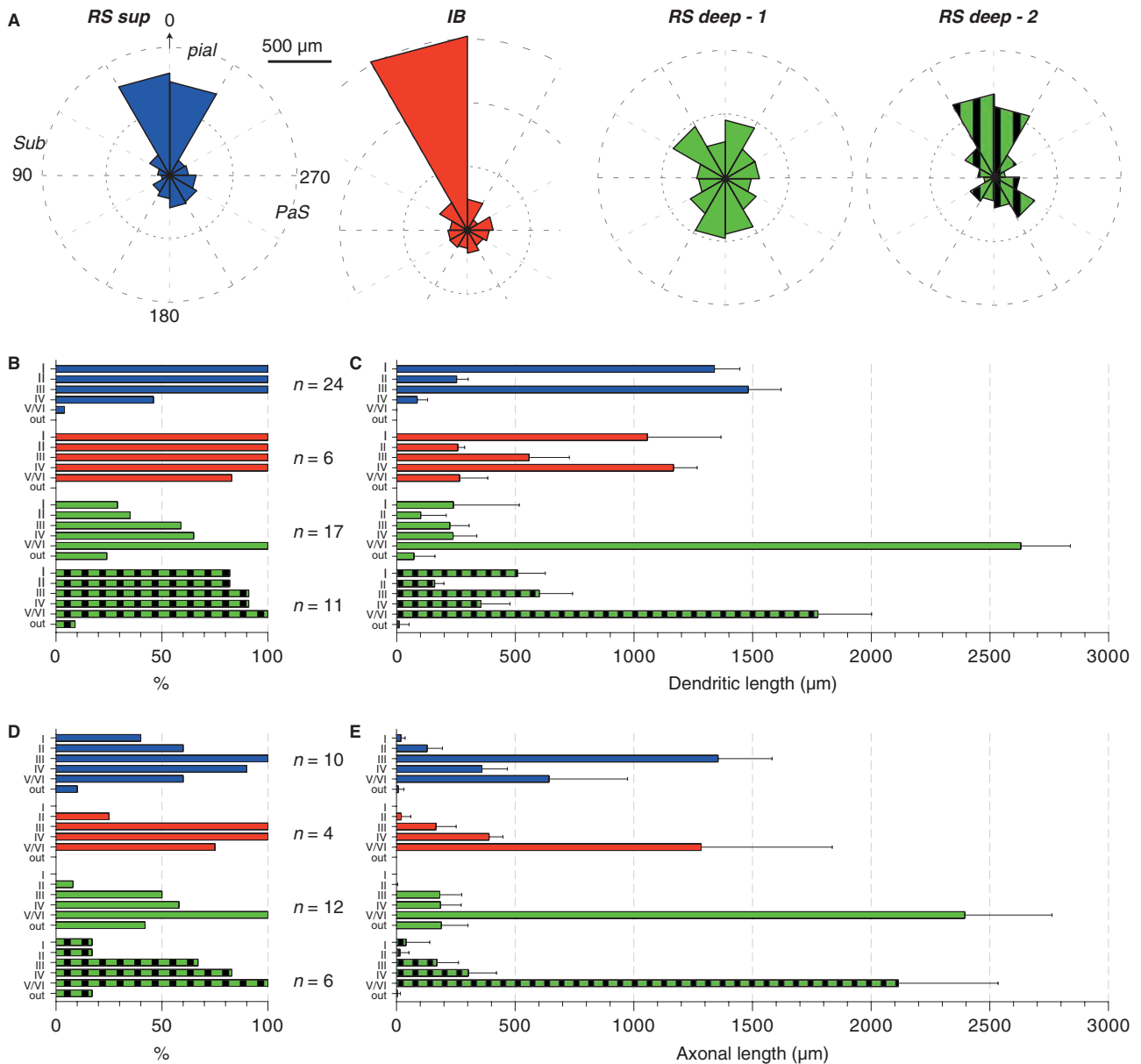


FIG. 7. Dendritic and axonal projections of presubicular neurons in different clusters. (A) Directionality of dendrite distribution, evaluated by 'wedge analysis' (NeuroLucida). Group-averaged results for dendritic length in each of 12 segments. Layer-specific distribution of dendrites (B and C) and axons (D and E) for neurons of different clusters. Graphs indicate the percentage of cells with dendrites (B) and axons (D) present in each layer. The mean dendritic length in each layer is given for each cluster in C and mean axonal length in each layer in E. Cluster 1 (RS sup cells) in blue ( $n = 24$ ); cluster 2 [intrinsic bursting (IB) cells] in red ( $n = 5$ ); cluster 3.1 (RS deep cells-1) in green ( $n = 19$ ); cluster 3.2 (RS deep-2) in green with black stripes ( $n = 12$ ). PaS, parasubiculum; Sub, subiculum.

## Discussion

We have classified presubicular principal cells, using an unsupervised cluster analysis based on cellular position, form and physiology obtained from *in vitro* records. The presubicular cell types from our analysis tend to correspond to neuronal types in other cortical regions. The presubiculum is situated at the transition between the archicortex and neocortex. Our data suggest that the neuronal types and their spatial arrangement in this region are closer to those of the entorhinal cortex than the cloud-like architecture of the subiculum. In particular, our cluster analysis revealed groups of neurons with similar properties arranged in the superficial, intermediate and deep

layers of the presubiculum. Two specific features of the presubicular neurons are of interest. First, layer IV cells, of the sparsely populated lamina dissecans, fired in bursts of APs, whereas principal cells from other superficial and deep layers discharged regularly. Second, repetitively firing principal neurons showed very little frequency adaptation consistent with a possible role in a maintained signalling of head direction.

### *The presubicular cortex is a transitional cortical region*

The presubiculum can be divided into six cytoarchitecturally distinct horizontal layers. None of the layers are as densely packed as the

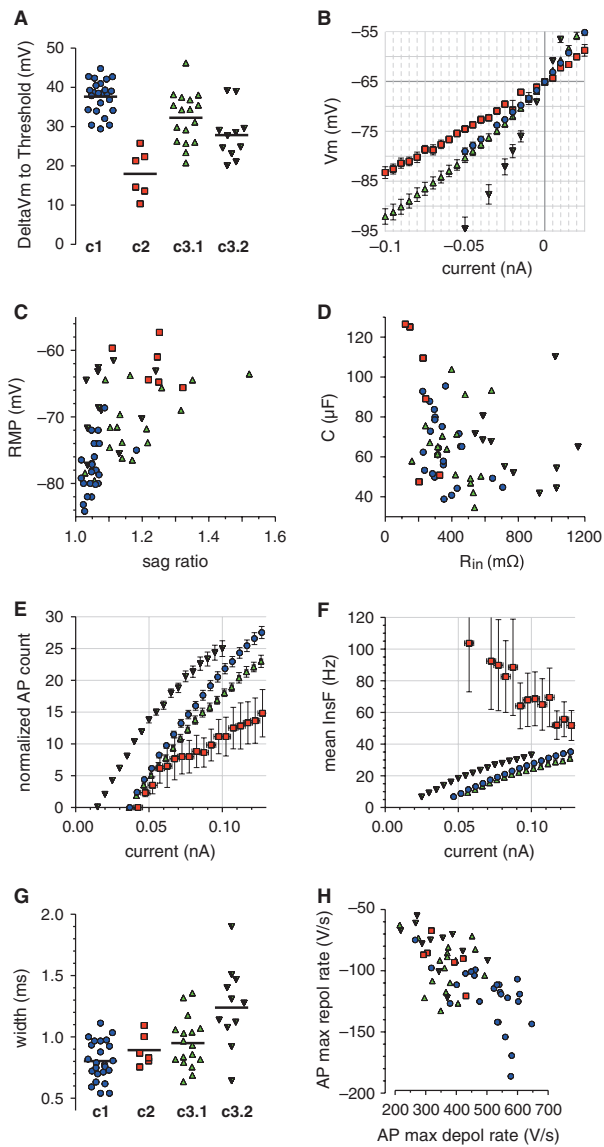


FIG. 8. Electrophysiological comparison of presubicular neurons. Cluster 1 (RS sup cells), blue circles ( $n = 24$ ); cluster 2 [intrinsic bursting (IB) cells], red squares ( $n = 5$ ); cluster 3.1 (RS deep-1 cells), green triangles ( $n = 17$ ); cluster 3.2 (RS deep-2 cells), green and black inverted triangles ( $n = 11$ ). (A) Voltage difference between resting membrane potential (RMP) and threshold. (B) Current–voltage relation at subthreshold potentials. The slope resistance is lowest for IB cells (cluster 2), and highest for cluster 3.2 cells. (C) RMP plotted against the sag ratio for each neuron. Low sag ratios and hyperpolarized RMPs are characteristic of cluster 1 neurons of layer II/III. (D) Capacitance (C) plotted against  $R_{in}$ . (E and F) Group averaged input–output curves. The number of APs/s (E) or the mean instantaneous frequency (InsF) (F) plotted against the amplitude of depolarizing current steps. Cells of cluster RS deep-2 cells had the lowest rheobase. AP numbers were lower in IB cells than RS cells, but occurred in bursts at higher InsF. (G) AP half-width. (H) AP maximal repolarization rate plotted against maximum depolarization rate. The fastest rate of rise was observed in RS sup cells. Each cell is represented by a symbol in A, C, D, G and H, and horizontal lines indicate mean values in A and G. In B, E, F, symbols indicate mean values  $\pm$  SEM for each group.  $V_m$ , membrane potential.

stratum pyramidale of the hippocampus proper, even though layers II and III contain a high pyramidal cell density (Figs 1 and 3). We show that the presubiculum shares features with the isocortex, where

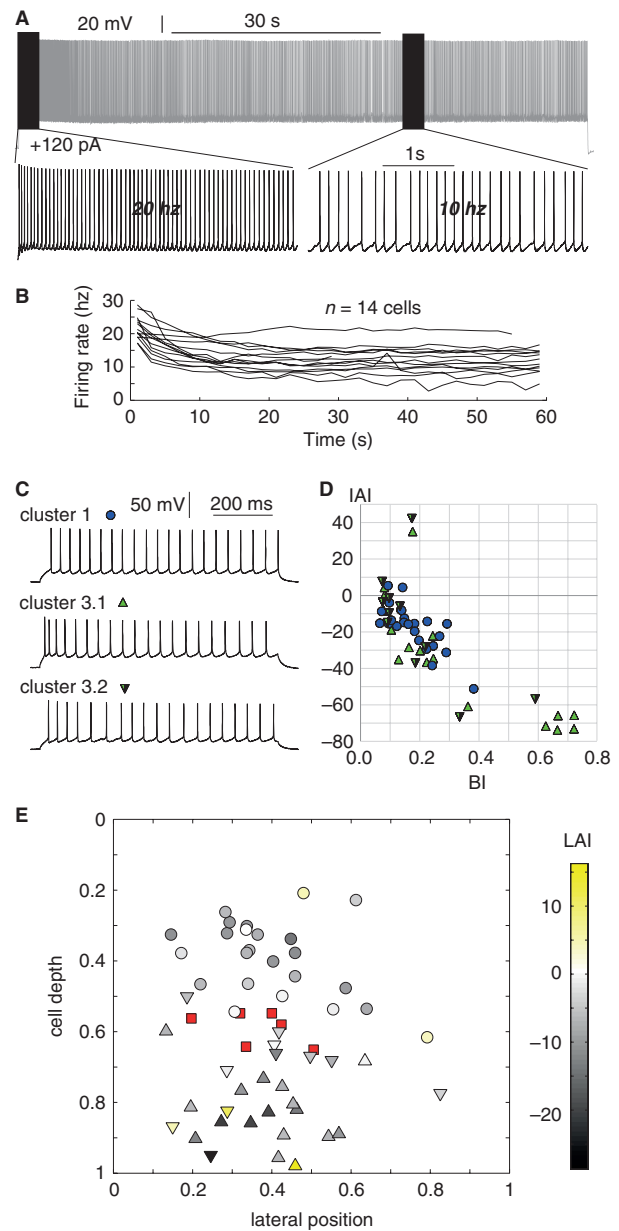


FIG. 9. Presubicular RS neurons sustain repetitive firing with little adaptation. (A) Sustained firing over 1 min in response to a suprathreshold depolarizing current of 120 pA. The initial firing frequency was close to 20 Hz, then dropped to 10 Hz. (B) Evolution of firing frequency, calculated by averaging instantaneous frequencies over successive 2 s periods. (C) Low AP frequency adaptation for cells of clusters 1 (RS sup,  $n = 24$ ) and 3 (RS deep-1,  $n = 17$ ; RS deep-2,  $n = 11$ ). The instantaneous firing frequency initially dropped in some cells, at the onset of a depolarizing pulse, then remained stable (step duration 800 ms). (D) Most presubicular neurons show little initial adaptation. A high IAI correlates with a high burst index in some cluster 3 neurons with a short interval between the first two APs. (E) LAI plotted as a function of soma position. The LAI of most neurons of layers II, III, V and VI is between  $-15$  and  $0\%$ . No adaptation index was calculated for layer IV neurons (cluster 2, red squares).

distinct cell populations are found in distinct layers. The firing patterns of presubicular neurons correspond to the RS and intrinsically bursting neurons of the neocortex (Connors & Gutnick, 1990). We also detected interneurons (Fig. 1D). Cells identified as interneurons

on the basis of anatomical and physiological criteria (Materials and methods) were encountered at a frequency similar to the estimated proportion of GABAergic neurons in the cortex. They were not included in the cluster analysis.

Columnar borders were not obvious in our slices of the presubiculum, even though columnar structures are transiently visible in young mice (Nishikawa *et al.*, 2002). However, axons of layer II and III neurons are radially oriented towards deep layers and may form elements of a vertical functional orientation (cf. Fig. 3). Deep layer axons may project out of the presubiculum as in the canonical neocortex. Ontogenetically, the presubiculum, together with the entorhinal cortex, belongs to an intermediate periallocortex (Filimonoff, 1947). Presubicular cells share some functional properties with the medial entorhinal cortex, in that both code for head direction and also for spatial grid information (Boccaro *et al.*, 2010). The deep presubicular layers V and VI and the neuronal types situated in them (Fig. 1) seem to be similar in form and physiology to analogous layers of the entorhinal cortex (Hamam *et al.*, 2000; Tahvildari & Alonso, 2005; Canto & Witter, 2012). Layer III presubicular cells extend only a very small portion of their basilar dendrites to deep layers as do the cells of this layer in the medial entorhinal cortex. There are some differences, however, including an absence in the presubiculum of 'fanned' cells like those of layer II of the lateral entorhinal cortex (Tahvildari & Alonso, 2005). In presubiculum layer II we find mainly pyramidal neurons and only rare stellate cells as in the medial entorhinal cortex (Canto & Witter, 2012). Furthermore, in contrast to the lamina dissecans of the entorhinal cortex (Canto & Witter, 2012), presubicular layer IV contains burst firing neurons (Figs 2 and 4). The anatomical continuity of layer IV with the subiculum, and the presence of bursting cells in both regions (Jarsky *et al.*, 2008) may reflect a common origin.

#### Cluster classification of presubicular neurons

Principal cells were classified with an unsupervised cluster analysis based on the somatic location, morphology and firing pattern. We focused on a limited dorsoventral portion at the centre of the presubiculum. At this level, superficial cells (layers II and III; cluster 1) were separated from deep cells (layers V and VI; cluster 3), and burst firing pyramidal neurons of layer IV emerged as a distinct third group (cluster 2, Fig. 2). These three clusters coincided with the neuronal somatic location. Our analysis suggests that neurons from the deep layers may be separated into two subgroups (clusters 3.1 and 3.2).

The presubicular principal cells of superficial layers II/III discharged regularly and were grouped into cluster 1. The form and electrophysiology of neurons from layers II and III was rather homogeneous, even though 4',6'-diamidino-2-phenylindole staining may suggest cytoarchitectural differences between these layers. The principal cells of the superficial layers in cluster 1 were the least excitable neurons recorded. The apical dendrites of superficial pyramidal cells may be innervated by afferents from the retrosplenial and visual cortices as well as the thalamus and hippocampus (van Groen & Wyss, 1990; Van Strien *et al.*, 2009; Kononenko & Witter, 2012). The axons of presubicular cells from layers II/III typically project towards deep layers (Fig. 3; cf. Funahashi & Stewart, 1997a).

Burst firing layer IV pyramidal cells, grouped in cluster 2, have not been described previously (Funahashi & Stewart, 1997a,b; Yoshida & Hasselmo, 2009). These neurons have rather depolarized resting potentials and relatively hyperpolarized firing thresholds resulting in the smallest potential difference between rest and thresh-

old of all clusters (Fig. 8A). They express the h-current strongly. Their apical dendrites extend to layer I where they may receive visual and entorhinal cortex inputs (van Groen & Wyss, 1990). Burst firing transmitted by local axons of layer IV cells should reliably excite postsynaptic targets within the presubiculum and help define functional units for processing head direction, whereas longer range targets of these cells probably include the lateral mammillary nucleus (Yoder & Taube, 2011).

Deep, layer V and VI cells of cluster 3 fired regularly, as did cells of cluster 1. Cells of clusters 1 and 3 exhibited little firing frequency adaptation consistent with a role in maintained signalling of head position. However, both the physiology and morphology of cluster 3 cells were more variable than those of cluster 1. Deep pyramidal cells of other cortical regions also tend to be diverse and layer VI cells include non-pyramidal glutamatergic neurons (Hamam *et al.*, 2000; Andjelic *et al.*, 2009; Canto & Witter, 2012). Some multiform cells of cluster 3 may possibly have been GABAergic, although their dendrites were typically spiny.

Our analysis suggests that cluster 3 may be divided into two subclusters, 3.1 and 3.2. The neurons of cluster 3.1 are morphologically and electrophysiologically diverse. The pyramidal cells of cluster 3.2 possess rare oblique dendrites and a high  $R_{in}$ . The majority of their cell bodies are located in the upper portion of layer V/VI, close to layer IV. Cluster 3.2 neurons could also correspond to the cells projecting to the lateral mammillary nucleus described by Yoder & Taube (2011). The responses to somatic current injection showed that neurons of subcluster 3.2 were more excitable than cells of subcluster 3.1. An enhanced excitability of layer V bursting cells in the barrel cortex depends partly on a reduced inhibitory control (Schubert *et al.*, 2001). It remains to be shown if cluster 3.2 presubicular cells are also less inhibited than RS neurons in cluster 1 or 3.1. Profiling the gene expression (Belgard *et al.*, 2011) in single cells from clusters 3.1 and 3.2 might define still further subclasses in these deep layer cells or show that they form a continuum with a range of overlapping phenotypes.

With distinct laminar termination patterns for presubicular afferents (van Groen & Wyss, 1990), deep cells with dendrites restricted to deep layers and superficial cells presumably receive different inputs. A minority of deep cells of cluster 3 possess dendrites that span all layers, and could perhaps integrate information from distinct sources. The axons of layer V/VI cells ramify locally in superficial presubicular layers (Honda *et al.*, 2011) and project to the anterodorsal thalamus (van Groen & Wyss, 1990). It is not clear whether single deep layer neurons that receive thalamic inputs also project back to the anterodorsal thalamus.

#### Presubicular microcircuit structure and function

Cells in both the deep and superficial layers of the presubiculum signal head direction in the intact animal, even if not all presubicular cells are also head direction cells (Boccaro *et al.*, 2010). Afferents to the region are crucial to construct head direction signals. Our data show that the physiological properties of presubicular cells are well suited to sustain neuronal firing for a given orientation. We examined adaptation at discharge frequencies close to those measured *in vivo* (20 Hz) (Taube *et al.*, 1990). The superficial and deep layer presubicular neurons supported prolonged maintained firing (Fig. 9). Their low adaptation contrasts with the accommodation of CA1 (Madison & Nicoll, 1984) and somatosensory cortex pyramidal cells (Fleiderovich *et al.*, 1996).

Pyramidal cells in neocortical slice preparations (Connors *et al.*, 1982) are typically silent. *In vivo*, state-dependent modulation may

favour pyramidal cell firing. Even so, RS pyramidal neurons in deep layers of the entorhinal cortex remain silent during exploration (Burgalossi *et al.*, 2011). Head direction cells in the presubiculum *in vivo* fire only when the head orients to its preferred orientation. In the CA1 region, only a subset of neurons discharge in a spatially tuned manner while other cells remain silent (Epszstein *et al.*, 2011). Possibly, as in other cortical regions, highly divergent inhibitory neurons (Fino & Yuste, 2011) dominate the operation of presubicular microcircuits in spatial signalling (Chrobak & Buzsaki, 1996). We detected many spontaneous inhibitory events in records from pyramidal cells (Simonnet, J. & Fricker, D., unpublished observation). As interneurons shape tuning width in the visual cortex (Katzner *et al.*, 2011) they also seem likely to contribute to the direction selectivity of presubicular principal cells (Taube, 2007; Isaacson & Scanziani, 2011).

When do presubicular pyramidal neurons fire? We found resting potentials that were 30 or 38 mV hyperpolarized from threshold in RS neurons of superficial and deep layers, respectively (Fig. 8A). Thus, only strong, synchronous and sustained synaptic inputs from afferents corresponding to a given head direction seem likely to assure maintained firing (Jerome *et al.*, 2011). The tetrodotoxin-insensitive, dendritic sodium current of presubicular principal cells (Fricker *et al.*, 2009) might function in a similar way to dendritic calcium signals in direction-sensitive visual cortex cells (Jia *et al.*, 2010), boosting correlated inputs to induce firing in response to directional inputs (Gasparini *et al.*, 2004; Losonczy *et al.*, 2008).

In conclusion, the cytoarchitectonics of the presubicular microcircuit provide this transitional region with a distinct organization. Our data on layer-specific differences in neuronal type, shape, intrinsic currents and discharge patterns provide a basis to understand how this region integrates afferent information by transforming synaptic signals in a voltage- and site-dependent manner.

## Supporting Information

Additional supporting information can be found in the online version of this article:

Fig. S1. Soma size estimates. (A) Shown are 60 × photographs of biocytin filled neuron somata for each cluster. (B) Measures for soma cross-sectional area in  $\mu\text{m}^2$ , obtained from measurement with Velocity image analysis software.

Table S1. Statistical tests.

Table S2. Electrophysiological and dendrite properties of presubicular neuron clusters. Given are 25%, 50% and 75% quantiles, in addition to mean and SEM.

## Acknowledgements

We thank Christophe Pouzat for comments on cluster analysis methods. The authors declare no competing financial interests. This work was supported by ANR Grant JCJC R10206DD (D.F.), the Région Ile-de-France (J.S.) and INSERM.

## Abbreviations

AHP, afterhyperpolarization; AP, action potential; BI, bursting index; IAI, initial adaptation index;  $I_h$ , hyperpolarization-activated current; LAI, late adaptation index;  $R_{in}$ , input resistance; RS, regular spiking.

## References

Andjelic, S., Gallopin, T., Cauli, B., Hill, E.L., Roux, L., Badr, S., Hu, E., Tamas, G. & Lambolez, B. (2009) Glutamatergic nonpyramidal neurons

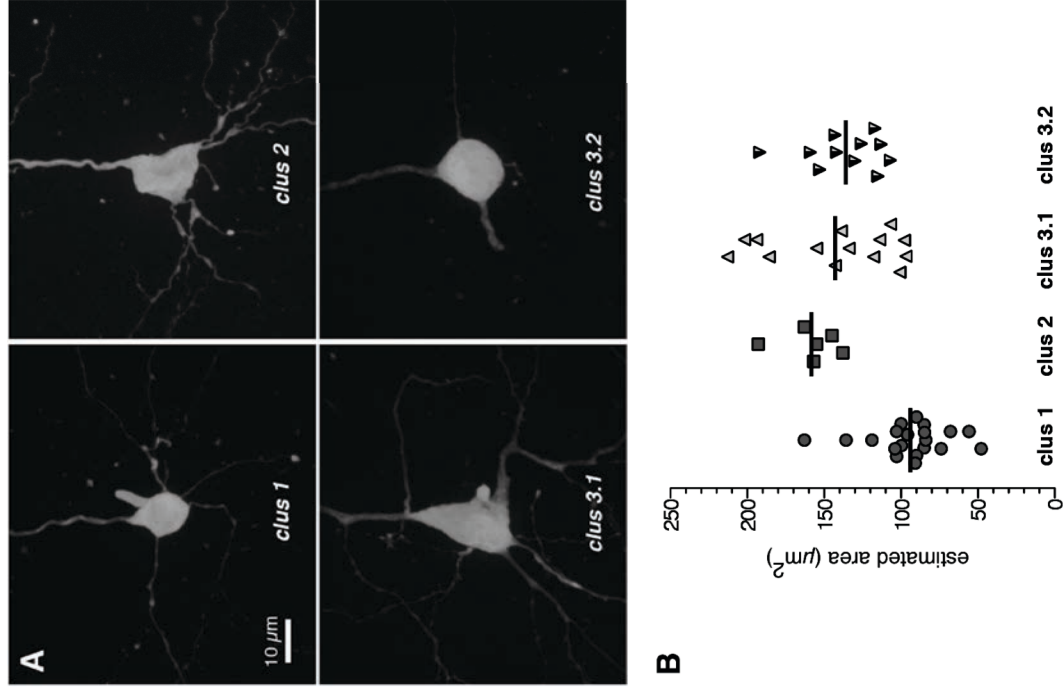
- from neocortical layer VI and their comparison with pyramidal and spiny stellate neurons. *J. Neurophysiol.*, **101**, 641–654.
- Belgard, T.G., Marques, A.C., Oliver, P.L., Abaan, H.O., Sirey, T.M., Hoerder-Suabedissen, A., Garc a-Moreno, F., Moln r, Z., Margulies, E.H. & Ponting, C.P. (2011) A transcriptomic atlas of mouse neocortical layers. *Neuron*, **71**, 605–616.
- Boccaro, C.N., Sargolini, F., Thoresen, V.H., Solstad, T., Witter, M.P., Moser, E.I. & Moser, M.-B. (2010) Grid cells in pre- and parasubiculum. *Nat. Neurosci.*, **13**, 987–994.
- Burgalossi, A., Herfst, L., von Heimendahl, M., F rste, H., Haskic, K., Schmidt, M. & Brecht, M. (2011) Microcircuits of functionally identified neurons in the rat medial entorhinal cortex. *Neuron*, **70**, 773–786.
- Cacucci, F., Lever, C., Wills, T.J., Burgess, N. & O'Keefe, J. (2004) Theta-modulated place-by-direction cells in the hippocampal formation in the rat. *J. Neurosci.*, **24**, 8265–8277.
- Canto, C.B. & Witter, M.P. (2012) Cellular properties of principal neurons in the rat entorhinal cortex. II. The medial entorhinal cortex. *Hippocampus*, **22**, 1277–1299.
- Canto, C.B., Wouterlood, F.G. & Witter, M.P. (2008) What does the anatomical organization of the entorhinal cortex tell us? *Neural Plast.*, **2008**, 1–18.
- Cauli, B., Porter, J.T., Tsuzuki, K., Lambolez, B., Rossier, J., Quenet, B. & Audinat, E. (2000) Classification of fusiform neocortical interneurons based on unsupervised clustering. *Proc. Natl. Acad. Sci. USA*, **97**, 6144–6149.
- Chrobak, J.J. & Buzsaki, G. (1996) High-frequency oscillations in the output networks of the hippocampal-entorhinal axis of the freely behaving rat. *J. Neurosci.*, **16**, 3056–3066.
- Cohen, I. & Miles, R. (2000) Contributions of intrinsic and synaptic activities to the generation of neuronal discharges in *in vitro* hippocampus. *J. Physiol. (Lond.)*, **524** Pt 2, 485–502.
- Connors, B.W. & Gutnick, M.J. (1990) Intrinsic firing patterns of diverse neocortical neurons. *Trends Neurosci.*, **13**, 99–104.
- Connors, B.W., Gutnick, M.J. & Prince, D.A. (1982) Electrophysiological properties of neocortical neurons *in vitro*. *J. Neurophysiol.*, **48**, 1302–1320.
- Ding, S.L. & Rockland, K.S. (2001) Modular organization of the monkey presubiculum. *Exp. Brain Res.*, **139**, 255–265.
- Douglas, R.J. & Martin, K.A.C. (2007) Mapping the matrix: the ways of neocortex. *Neuron*, **56**, 226–238.
- Epszstein, J., Brecht, M. & Lee, A.K. (2011) Intracellular determinants of hippocampal CA1 place and silent cell activity in a novel environment. *Neuron*, **70**, 109–120.
- Filimonoff, I.N. (1947) A rational subdivision of the cerebral cortex. *Arch. Neurol. Psychiatry*, **58**, 296–311.
- Fino, E. & Yuste, R. (2011) Dense inhibitory connectivity in neocortex. *Neuron*, **69**, 1188–1203.
- Fleiderovich, I.A., Friedman, A. & Gutnick, M.J. (1996) Slow inactivation of  $\text{Na}^+$  current and slow cumulative spike adaptation in mouse and guinea-pig neocortical neurones in slices. *J. Physiol. (Lond.)*, **493**, 83–97.
- Fricker, D., Verheugen, J.A. & Miles, R. (1999) Cell-attached measurements of the firing threshold of rat hippocampal neurones. *J. Physiol. (Lond.)*, **517**, 791–804.
- Fricker, D., Dinocourt, C., Eug ne, E., Wood, J.N., Wood, J. & Miles, R. (2009) Pyramidal cells of rodent presubiculum express a tetrodotoxin-insensitive  $\text{Na}^+$  current. *J. Physiol. (Lond.)*, **587**, 4249–4264.
- Funahashi, M. & Stewart, M. (1997a) Presubicular and parasubicular cortical neurons of the rat: functional separation of deep and superficial neurons *in vitro*. *J. Physiol. (Lond.)*, **501**, 387–403.
- Funahashi, M. & Stewart, M. (1997b) Presubicular and parasubicular cortical neurons of the rat: electrophysiological and morphological properties. *Hippocampus*, **7**, 117–129.
- Gasparini, S., Migliore, M. & Magee, J.C. (2004) On the initiation and propagation of dendritic spikes in CA1 pyramidal neurons. *J. Neurosci.*, **24**, 11046–11056.
- Goldman-Rakic, P.S., Selemon, L.D. & Schwartz, M.L. (1984) Dual pathways connecting the dorsolateral prefrontal cortex with the hippocampal formation and parahippocampal cortex in the rhesus monkey. *Neuroscience*, **12**, 719–743.
- van Groen, T. & Wyss, J.M. (1990) The connections of presubiculum and parasubiculum in the rat. *Brain Res.*, **518**, 227–243.
- Hamam, B.N., Kennedy, T.E., Alonso, A. & Amaral, D.G. (2000) Morphological and electrophysiological characteristics of layer V neurons of the rat medial entorhinal cortex. *J. Comp. Neurol.*, **418**, 457–472.
- Honda, Y., Umitsu, Y. & Ishizuka, N. (2008) Organization of connectivity of the rat presubiculum: II. Associational and commissural connections. *J. Comp. Neurol.*, **506**, 640–658.

- Honda, Y., Furuta, T., Kaneko, T., Shibata, H. & Sasaki, H. (2011) Patterns of axonal collateralization of single layer V cortical projection neurons in the rat presubiculum. *J. Comp. Neurol.*, **519**, 1395–1412.
- Isaacson, J.S. & Scanziani, M. (2011) How inhibition shapes cortical activity. *Neuron*, **72**, 231–243.
- Jarsky, T., Mady, R., Kennedy, B. & Spruston, N. (2008) Distribution of bursting neurons in the CA1 region and the subiculum of the rat hippocampus. *J. Comp. Neurol.*, **506**, 535–547.
- Jerome, J., Foehring, R.C., Armstrong, W.E., Spain, W.J. & Heck, D.H. (2011) Parallel optical control of spatiotemporal neuronal spike activity using high-speed digital light processing. *Front. Syst. Neurosci.*, **5**, 70.
- Jia, H., Rochefort, N.L., Chen, X. & Konnerth, A. (2010) Dendritic organization of sensory input to cortical neurons in vivo. *Nature*, **464**, 1307–1312.
- Katzner, S., Busse, L. & Carandini, M. (2011) GABAA inhibition controls response gain in visual cortex. *J. Neurosci.*, **31**, 5931–5941.
- Kononenko, N.L. & Witter, M.P. (2012) Presubiculum layer III conveys retrosplenial input to the medial entorhinal cortex. *Hippocampus*, **22**, 881–895.
- Kruger, L., Saporta, S. & Swanson, L.W. (1995) *Photographic Atlas of the Rat Brain*. Cambridge University Press, New York, USA.
- Longson, D., Longson, C.M. & Jones, E.G. (1997) Localization of CAM II kinase- $\alpha$ , GAD, GluR2 and GABA(A) receptor subunit mRNAs in the human entorhinal cortex. *Eur. J. Neurosci.*, **9**, 662–675.
- Lorente de No, R. (1934) Studies on the structure of the cerebral cortex. II. Continuation of the study of ammonic system. *J. Psychol. Neurol.*, **46**, 113–177.
- Losonczy, A., Makara, J.K. & Magee, J.C. (2008) Compartmentalized dendritic plasticity and input feature storage in neurons. *Nature*, **452**, 436–441.
- Lübke, J. & Feldmeyer, D. (2007) Excitatory signal flow and connectivity in a cortical column: focus on barrel cortex. *Brain Struct. Funct.*, **212**, 3–17.
- Madison, D.V. & Nicoll, R.A. (1984) Control of the repetitive discharge of rat CA 1 pyramidal neurones in vitro. *J. Physiol. (Lond.)*, **354**, 319–331.
- Mountcastle, V.B. (1997) The columnar organization of the neocortex. *Brain*, **120**, 701–722.
- Nishikawa, S., Goto, S., Hamasaki, T., Yamada, K. & Ushio, Y. (2002) Involvement of reelin and Cajal-Retzius cells in the developmental formation of vertical columnar structures in the cerebral cortex: evidence from the study of mouse presubicular cortex. *Cereb. Cortex*, **12**, 1024–1030.
- O'Mara, S.M., Commins, S., Anderson, M. & Gigg, J. (2001) The subiculum: a review of form, physiology and function. *Prog. Neurobiol.*, **64**, 129–155.
- Petilla Interneuron Nomenclature Group, Ascoli, G.A., Alonso-Nanclares, L., Anderson, S.A., Barrionuevo, G., Benavides-Piccione, R., Burkhalter, A., Buzsáki, G., Cauli, B., Defelipe, J., Fairén, A., Feldmeyer, D., Fishell, G., Fregnac, Y., Freund, T.F., Gardner, D., Gardner, E.P., Goldberg, J.H., Helmstaedter, M., Hestrin, S., Karube, F., Kisvárdy, Z.F., Lambollez, B., Lewis, D.A., Marin, O., Markram, H., Muñoz, A., Packer, A., Petersen, C.C.H., Rockland, K.S., Rossier, J., Rudy, B., Somogyi, P., Staiger, J.F., Tamas, G., Thomson, A.M., Toledo-Rodriguez, M., Wang, Y., West, D.C. & Yuste, R. (2008) Petilla terminology: nomenclature of features of GABAergic interneurons of the cerebral cortex. *Nat. Rev. Neurosci.*, **9**, 557–568.
- Ranck, J.J. (1984) Head direction cells in the deep layer of dorsal presubiculum in freely moving rats. *Soc. Neurosci. Abstr.*, **10**, 599.
- Rolls, E.T. (2006) Neurophysiological and computational analyses of the primate presubiculum, subiculum and related areas. *Behav. Brain Res.*, **174**, 289–303.
- Schubert, D., Staiger, J.F., Cho, N., Kötter, R., Zilles, K. & Luhmann, H.J. (2001) Layer-specific intracolumnar and transcolumnar functional connectivity of layer V pyramidal cells in rat barrel cortex. *J. Neurosci.*, **21**, 3580–3592.
- Shibata, H. & Honda, Y. (2012) Thalamocortical projections of the anterodorsal thalamic nucleus in the rabbit. *J. Comp. Neurol.*, **520**, 2647–2656.
- Shiple, M.T. & Sorensen, K.E. (1975) On the laminar organization of the anterior thalamus projections to the presubiculum in the guinea pig. *Brain Res.*, **86**, 473–477.
- Tahvildari, B. & Alonso, A. (2005) Morphological and electrophysiological properties of lateral entorhinal cortex layers II and III principal neurons. *J. Comp. Neurol.*, **491**, 123–140.
- Taube, J.S. (2007) The head direction signal: origins and sensory-motor integration. *Annu. Rev. Neurosci.*, **30**, 181–207.
- Taube, J.S. & Muller, R.U. (1998) Comparisons of head direction cell activity in the postsubiculum and anterior thalamus of freely moving rats. *Hippocampus*, **8**, 87–108.
- Taube, J.S., Muller, R.U. & Ranck, J.B. (1990) Head-direction cells recorded from the postsubiculum in freely moving rats. I. Description and quantitative analysis. *J. Neurosci.*, **10**, 420–435.
- Thorndike, R.L. (1953) Who belongs in the family? *Psychometrika*, **18**, 267–276.
- Van Strien, N.M., Cappaert, N.L.M. & Witter, M.P. (2009) The anatomy of memory: an interactive overview of the parahippocampal–hippocampal network. *Nat. Rev. Neurosci.*, **10**, 272–282.
- Vogt, B.A. & Miller, M.W. (1983) Cortical connections between rat cingulate cortex and visual, motor, and postsubicular cortices. *J. Comp. Neurol.*, **216**, 192–210.
- Ward, J.H. Jr. (1963) Hierarchical grouping to optimize an objective function. *J. Am. Stat. Assoc.*, **58**, 236–244.
- Williams, S.R. & Stuart, G.J. (1999) Mechanisms and consequences of action potential burst firing in rat neocortical pyramidal neurons. *J. Physiol. (Lond.)*, **521** Pt 2, 467–482.
- Witter, M.P., Groenewegen, H.J., Lopes da Silva, F.H. & Lohman, A.H. (1989) Functional organization of the extrinsic and intrinsic circuitry of the parahippocampal region. *Prog. Neurobiol.*, **33**, 161–253.
- Yoder, R.M. & Taube, J.S. (2011) Projections to the anterodorsal thalamus and lateral mammillary nuclei arise from different cell populations within the postsubiculum: implications for the control of head direction cells. *Hippocampus*, **21**, 1062–1073.
- Yoder, R.M., Clark, B.J. & Taube, J.S. (2011) Origins of landmark encoding in the brain. *Trends Neurosci.*, **34**, 561–571.
- Yoshida, M. & Hasselmo, M.E. (2009) Persistent firing supported by an intrinsic cellular mechanism in a component of the head direction system. *J. Neurosci.*, **29**, 4945–4952.

Supporting document

Suppl Fig. 1

Soma size estimates. A. Shown are 60x photographs of biocytin filled neuron somata for each cluster. B. Measures for soma cross-sectional area in  $\mu\text{m}^2$ , obtained from automated measurement with Volocity image analysis software. Each symbol represents one cell, horizontal bars indicate mean soma surface for each cluster.



Suppl. Table 1

Statistical tests.

Parameters	RMP	Rin	tau	Firing slope	Rheobase	Width	minslope	max slope
Normal distribution	YES	NO	NO	YES	NO	YES	YES	NO
ONE WAY ANOVA : if normality was passed ; if variances do not differ significantly								
degree of freedom between columns	F	p value		F	p value		F	p value
degree of freedom within columns	24.03	****		0.88	ns		11.25	****
Tukey's Multiple comparison test								
statistics	q	p value		q	p value		q	p value
RS deep - 2 vs RS deep - 1	2.503	ns		1.803	ns		2.862	ns
RS deep - 2 vs IB	3.553	ns		0.765	ns		1.376	ns
RS deep - 2 vs RS sup	8.124	****					7.497	***
RS deep - 1 vs IB	5.837	****					0.8617	ns
RS deep - 1 vs RS sup	6.275	****		1.322	ns		5.118	**
IB vs RS sup	10.43	****					4.451	*
Kruskal-Wallis : if normality test was not passed								
degree of freedom	K-W	p value		K-W	p value		K-W	p value
statistics	31.72	****	3	25.05	****	3	20.95	***
							17.71	***
							25.6	****
Dunn's Multiple comparison test								
statistics	Difference	p value		Difference	p value		Difference	p value
RS deep - 2 vs RS deep - 1	in rank sum			in rank sum			in rank sum	
RS deep - 2 vs IB	21.47	**		-23.78	**		-5.091	ns
RS deep - 2 vs RS sup	44.15	***		-28.55	**		-4.174	ns
RS deep - 1 vs IB	27.69	***		-25.89	***		-25.78	***
RS deep - 1 vs RS sup	22.69	*		-4.77	ns		0.9167	ns
IB vs RS sup	6.228	ns		-2.103	ns		-20.69	***
	-16.46	ns		2.667	ns		-21.6	*

Suppl. Table 2

	Cluster 1				Cluster 2				Cluster 3.1				Cluster 3.2			
	mean	sem	Quantiles (25% 50% 75 %)	n	mean	sem	Quantiles (25% 50% 75 %)	n	mean	sem	Quantiles (25% 50% 75 %)	n	mean	sem	Quantiles (25% 50% 75 %)	n
Lateral Position	0.40	0.03	0.30 0.35 0.47	24	0.36	0.04	0.32 0.37 0.42	6	0.39	0.03	0.31 0.42 0.46	17	0.39	0.06	0.26 0.41 0.48	11
Cell Depth	0.39	0.02	0.32 0.38 0.47	24	0.59	0.02	0.65 0.57 0.64	6	0.82	0.02	0.76 0.82 0.89	17	0.72	0.04	0.65 0.69 0.82	11
RMP (mV)	-77.5	0.8	-80.0 -78.0 -74.5	24	-62.1	1.4	-64.8 -62.7 -59.7	6	-71.1	1.3	-75.0 -71.6 -65.3	17	-67.9	1.6	-71.3 -68.6 -63.1	11
Rm (m $\Omega$ )	360	24	290 331 416	24	216	28	149 215 244	6	415	32	316 423 517	17	819	67	600 771 1028	11
Tau (ms)	22	1	18 21 28	24	18	2	17 18 22	6	26	3	19 24 29	17	52	7	40 43 54	11
Sag Ratio	1.06	0.01	1.04 1.05 1.07	24	1.23	0.03	1.22 1.25 1.25	6	1.18	0.03	1.10 1.14 1.23	17	1.10	0.02	1.04 1.07 1.13	11
Rheobase (pA)	37	2	30 40 45	24	43	8	30 38 60	6	36	4	20 35 50	17	15	1	15 15 15	11
Firing Rate at 100 pA	27	1	22 27 32	24	68	22	46 47 119	6	24	2	19 24 29	17	33	1	29 33 36	11
Input output slope (Hz.nA $^{-1}$ )	463	24	375 463 550	24	346	196	125 163 475	6	371	23	350 400 425	17	514	27	481 500 550	11
Bursting Index	0.18	0.02	0.11 0.15 0.23	24	0.88	0.04	0.75 0.94 0.96	6	0.32	0.06	0.12 0.22 0.63	17	0.19	0.05	0.09 0.13 0.21	11
AP width (ms)	0.80	0.03	0.71 0.78 0.95	24	0.89	0.05	0.80 0.85 1.00	6	0.95	0.05	0.81 0.89 1.06	17	1.24	0.10	1.09 1.15 1.45	11
AP AHP (mV)	-12.7	0.4	-14.4 -13.0 -11.6	24	-14.8	1.7	-18.3 -15.3 -11.6	6	-14.6	0.8	-17.3 -14.9 -11.8	17	-14.2	0.8	-16.4 -13.8 -12.7	11
AP Rise Amplitude (mV)	98.1	1.0	95.0 98.2 101.2	24	89.8	3.5	86.2 88.9 94.2	6	92.7	1.5	89.3 93.3 98.0	17	94.4	1.7	89.0 96.6 99.3	11
AP Max Depol Rate (V.s $^{-1}$ )	506	19	454 536 573	24	359	26	305 352 423	6	367	16	340 371 400	17	340	24	276 343 383	11
AP Max Repolarisation Rate (V.s $^{-1}$ )	-122	5	-134 -118 -105	24	-91	7	-93 -89 -85	6	-97	5	-112 -92 -82	17	-80	6	-90 -75 -68	11
AP FHP (mV)	-11.6	0.5	-13.2 -11.6 -10.2	24	2.8	1.2	2.2 2.9 4.7	6	-13.7	0.9	-15.9 -13.1 -10.6	17	-13.8	0.8	-16.0 -13.8 -11.6	11
Dendritic Count	4.5	0.3	3.5 5.0 5.5	24	5.3	0.6	5.0 5.0 5.0	6	5.4	0.4	5.0 5.0 6.0	17	3.9	0.4	3.0 4.0 4.8	11
Dendritic Length ( $\mu$ m)	3175	171	2711 3072 3605	24	3357	416	2499 3147 3908	6	3861	263	2936 3699 4781	17	3166	295	2300 2860 3986	11
Layer I dendritic length ( $\mu$ m)	1340	108	1041 1270 1583	24	1056	311	574 847 1095	6	239	151	0 0 238	17	510	106	113 672 786	11
Layer II dendritic length ( $\mu$ m)	254	48	90 186 270	24	258	28	218 240 319	6	102	63	0 0 124	17	161	34	76 183 226	11
Layer III dendritic length ( $\mu$ m)	1481	139	1056 1576 1932	24	558	171	285 393 957	6	224	63	0 105 480	17	602	133	292 540 1003	11
Layer IV dendritic length ( $\mu$ m)	87	30	0 0 116	24	1167	100	952 1154 1275	6	239	80	0 128 354	17	355	117	101 174 592	11
Layer V/VI dendritic length ( $\mu$ m)	0	0	0 0 0	24	266	109	71 165 548	6	2631	208	2045 2269 2848	17	1775	227	1174 1751 2241	11
0j Wedge dendritic length ( $\mu$ m)	1532	107	1357 1542 1866	24	1762	267	1283 1858 2269	6	748	132	348 503 1077	17	1208	242	784 1121 1595	11
60j Wedge dendritic length ( $\mu$ m)	276	59	0 214 439	24	383	171	191 240 313	6	695	200	74 482 1155	17	396	150	64 122 832	11
120j Wedge dendritic length ( $\mu$ m)	216	32	79 218 351	24	309	73	98 366 381	6	525	132	169 424 615	17	302	91	44 263 470	11
180j Wedge dendritic length ( $\mu$ m)	442	59	251 351 602	24	327	66	182 345 370	6	906	115	586 774 1327	17	428	72	198 416 644	11
240j Wedge dendritic length ( $\mu$ m)	451	60	191 473 600	24	311	40	247 329 387	6	484	90	172 333 764	17	564	129	338 513 661	11
300j Wedge dendritic length ( $\mu$ m)	281	58	55 190 446	24	292	42	242 261 278	6	535	52	341 579 694	17	283	76	30 260 500	11

## ARTICLE 2

# Properties of presubicular neurons that project to lateral mammillary nucleus or anterodorsal thalamus

In my previous work, I described the laminar specificity of integrative properties in the presubiculum (Simonnet et al. 2013). I hypothesized that distinct electrophysiological and morphological properties may be linked to the projection specificity of the different neuronal populations.

The present study is part of an ongoing work that aims to link the diversity of presubicular principal cells with their function. We are using an *in vivo* approach to identify the presubicular neurons that project to subcortical areas, the lateral mammillary nucleus (LMN) and the anterodorsal thalamus (ADN), in the *in vitro* slice preparation.

At its origin, the purpose of this work was to describe the properties of different projection-specific subpopulations of neurons, and we have obtained several interesting results: ADN projecting neurons and LMN projecting neurons have distinct morphological and electrophysiological properties. ADN projecting neurons are regular spiking neurons, which may correspond to a homogeneous population in deep layers, whereas LMN projecting neurons correspond to intrinsic burst firing neurons that I previously described in layer 4.

We next wish to combine projection-specific labeling of presubicular neurons with the optogenetic stimulation of their afferences, in order to address how the input-output conversion is operated in the presubiculum. In the general discussion, I suggest a possible pathway for relaying visual information in the presubiculum, and I present some hypotheses that can be tested in future studies.



# Properties of presubicular neurons that project to lateral mammillary nucleus or anterodorsal thalamus

Authors. Jean Simonnet, Roxanne Lofredi, Bertrand Mathon and Desdemona Fricker.

## Introduction

The head direction signal is thought to originate from subcortical areas, from the interconnection between lateral mammillary nucleus (LMN) and dorso tegmental nucleus (DTN) (Bassett et al., 2007; Clark and Taube, 2012). The LMN sends its projections to the anterodorsal thalamus (ADN) (Gonzalo-Ruiz et al., 1992) that is a critical relay of the head direction signal to cortical areas, including the presubiculum (Goodridge and Taube, 1997). The presubicular head direction signal is continuously updated by visual cues (Taube et al., 1990), receiving projections from both visual cortex (Vogt and Miller, 1983) and retrosplenial cortex (Vogt and Miller, 1983; van Groen and Wyss, 1990; Jones and Witter, 2007). Finally, the presubiculum exerts a visual landmark control on the subcortical head direction signal (Goodridge and Taube, 1997; Yoder et al., 2011) via direct projections to ADN (van Groen and Wyss, 1990; Ishizuka, 2001) and LMN (Allen and Hopkins, 1989; Gonzalo-Ruiz et al., 1992).

A recent tracing study has identified the elements of the presubicular microcircuit projecting to subcortical areas as two non-overlapping populations, cells in deep layer projecting to ADN and neurons in layer 4 projecting to LMN (Yoder and Taube, 2011). Yet, the morphological and electrical properties of these neurons have remained unknown. Given the location of their cell bodies, we suggest that the LMN projecting neurons might correspond to intrinsically burst firing neurons of layer 4, or upper layer 5 pyramidal neurons (Simonnet et al., 2013). ADN projecting neurons are located in deep layers, and we ask whether they constitute a homogeneous subpopulation within the diverse population of deep layer neurons (Simonnet et al., 2013). Our present study tested this hypothesis by *in vitro* recording of ADN

projecting neurons and LMN projecting neurons, identified by stereotaxic injections of retrograde tracers *in vivo*.

## **Methods**

Retrobeads (Lumafluor) are non-toxic fluorescent microspheres that can be taken up by presynaptic terminals, migrate retrogradely to the cell bodies in 48 hours, and allow for subsequent recordings from visually identified projecting neurons in the slice preparation (Katz et al., 1984; Kim and Spruston, 2011). We used 24- to 45-day-old mice that were anesthetized with ketamine hydrochloride and xylazine (80 and 12 mg/kg, respectively). Stereotaxic injections of 100-300  $\mu$ l of green or red retrobeads were performed into ADN and LMN. Coordinates were defined from the bregma according to the antero-posterior (AP), medio-lateral (ML) and dorso-ventral (DV) axis and were (AP / ML / DV) -0.82 / 0.75 / -2.85 for ADN (Fig. 1A, B) and -2.80 / 0.75 / -5.35 for LMN (Fig. 1D, E) (Franklin, 2001). After surgery, mice were returned to their home cages for at least 48 hours. We made acute slices, patch clamp recordings of the intrinsic electrophysiological properties and revealed morphological properties following the methods described in our previous study (Simonnet et al., 2013).

## **Results**

### *Laminar distribution of LMN and ADN projecting neurons*

Retrobeads appeared as small fluorescent spheres in the somata of specific neuronal populations in the slice preparation. The topographical distributions of ADN and LMN projecting neurons followed those described by Yoder and Taube (2011). ADN projecting neurons were confined to deep layers (Fig. 1C) whereas LMN projecting neurons were found in layer 4 (Fig 1F). Many stained neurons were also found in nearby subiculum, which is known to project to the Medial Mammillary Bodies (Ishizuka, 2001), an area very close to LMN and difficult to avoid by injecting into the LMN. However, the specific patterns of thalamic and LMN projecting neurons within the hippocampal and parahippocampal areas allowed to verify the accuracy of the injection (Ishizuka, 2001). We excluded animals if the distribution of projecting neurons did not match the expected results.

### *Properties of ADN and LMN projecting neurons*

The post-hoc revelation of recorded neurons revealed that LMN projecting neurons were pyramidal cells in layer 4 (Fig 2A, D) similar to those described in rat. They had ascending apical dendritic trees ramifying in layer 1 and basal dendrites mainly covering layer 4, with

some extension in layer 3 and deep layers. ADN projecting neurons were located in deep layers, mostly pyramidal cells and extended their dendritic arborization across all layers of the presubiculum. For now, the morphology of only a small number of neurons has been revealed, so we cannot exclude that cells with other morphologies project to ADN.

Table 1 and Figure 2 describe the passive, firing and action potential properties of the two neuronal populations. Differences in firing patterns can be observed in two representative examples in Figure 2: regular firing for ADN cells and initial single spike or intrinsic burst followed by irregular spiking for LMN cells.

In LMN neurons ( $n = 17$ ), the fast membrane time constant ( $12.9 \pm 1.3$  ms) and the presence of a depolarizing current at the onset of a depolarization (Fig 2. E, inset) promoted short latency firing ( $55 \pm 4.2$  ms) of either bursts or single spikes. After the initial discharge, the cell fired regular sparse firing (Fig 2F). When neurons did not fire in bursts, a depolarizing envelope always underlied the single spike, and the after hyperpolarization amplitude was low ( $-10.4 \pm 1$  mV, compared to  $-17 \pm 0.9$  mV for ADN projecting neurons), an evidence for the ability to fire bursts (Connors and Gutnick, 1990; Simonnet et al., 2013). Our results therefore confirmed the hypothesis that LMN projecting neurons correspond to the intrinsic bursting neurons in layer 4, previously described in rat presubiculum (Simonnet et al., 2013).

The firing onset of ADN projecting neurons ( $n = 9$ ) was different as they had a longer membrane time constant ( $36 \pm 2.8$  ms) and latency to fire at rheobase ( $328 \pm 105.1$  ms) but contrary to LMN neurons, they were able to sustain high firing frequency (30 spikes per second at two times the rheobase).

**Table 1:** Intrinsic electrophysiological properties of LMN and ADN projecting neurons. Tau: membrane time constant. Rin: Input resistance ; inst freq: instantaneous frequency (Hz). CV: inst freq coefficient of variation. AHP: after hyperpolarization. AP: action potential.

	ADN projecting neurons			LMN projecting neurons		
	mean	sem	count	mean	sem	count
Resting membrane potential (mV)	-69.5	2.8	9	-66.0	1.6	16
Tau (ms)	36.1	6.4	9	12.9	1.3	17
Rin (M $\Omega$ )	419.7	28.3	9	191.0	20.7	17
Rheobase (pA)	71	15.1	9	74	6.2	17
Firing latency (ms)	328	105.1	9	55	4.3	17
Two times rheobase - Spikes per sec	32.8	6.0	9	14.0	3.6	17
Two times rheobase - Mean inst freq (Hz)	42.2	6.3	9	49.1	12.1	17
Two times rheobase - CV	0.26	0.05	9	1.01	0.18	13
AP - rise amplitude (mV)	73.1	2.0	9	75.0	3.1	17
AP - half width duration (ms)	0.570	0.049	9	0.502	0.020	17
AP - AHP amplitude	-17.8	0.9	9	-10.4	1.0	17
AP - max depolarization rate (Hz/pA)	384	16	9	480	38	17
AP - max repolarization rate (Hz/pA)	-136	15	9	-153	7	17

**Figure 1. Retrograde labeling of specific efferent neurons in different layers of the presubiculum. A, B.** Coronal plates from (Franklin, 2001) corresponding to the theoretical anteroposterior level for stereotaxic injections in ADN (**A**) and LMN (**D**). **C, D.** Coronal section showing the injection sites for the defined coordinates in ADN (**C**, Fluororuby) and LMN (**D**, red retrobeads, superimposed with bright field image). **E, F.** Labeled cell bodies of projecting neurons in presubiculum for injection in ADN (**E**) and LMN (**F**). Green retrobeads injected in ADN retrogradly stained deep layer (5/6) neurons in the presubiculum, in a very specific manner. Red retrobeads injected in the LMN retrogradly stained neurons within layer 4, but also subicular neurons that projected to medial mammillary nucleus (MM), next the the LMN (see on B).

**Figure 2. Electrophysiological and morphological properties of ADN and LMN neurons (A-C),** ADN projecting neurons. (**A**) Morphology, dendrite in light blue and axon in orange, layers in green. The arrow indicates the vertical axis determined as defined in (Simonnet et al. (2013)). (**B**) Membrane voltage responses to negative and positive current steps of 800 ms up to rheobase. (**C**) Evolution of discharge from rheobase, for the neuron in (A). (**D-F**) same as A-C, but for a LMN projecting neuron. In (**E**), see the magnification of the depolarizing onset that causes discharge with short latency. The framed inset is a magnification showing the intrinsic bursting behaviour in another LMN projecting neuron. (**G**) Membrane time constant as a function of input resistance suggests two populations with distinct properties, although some overlap exists. (**H-I**) The action potential afterhyperpolarization tended to be deeper for ADN than LMN neurons, because of the depolarization underlying firing and causing bursts in LMN neurons (A, inset).

**Figure 1**

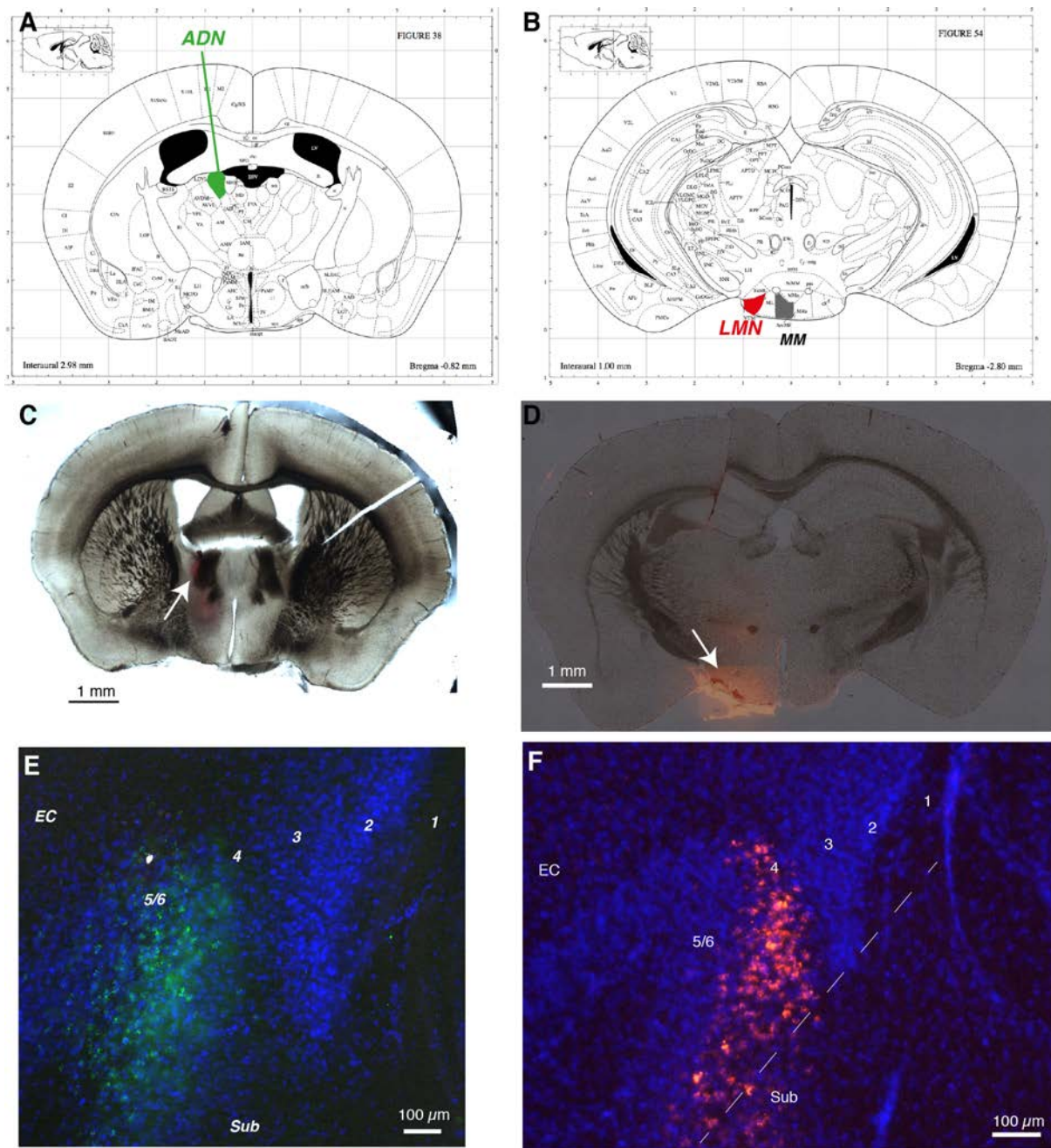


**Figure 1. Retrograde labeling of specific efferent neurons in different layers of the presubiculum.** **A, B.** Coronal plates from (Franklin, 2001) corresponding to the theoretical anteroposterior level for stereotaxic injections in ADN (**A**) and LMN (**D**). **C, D.** Coronal section showing the injection sites for the defined coordinates in ADN (**C**, Fluororuby) and LMN (**D**, red retrobeads, superimposed with bright field image). **E, F.** Labeled cell bodies of projecting neurons in presubiculum for injection in ADN (**E**) and LMN (**F**). Green retrobeads injected in ADN retrogradly stained deep layer (5/6) neurons in the presubiculum, in a very specific manner. Red retrobeads injected in the LMN retrogradly stained neurons within layer 4, but also subicular neurons that projected to medial mammillary nucleus (MM), next the the LMN (see on B).

**Figure 2**

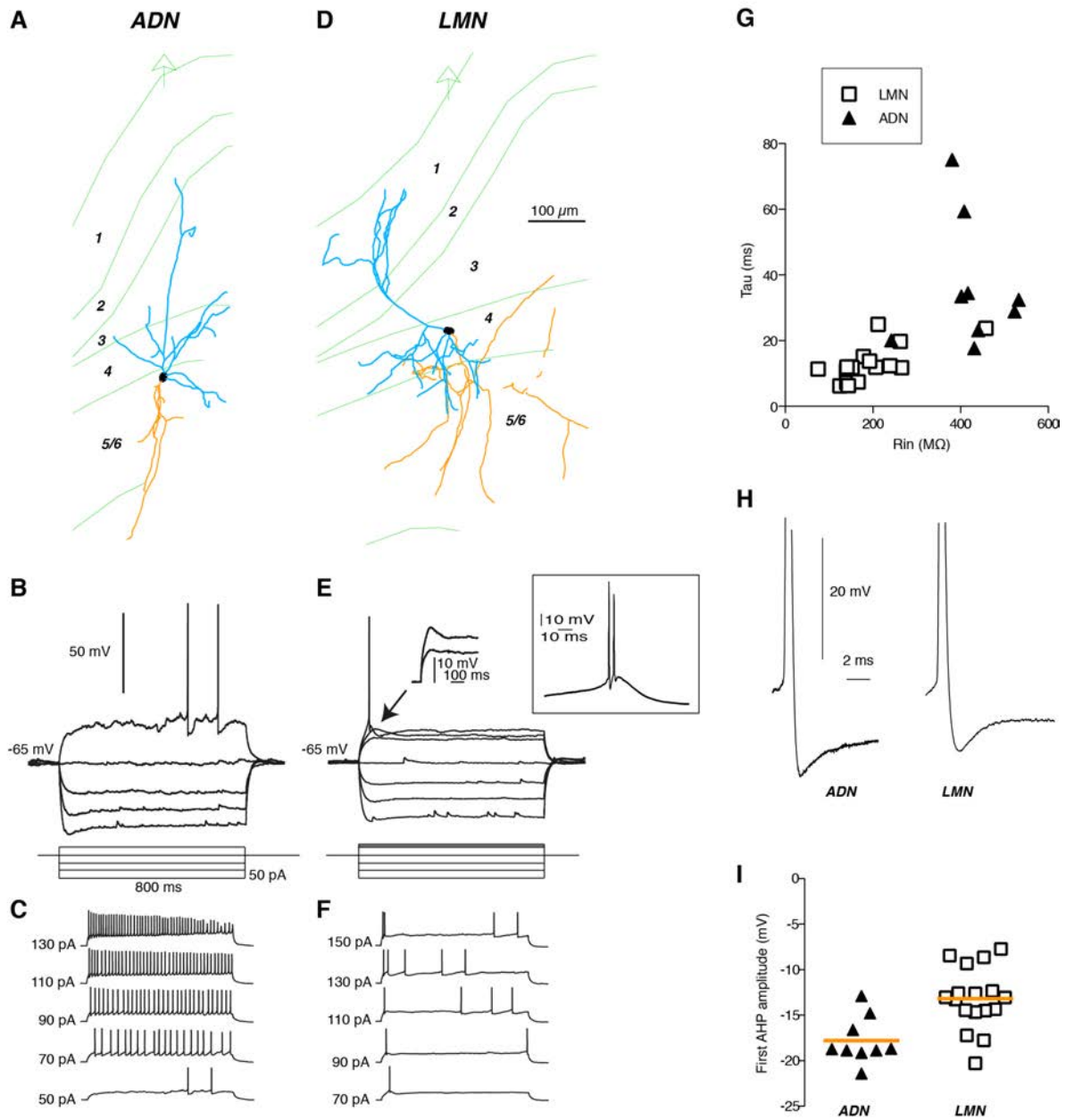


**Figure 2. Electrophysiological and morphological properties of ADN and LMN neurons**

(A-C), ADN projecting neurons. (A) Morphology, dendrite in light blue and axon in orange, layers in green. The arrow indicates the vertical axis determined as defined in Simonnet et al. (2013). (B) Membrane voltage responses to negative and positive current steps of 800 ms up to rheobase. (C) Evolution of discharge from rheobase, for the neuron in (A). (D-F) same as A-C, but for a LMN projecting neuron. In (E), see the magnification of the depolarizing onset that causes discharge with short latency. The framed inset is a magnification showing the intrinsic bursting behaviour in another LMN projecting neuron. (G) Membrane time constant as a function of input resistance suggests two populations with distinct properties, although some overlap exists. (H-I) The action potential afterhyperpolarization tended to be deeper for ADN than LMN neurons, because of the depolarization underlying firing and causing bursts in LMN neurons (A, inset).

- Allen GV, Hopkins DA (1989) Mammillary body in the rat: topography and synaptology of projections from the subicular complex, prefrontal cortex, and midbrain tegmentum. *J Comp Neurol* 286:311–336.
- Bassett JP, Tullman ML, Taube JS (2007) Lesions of the Tegmentomammillary Circuit in the Head Direction System Disrupt the Head Direction Signal in the Anterior Thalamus. *Journal of Neuroscience* 27:7564–7577.
- Clark BJ, Taube JS (2012) Vestibular and attractor network basis of the head direction cell signal in subcortical circuits. *Front Neural Circuits* 6:7.
- Connors BW, Gutnick MJ (1990) Intrinsic firing patterns of diverse neocortical neurons. *Trends in Neurosciences* 13:99–104.
- Franklin GPKBJ (2001) *The Mouse Brain in Stereotaxic Coordinates*. :1–350.
- Gonzalo-Ruiz A, Alonso A, Sanz JM, Llin s RR (1992) Afferent projections to the mammillary complex of the rat, with special reference to those from surrounding hypothalamic regions. *J Comp Neurol* 321:277–299.
- Goodridge JP, Taube JS (1997) Interaction between the postsubiculum and anterior thalamus in the generation of head direction cell activity. *J Neurosci* 17:9315–9330.
- Ishizuka N (2001) Laminar organization of the pyramidal cell layer of the subiculum in the rat. *J Comp Neurol* 435:89–110.
- Jones BF, Witter MP (2007) Cingulate cortex projections to the parahippocampal region and hippocampal formation in the rat. *Hippocampus* 17:957–976.
- Katz LC, Burkhalter A, Dreyer WJ (1984) Fluorescent latex microspheres as a retrograde neuronal marker for in vivo and in vitro studies of visual cortex. *Nature* 310:498–500.
- Kim Y, Spruston N (2011) Target-specific output patterns are predicted by the distribution of regular-spiking and bursting pyramidal neurons in the subiculum. *Hippocampus*.
- Simonnet J, Eugène E, Cohen I, Miles R, Fricker D (2013) Cellular neuroanatomy of rat presubiculum. *Eur J Neurosci* 37:583–597.
- Taube JS, Muller RU, Ranck JB (1990) Head-direction cells recorded from the postsubiculum in freely moving rats. II. Effects of environmental manipulations. *J Neurosci* 10:436–447.
- van Groen T, Wyss JM (1990) The postsubicular cortex in the rat: characterization of the fourth region of the subicular cortex and its connections. *Brain Res* 529:165–177.
- Vogt BA, Miller MW (1983) Cortical connections between rat cingulate cortex and visual, motor, and postsubicular cortices. *J Comp Neurol* 216:192–210.
- Yoder RM, Clark BJ, Brown JE, Lamia MV, Valerio S, Shinder ME, Taube JS (2011) Both Visual and Idiothetic Cues Contribute to Head Direction Cell Stability During Navigation Along Complex Routes. *Journal of Neurophysiology*.
- Yoder RM, Taube JS (2011) Projections to the anterodorsal thalamus and lateral mammillary nuclei arise from different cell populations within the postsubiculum: Implications for the control of head direction cells. *Hippocampus* 21:1062–1073.



## ARTICLE 3

# A continuum of diversity of Parvalbumin or Somatostatin expressing interneurons in mouse presubiculum

Head direction cells are found in many subcortical and cortical areas. A specificity of presubicular head direction cells is the narrower directional firing range and the lower firing rate compared to the afferent anterodorsal thalamus. I think that this could be due to the refinement operated by the presubicular cortical circuit, which possesses different layers to process the information. During my first study, I had noticed frequent spontaneous inhibitory activity in recordings of principal cells (not shown). GABAergic interneurons generally regulate activity by balancing excitation, selecting incoming information or synchronizing the activity of neuronal assemblies, and I think that they constitute major regulators of the head direction signal in the presubiculum.

Similarly to my previous study, a first step to understand the role of inhibition in the presubiculum was to understand its cellular basis. Cortical interneurons are very diverse. The few data that I had obtained in presubicular rat slices was definitely not enough to describe fully the interneuronal population. Identification of interneurons in rat slices is complicated because cellular bodies of both pyramidal neurons and interneurons have a similar size. I never succeeded to identify interneurons by their somatic shape. I therefore switched to transgenic mouse models, enabling the identification of different subtypes of interneurons, the Parvalbumin (PV+) and Somatostatin (SOM+) containing interneurons. We used the Pvalb-Cre mice for identification of PV+ interneurons and Sst-IRES-Cre and X98-SST for identifying SOM+ interneurons. At this time, Mérie Nassar joined the lab and we worked together on this subject. We used the same experimental approaches and the analysis tools that I had developed for my first study. Our results show that the presubicular

diversity of interneurons is comparable to what is found in other cortical areas. We found the typical PV+ fast spiking basket cells, and other interneurons resembling the typical SOM+ low threshold spiking Martinotti cells. These cells were identified in two distinct subgroups of our unsupervised classification. However, a third group lay between the two, grouping together neurons with intermediate features: quasi fast spiking cells with diverse morphologies.

In the future, it will be important to understand if these identified interneurons have distinct functional roles by identifying their specific targets and afferences. This will be an essential step to better understand the regulation of information flow in the circuit and how a specific head direction signal emerges from this cortex.

Title: A continuum of diversity of Parvalbumin or Somatostatin  
expressing interneurons in mouse presubiculum

running title: Interneuron diversity in mouse presubiculum

Mérie Nassar\*, Jean Simonnet\*, Ivan Cohen, Etienne Savary,  
Richard Miles and Desdemona Fricker

Institut du Cerveau et de la Moelle Epinière ICM,  
UPMC / INSERM U1127 / CNRS UMR7225, Paris, France.

Associate editor?

Zoltan Nusser ?

*Synaptic Neurotransmission; Molecular and Cellular Neuroanatomy; Cellular  
Neurophysiology*

Laboratory of Cellular Neurophysiology, Institute of Experimental Medicine, Budapest,  
Hungary

Corresponding author: Desdemona Fricker, ICM - CNRS UMR7225, CHU Pitié-Salpêtrière,  
47 Bd de l'Hôpital, 75013 Paris, France  
email: [desdemona.fricker@upmc.fr](mailto:desdemona.fricker@upmc.fr)

Keywords: inhibition, excitability, morphology, postsubiculum, head direction

## ABSTRACT *not exceeding 250 words*

The presubiculum is located between hippocampus and entorhinal cortex and plays an important role in spatial information processing and notably in signaling heading direction. We have recently examined presubicular principal neurons (Simonnet et al. 2013) but little is known about inhibitory interneurons in this region. Here, we examined the electrophysiological and morphological properties of parvalbumin-expressing (PV) and somatostating-expressing (SOM) interneurons from three transgenic mouse lines, Pvalb-Cre, Sst-Cre and X98, where interneurons are labeled with red (RFP) or green (GFP) fluorescent protein. Pvalb-Cre RFP neurons preferentially concentrated in superficial layers of presubiculum, as well as the less abundant interneurons of the X98 line. Sst-Cre RFP interneurons were more densely distributed in deep layers.

PV and SOM containing interneurons in presubiculum are diverse, and we used Ward's unsupervised cluster analysis based on electrophysiological parameters describing passive properties, firing patterns and AP shapes, to classify these interneurons according to their similarities. This revealed two main groups of interneurons: On one extreme of the spectrum are SOM-positive low-threshold spiking Martinotti type cells (cluster 1). On the other end we find archetypal PV-positive fast spiking basket cells (cluster 2b). An intermediate cluster, cluster 2a, contained a mix of PV or SOM expressing interneurons with intermediate electrical properties and mostly basket like morphologies. This result suggests a graded continuum of diversity for PV and SOM interneurons in presubiculum.

## INTRODUCTION *not exceeding 500 words;*

The presubicular cortex is located between the hippocampus and the medial entorhinal cortex, and it is thought to play a major role in spatial navigation. It contains "head direction" cells which discharge as a function of the animal's head in the environment, contributing to the sense of orientation (Taube et al. 1990; Van Strien et al. 2009; Boccara et al. 2010). Visual information from the visual and retrosplenial cortices, and head directional information of vestibular origin are both processed in presubiculum (Calton et al. 2003). Presubicular output neurons provide directional information to the grid cells in the superficial layers of the entorhinal cortex (van Groen and Wyss 1990a; van Haeften et al. 1997; Honda and Ishizuka 2004; Yoder et al. 2011; Kononenko and Witter 2012; Rowland et al. 2013).

We have shown previously three major principal cell types in superficial and deep layers of presubiculum (Simonnet et al. 2013). Inhibitory synaptic events were frequently observed in recordings from principal cells, and presubicular signal processing involves interactions between excitatory glutamatergic neurons and inhibitory GABAergic interneurons. The physiological and anatomical features of presubicular interneurons and their distributions across superficial and deep layers are insufficiently known however. In the hippocampus and in neocortex, distinct subsets of interneurons are believed to play distinct roles. In particular, soma targeting inhibitory neurons control timing and frequency of action potential discharge (Miles et al. 1996; Fricker and Miles 2001) and may contribute to the generation of fast oscillations (Cobb et al. 1995; Chrobak and Buzsaki 1996; Somogyi and Klausberger 2005). Dendrite targeting interneurons rather select input signals to pyramidal neurons and could affect head directional signal processing in the presubicular microcircuit in this way (Taube 2007; Isaacson and Scanziani 2011).

The diversity of interneuron function relies on a heterogeneous population of GABAergic neurons known to derive from multiple embryonic sources (Kepecs and Fishell 2014). Interneurons may be subdivided according to their anatomy, electrophysiological and neurochemical features, as well as their synaptic connectivity (Freund and Buzsáki 1996; Cauli et al. 1997; Kawaguchi and Kubota 1997; Parra et al. 1998; Markram et al. 2004; Rudy et al. 2010; Defelipe et al. 2013; Kubota 2014). What constitutes an interneuron type is still matter of debate, and classifications based on unsupervised clustering methods are a way to define neuronal classes through sets of common functional features (Ma et al. 2006; Karagiannis et al. 2009; McGarry et al. 2010; Perrenoud et al. 2012; Helm et al. 2013). Even so, as Battaglia and coworkers (Battaglia et al. 2013) pointed out, a structured continuum of

phenotypes with 'atypical' interneurons positioned at frontiers between distinct groups may exist.

We therefore performed a detailed electrophysiological and anatomical characterization of two major populations of interneurons in mouse presubiculum, those expressing the calcium binding protein parvalbumin (PV) and those expressing the neuropeptide somatostatin (SOM), identified from three transgenic mouse lines, Pvalb-Cre- or Sst-Cre-RFP and X98 GFP mice. Using unsupervised cluster analysis, we revealed two main groups of interneurons. The subsets so-defined by similarity of electrophysiological parameters did not entirely coincide with the expression of neurochemical markers. Our results establish the dichotomy between Pvalb and X98 interneurons in presubiculum, while Sst-Cre neurons showed similarities with either the X98 or the Pvalb interneurons.

## MATERIALS AND METHODS

### ***Animals***

Experiments were performed in male and female Pvalb-Cre mice (Jax 008069; (Hippenmeyer et al. 2005)) or Sst-IRES-Cre mice (Jax n°013044; (Taniguchi et al. 2011)) crossed with the Ai14 Cre reporter line (Jax n°007914; (Madisen et al. 2010)). Cre-mediated recombination resulted in the expression of red fluorescent tdTomato (RFP) labeling in subsets of GABAergic neurons. The terms "Sst-Cre" or "Pvalb-Cre" will be used when referring to the mouse line. The abbreviations "SOM" and "PV" will be used when referring to the expression of the neuropeptide, which, as we will show, is not always equivalent. Additionally we used the transgenic mouse line X98 (Jax n°006340), in which GFP expression is driven by the GAD67 promoter. Labeled is a subset of somatostatin positive neurons with axonal arborizations in layer I (Martinotti-type morphology in neocortex; (Ma et al. 2006)). Our care and use of the animals conformed to the European Communities Council Directive of 22 September 2010 (2010/63/EU) and French law (87/848). Our study was approved by the local ethics committee Charles Darwin N°5.

### ***Slices preparation***

Acute slices containing the hippocampus, subicular complex and entorhinal cortex were obtained from 25-31 days-aged mice. After ketamine hydrochloride and xylazine anesthesia (80 and 12 mg.kg<sup>-1</sup>, respectively), the animals were perfused through the heart with a cutting

solution containing 125 NaCl, 25 sucrose, 2.5 KCl, 25 NaHCO<sub>3</sub>, 1.25 NaH<sub>2</sub>PO<sub>4</sub>, 2.5 D-glucose, 0.1 CaCl<sub>2</sub>, 7 MgCl<sub>2</sub> (in mM) cooled to 4 °C and equilibrated with 5% CO<sub>2</sub> in O<sub>2</sub>. Animals were decapitated and horizontal, 250-300 µm thick brain sections were prepared in the same cutting solution using a vibratome (Leica VT1000S or Microm HM650V). Slices were stored for at least 1 h at 22–25 °C in a holding chamber filled with ACSF containing (in mM): 124 NaCl, 2.5 KCl, 26 NaHCO<sub>3</sub>, 1 NaH<sub>2</sub>PO<sub>4</sub>, 2 CaCl<sub>2</sub>, 2 MgCl<sub>2</sub>, and 11 D-glucose, bubbled with 5% CO<sub>2</sub> in O<sub>2</sub> (pH 7.3, 305–315 mOsm/L). They were then transferred to the recording chamber (volume 2-3 ml), heated at 33-35 °C, of either an Axioskop 2 FS plus microscope (Zeiss, France) or an BX51WI microscope (Olympus, France).

### ***Whole-cell patch-clamp recordings***

Recordings were made with glass pipettes pulled using a Brown–Flaming electrode puller (Sutter Instruments) from borosilicate glass of external diameter 1.5 mm (Hilgenberg, Germany). The electrode resistance was 3–6 MΩ after filling with a solution containing (in mM): 135 K-gluconate, 1.2 KCl, 10 HEPES, 0.2 EGTA, 2 MgCl<sub>2</sub>, 4 MgATP, 0.4 Tris-GTP, 10 Na<sub>2</sub>-phosphocreatine and 2.7 biocytin. This internal solution was adjusted to a pH of 7.3 with KOH and an osmolarity of 300 mOsm. Slices were visualized using infrared-differential interference contrast optics, and fluorescently labeled PV, SST or X98 interneurons were identified using LED illumination coupled to appropriate emission/excitation filters (OptoLED, Cairn Research, Faversham, UK). Whole-cell current-clamp recordings were made using a MultiClamp 700B amplifier and pCLAMP software (Molecular Devices, Union City, CA). The signal was filtered at 6 kHz and digitized at 20 kHz. The estimated junction potential of ~15 mV was not corrected.

### ***Electrophysiological analysis***

Recorded signals were analyzed with AxographX and routines written in MATLAB (The Mathwork). After break-in, we waited for 3–5 min before measuring cellular parameters. Resting membrane potential (RMP) was the mean potential over at least 10 seconds. Most electrophysiological parameters were measured from responses to step current injections of 800 ms duration applied from a fixed membrane potential of -65 mV. Injected currents increased from negative to positive values, with a range of amplitudes that resulted in hyperpolarization to about -100 mV during the first step and depolarizations to maximum sustainable firing frequency. Maximum sustainable firing frequency was defined as

maximum firing frequency before spike inactivation became evident, even though instantaneous frequency continued to rise or remained stable. Neuronal input resistance ( $R_{in}$ ) was determined as the slope of the current-voltage (IV) relationship between -71 and -64 mV. Membrane time constants ( $\tau$ ) were estimated by fitting a double exponential to the negative deflection of membrane voltage (Levenberg-Marquardt algorithm; (Golowasch et al. 2009)) observed after applying a 800 ms hyperpolarizing current injection inducing a voltage change that did not exceed 15 mV. A “sag ratio”, indicative of  $I_h$  expression, was calculated as the ratio of the maximal negative potential (sag, reached typically between 0-200 ms), divided by the mean steady state voltage deflection (typically between 400-800 ms).

Action Potentials (APs) were detected from continuous periods of rising membrane potential with a minimum amplitude of 30 mV. Rheobase (or threshold current for firing) was defined as the smallest current step of 800 ms that elicited at least one AP. Firing frequency (Hz) was deduced either by averaging all instantaneous frequencies of a given step (*MeanInsF*) or dividing the number of APs over time (*APs/sec*). Input-output (I-O) curves were constructed by plotting firing frequency (either *MeanInsF* or *APs/sec*) as a function of the injected current; their initial slopes (I-O gain) were obtained with a linear fit of the first 9 steps beyond rheobase. Coefficient of variation (CV) was calculated as standard deviation divided by the mean of instantaneous frequencies when at least 3 APs were elicited. This value gave an index of firing regularity; the higher the value, the more irregular the firing would be. First AP-Latency was calculated from the first AP in the spike trains following a two-fold rheobase current injection. Adaptation index (AI) was defined as the ratio of the mean of the three last instantaneous frequencies divided by the first instantaneous frequency.

AP waveform features were obtained by the averaging the measures from the first AP elicited from three consecutive depolarizing steps with a firing latency less than 100 ms. AP threshold was defined as the membrane potential at the point at which  $dV/dt > 30$  mV/ms. AP peak was its maximum potential. AP rising amplitude was measured as the difference between the threshold and the AP peak voltage. The AP rising amplitude was the difference between the threshold and the peak AP voltage. AP width was measured at the half-height of the AP rising phase. *Max depolarization rate* and *max repolarization rate* were defined as the maximum and minimum  $dV/dt$ , occurring during rising phase and falling phase respectively.

### **Cluster analysis**

We performed unsupervised cluster analysis using 17 electrophysiological parameters gathered from 142 neurons from superficial and deep layers of the presubiculum. Interneurons were grouped based on similarities of the electrophysiological variables considered, using Ward's method, and Euclidean distances as the distance measure (Ward 1963), as described previously (Simonnet et al. 2013). Cluster analysis was implemented using MATLAB (The Mathwork) and its statistics toolbox. The number of clusters in our analysis was examined using the Thorndike procedure (Thorndike 1953), where jumps in distances within clusters indicate prominent differences between neurons.

We based our classification on (1) RMP, (2) Rin, (3) Tau, (4), Sag ratio; I-O gain ((5) *MeanInsF* or (6) *APs/sec*); (7) *MeanInsF* with (8) CV; (9) latency and (10) AI at the 2-fold rheobase step; AP properties including (11) threshold, (12) width, (13) amplitude, (14) AHP, (15) rising amplitude, (16) maximum depolarization rate and (17) maximum repolarization rate.

## **Statistics**

Results are given as mean +/- SEM. Statistical analysis was performed with Prism (GraphPad Software, Inc.) and MATLAB (The Mathwork).

## ***Morphology revelation and 3D reconstruction***

After recording with pipettes containing biocytin (1-3 mg.ml<sup>-1</sup>), slices were fixed in 4% paraformaldehyde in 0.1 M phosphate buffer (PB) at 4°C for 24 hours. Thereafter, slices were rinsed three times in PBS and cryoprotected in 30% sucrose mixture at 4°C overnight. Membranes were permeabilized by three cycles of freezing/defrosting over dry ice followed by three rinses with PBS. Slices were incubated in a blocking solution containing PBS (0.1M), milk 2% and 0.3% TritonX100 for 3h at room temperature. Then, we added the nuclear marker 4,6-diamidino-2-phenylindole (DAPI) (1:1000), Streptavidin–Cy3 or Cy5 conjugate (1:500, Invitrogen, Eugene, OR, USA) in the same blocking solution for 3 hours at room temperature. After washing with PBS three times, slices were mounted on coverslips using anti-fade Prolong Gold medium. Filled cells were visualized with a QImaging Retiga EXI camera (Qimaging Surrey, BC, Canada), and scanned with an Optigrd II (Thales Optem, Qioptik, Rochester, NY, USA) on an inverted Olympus IX81 microscope. The Optigrd system permitted the acquisition of structured images and the subsequent three-dimensional reconstruction of filled neurons with the software Volocity (Improvision, Perkin-

Elmer, Coventry, UK). Stacks of 75–250 images were acquired using a 20X oil immersion objective. Stacks were then imported in NeuroLucida (MicroBrightfield, Williston, VT, USA) for digital reconstructions. The NeuroLucida explorer program was used for "layer length" analysis allowing us to determine directionality and length per layer of dendritic and axonal distribution as described previously (Simonnet et al. 2013). Layers and boundaries of the presubiculum were determined using DAPI staining. No correction for tissue shrinkage was applied.

### ***Immunohistochemistry***

Mice were anesthetized intraperitoneally with ketamine hydrochloride and xylazine (80 and 12 mg.kg<sup>-1</sup>, respectively), transcardially perfused with 0.9% saline containing heparin (100–200 UI/ml followed by 30–50 ml of a fixative solution containing 4% paraformaldehyde in 0.1 M phosphate buffer (PB). Dissected brains were post-fixed overnight in the same fixative solution at 4°C and then placed in a 30% sucrose solution at 4°C for at least 24 h. Using a slicing vibratome (Leica), 50 µm-thick horizontal sections were collected in 0.1M PBS.

## RESULTS

### ***Interneuron subtypes in presubiculum: layer distribution and immunohistochemistry in three transgenic mouse lines***

The mouse presubiculum is shown in the context of the hippocampal formation in Fig. 1A. It is similar to rat presubiculum, with high density of cell bodies in layer II.

[Figure One near here]

To examine the diversity of PV and SOM expressing interneurons in the presubiculum, we recorded from 142 interneurons from three transgenic mouse lines. To target PV interneurons, we used Pvalb-Cre mice (Hippenmeyer et al. 2005), crossed with a reporter line expressing a red fluorescent protein (RFP), td-Tomato (Ai14, (Madisen et al. 2010); Fig 1D). To target SOM interneurons, we used SST-IRES-Cre mice (Taniguchi et al. 2011) crossed with the same reporter line Ai14 (Fig 1E), and the X98 line (Ma et al. 2006), where a subset of SOM interneurons is GFP labeled (Fig 1F). Neuronal somatic location of recorded

neurons was situated on a schematic of a standardized presubiculum (Fig. 1B). To assess the laminar distribution of different interneurons subtypes, we quantified the number of fluorescently labeled interneurons in these three lines in superficial and deep layers of presubiculum. Pvalb-Cre interneurons were more numerous in superficial layers than in deep layers, while tomato-labeled Sst-Cre interneurons were more abundant in deep than in superficial layers (numbers). The expression of GFP-labeled neurons in the X98 line was more restricted, with lower absolute numbers of labeled interneurons, and a preferential distribution to superficial layers (numbers). A potential dorso-ventral gradient in the density of interneuron subtypes was examined. We counted the neurons in horizontal slices in three different depths ((a), DV xx; (b), DV xx; (c), DV xx; cf. Fig. 1C). Gradient exists or not? Panel D-E show the middle depth that was used for most recordings (close to DV xx.x, Paxinos Mouse Atlas or Allen brain atlas).

We next examined the recombination specificity of the Pvalb-Cre and Sst-Cre mouse lines, and validated the somatostatin expression in GFP labeled neuron from X98 mice. Horizontal sections of presubiculum from adult animals were stained with antibodies to PV and SOM (Fig 2A-F). The fraction of RFP+ or GFP+ cells that were immunopositive for each marker was quantified in slices from 3 animals from each line. Virtually all RFP+ neurons in the Pvalb-Cre line were PV immunopositive (count), while a small percentage was positive for SOM (count). All GFP+ neurons of the X98 line were positive for SOM and no PV labeling was found. In the Sst-Cre line, the result was less clear-cut as expected from previously described off-target recombination (Hu et al. 2013). In the presubiculum, about 15 % of Sst-Cre RFP+ cells were positive for PV, while only 85% colocalised with SOM immunostained cells (count).

[Figure two near here]

### **Cluster analysis revealed two main groups of presubicular interneurons based on electro-physiological parameters.**

To examine how presubicular PV or SOM positive interneurons classify on the basis of electrophysiological parameters, we recorded from 46 Pvalb-Cre RFP+ neurons, 61 Sst-Cre RFP+ neurons and 35 GFP+ neurons of the X98 line, in order to determine their firing patterns, passive membrane properties and action potential waveforms. Seventeen superficial layer pyramidal neurons were included as controls, to validate the analysis

method. Neurons were biocytin-filled for post-hoc revelation of their anatomy. For a subset of completely reconstructed neurons, we matched the morphology with the electrophysiological definition of interneuron clusters. Unsupervised cluster analysis using Ward's method (Ward 1963) was performed based on 17 variables listed in Table 1. Figure 3A shows the hierarchical tree diagram of clusters that emerged. The tree diagram initially separated two populations: the first branch (I.) included all principal neurons, all X98 GFP+ cells, and some Sst-Cre RFP+ cells; the second branch (II.) included all Pvalb-Cre RFP+ cells and some Sst-Cre RFP+ cells. Decreasing the cut-off value for cluster separation allowed us to completely isolate the pyramidal neurons, as a highly homogenous population of cells, in cluster 0 (cf. Fig 3A, broken vertical line). An archetypical glutamatergic cell is shown in Fig 3B. This separation comforts us with the validity of our clustering method, and while the pyramidal neurons were not considered in further detail, they served as an external reference for the interneuron containing clusters. We found two interneuron containing clusters, cluster 1 and 2, suggesting that two main inhibitory cell types were present in our data set of presubicular interneurons. Indeed, cluster 1 and cluster 2 strictly segregated X98 GFP+ neurons from Pvalb-Cre RFP+ neurons. These two mouse lines are expected to specifically label distinct interneuron types, and this is confirmed by their distribution in two distinct clusters. Many RFP+ interneurons recorded in Sst-Cre mice were similar to the somatostatin expressing X98 GFP+ neurons in cluster 1, while others, in contrast, were highly similar to Pvalb-Cre RFP+ interneurons in cluster 2.

While the Thorndike procedure suggested 3 main separations, we decided on a somewhat lower cutoff value for cluster separation, yielding two subclusters, 2a and 2b, both containing Pvalb and Sst-Cre RFP + cells. We noticed similar within-cluster Euclidean distances of clusters 1, 2a and 2b (13, 12 and 13, respectively) that will be now described in detail.

[Table One near here]//[Figure Tree near here]

### ***Cluster 1: Somatostatin expressing low rheobase adapting interneurons***

Cluster I comprised n = 65 interneurons, among which 55% were GFP+ cells from the X98 mouse line, and 45% Sst-Cre RFP+ cells. A representative cluster 1 neuron is shown in Fig. 3C, a Martinotti type X98 neuron, with adapting firing pattern and broad action potential waveform. This cell was located in layer III, and may be considered as **archetypal** for the somatostatin expressing, adapting interneurons of cluster 1.

Many cluster 1 interneurons discharged spontaneously (numbers), even before rupturing the membrane for whole-cell recording. The resting membrane potential was relatively depolarized at  $-54 \pm 1$  mV, more positive than in the other clusters. Their mean AP threshold was  $-38.6 \pm 0.4$  mV.  $R_{in}$  was  $374 \pm 17$  M $\Omega$ , about twice as high as for cluster 2 cells, and membrane time constant, tau, was  $32 \pm 2$  ms, almost three times longer than for cluster 2 cells. The firing pattern of cluster 1 cells was regular or irregular, with the highest CV at two-fold rheobase current levels ( $0.24 \pm 0.02$ ) and a stronger frequency adaptation (AI,  $0.70 \pm 0.01$ ) compared to cluster 2 cells. Examples of firing patterns from three different cells of cluster 1 are illustrated in Fig. 4A and B. Action potentials were easily initiated by positive current injection, with a mean rheobase of  $40 \pm 3$  pA. Hyperpolarizing current injections induced a pronounced voltage sag (Fig. 4B; sag ratio  $1.04 \pm 0.00$ ). Input-output curves, constructed by plotting the frequency of action potentials against injected current (Fig. 4C), had a mean initial slope of  $778 \pm 28$  Hz.nA $^{-1}$ . The firing frequency reached at double rheobase current level was  $35 \pm 2$  Hz, and the latency of the first action potential following a depolarizing current step was  $21 \pm 1$  ms. Action potentials were rather high and broad, with mean amplitudes of  $82 \pm 1$  mV and widths of  $0.29 \pm 0.01$  ms. The maximum action potential depolarization and repolarization rates were  $567 \pm 11$  and  $-329 \pm 9$  V.s $^{-1}$  respectively. Spike after-hyperpolarization was typically complex or bi-phasic (Fig. 3C), with mean maximal amplitude of  $-24 \pm 0$  mV.

### ***Cluster 2b: fast-spiking parvalbumin expressing interneurons***

Cluster 2b comprised  $n = 29$  neurons, 75% of which were RFP+ neurons from the Pvalb-Cre line, and 25% from the Sst-Cre line. An archetypal neuron for this cluster is shown in Fig. 3E, a parvalbumin expressing basket shaped interneuron with fast-spiking (FS) firing pattern. The cell body was located in layer III, and in fact all recovered neurons in this cluster were superficial layer cells.

Cluster 2b interneurons had a hyperpolarized resting membrane voltage at  $-70 \pm 1$  mV, more negative than the average of cells in clusters 1 or 2a. Their mean firing threshold was  $-42.2 \pm 0.7$  mV.  $R_{in}$  was  $137 \pm 17$  M $\Omega$ , which is half the value of cluster 2a and 3 times less than cluster 1. The membrane time constant, tau, was  $13 \pm 2$  ms, similar to cluster 2a, but almost three times lower than for cluster 1 cells. The firing pattern of cluster 2b cells was the typical non-accommodating, fast-spiking pattern of basket cells, characterized by a low CV at two-fold rheobase current levels ( $0.08 \pm 0.02$ ) and a corresponding adaptation index of  $1.00 \pm 0.02$ . Fig. 4A and B shows examples of firing patterns from three different cells of cluster 2b

(right column), which are quite stereotyped. The minimum current to drive these neurons to fire was  $202 \pm 23$  pA, a high rheobase compared to cells in cluster 1 or 2a. Virtually no voltage sag was observed in response to hyperpolarizing current injections (Fig 4.B; sag index  $1.09 \pm 0.01$ ). The input-output curves rose steeply, with a high I-O gain of  $1437 \pm 131$  Hz.nA<sup>-1</sup>. The firing frequency reached at double rheobase was very high at  $297 \pm 27$  Hz, and the latency of the first action potential in a step was short ( $8 \pm 2$  ms). Cluster 2b fast-spiking cells generated single action potentials with the shortest half width ( $0.18 \pm 0.01$  ms). Spike amplitudes were  $69 \pm 2$  mV and the maximum rates of depolarization and repolarization were  $623 \pm 26$  and  $-547 \pm 30$  V.s<sup>-1</sup> respectively. Spike afterhyperpolarization was typically simple with a mean amplitude of  $-23 \pm 1$  mV.

### ***Cluster 2a: quasi fast-spiking parvalbumin or somatostatin expressing interneurons***

Cluster 2a grouped together  $n = 48$  neurons, that were either RFP+ neurons from the Pvalb-Cre line (50%) or from the Sst-Cre line (50%). While cluster 1 adapting SOM cells and cluster 2b fast-spiking cells formed the two distinct extremes of our data set, cluster 2a contained a mix of somatostatin and parvalbumin expressing cells with intermediate values for most electrophysiological parameters. An illustrative example for cluster 2a is shown in Fig. 3D, a Sst-Cre RFP+ neuron, with quasi-FS properties and basket-cell like morphology, located in layer 5/6.

The membrane voltage of cluster 2a cells was intermediate at  $-60 \pm 1$  mV. The firing threshold was  $-37.4 \pm 0.5$  mV.  $R_{in}$  ( $189 \pm 11$  M $\Omega$ ) and membrane time constant ( $11 \pm 1$  ms) were also intermediate. The firing pattern of cluster 2a cells could be regular or quasi-fast spiking with a low CV ( $0.07 \pm 0.00$ ), similar to cluster 2b, and an adaptation index of  $0.92 \pm 0.02$ . Examples of firing patterns are shown in Fig. 4A and B. A voltage sag was moderately distinguishable (sag ratio,  $1.11 \pm 0.01$ ). Action potentials were obtained from a rheobase current level of  $113 \pm 8$  pA. Input-output curves, constructed by plotting the frequency of action potentials against injected current (Fig. 4C), had a mean initial slope of  $762 \pm 41$  Hz.nA<sup>-1</sup>, close to that of cluster 1. The firing frequency at double rheobase current level was quasi fast-spiking at  $128 \pm 7$  Hz, and the latency of the first action potential in a step was  $14 \pm 2$  ms. Action potential amplitude was  $76 \pm 1$  mV and the half width was  $0.23 \pm 0.01$  ms. The maximum action potential depolarization and repolarization rates were  $627 \pm 14$  and  $-409 \pm 15$  V.s<sup>-1</sup> respectively. Spike after-potential waveforms were either simple or complex with mean amplitude of  $-24 \pm 1$  mV.

## Morphology

Among the 142 recorded interneurons, the axonal and dendritic morphology of a subset of 28 biocytin filled cells was reconstructed using NeuroLucida. We examined how their morphologies correlated with our electrophysiologically defined groups of interneuron clusters, and with the morphological features of somatostatin or parvalbumin positive interneuron archetypes described in other cortical areas.

Figure 5A shows the somatodendritic form of five somatostatin expressing neurons that were grouped in cluster 1. Somata were ovoid, located either in superficial or deep layers. The axons emerged from the cell body or from an ascending dendritic trunk. X98 axonal tree was compact with one part that ramified immediately above the cell body in layer III. Multiple ascending axon branches extended towards layer I where dense axon collaterals branched horizontally for distances as long as 300 $\mu$ m (Martinotti type interneurons, Wang et al. 2004). The dendritic arbor of X98 neurons was multipolar. Sst-Cre RFP+ neurons of cluster 1 emitted a local axonal arbor in the vicinity of the cell body. Some axon collaterals reached layer I, but had little ramifications there. Sst-Cre RFP+ neuron dendrites were locally distributed around the perisomatic region within a radius of 150-200  $\mu$ m and preferentially oriented towards deeper layers. The mean total axonal length of reconstructed cluster 1 interneurons ( $n = 3$ ) was  $11548 \pm 1201 \mu\text{m}$ , which is significantly higher compared to cluster 2a and 2b interneurons. Their mean dendritic length was significantly shorter ( $1500 \pm 1201 \mu\text{m}$ ;  $n = 3$ ;  $p$  value). Seven representative cluster 2a interneurons are shown in Figure 5B. Their somata were located either in superficial or deep layers. Some superficial layer neurons including Pvalb3 with putative chandelier morphology, and Sst5, had their axon and dendrites entirely limited to superficial layers. Some deep layer neurons, Pvalb2 and Sst4, (and 8 other neurons, not shown) were exclusively covering deep layers with axons and dendrites. In these examples, axonal trees were distributed locally around the soma in their home layer, with little asymmetrical upward or downward shift, or sideways shift, with respect to the soma. Such local axons are typical for basket cells. Sst3 had some dendrites extending farther away from its home layer, to superficial layers II and III. Pvalb1, conversely, had its soma in layer V, but the axon projected across deep and superficial layers, with dense ramifications specifically in layer II. Sst6 was atypical, with its cell body located in superficial layer III but its expansive axon - quasi non-overlapping with the dendrites - crossed downward to the deep layers, sparsely covering a large area. Some neurons ( $n = 6$ ) had axon endings in the neighboring region of the parasubiculum, as indicated with broken vertical lines for Sst1 (3063  $\mu\text{m}$ , about 4% of total length), Pvalb1 (2187  $\mu\text{m}$ ) and Pvalb3 (xxx  $\mu\text{m}$ ).

The mean total axonal length for all reconstructed interneurons of cluster 2a was  $6589 \pm 944 \mu\text{m}$  ( $n = 13$ ). Dendrites in cluster 2a interneurons usually emanated in all directions, some running up to  $500 \mu\text{m}$  away from the soma, and their mean total length was  $2201 \pm 138 \mu\text{m}$  ( $n = 13$ ).

Examples of interneurons of cluster 2b are shown in Fig. 5C, with their somata located in superficial layers. In 3 out of 4 neurons, the axon remained restricted to the superficial home layers, with ascending rather than downward projecting collaterals (Pvalb4, Pvalb5 and Sst7). The axonal tree was usually dense ( $n = 6$ ). Pvalb5 had a particularly dense and huge axon ramifying in all directions with farther-reaching axon collaterals, reminiscent of large basket cells (Wang et al. 2002). Similar to cluster 2a, cluster 2b interneurons were mostly multipolar at the somato-dendritic level with an evenly distributed dendritic arbor that ramified near the cell body. Pvalb4 and one other similar neuron (not shown;  $n = 2$ ) had a vertically biased dendritic arbor that projected into both deep and superficial neighboring layers. Dendrites could spread towards superficial layer (Pvalb5) and/or deep layers (Sst7). One atypical cell was located at the boundary between layer 3 and 4: primary dendrites were distributed around the whole perimeter of the cell body surrounded by a dense axonal tree; a dendritic tuft extended towards the pial surface, ending in layer II. The mean total axonal and dendritic length of cluster 2b interneurons was respectively of  $8165 \pm 1658 \mu\text{m}$  and  $2277 \pm 403 \mu\text{m}$  ( $n = 8$ ).

## DISCUSSION

This study provides the first electrophysiological and morphological characterization of PV expressing and SOM expressing interneurons in mouse presubiculum. Firing patterns and active and passive membrane properties were examined in interneurons from three transgenic mouse lines, Pvalb-Cre Sst-Cre and X98 mice. Unsupervised cluster analysis based on electrophysiological parameters grouped the recorded interneurons into 3 clusters. This classification partly followed neurochemical marker expression, and we found the classical archetypes of SOM adapting neurons (in cluster 1) and fast-spiking PV neurons (in cluster 2b) in presubiculum. An intermediate cluster (cluster 2a) revealed similarities between subpopulations of some quasi fast spiking PV or SOM expressing neurons. The reliability of our clustering approach was supported by its ability to group pyramidal cells taken as controls. The electrical and morphological profile of interneurons in superficial and deep layers of presubiculum is found to share common features with the diversity of

interneurons in hippocampus and neocortex. Our results suggest that the inhibitory network of the presubicular microcircuit is likely to be subdivided into distinct functional territories.

### ***Mouse lines and neurochemical marker expression pattern in presubiculum***

The use of genetically modified mouse lines is a helpful tool to study specific subsets of neurons. We find a distinct distribution of Pvalb-Cre RFP, Sst-Cre RFP and X98 GFP interneurons in superficial versus deep layers of presubiculum: presubicular Pvalb-Cre RFP cells were preferentially distributed in thalamorecipient superficial layers (L-II/III) while Sst-Cre RFP cells were more densely located in deep layers (L-V/VI). Previous work in mouse visual cortex on the contrary found that PV and SOM interneurons were rather evenly distributed across superficial and deep layers (Gonchar et al. 2007). Xu et al. (2010) and Ma et al. (2006) found - similarly to our results - higher SOM positive cell densities in deep layers, even though there are also region specific differences between visual, frontal and somatosensory cortical areas, as well as species specific differences between mouse and rat cortex (Ma et al. 2006; Xu et al. 2010). The PV cell counts in the study by Xu et al. (2010) were rather higher in deep layers, unlike the higher densities we find for PvalbCre RFP cells in superficial layers of presubiculum. Our study therefore reveals a unique distribution of interneuron subtypes that accumulate in distinct layers of presubiculum.

Immunohistochemistry confirmed that the Pvalb-Cre line almost exclusively labels PV expressing neurons, while hardly any were SOM positive. Conversely, all X98 GFP neurons were positive for SOM. The validation of SOM expression in the Sst-Cre RFP+ cells was less clear cut in our hands. The same Sst-Cre line has been used previously by several authors, and it was generally assumed that Cre-mediated recombination was restricted to SOM interneurons (Gentet et al. 2012; Cottam et al. 2013; Kvitsiani et al. 2013; Xu et al. 2013). Only recently it was pointed out by Hu et al. (2013), that an average of 6-10% of Sst-Cre RFP+ neurons in five different cortical areas (cingulate, M1, S1, A1, and V1) were in fact fast-spiking PV expressing interneurons. In presubiculum, about 85% of Sst-Cre RFP+ cells were SOM positive, while 15% were PV positive. This result may be explained by off-target recombination, which may occur in PV cells that transiently expressed SOM during development (Hu et al., 2013). In that case, the off-target recombination rate could be higher in presubiculum than in other brain regions. Even though PV and SOM expression do not overlap in neocortical adult interneurons in rat or mouse (Gonchar and Burkhalter 1997; Kawaguchi and Kubota 1997; Xu et al. 2010; Kubota et al. 2011), on the mRNA level, both PV and SOM mRNA may be detected in a same interneuron (Cauli et al. 2000). In the

hippocampus, on the other hand, bistratified neurons or oriens-locunosum-moleculare interneurons may coexpress PV and SOM (Jinno and Kosaka 2000; Klausberger et al. 2003; Somogyi and Klausberger 2005; Fishell and Rudy 2011; Katona et al. 2014). We therefore consider the possibility that in the presubiculum some PV positive Sst-Cre RFP+ neurons might also coexpress the two neuropeptides.

### ***Interneuron classification***

Since the early work of Ramon y Cajal (Ramon y Cajal 1911), numerous subtypes of interneurons have been described as a functionally heterogeneous population according to their electrophysiological, morphological, molecular and developmental characteristics in different areas of the brain. Here we asked whether in presubiculum, neurochemically defined interneurons from the three transgenic mouse lines were electrophysiologically and anatomically distinct. The fundamental question of how to define different classes of interneurons (Parra et al. 1998) or their structured continuum (Battaglia et al. 2013) still remains, objective criteria have been proposed to classify interneurons into distinct groups which should help to understand the organizing principles of interneuron diversity (Markram et al. 2004; Petilla Interneuron Nomenclature Group et al. 2008; Druckmann et al. 2012). Ward's unsupervised classification method allowed us to objectively identify neuron types based on a combination of 17 electrophysiological parameters. Morphological criteria were then correlated with the resulting groups.

We expected fluorescently labeled interneurons in the PvalbCre and X98 line to differ in their electrical properties, and presumed similarities between Sst-Cre and X98 fluorescent cells. Ward's method has the advantage not to require any preliminary supposition about the number of cell types, while it tends to achieve a lesser significant separation between neuronal classes compared to K-means clustering (Cauli et al. 2000; Karagiannis et al. 2009). Our cluster analysis completely separated presubicular glutamatergic pyramidal cells, that were included as controls (cluster 0), from GABAergic inhibitory interneurons (clusters 1 and 2), thus validating and supporting the reliability of our analysis scheme. This separation also indicated a meaningful cutoff value for the number of distinct clusters. We were satisfied to find interneurons originating from the X98 mouse line only in cluster 1, while interneurons from the Pvalb-Cre line grouped together on a separate branch, in cluster 2 (Fig. 3). Indeed the X98 interneurons correspond closely to the archetypical adapting SOM cells (Fig. 3C), while Pvalb-cre neurons had a classical fast-spiking firing pattern (Fig. 3E). These two interneuron classes have been defined previously in both hippocampus and

neocortical areas (Cauli et al. 1997; Kawaguchi and Kubota 1997; Markram et al. 2004; Somogyi and Klausberger 2005; Petilla Interneuron Nomenclature Group et al. 2008; Fishell and Rudy 2011).

The “right” number of clusters using the Wards method may be suggested by the Thorndike procedure. Thorndike yields the mathematically optimal cut-off value for maximizing information content. Biologically meaningful interneuron clusters however would ideally correspond to functionally distinct interneuron types. We therefore tentatively set a cut-off threshold a bit lower, so that Cluster 2 became subdivided in 2 subclusters 2a and 2b. Somewhat surprisingly, interneurons from the Sst-cre line were found in all interneuron containing clusters (cluster 1, 2a and 2b).

### ***Two main archetypes of GABAergic interneurons***

Cluster 1 interneurons corresponded typically to adapting-SOM type interneurons. As described in hippocampus (oriens-lacunosum-moleculare interneurons) and neocortex (Martinotti cells), these cells were highly excitable and characterized by rather depolarized membrane potentials and pronounced voltage sags. All cells in this cluster were from SOM expressing X98 interneurons or from the Sst-Cre line. They displayed a regular-spiking firing pattern with a consistently marked frequency adaptation. Action potentials were characterized by their high amplitude and half-durations (Wang et al. 2004; Halabisky et al. 2006; Ma et al. 2006; Uematsu et al. 2007; Karagiannis et al. 2009; Xu et al. 2013).

The morphologies of cluster 1 interneurons revealed that X98 GFP+ cells generally had multipolar dendrites and axons sending several collaterals to layers 2/3 and particularly layer 1 where the collaterals branched horizontally for distances as long as 300µm, as previously described for Martinotti-cells (Wang et al. 2004; Ma et al. 2006). Sst-Cre RFP+ cells of cluster 1 had a sparse and local axonal arborization similar to subtypes of SOM neurons described in the GIN mouse line (McGarry et al. 2010). Cluster 1 interneurons are well suited to control inputs to principal cell apical dendrites and tufts. Specifically, they could interact with afferent excitatory projections to presubicular layer I or III, such as retrosplenial and thalamic inputs (van Groen and Wyss 1990b).

Cluster 2b corresponded to the well-established FS cells, that are similarly found in hippocampus (Somogyi and Klausberger 2005) and neocortex (Kawaguchi 1995). Most of these interneurons were recorded from the Pvalb-Cre line, and a small fraction from the Sst-Cre line. If off-target recombination falsely labeled PV interneurons in the Sst-Cre line, these

neurons could well be grouped together with the other FS-PV cells in cluster 2b. Presubicular FS cells were characterized by a hyperpolarized resting membrane voltage, the lowest input resistance and the shortest membrane time constant. They displayed the lowest electrical excitability when probed with somatic current injections, and showed the least marked voltage sag in response to hyperpolarizing steps. A delay from depolarization to the appearance of the first AP commonly found in FS cells is likely to be correlated with a more depolarized threshold mediated by the Kv1.1 subunit (Goldberg et al. 2008). Stronger depolarizing stimuli gave rise to sustained high-frequency trains of narrow and fast spikes with little or no frequency adaptation, that requires fast delayed rectifier Kv3-mediated currents (Martina et al. 1998; Erisir et al. 1999). Hence, the AP firing pattern can be described as fast spiking, with subpartitions including continuous, delayed or stuttering firing (Druckmann et al. 2012).

Anatomically, FS cells have been well characterized in neocortical superficial layers where they correspond mainly to basket cells and chandelier cells (Kawaguchi 1995; Wang et al. 2002) and to basket cells as well in hippocampus (Freund and Buzsáki 1996; Somogyi and Klausberger 2005). We cannot identify their postsynaptic target cells from our data, but with analogy to other cortical areas we presume that cluster 2b basket cells contact the perisomatic region of presubicular principal neurons. Most presubicular cluster 2b FS cells had multipolar dendrites and based on their axonal arbor, they have been shown to vary in size (small or large basket-cell) and axonal projections (mostly local, some translaminar or transcolumnar) similarly to previous studies (Wang et al. 2002; Karube et al. 2004; Markram et al. 2004). The RFP cells from the Sst-Cre line had basket like morphologies similar to the Pvalb-Cre RFP neurons in this cluster.

### ***... and a transitional edge cluster***

Cluster 2a grouped together a large subset of Sst-Cre RFP interneurons with an equal number of Pvalb-Cre RFP interneurons. It is known from other neocortical areas that the population of SOM positive neurons comprises several subtypes, such as the Martinotti type cells (Wang et al. 2004), the SOM cells in the X94 line (Ma et al. 2006), as well as other subtypes (Halabisky et al. 2006; Mcgarry et al. 2010). These cluster 2a Sst-cre RFP cells in presubiculum are clearly separate from the classical adapting SOM-archetype that is represented in our cluster 1. Their electrical features, as well as those of Pvalb-Cre RFP cells in cluster 2a, include intermediate values for membrane potential, a relatively small resistance and short time constant approaching that of archetypal FS cells. Cluster 2a cells

from both Cre mouse lines had spikes of short duration and produced diverse firing patterns ranging from single spiking, to stuttering, to regular spiking. At higher firing frequencies, they displayed a quasi-fast-spiking firing pattern due to their weak to absent frequency adaptation. But cluster 2a cells are also distinct from the classical fast-spiking PV cells in cluster 2b.

Somato-dendritic morphology was mostly similar to basket cells, for both, RFP cells originating from the Sst-Cre and the Pvalb-Cre line (Wonders and Anderson 2006; Kubota 2014). These cells tended to branch within their home layer revealing intra-laminar projections that could mediate early and late blanket inhibition (Karnani et al. 2014). Some basket cell morphologies did not follow this pattern, with dendrites oriented upwards to seemingly target layer II cell-bodies, but also downward to deep layer V/VI. Or conversely, a soma and dendritic arborization in superficial layers with an axonal arbor extending to deep layers. Such cells could be specialized in translaminar inhibition (Bortone et al. 2014).

### ***A structured continuum of diversity***

We suggest that in presubiculum, a continuum of diversity exists within the interneuron populations that we have examined, ranging from the archetypal SOM adapting cells to the archetypal fast-spiking PV cells. This continuum is graded, with the existence of intermediate cluster 2a interneurons, at the edge between these archetypes, containing equally Pvalb-Cre and Sst-Cre RFP cells. Based on the theory of fuzzy sets, a structured continuum has been suggested previously as an alternative classification scheme for cortical interneurons (Battaglia et al. 2013). This seems helpful whenever the attribution of specific neurons to a single defined class is difficult. In presubiculum, cluster 2a manifests the convergence of traits from the SOM-adapting and the PV fast-spiking archetype.

Interneuron diversity is correlated with the developmental origins of interneurons. Both PV and SOM interneurons along with the majority of neocortical interneurons originate from the medial ganglionic eminence (Xu et al. 2004; Wonders and Anderson 2006; Batista-Brito and Fishell 2009; Miyoshi et al. 2010; Kepecs and Fishell 2014). While the adapting-SOM and the FS-PV cells may be archetypal, their common origin could have left intermediate “edge cells” at the transition between these two archetypes, reflecting a relic of their shared embryonic origin. Interestingly, clones from a same progenitor lineage are equally likely to be comprised of mixed SST- and PV-expressing interneurons rather than one subtype (Kepecs and Fishell 2014). Could that explain the equal presence of Sst-Cre and Pvalb-cre RFP cells

in a same interneuron class? Even if SOM was only expressed transiently in Sst-Cre cells of cluster 2a, they would still be RFP+ for life, due to Cre-recombinase expression and Cre-mediated recombination (Hu et al. 2013). In future studies it will be interesting to determine the molecular phenotypes of these quasi-FS RFP+ Sst-Cre interneurons and identify any differentially expressed calcium binding proteins or neuropeptides.

PV and SOM neurons not only share a common origin, the MGE, but here we consider a population of interneurons that have migrated in a similar spatio-temporal fashion, and in the presubiculum they arguably receive shared **local cues** that could control neuritic branching and orientate phenotypic traits (Adams and Eichmann 2010; Battaglia et al. 2013). The presubiculum lies at the junction between the hippocampal archicortex and the neocortex (O'Mara et al. 2001; Simonnet et al. 2013) and even though its six-layered cytoarchitecture is similar to a neocortical organization, the heterogeneous and somewhat atypical populations of presubicular PV and SOM interneurons described in the present work could have emerged due to the transitional location of this cortical region. Possibly uncommonly similar electrophysiological and anatomical features between Sst-Cre and Pvalb-Cre RFP cells in cluster 2a could have been generated due to local signals in the presubiculum.

### ***Implication of interneurons in presubicular microcircuit function***

Studying neuronal diversity is a tool to establish a correspondence between neuronal types and their respective connectivity patterns and functions in the brain. By analogy with other cortical areas, it is probable that GABAergic inhibition in the presubiculum is involved in temporal processing, in controlling sensitivity or sharpening selectivity of the head directional signal.

FS cells of cluster 2b may form proximal, perisomatic synapses on target neurons, and so could quickly suppress the output of target neurons, mediating fast inhibition, and precision timing as in hippocampus or somatosensory cortex (Miles et al. 1996; Fricker and Miles 2000; Pouille and Scanziani 2001; Gabernet et al. 2005). In contrast, cluster 1 Martinotti cell inhibition might be more graded and selective by inhibit excitatory inputs arriving at dendritic sites close to the location of inputs, such as retrosplenial or thalamic inputs to layer I of presubiculum. Presubicular Martinotti cells are often reciprocally connected with principal neurons (Simonnet and Fricker, not shown, manuscript in preparation), and their recruitment might limit excitatory inputs or mediate lateral inhibition onto nearby cells (Silberberg and Markram 2007). Mapping studies using two-photon glutamate uncaging showed a lack of

fine level of connectivity of both PV and SOM interneurons in the mouse somatosensory and frontal cortex (Fino and Yuste 2011; Packer and Yuste 2011). Presubicular PV or SOM interneurons with local, sparse or dense axonal trees similar to basket-cells could innervate their postsynaptic targets without any evident specificity, as if they were spreading a “blanket of inhibition” into the microcircuit (Karnani et al. 2014). Futures studies combining recordings from principal cells and interneurons will let us examine connectivity motifs of interneuron subclasses in presubiculum, and determine similarities and differences with the inhibitory circuit design in other parts of the cortex.

## ACKNOWLEDGEMENTS

The authors declare no competing financial interests. We thank Alberto Bacci and Caroline Mailhes for help and support. This work was supported by ANR Grant JCJC R10206DD (D.F.); French Ministry (M.N.); the Région Ile-de-France and FRM (J. S.) and INSERM.

## ABBREVIATIONS

ADP, after-depolarisation	InsF, instantaneous frequency
AP, action potential	LAI, late adaptation index
AHP, after-hyperpolarization	PV, parvalbumin
BI, bursting index	RFP, red fluorescent protein (tdTomato)
C, capacitance	RMP, resting membrane potential
DAPI, 4',6-diamidino-2-phenylindole	RS, regular spiking
EGTA, ethylene glycol tetraacetic acid	$R_{in}$ , input resistance
FHP, first after-hyperpolarization	SHP, second after-hyperpolarization
GFP, green fluorescent protein	SOM, somatostatin
IAI, initial adaptation index	TTX, tetrodotoxin
IB, intrinsic bursting	$V_m$ , membrane potential

## REFERENCES

- Adams RH, Eichmann A. 2010. Axon guidance molecules in vascular patterning. *Cold Spring Harbor Perspectives in Biology*. 2:a001875.
- Batista-Brito R, Fishell G. 2009. The developmental integration of cortical interneurons into a functional network. *Current topics in developmental biology*. 87:81–118.
- Battaglia D, Karagiannis A, Gallopin T, Gutch HW, Cauli B. 2013. Beyond the frontiers of neuronal types. *Front Neural Circuits*. 7:13.
- Boccarda CN, Sargolini F, Thoresen VH, Solstad T, Witter MP, Moser EI, Moser M-B. 2010. Grid cells in pre- and parasubiculum. *Nature Publishing Group*. 13:987–994.
- Bortone DS, Olsen SR, Scanziani M. 2014. Translaminar Inhibitory Cells Recruited by Layer 6 Corticothalamic Neurons Suppress Visual Cortex. *Neuron*. 1–12.
- Calton JL, Stackman RW, Goodridge JP, Archey WB, Dudchenko PA, Taube JS. 2003. Hippocampal place cell instability after lesions of the head direction cell network. *Journal of Neuroscience*. 23:9719–9731.

- Cauli B, Audinat E, Lambolez B, Angulo MC, Ropert N, Tsuzuki K, Hestrin S, Rossier J. 1997. Molecular and physiological diversity of cortical nonpyramidal cells. *J Neurosci.* 17:3894–3906.
- Cauli B, Porter JT, Tsuzuki K, Lambolez B, Rossier J, Quenet B, Audinat E. 2000. Classification of fusiform neocortical interneurons based on unsupervised clustering. *Proc Natl Acad Sci USA.* 97:6144–6149.
- Chrobak JJ, Buzsaki G. 1996. High-frequency oscillations in the output networks of the hippocampal-entorhinal axis of the freely behaving rat. *J Neurosci.* 16:3056–3066.
- Cobb SR, Buhl EH, Halasy K, Paulsen O, Somogyi P. 1995. Synchronization of neuronal activity in hippocampus by individual GABAergic interneurons. *Nature.* 378:75–78.
- Cottam JCH, Smith SL, Hausser M. 2013. Target-Specific Effects of Somatostatin-Expressing Interneurons on Neocortical Visual Processing. *Journal of Neuroscience.* 33:19567–19578.
- Defelipe J, López-Cruz PL, Benavides-Piccione R, Bielza C, Larrañaga P, Anderson S, Burkhalter A, Cauli B, Fairén A, Feldmeyer D, Fishell G, Fitzpatrick D, Freund TF, González-Burgos G, Hestrin S, Hill S, Hof PR, Huang J, Jones EG, Kawaguchi Y, Kisvárdy Z, Kubota Y, Lewis DA, Marin O, Markram H, Mcbain CJ, Meyer HS, Monyer H, Nelson SB, Rockland K, Rossier J, Rubenstein JLR, Rudy B, Scanziani M, Shepherd GM, Sherwood CC, Staiger JF, Tamas G, Thomson A, Wang Y, Yuste R, Ascoli GA. 2013. New insights into the classification and nomenclature of cortical GABAergic interneurons. *Nat Rev Neurosci.* 14:202–216.
- Druckmann S, Hill S, Schürmann F, Markram H, Segev I. 2012. A Hierarchical Structure of Cortical Interneuron Electrical Diversity Revealed by Automated Statistical Analysis. *Cerebral Cortex.* 23:2994–3006.
- Dumitriu D, Cossart R, Huang J, Yuste R. 2006. Correlation Between Axonal Morphologies and Synaptic Input Kinetics of Interneurons from Mouse Visual Cortex. *Cerebral Cortex.* 17:81–91.
- Erisir A, Lau D, Rudy B, Leonard CS. 1999. Function of specific K(+) channels in sustained high-frequency firing of fast-spiking neocortical interneurons. *Journal of Neurophysiology.* 82:2476–2489.
- Fino E, Yuste R. 2011. Dense inhibitory connectivity in neocortex. *Neuron.* 69:1188–1203.
- Fishell G, Rudy B. 2011. Mechanisms of Inhibition within the Telencephalon: “Where the Wild Things Are.” *Annu Rev Neurosci.* 34:535–567.
- Freund TF, Buzsáki G. 1996. Interneurons of the hippocampus. *Hippocampus.* 6:347–470.
- Fricker D, Miles R. 2000. EPSP amplification and the precision of spike timing in hippocampal neurons. *Neuron.* 28:559–569.
- Fricker D, Miles R. 2001. Interneurons, spike timing, and perception. *Neuron.* 32:771–774.
- Gabernet L, Jadhav SP, Feldman DE, Carandini M, Scanziani M. 2005. Somatosensory integration controlled by dynamic thalamocortical feed-forward inhibition. *Neuron.* 48:315–327.
- Gentet LJ, Kremer Y, Taniguchi H, Huang ZJ, Staiger JF, Petersen CCH. 2012. Unique functional properties of somatostatin-expressing GABAergic neurons in mouse barrel cortex. *Nature Publishing Group.* 15:607–612.
- Goldberg EM, Clark BD, Zaghera E, Nahmani M, Erisir A, Rudy B. 2008. K+ channels at the axon initial segment dampen near-threshold excitability of neocortical fast-spiking GABAergic interneurons. *Neuron.* 58:387–400.
- Golowasch J, Thomas G, Taylor AL, Patel A, Pineda A, Khalil C, Nadim F. 2009. Membrane capacitance measurements revisited: dependence of capacitance value on measurement method in nonisopotential neurons. *Journal of Neurophysiology.*

102:2161–2175.

- Gonchar Y, Burkhalter A. 1997. Three distinct families of GABAergic neurons in rat visual cortex. *Cereb Cortex*. 7:347–358.
- Gonchar Y, Wang Q, Burkhalter A. 2007. Multiple distinct subtypes of GABAergic neurons in mouse visual cortex identified by triple immunostaining. *Front Neuroanat*. 1:3.
- Halabisky B, Shen F, Huguenard JR, Prince DA. 2006. Electrophysiological classification of somatostatin-positive interneurons in mouse sensorimotor cortex. *Journal of Neurophysiology*. 96:834–845.
- Helm J, Akgul G, Wollmuth LP. 2013. Subgroups of parvalbumin-expressing interneurons in layers 2/3 of the visual cortex. *Journal of Neurophysiology*. 109:1600–1613.
- Hippenmeyer S, Vrieseling E, Sigrist M, Portmann T, Laengle C, Ladle DR, Arber S. 2005. A developmental switch in the response of DRG neurons to ETS transcription factor signaling. *PLoS Biol*. 3:e159.
- Honda Y, Ishizuka N. 2004. Organization of connectivity of the rat presubiculum: I. Efferent projections to the medial entorhinal cortex. *J Comp Neurol*. 473:463–484.
- Hu H, Cavendish JZ, Agmon A. 2013. Not all that glitters is gold: off-target recombination in the somatostatin-IRES-Cre mouse line labels a subset of fast-spiking interneurons. *Front Neural Circuits*. 7:195.
- Isaacson JS, Scanziani M. 2011. How Inhibition Shapes Cortical Activity. *Neuron*. 72:231–243.
- Jinno S, Kosaka T. 2000. Colocalization of parvalbumin and somatostatin-like immunoreactivity in the mouse hippocampus: quantitative analysis with optical dissector. *J Comp Neurol*. 428:377–388.
- Karagiannis A, Gallopin T, Dávid C, Battaglia D, Geoffroy H, Rossier J, Hillman EMC, Staiger JF, Cauli B. 2009. Classification of NPY-expressing neocortical interneurons. *Journal of Neuroscience*. 29:3642–3659.
- Karnani MM, Agetsuma M, Yuste R. 2014. ScienceDirectA blanket of inhibition: functional inferences from dense inhibitory connectivity. *Current Opinion in Neurobiology*. 26:96–102.
- Karube F, Kubota Y, Kawaguchi Y. 2004. Axon Branching and Synaptic Bouton Phenotypes in GABAergic Nonpyramidal Cell Subtypes. *Journal of Neuroscience*. 24:2853–2865.
- Katona L, Lapray D, Viney TJ, Oulhaj A, Borhegyi Z, Micklem BR, Klausberger T, Somogyi P. 2014. Sleep and movement differentiates actions of two types of somatostatin-expressing GABAergic interneuron in rat hippocampus. *Neuron*. 82:872–886.
- Kawaguchi Y. 1995. Physiological subgroups of nonpyramidal cells with specific morphological characteristics in layer II/III of rat frontal cortex. *J Neurosci*. 15:2638–2655.
- Kawaguchi Y, Kubota Y. 1997. GABAergic cell subtypes and their synaptic connections in rat frontal cortex. *Cereb Cortex*. 7:476–486.
- Kepecs A, Fishell G. 2014. Interneuron cell types are fit to function. *Nature*. 505:318–326.
- Klausberger T, Márton LF, Baude A, Roberts JDB, Magill PJ, Somogyi P. 2003. Spike timing of dendrite-targeting bistratified cells during hippocampal network oscillations in vivo. *Nat Neurosci*. 7:41–47.
- Kononenko NL, Witter MP. 2012. Presubiculum layer III conveys retrosplenial input to the medial entorhinal cortex. *Hippocampus*. 22:881–895.
- Kubota Y. 2014. Untangling GABAergic wiring in the cortical microcircuit. *Current Opinion in Neurobiology*. 26:7–14.
- Kubota Y, Shigematsu N, Karube F, Sekigawa A, Kato S, Yamaguchi N, Hirai Y, Morishima

- M, Kawaguchi Y. 2011. Selective Coexpression of Multiple Chemical Markers Defines Discrete Populations of Neocortical GABAergic Neurons. *Cerebral Cortex*. 21:1803–1817.
- Kvitsiani D, Ranade S, Hangya B, Taniguchi H, Huang JZ, Kepecs A. 2013. Distinct behavioural and network correlates of two interneuron types in prefrontal cortex. *Nature*. 498:363–366.
- Ma Y, Hu H, Berrebi AS, Mathers PH, Agmon A. 2006. Distinct subtypes of somatostatin-containing neocortical interneurons revealed in transgenic mice. *Journal of Neuroscience*. 26:5069–5082.
- Madisen L, Zwingman TA, Sunkin SM, Oh SW, Zariwala HA, Gu H, Ng LL, Palmiter RD, Hawrylycz MJ, Jones AR, Lein ES, Zeng H. 2010. A robust and high-throughput Cre reporting and characterization system for the whole mouse brain. *Nature Publishing Group*. 13:133–140.
- Markram H, Toledo-Rodriguez M, Wang Y, Gupta A, Silberberg G, Wu C. 2004. Interneurons of the neocortical inhibitory system. *Nat Rev Neurosci*. 5:793–807.
- Martina M, Schultz JH, Ehmke H, Monyer H, Jonas P. 1998. Functional and molecular differences between voltage-gated K<sup>+</sup> channels of fast-spiking interneurons and pyramidal neurons of rat hippocampus. *J Neurosci*. 18:8111–8125.
- McGarry LM, Packer AM, Fino E, Nikolenko V, Sippy T, Yuste R. 2010. Quantitative classification of somatostatin-positive neocortical interneurons identifies three interneuron subtypes. *Front Neural Circuits*. 4:12.
- Miles R, Tóth K, Gulyás AI, Hajos N, Freund TF. 1996. Differences between somatic and dendritic inhibition in the hippocampus. *Neuron*. 16:815–823.
- Miyoshi G, Hjerling-Leffler J, Karayannis T, Sousa VH, Butt SJB, Battiste J, Johnson JE, Machold RP, Fishell G. 2010. Genetic Fate Mapping Reveals That the Caudal Ganglionic Eminence Produces a Large and Diverse Population of Superficial Cortical Interneurons. *Journal of Neuroscience*. 30:1582–1594.
- O'Mara SM, Commins S, Anderson M, Gigg J. 2001. The subiculum: a review of form, physiology and function. *Prog Neurobiol*. 64:129–155.
- Packer AM, Yuste R. 2011. Dense, unspecific connectivity of neocortical parvalbumin-positive interneurons: a canonical microcircuit for inhibition? *Journal of Neuroscience*. 31:13260–13271.
- Parra P, Gulyás AI, Miles R. 1998. How many subtypes of inhibitory cells in the hippocampus? *Neuron*. 20:983–993.
- Perrenoud Q, Rossier J, Geoffroy H, Vitalis T, Gallopin T. 2012. Diversity of GABAergic Interneurons in Layer VIa and VIb of Mouse Barrel Cortex. *Cerebral Cortex*.
- Petilla Interneuron Nomenclature Group, Ascoli GA, Alonso-Nanclares L, Anderson SA, Barrionuevo G, Benavides-Piccione R, Burkhalter A, Buzsáki G, Cauli B, Defelipe J, Fairén A, Feldmeyer D, Fishell G, Fregnac Y, Freund TF, Gardner D, Gardner EP, Goldberg JH, Helmstaedter M, Hestrin S, Karube F, Kisvárdy ZF, Lambollez B, Lewis DA, Marin O, Markram H, Muñoz A, Packer A, Petersen CCH, Rockland KS, Rossier J, Rudy B, Somogyi P, Staiger JF, Tamas G, Thomson AM, Toledo-Rodriguez M, Wang Y, West DC, Yuste R. 2008. Petilla terminology: nomenclature of features of GABAergic interneurons of the cerebral cortex. *Nat Rev Neurosci*. 9:557–568.
- Pouille F, Scanziani M. 2001. Enforcement of temporal fidelity in pyramidal cells by somatic feed-forward inhibition. *Science*. 293:1159–1163.
- Ramon y Cajal S. 1911. *Histologie du Systeme Nerveux de L'Homme et des Vertebres*. Maloine. ed. Paris.
- Rowland DC, Weible AP, Wickersham IR, Wu H, Mayford M, Witter MP, Kentros CG. 2013.

- Transgenically Targeted Rabies Virus Demonstrates a Major Monosynaptic Projection from Hippocampal Area CA2 to Medial Entorhinal Layer II Neurons. *Journal of Neuroscience*. 33:14889–14898.
- Rudy B, Fishell G, Lee S, Hjerling-Leffler J. 2010. Three groups of interneurons account for nearly 100% of neocortical GABAergic neurons. *Devel Neurobio*. 71:45–61.
- Silberberg G, Markram H. 2007. Disynaptic inhibition between neocortical pyramidal cells mediated by Martinotti cells. *Neuron*. 53:735–746.
- Simonnet J, Eugène E, Cohen I, Miles R, Fricker D. 2013. Cellular neuroanatomy of rat presubiculum. *Eur J Neurosci*. 37:583–597.
- Somogyi P, Klausberger T. 2005. Defined types of cortical interneurone structure space and spike timing in the hippocampus. *J Physiol (Lond)*. 562:9–26.
- Taniguchi H, He M, Wu P, Kim S, Paik R, Sugino K, Kvitsani D, Fu Y, Lu J, Lin Y, Miyoshi G, Shima Y, Fishell G, Nelson SB, Huang ZJ. 2011. A Resource of Cre Driver Lines for Genetic Targeting of GABAergic Neurons in Cerebral Cortex. *Neuron*. 71:995–1013.
- Taube JS. 2007. The head direction signal: origins and sensory-motor integration. *Annu Rev Neurosci*. 30:181–207.
- Taube JS, Muller RU, Ranck JB. 1990. Head-direction cells recorded from the postsubiculum in freely moving rats. II. Effects of environmental manipulations. *J Neurosci*. 10:436–447.
- Thorndike RL. 1953. Who belongs in the family? *Psychometrika*. 18:267–276.
- Uematsu M, Hirai Y, Karube F, Ebihara S, Kato M, Abe K, Obata K, Yoshida S, Hirabayashi M, Yanagawa Y, Kawaguchi Y. 2007. Quantitative Chemical Composition of Cortical GABAergic Neurons Revealed in Transgenic Venus-Expressing Rats. *Cerebral Cortex*. 18:315–330.
- van Groen T, Wyss JM. 1990a. The connections of presubiculum and parasubiculum in the rat. *Brain Res*. 518:227–243.
- van Groen T, Wyss JM. 1990b. The postsubicular cortex in the rat: characterization of the fourth region of the subicular cortex and its connections. *Brain Res*. 529:165–177.
- van Haften T, Wouterlood FG, Jorritsma-Byham B, Witter MP. 1997. GABAergic presubicular projections to the medial entorhinal cortex of the rat. *J Neurosci*. 17:862–874.
- Van Strien NM, Cappaert NLM, Witter MP. 2009. The anatomy of memory: an interactive overview of the parahippocampal-hippocampal network. *Nat Rev Neurosci*. 10:272–282.
- Wang Y, Gupta A, Toledo-Rodriguez M, Wu CZ, Markram H. 2002. Anatomical, physiological, molecular and circuit properties of nest basket cells in the developing somatosensory cortex. *Cereb Cortex*. 12:395–410.
- Wang Y, Toledo-Rodriguez M, Gupta A, Wu C, Silberberg G, Luo J, Markram H. 2004. Anatomical, physiological and molecular properties of Martinotti cells in the somatosensory cortex of the juvenile rat. *J Physiol (Lond)*. 561:65–90.
- Ward JH Jr. 1963. Hierarchical grouping to optimize an objective function. *Journal of the American statistical association*. 236–244.
- Wonders CP, Anderson SA. 2006. The origin and specification of cortical interneurons. *Nat Rev Neurosci*. 7:687–696.
- Xu H, Jeong H-Y, Tremblay R, Rudy B. 2013. Neocortical Somatostatin-Expressing GABAergic Interneurons Disinhibit the Thalamorecipient Layer 4. *Neuron*. 77:155–167.
- Xu Q, Cobos I, La Cruz De E, Rubenstein JL, Anderson SA. 2004. Origins of cortical interneuron subtypes. *Journal of Neuroscience*. 24:2612–2622.
- Xu X, Roby KD, Callaway EM. 2010. Immunochemical characterization of inhibitory mouse cortical neurons: three chemically distinct classes of inhibitory cells. *J Comp Neurol*.

518:389–404.

Yoder RM, Clark BJ, Taube JS. 2011. Origins of landmark encoding in the brain. *Trends Neurosci.* 34:561–571.

## LEGENDS

**Fig. 1. Distribution patterns of interneurons in the mouse presubiculum** (A) horizontal section of mouse presubiculum stained with DAPI. (B) schematic indicating the somatic locations of a sample of the recorded interneurons from three mouse lines: Green, Pvalb-Cre RFP; red, Sst-Cre RFP; blue, X98. (C) a,b,c indicates schematically the level of horizontal sections at different dorsoventral levels. Shown in A,D,E,F are section at intermediate level b. (D-F), fluorescently labeled interneurons of the Pvalb-Cre (D), Sst-Cre (E) and X98 GFP mouse lines (F).

**Fig. 2. Immunostaining of RFP or GFP expressing interneurons.** (A-C), anti-PV labeling. (D-F), anti-SOM labeling, on mouse lines Pvalb-Cre (A, D), Sst-Cre (B, E) and X98 (C, F).

**Table 1. Electrophysiological properties of presubicular neurons.** Values are given for each of the three mouse lines (A) and grouped into clusters (B). These 17 parameters were used for Ward's unsupervised cluster analysis.

**Fig. 3. Classification of 142 presubicular interneurons and 17 presubicular glutamatergic neurons using Ward's unsupervised cluster analysis.** (A) Dendrogram. The broken vertical line indicates the first level of cut-off, which isolates cluster 0, containing only pyramidal neurons (grey boxes, representative example shown in (B)). Cluster 1 is composed of SST interneurons from the X98 (blue) and Sst-Cre (red) mouse lines. Cluster 2 subdivides into cluster 2a and cluster 2b. Cluster 2a comprises a mix of Sst-Cre (red) and Pvalb-Cre (green) interneurons. Cluster 2b contains mostly fast-spiking Pvalb-Cre (green) cells. Somatic location was either superficial (yellow) or deep (orange). For each cluster, one neuron is shown as an illustrative example: (B, grey box), pyramidal neuron of cluster 0. (C, blue box), Martinotti type adapting neuron of cluster 1. (D, red box), Sst-Cre quasi fast-

spiking interneuron from cluster 2a. (E, green box), fast-spiking Pvalb-Cre neurons from cluster 2b. (B-E), current-clamp recordings in response to a negative current pulse that hyperpolarizes the cell to -100 mV and a current pulses at rheobase. Insets: details of the first AP repolarization phase (red trace). Morphologies with axons in red and dendrites in blue.

**Fig. 4. Electrophysiological diversity of PV and SOM interneurons.** (A) Examples of firing patterns of three different interneurons per cluster are shown during an 800 ms rheobase current pulse. (B) Discharge patterns obtained in response to rheobase\*2 and a negative current pulse that hyperpolarizes the cell to -100 mV . Note the low input resistance of the cluster 1 neurons compared with that of the cluster 2a and 2b (larger current steps required to elicit similar voltage changes). Cluster 1 neurons had the most pronounced voltage sag apparent upon hyperpolarization. (C) Input-output curves (upper) and current-voltage relation at sub-threshold potentials (lower) are plotted for three example interneurons from each cluster. Green, Pvalb-Cre RFP; red, Sst-Cre RFP; blue, X98. (D) RMP, rheobase, adaptation index and CV for each cluster. Each cell is represented by a dot. Horizontal lines (red) indicate mean values. (E) AP width plotted against the  $R_{in}$  for each neuron. Low AP width and  $R_{in}$  are characteristics of cluster 1 interneurons. Each cell is represented by a symbol.

**Fig. 5. Morphological variability of presubicular interneurons.** (A, B, C) Representative axo-dendritic trees of 15 biocytin-filled and NeuroLucida-reconstructed interneurons in cluster 1, cluster 2a and cluster 2b respectively. Axons are shown in red, dendrites in blue and cell bodies in black. Cluster 1 was in part composed of Martinotti-like interneurons. Cluster 2a and 2b contained mainly multipolar basket-cell like interneurons.

Figure 1: Distribution patterns of interneurons in the mouse presubiculum

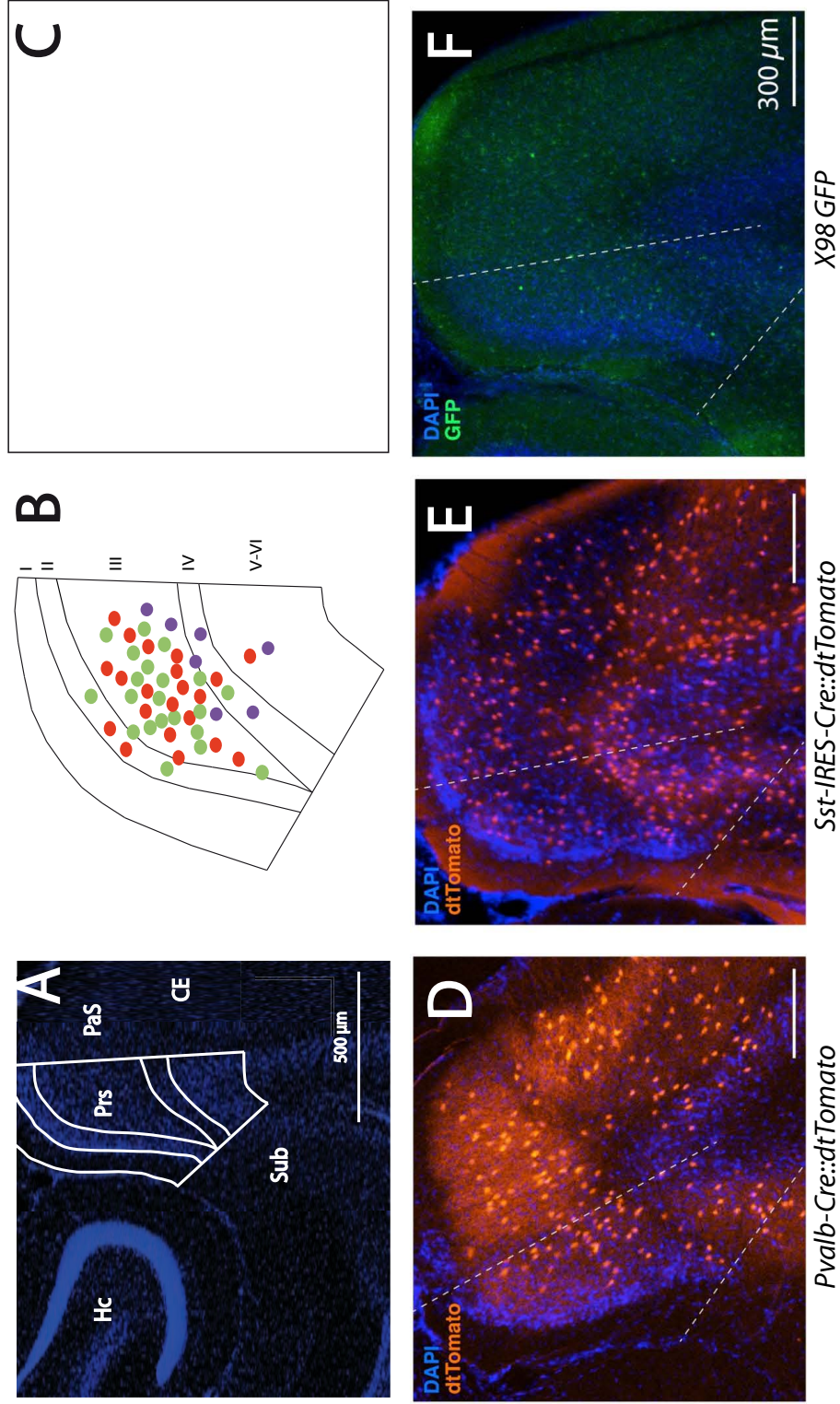


Fig. 2. Immunostaining of RFP and GFP expressing interneurons

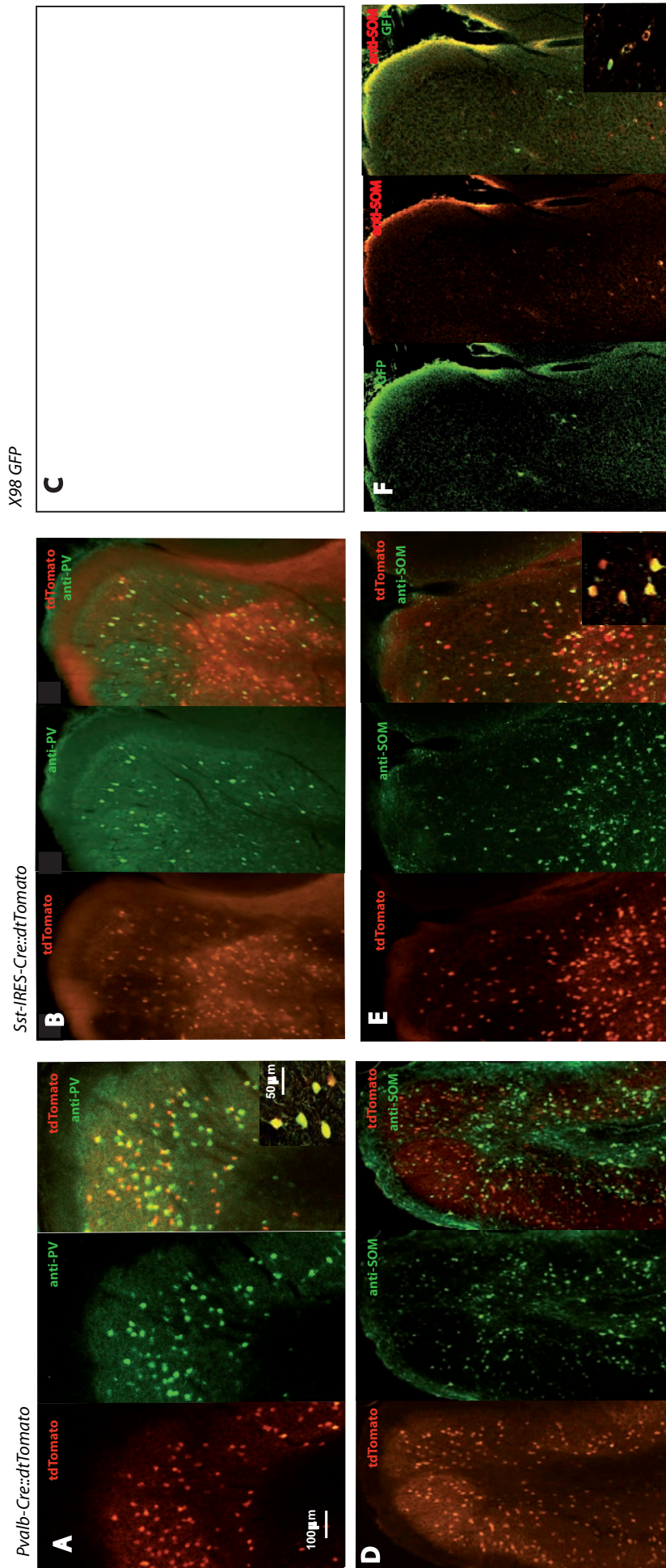


Table 1

	X98			SST tom			PV tom			PC		
	mean	sem	n	mean	sem	n	mean	sem	n	mean	sem	n
RMP (mV)	-54	1	35	-58	1	61	-65	1	46	-78	1	17
Rin (Mohm)	376	22	35	285	20	61	148	9	46	250	24	17
Time constant (ms)	36	3	35	21	2	61	10	1	46	28	4	17
Sag	1.25	0.02	35	1.15	0.01	61	1.10	0.01	46	1.04	0.00	17
Rheobase (pA)	40	4	35	72	9	61	175	14	46	84	9	17
I-O gain (Hz/nA)(MeanInsF)	748.12	38.00	35	916.83	53.87	61	1014.75	92.16	46	275.16	23.25	17
I-O gain (Hz/nA)(APs/sec)	731.79	46.22	35	884.59	58.66	61	1065.18	98.48	46	270.32	22.11	17
MeanInsF (Hz)	33	3	35	74	8	61	247	19	46	33	3	17
Coefficient of variation	0.28	0.03	35	0.15	0.01	61	0.06	0.00	46	0.20	0.02	17
Latency (ms)	21	2	35	15	1	61	13	2	46	27	3	17
Adaptation Index	0.66	0.02	35	0.86	0.02	61	0.94	0.02	46	0.72	0.04	17
Threshold (mV)	-38.2	0.4	35	-38.5	0.5	61	-39.6	0.6	46	-35.0	0.7	17
Width (ms)	0.27	0.01	35	0.27	0.01	61	0.20	0.01	46	0.55	0.01	17
Amplitude (pA)	83	1	35	77	1	61	72	1	46	84	1	17
AHP (mV)	-23.8	0.7	35	-23.5	0.5	61	-23.7	0.6	46	-15.3	0.5	17
Max depolarization rate (V.s-1)	598	14	35	571	13	61	637	18	46	534	20	17
Min depolarization rate (V.s-1)	-355	11	35	-353	14	61	-498	22	46	-135	5	17

	Cluster 0			Cluster 1			Cluster 2a			Cluster 2b		
	mean	sem	n	mean	sem	n	mean	sem	n	mean	sem	n
RMP (mV)	-78	1	17	-54	1	65	-60	1	48	-70	1	29
Rin (Mohm)	250	24	17	374	17	65	189	11	48	137	17	29
Time constant (ms)	28	4	17	32	2	65	11	1	48	13	2	29
Sag	1.04	0.00	17	1.22	0.01	65	1.11	0.01	48	1.09	0.01	29
Rheobase (pA)	84	9	17	40	3	65	113	8	48	202	23	29
I-O gain (Hz/nA)(MeanInsF)	275	23	17	778	28	65	762	41	48	1437	131	29
I-O gain (Hz/nA)(APs/sec)	270	22	17	746	35	65	747	43	48	1525	132	29
MeanInsF (Hz)	33	3	17	35	2	65	128	7	48	297	27	29
Coefficient of variation	0.20	0.02	17	0.24	0.02	65	0.07	0.00	48	0.08	0.02	29
Latency (ms)	27	3	17	21	1	65	14	2	48	8	2	29
Adaptation Index	0.72	0.04	17	0.70	0.01	65	0.92	0.02	48	1.00	0.02	29
Threshold (mV)	-35.5	0.5	17	-38.4	0.4	65	-37.4	0.5	48	-42.2	0.7	29
Width (ms)	0.56	0.02	17	0.29	0.01	65	0.23	0.00	48	0.18	0.01	29
Amplitude (pA)	84	2	17	82	1	65	76	1	48	69	2	29
AHP (mV)	-14.7	0.6	17	-23.8	0.5	65	-23.8	0.5	48	-22.9	0.8	29
Max depolarization rate (V.s-1)	517	22	17	567	11	65	627	14	48	623	26	29
Min depolarization rate (V.s-1)	-134	6	17	-329	9	65	-409	15	48	-547	30	29

Figure 3: Dendrogram

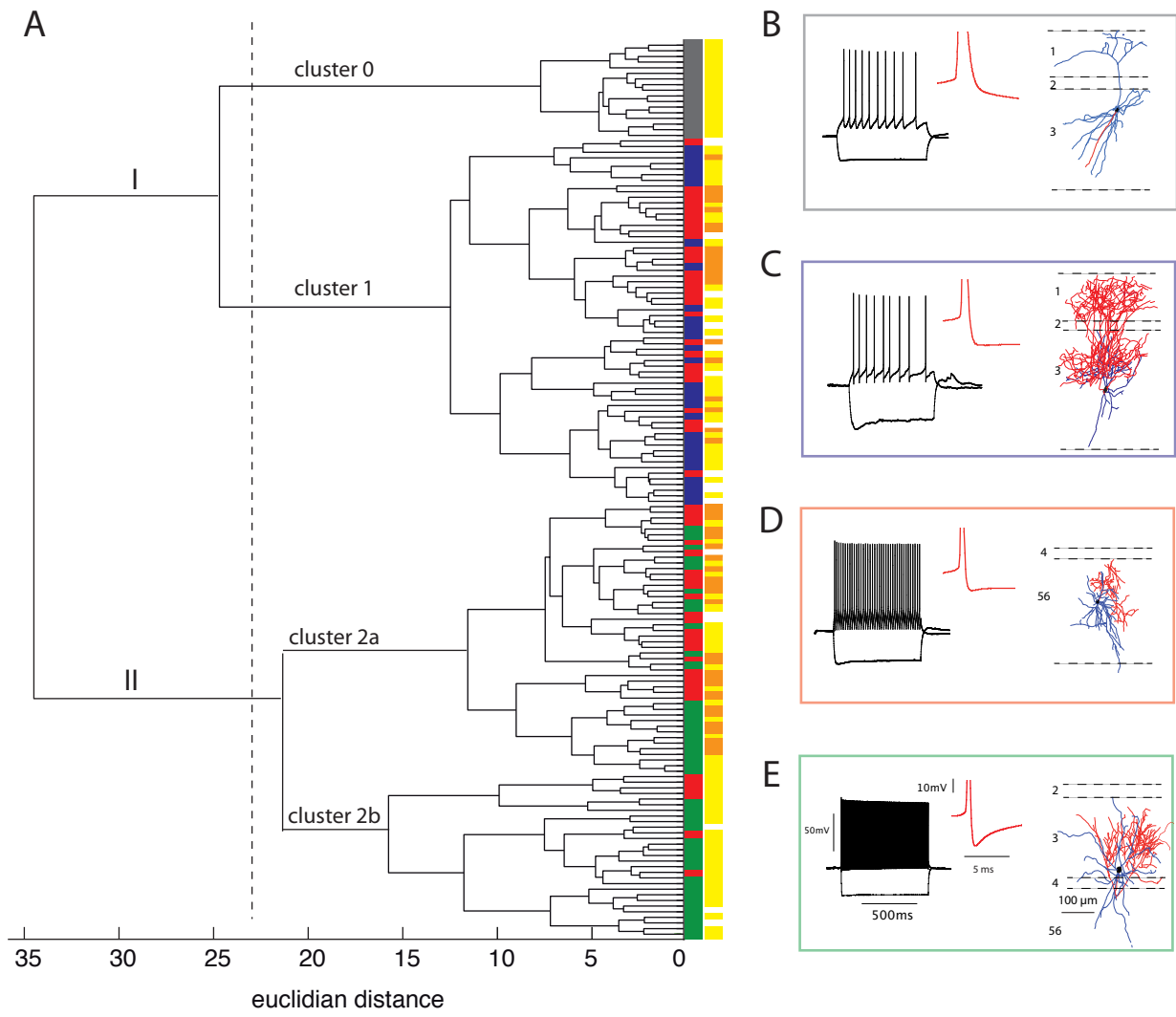


Figure 4: Electrophysiological diversity

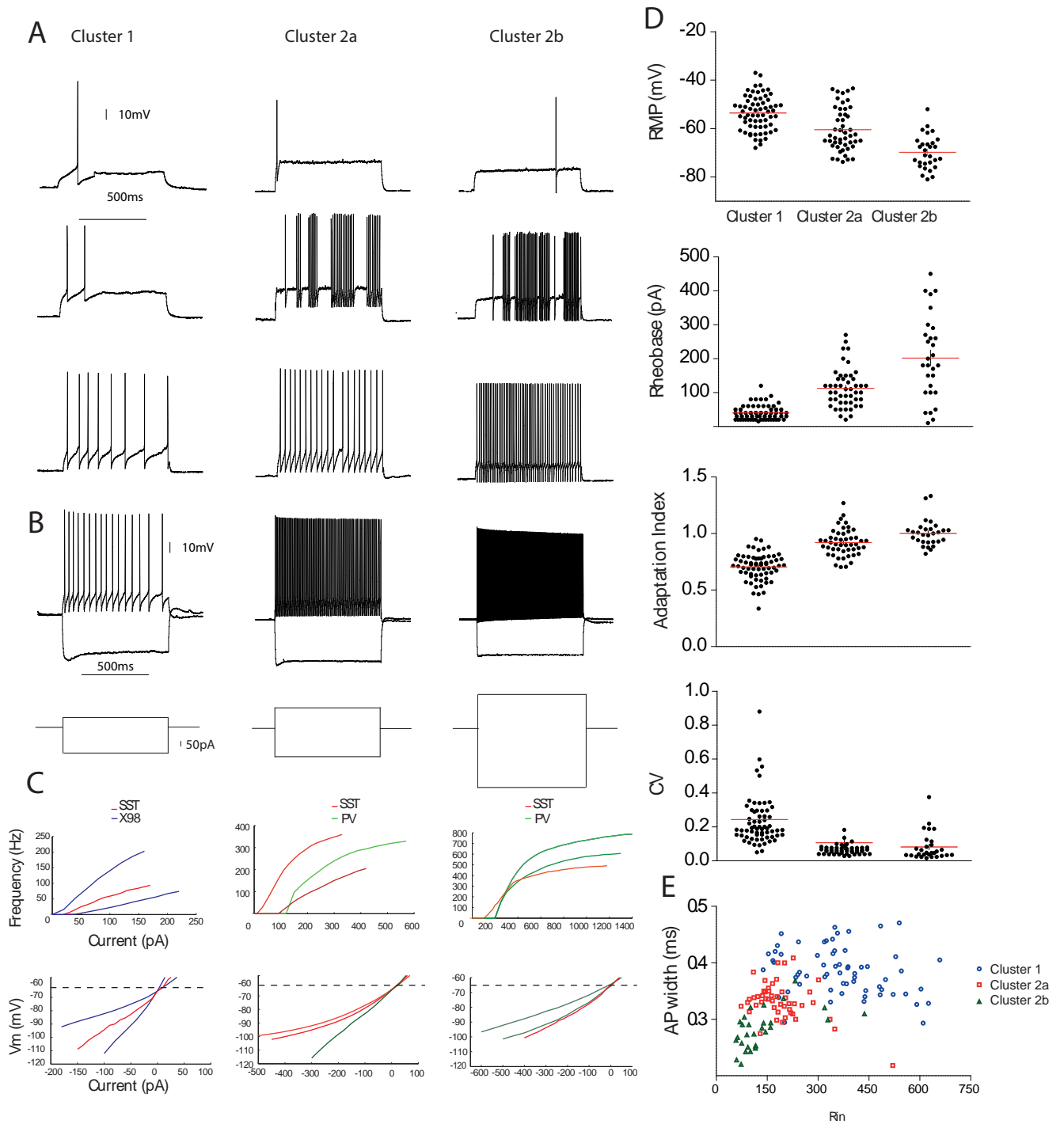
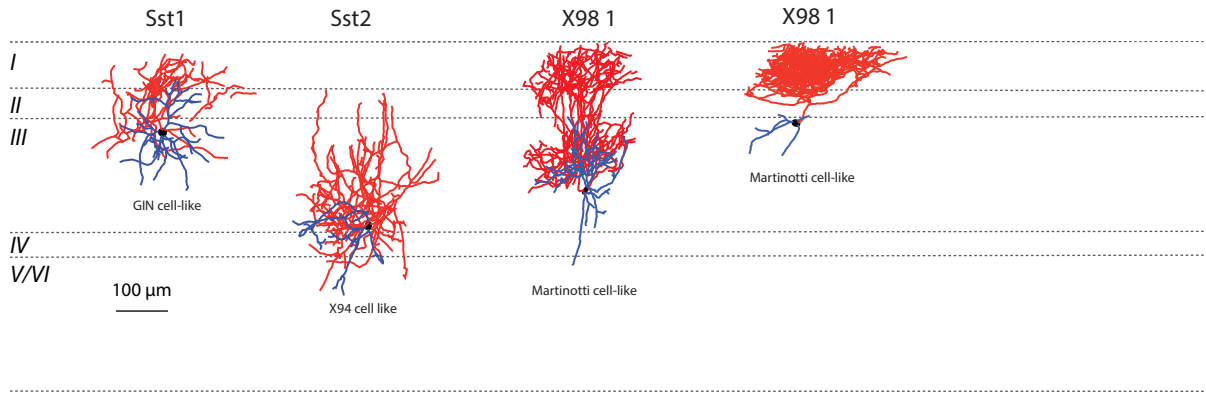
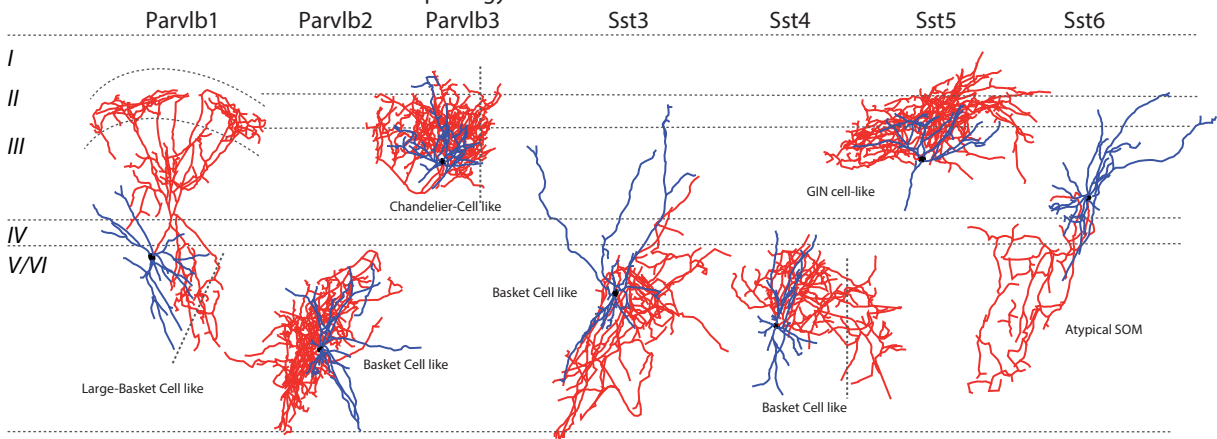


Figure 5: Morphological Diversity

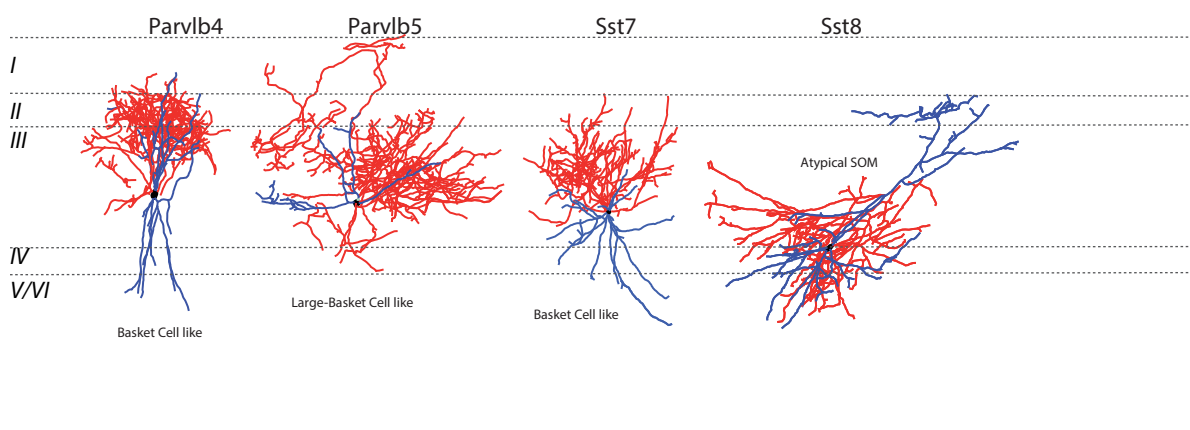
**A** Cluster 1: Typical morphology of SOM-like interneurons



**B** Cluster 2a: Interneurons with variable morphology



**C** Cluster 2b: Multipolar basket-cell like interneurons



## ARTICLE 4

# Memory of past activity determines the recruitment of a Martinotti cell-mediated inhibitory feedback loop in mouse presubiculum

My previous studies characterized principal cells and interneurons in the different layers of the presubiculum. Different bricks of the microcircuit have therefore been identified, but the synaptic connectivity in the presubicular network is still unknown. The full presubicular intrinsic connectivity and its dynamics remain to be unraveled to understand the presubicular information processing. Revealing the excitatory information flows and their regulation by the different interneurons is difficult to do in only one stage. I therefore chose to address one more specific question: the recruitment of dendritic inhibition.

In the present work, I have been studying the interaction between pyramidal cells and Martinotti cells in superficial layers of presubiculum. The morphologies of these two neuronal types suggest their interconnections: axons of Martinotti cells innervate mainly layer 1 and 3, where pyramidal cell dendrites ramify; axons of pyramidal cells innervate layer 3, where Martinotti cell dendrites are located. Using dual patch clamp recordings, I confirmed the presence of a high degree of interconnections between pyramidal cells and Martinotti cells. Martinotti cells provided weak inhibition that might influence spiking activity at the soma. It is worth noting that the inhibitory effect is lower when the Martinotti cell action potential is timed immediately after the pyramidal cell discharge. The pyramidal cell to Martinotti cell synapse is facilitating with unexpectedly slow kinetics. The synaptic transfer rate is almost zero for single spikes and becomes more reliable after repetitive firing at high frequency. This synaptic enhancement may persist for several hundreds of

milliseconds after the end of high frequency stimulation.

Taken together, these results suggest that the pyramidal cells and Martinotti cells form a feedback inhibitory loop recruited during persistent firing. The spike timing dependent inhibitory strength of Martinotti cells might provide a filter that favors lateral inhibition but not self-induced inhibition. This loop could therefore be used to refine persistent head direction signaling in the presubiculum by the preferential inhibition of cells with different directional tuning.

Title:

Memory of past activity determines the recruitment of a  
Martinotti cell-mediated inhibitory feedback loop in  
mouse presubiculum

Authors:

Jean Simonnet<sup>1</sup>, Charlotte N. Boccara<sup>2</sup>, Ivan Cohen<sup>3</sup>,  
Richard Miles<sup>1</sup> and Desdemona Fricker<sup>1</sup>

(1) Institut du Cerveau et de la Moelle épinière - Université Pierre et Marie Curie, Hôpital Pitié  
Salpêtrière 47 Bd de l'Hopital 75013 Paris; (2) IST Austria, Am Campus 1, 3400 Klosterneuburg,  
Austria ; (3) Neurosciences Paris Seine - Université Pierre et Marie Curie, Campus Jussieu Quai St  
Bernard, 75005 Paris

## **Introduction**

The presubiculum is an understudied cortical region located between the hippocampus and the entorhinal cortex (Amaral and Witter, 1989; van Strien et al., 2009). Around sixty percent of neurons in the presubiculum are head direction cells (Taube et al., 1990; Boccara et al., 2010), which fire persistently as the animal's head is turned toward the preferred directional firing range. Presubiculum plays a major role in visual landmark encoding, controlling the accuracy of the head direction signal and providing visual cues for hippocampal-based landmark navigation (Yoder et al., 2011).

The presubicular head direction signal arises from the combination of subcortical signals, mainly from anterior thalamus (Goodridge and Taube, 1997), and visual information (Taube et al., 1990) from visual cortex (Vogt and Miller, 1983) or relayed by retrosplenial cortex (van Groen and Wyss, 1990). Yet, integrative properties of the presubicular microcircuit that generates the local head direction signal are poorly understood.

The electrophysiological and morphological properties of excitatory and inhibitory neurons contained in the six layers of this transitional cortex have been described previously (Abbasi and Kumar, 2013; Simonnet et al., 2013). Inter- and intralaminar recurrent projections have been studied to some degree (Funahashi and Stewart, 1997; Honda et al., 2008), but the fine interconnection and the dynamics of information within the circuit have not been established yet. It has been shown that presubicular neurons can experience (Simonnet et al., 2013) or even generate (Yoshida and Hasselmo, 2009) persistent firing during tens of seconds to minutes *in vitro*, which constitutes a cellular basis for the head direction signal. This persistent activity should be balanced by the recruitment of the local inhibitory network that may ensure the specificity of the head direction signal over time (Isaacson and Scanziani, 2011), as suggested in continuous attractor models of the head direction signal (McNaughton et al., 2006). High frequency burst firing of neocortical layer 5 pyramidal cells recruit local dendrite-targeting interneurons, the Martinotti cells, which provide feedback inhibition (Silberberg and Markram, 2007; Zhu et al., 2011). This recurrent inhibition strongly regulates the integration of inputs arriving onto the apical dendritic tree *in vivo* (Murayama et al., 2009).

We have previously identified dendrite-targeting neurons in the presubiculum that we defined as Martinotti cells (Nassar et al. in preparation) and here we study their interconnectivity with pyramidal cells. We determined that presubicular Martinotti cells are part of a feedback inhibitory pathway in superficial layers of mouse presubiculum. The recruitment of Martinotti cells is time and frequency dependent, and the synapse has a low reliability during sparse

firing. Moreover, the un-muting of the synapse outlasts the high frequency stimulation for seconds, constituting a memory of past activity that enhances synapse reliability for subsequent firing. This may constitute an important mechanism that controls the tuning properties of head direction cells as they persistently fire.

## **Methods**

### *Slice preparation and recording.*

Horizontal slices of hippocampal and parahippocampal areas were prepared from 24- to 35-day-old male and female transgenic mice expressing GFP in a subpopulation of SST-positive neurons corresponding to Martinotti cells in neocortex (X98 line, JAX stock n° 006340; Ma et al., 2006). Our care and use of the animals conformed to the European Communities Council Directive of 22 September 2010 (2010/63/EU) and French law (87/848). Our study was approved by the local ethics committee Charles Darwin N°5. After anesthesia with ketamine hydrochloride and xylazine (80 and 12 mg/kg, respectively), animals were perfused via the heart with at least 30 ml of a solution containing (in mM): 125 NaCl, 25 sucrose, 2.5 KCl, 25 NaHCO<sub>3</sub>, 1.25 NaH<sub>2</sub>PO<sub>4</sub>, 2.5 D-glucose, 0.1 CaCl<sub>2</sub> and 7 MgCl<sub>2</sub>, cooled to 2–6 °C and equilibrated with 5% CO<sub>2</sub> in O<sub>2</sub>. The forebrain was dissected, and horizontal slices (260–320 µm thick) were cut on a vibratome (Leica VT1200S). Slices were transferred to a storage chamber containing warmed (37°C) artificial cerebrospinal fluid (ACSF) containing (in mM): 124 NaCl, 2.5 KCl, 26 NaHCO<sub>3</sub>, 1 NaH<sub>2</sub>PO<sub>4</sub>, 2 CaCl<sub>2</sub>, 2 MgCl<sub>2</sub>, and 11 D-glucose, gently bubbled with 5% CO<sub>2</sub> in O<sub>2</sub> (pH 7.3, 305–310 mOsm/L). ACSF was allowed to progressively cool down to room temperature (22–25°C) and slices were kept during at least 1 h.

The recording chamber (volume ~2 mL) was heated to 32 – 34 °C. Neurons were visualized with an EMCCD Luca-S camera (Andor) on a Axioskop 2 FS plus microscope (Zeiss, France) with infrared differential interference contrast.

Patch clamp glass pipettes were pulled from borosilicate glass of external diameter 1.5 mm (Hilgenberg, Germany) using a Brown-Flaming electrode puller (Sutter Instruments). The electrode resistance was 3–6 MΩ, when filled with a solution containing (in mM): 135 K-gluconate, 2 KCl, 10 HEPES, 0–0.2 ethylene glycol tetra-acetic acid (EGTA), 2 MgCl<sub>2</sub>, 4 MgATP, 0.4 Tris-GTP, 10 Na<sub>2</sub>-phosphocreatine. Whole-cell records were made with a Multiclamp 700B amplifier and acquired with pClamp software (Molecular Devices, Sunnyvale, CA, USA). Recordings were filtered at 6 KHz in current clamp mode and at 2 KHz

in voltage clamp mode. Recordings were not corrected for junction potential (~15 mV). Spike trains of *in vivo* recorded presubicular head direction cells (Boccarda et al. 2010) were extracted with MATLAB (The Mathwork) and imported in pClamp to generate command protocols. Access resistance was continuously monitored and was stable within  $\pm 15\%$  for all included recordings. All salts and anesthetics were obtained from Sigma (Lyon, France).

### *Data analysis*

Signals were analysed with AxoGraphX, and software written in Labview (National Instruments) or MATLAB (The Mathwork).

*Cellular properties and action potentials.* Methods for detection of action potentials and description of electrophysiological parameters were similar to those in our previous studies (Simonnet et al, Nassar et al.).

*Synapses.* Excitatory and inhibitory postsynaptic events in paired recordings were measured in either voltage clamp or current clamp mode, and two different methods served to determine synaptic efficiency (failure rate, transfer rate, dynamics). *Peak amplitude method.* To obtain shape parameters of synaptic events, traces were aligned at the peak of the presynaptic action potential and averaged. Amplitudes of synaptic events could also be measured from single trials using a fixed 3 ms time window starting from action potential peak. Noise was determined as the maximum amplitude of baseline fluctuations within a 3 ms time window prior to the action potential peak. Synaptic responses that were smaller than 1.6 RMS (root mean square) of the noise were considered as failures (Markram et al., 1997; Beierlein et al., 2003). Failure rate was the number of failures divided by the number of presynaptic activations, and conversely, transfer rate was  $1 - \text{failure rate}$ . In an alternative, *automatic detection method*, all postsynaptic events (spontaneous and spike-locked) were detected as continuous periods of rising membrane potential (low-pass filtered at 400 Hz for current clamp or 1000 Hz for voltage clamp), with an amplitude threshold at 0.3-0.6 mV for current clamp or 4-7 pA for voltage clamp recordings. This amplitude threshold was determined for individual recordings and set as a value that minimized errors, both false positive and missed events, as judged by eye. Detected synaptic responses were considered spike-locked if their delay (at mid-rise amplitude) from the action potential peak was comprised between 0.5 and 3 ms. Synaptic transfer rate was the number of spike-locked events divided by the number of presynaptic activations. We confirmed that the performance of the automatic detection method was comparable to the peak amplitude method (Fig. 5F), and we used it routinely for the analysis of synaptic transmission after repeated presynaptic

activation. Spontaneous activity can bias transfer rate calculation, which is why a correction based on the RMS of the noise was performed for the *peak amplitude method*. We also determined the noise level for the *automatic detection method*. Presynaptic firing patterns were aligned to a “control window”, generally prior to the stimulation, and transfer rate, corresponding to a noise value, was calculated. This procedure was applied multiple (250 - 300) times using different starting points in the same control window to obtain an estimate of false positives. The probability of false positives was very low for all our recordings. While it may depend on the level of background synaptic activity, it never exceeded 0.05, and was not correlated to presynaptic firing frequency.

### *Cellular anatomy.*

For some experiments, biocytin (1mg / ml) was added to the internal solution. The procedure for post-hoc anatomical revelation was described previously (Simonnet et al. 2013).

NeuroLucida software (MicroBrightfield, Williston, VT, USA) was used to reconstruct axo-dendritic morphologies in three dimensions from stacks of acquired images.

## **Results**

We studied interactions between Martinotti cells (MC) and Pyramidal cells (PC) in layer 2 and 3 of mouse presubiculum. Presubicular MCs were identified in horizontal slices of 24- to 35-day-old male and female X98-SST transgenic mice. In terms of electrophysiological and morphological properties, they were similar to neocortical Martinotti cells (Ma et al., 2006, Nassar et al 2014). GFP neurons were found in all layers of presubiculum, except in layer 1; all expressed somatostatin and one third also expressed calbindin (not shown).

### *Martinotti cell and pyramidal cell electrophysiological properties*

Properties of MC and PC are summarized in table 1 and Fig. 1. Pyramidal cells in superficial layers of mouse presubicular cortex were regular spiking, similar to those previously described in rat (Simonnet et al., 2013). Their resting membrane potential was rather hyperpolarized at  $-77.5 \pm 0.7$  mV (Fig, 1A, B). They were little excitable neurons, with a low input resistance (Fig, 1D, E;  $233.8 \pm 16.9$  M $\Omega$ ), high rheobase (Fig, 1F, G;  $88.6 \pm 7$  mV) and a low input-output gain (Fig, 1F, G;  $0.296 \pm 0.019$  Hz.pA $^{-1}$ ).

Martinotti cells on the contrary were highly excitable. Their resting membrane potential was  $-53.3 \pm 0.9$  mV and some of them were spontaneously active (23 out of 30) (Fig. 1A, B). They had a higher input resistance ( $342.4 \pm 22.3$  M $\Omega$ ) than pyramidal cells (fig 1.E) and a low threshold spiking behavior; rheobase was  $44.2 \pm 4.3$  pA, firing gain was  $0.728$  Hz.pA $^{-1}$  and frequency could reach more than 150 Hz (Fig. 1F). The presence of a hyperpolarization activated current I<sub>h</sub> was suggested by a prominent voltage sag (Fig. 1H). Thus, they have the electrophysiological intrinsic properties of neocortical X98-SST/Martinotti cells (Ma et al., 2006).

#### *High level of interconnectivity between Martinotti cells and Pyramidal cells*

The comparison of Martinotti and pyramidal cell morphologies suggested that one could be the preferential target of the other (Fig. 2A). Dendrites of pyramidal cells ramified in layer 1 and 3, the main areas targeted by Martinotti cell axons. Martinotti cell dendrites principally ramified in layer 3 where pyramidal cell axons had collaterals. These overlapping morphologies might reflect the presence of a feedback loop between the two neuronal populations. We therefore tested the interconnection between Martinotti and nearby pyramidal cells in superficial layers using dual recordings. Connectivity was high, as summarized on panel 2B. The proportion of connected pairs was 60 % (43 out of 72 tested) for Martinotti cell to pyramidal cells and 41 % (35 out of 85 tested) for pyramidal cell to Martinotti cells. About 29 % (20 out of 69 tested) of dual recorded neurons were reciprocally connected. Synaptic strength and its dynamics (short term plasticity) indicate how and when a given synapse participates to microcircuit information processing (Abbott and Regehr, 2004; Silberberg et al., 2005; Regehr, 2012). We therefore investigated synaptic features of the MC-to-PC and PC-to-MC connections in detail.

#### *Martinotti cells provide reliable inhibition onto pyramidal cell dendrites*

We investigated the electrophysiological properties of the inhibitory MC-to-PC synapse and confirmed its dendritic location suggested by morphology. At -50 mV, the amplitudes of the averaged GABAergic current responses (see method) were comprise between 2.3 and 32.3 pA ( $13.8 \pm 2.36$  pA; Fig. 3A-C). Even if the amplitudes were small, the failure rate was low (0.07, n=4, certainly overestimated, see discussion), showing the high reliability of this inhibitory synapse. The amplitude of synaptic events was progressively reduced between the beginning and the end of presynaptic action potential trains elicited at 20, 50 or 100 Hz (Fig.

3D). The paired pulse ratio at 50 Hz was  $0.81 \pm 0.04$  ( $n=8$ ), indicating short-term depression. The low amplitude of synaptic events is partly due to a low driving force for GABA<sub>A</sub> currents, the theoretical reversal potential of chloride being only 13 mV more negative than the holding voltage in our conditions. The experimental reversal potential of synaptic current was more negative than chloride reversal potential ( $n = 2$ , not shown), which is a typical distortion of dendritic currents recorded with somatic patch clamp (Silberberg and Markram, 2007; Williams and Mitchell, 2008) and therefore indicative of the dendritic origin of these GABAergic currents.

The efficacy of inhibition was examined by looking at MC ability to delay a spike during a 30-40 Hz somatic-induced firing of PC (Fig. 4A, B). The variation between the duration of PC inter-spike-interval (ISI) during which inhibition occurred (post-ISI) and the previous ISI (pre-ISI) was used as an index of inhibitory effect (Fig. 4A). This index was low, as PC inter-spike-intervals were only slightly increased by MC firing (Fig 4B, 6-30 %,  $n=4$ ) which further indicates the dendritic origin of inhibition (Williams and Stuart, 2003). Nonetheless, we noticed that the inhibitory effect depended on MC spike timing; it was lower if MC fired earlier during post-ISI (Fig. 4B). This occurred in particular for reciprocally connected MC-PC pairs (Fig. 4C), when a PC discharged a MC with short latency, the inhibitory event in return increased the afterhyperpolarization (AHP) of the PC action potential, but it did not really affect post-ISI (Fig. 4C). To better understand the role of this feedback inhibition, we then investigated how pyramidal cells recruited Martinotti cells.

#### *Repetitive stimulation un-mutes PC-to-MC connection*

The probability for evoking a postsynaptic excitatory event in a MC with a single spike in the PC was very low (range = 0 - 0.35; Median = 0.08; 75% percentile = 0.19;  $n = 23$ ). However, synaptic transfer increased significantly after a 30 Hz train of 30 action potentials (Fig. 5,  $n = 7$ ). Early and late transfer rates were calculated based on synchronous excitatory postsynaptic events, elicited for the 5 first and the 5 last action potentials, respectively, showing an increase in synaptic transfer by  $3.45 \pm 0.91$  ( $n = 7$ ) at the end of the train. The amplitude of the postsynaptic events also increased significantly (multiplied by  $1.34 \pm 0.44$ ;  $n = 7$ ), but to a lesser degree compared to the increase in transfer rate. The repetitive stimulations at the PC-to-MC synapse thus increased the PC-to-MC synaptic efficacy;

#### *Transfer probability depends on presynaptic firing frequency*

Short term plasticity mechanisms typically depend on dynamical properties in the presynaptic compartment (Zucker and Regehr, 2002; Regehr, 2012). We therefore compared how presynaptic firing frequency would influence postsynaptic responses. Trains of equivalent numbers of action potentials were elicited in the pyramidal neuron, at a frequency of either 30 Hz or 10 Hz (Fig. 6A, B), with silent periods of at least 10 seconds between trains (Fig. 6A). The synaptic transfer rate was always higher for 30 Hz trains ( $0.32 \pm 0.06$ ) compared to 10 Hz trains ( $0.18 \pm 0.05$ ;  $n = 9$ , Table 3, Fig. 6B,C). Therefore, increasing the firing frequency clearly enhanced synaptic reliability. If the transfer rate is normalized to a 1 second period of action potential firing, the increase in synaptic transfer is even more striking, going up by a factor of  $6.2 \pm 1.1$  when presynaptic firing frequencies increase from 10 to 30 Hz. (see Table 3). An alternative protocol, consisting of consecutive step current injections with increasing amplitude, from 15 to 50 Hz (Fig. 6D,  $n = 6$  different pairs). Once again, the PC-to-MC transfer rate, calculated for the first ten spikes, increases progressively from 10 to 50 Hz (Fig. 6E). This frequency dependent transfer rate at PC-to-MC synapses was observed in all tested pairs ( $n = 27$  in total).

#### *Increase of transfer rate as a medium term memory process*

The change of transfer rate was related not only to the present presynaptic firing frequency, but also to the recent past of presynaptic activity, as suggested by the facilitating dynamics. Figure 7A-C shows how an initial 10 Hz spike train is scarcely transmitted, with a subsequent sharp increase in the transfer rate for a 30 or 40 Hz train of action potential firing. Interestingly, this apparent “un-muting” of the synapse was then maintained, and the immediately succeeding 10 Hz train had a much higher transfer rate compared to the initial one. In fact, the probability to get a postsynaptic event was almost as high as during the high frequency un-muting stimulus (1-2 seconds;  $n = 3$ ). This plasticity of transfer rate was fully reversible with longer silent inter-stimulus intervals: synapses were no longer un-muted for a 10 Hz spike train that was applied more than 10 seconds after a 30 Hz train (cf. Fig. 6B, 7B).

*In vivo*, head direction cells of the presubiculum sustain firing if the head is still (Taube et al., 1990). *In vitro*, principal cells of presubiculum can sustain firing during several seconds in response to DC (direct current) injection, even though their discharge frequency slightly adapts over time (Yoshida and Hasselmo, 2009; Simonnet et al., 2013). We therefore tested the dynamics of the PC-to-MC synapse during the progressive decrease of firing frequency induced by maintained DC injection (Fig. 7D-F). Two cases were distinguished for each neuron. First, initial firing was not high enough to un-mute synapses and synaptic transfer

stayed low (Fig. 7D and 7F, orange lines); Secondly, the initial high frequency firing un-muted the PC-to-MC synapse, and transfer rate remained stable thereafter, even if firing frequency decreased (Fig. 7D and 7F, blue lines). These results confirmed that the initial discharge had a significant impact on further information transfer. However, these sustained discharges may not correspond to firing patterns of head direction cells *in vivo*.

*The PC-to-MC synaptic dynamics account for more natural firing patterns.*

*In vivo* studies of head direction (HD) cells in the presubiculum reported variable peak firing rates, from 5 to 115 spikes per seconds, 2/3 being < 40 Hz (Taube et al., 1990b). In recordings of head direction cells from freely moving animals, we found that the mean peak-firing rate was  $10 \pm 2$  spikes per seconds ( $n = 5$  HD cells, Fig. 8A). Firing patterns were highly irregular (Fig. 8B, C), with peak instantaneous frequencies up to 250 Hz. We extracted stretches of sustained spiking activity, corresponding to maintained HD cell firing (Fig. 8D), and played those as depolarizing current commands into a pyramidal cell. Figure 8E, F shows the spike pattern initiated in the pyramidal cell and the simultaneous recording from a postsynaptically connected Martinotti cell, either in current clamp or voltage clamp mode. As expected from our previous results, single pyramidal cell action potentials at the beginning of the *in vivo* spike pattern were rarely transmitted, but the PC-to-MC synaptic efficiency was enhanced during period of sustained and high frequency natural firing (Fig. 8E-G). Synaptic un-muting could persist during silent periods following an enhancement. For one pair with a relatively high basal transfer rate, the pyramidal cell fired the Martinotti cell but only specifically during sustained and high frequency firing (Fig. 8E, G).

## **Conclusion**

Our present work constitutes the first study of dynamical synaptic properties in the rodent presubicular microcircuit. We have identified elements of an inhibitory feedback circuit in superficial layers: a Pyramidal Cell (PC) exciting a Martinotti Cell (MC), which in return inhibits the Pyramidal Cell. MCs target mainly layers 1 and 3 and provide reliable dendritic inhibition. The efficiency of inhibition in terms of delaying PC firing induced with somatic DC injection seemed rather weak. Nonetheless, we noticed that the strength of inhibition depended on MC spike timing, that is, if inhibition was synchronized with the pyramidal cell AHP, the inhibitory effect was the lowest. The synaptic transfer from PC to MC was activity dependent, as it increased with the duration and frequency of the presynaptic discharge. Excitatory post-synaptic events were rarely detected in MC upon single spike firing of PC. However, the synaptic transfer rate was significantly increased at the end of a PC spike train at 30 Hz. This “un-muting” of the PC-to-MC synapse also enhanced subsequent synaptic transfer during hundreds of milliseconds and up to seconds after the end of a stimulus. Following un-muting, even single spikes, or low frequency discharge, could effectively transfer information. Natural firing patterns of head direction cell spike trains were injected into a pyramidal cell to confirm that MCs could be recruited by in vivo discharge patterns. Martinotti cells may be tuned to refine the head directional signal during sustained firing of Head Direction Cells.

## **Discussion and perspectives**

*Martinotti cells and pyramidal cells constitute the highly interconnected elements of a feedback subcircuit in the presubiculum.*

A high proportion of connections were found in our recordings: 40 % from PC to MC, 60% from MC to PC and 30% of pairs were reciprocally connected. As the slice preparation cannot preserve the integrity of all connections, our estimation of the overall connectivity is certainly on the low side. The amount of inhibitory connections and the transfer rate at connected pairs might have been further underestimated because of the very low amplitude of inhibitory synaptic events at distal dendritic contacts. The MC-to-PC connectivity, as well as the reliability at these synapses, may be higher than our estimation. In order not to miss small amplitude events, the internal recording solution could be modified to increase the driving force for chloride, which would produce synaptic events of higher amplitude and the reliability of these synapses (failure/transfer rate) could be better addressed. Adapting the

recording conditions in this way should also help the observation of the kinetics of the evoked IPSCs, as well as their short-term synaptic dynamics.

The high proportion of MC-to-PC connections in presubiculum is similar to what is found in neocortex, where Martinotti cells provide a dense, reliable and non-specific inhibition onto neighboring pyramidal cells (Fino and Yuste, 2011). Together with the high number of PC to MC connections, this indicates that MC provide a recurrent inhibitory control onto superficial layer pyramidal cells (Kapfer et al., 2007; Silberberg and Markram, 2007; Berger et al., 2009). We have recently shown that the optogenetic activation of afferent fibers from anterodorsal thalamus, a determinant area of presubicular function (Goodridge and Taube, 1997), directly activated pyramidal cells, but rarely SST+ interneurons. This further supports the feedback inhibitory role of MCs in the presubiculum (Mathon, Nassar, Simonnet and Fricker, unpublished).

The direct PC-to-PC connectivity seems very low in the presubiculum (0 out of 22 checked connections, not shown). Thus the inhibition provided by Martinotti cells might be a prominent way to interact between presubicular pyramidal cells, similarly to Martinotti cells in neocortex during high frequency burst (Silberberg and Markram, 2007). Given the high degree of connectivity and the dense ramification of the Martinotti cell axon in superficial layer, the presence of disynaptic inhibition will be certainly confirmed in future studies combining dually recorded pyramidal cells.

#### *Facilitating synaptic transfer rate at the PC to MC synapse.*

Single spikes in PC rarely excited MC, but sustained and high frequency stimuli could evoke postsynaptic EPSCs following facilitating dynamics: the transfer rate increased gradually during the stimulation, and could eventually fire the MC (Fig. 6D, 8G) when excitatory postsynaptic events started to sum. In neocortex and hippocampus, short-term dynamics of pyramidal cell excitatory synapses depend on the target interneuron (Ali and Thomson, 1998; Ali et al., 1998; Markram et al., 1998; Beierlein et al., 2003; Koester, 2005; Silberberg et al., 2005; Silberberg and Markram, 2007). The dynamics of the PC-to-MC synapse match well with the corresponding excitatory synapses in hippocampus (Ali and Thomson, 1998) and neocortex (Beierlein et al., 2003; Silberberg and Markram, 2007; Fanselow et al., 2008); all these synapses are strengthened during repetitive stimulations. However, we could not address the dynamics of amplitude changes with a classical paired-pulse protocol (as we did for the MC to PC synapse), because most synapses stayed silent during a paired pulse. Amplitudes tended to increase somewhat during repetitive stimuli (Fig. 5, 6D), especially in recordings

with a high initial transfer rate (Fig. 5D, 8G). The frequency dependent increase of transfer rate that we observe in presubiculum may go with the frequency dependent amplitude increase described in many facilitating synapses, such as the excitatory synapses onto Martinotti cells in neocortex (Markram et al., 1998; Faselow et al., 2008). Finally, the facilitation of synaptic efficacy may last several hundreds of milliseconds after the end of a stimulation (Gupta et al., 2000; Regehr, 2012). This slow decay seems similar to the persistent increase of transfer rate that we observe after high frequency stimuli (Fig. 7, 8). Nevertheless, the transfer rate always stays relatively low, even after un-muting, compared to sustained stimulations in neocortical layer 3 (Faselow et al., 2008) or layer 5 (Silberberg and Markram, 2007) PC-to-MC synapses. We therefore suggest that the PC-to-MC synaptic transmission in the presubiculum is regulated by an activity dependent mechanism, distinct from presynaptic short term facilitation (Zucker and Regehr, 2002; Regehr, 2012), acting either in the axon or at the presynaptic site. (Debanne et al., 2013).

#### *Function of frequency-dependent dendritic inhibition in the presubiculum.*

Frequency dependent mechanisms at the synapse regulate information transfer in neuronal networks (Abbott and Regehr, 2004). In somatosensory cortex, the switch between two regimes of activity, sparse firing to burst firing, reroutes the information from depressing pyramidal-to-pyramidal synapse to facilitating pyramidal-to-Martinotti synapse (Silberberg and Markram, 2007). We have no information about the pyramidal-to-pyramidal connection in the presubiculum, but presubicular pyramidal-to-Martinotti synapse follows the same logic.

Sixty percent of presubicular neurons are head direction cells (Boccaro et al., 2010) and these neurons can sustain firing, sometimes at high frequency (Fig. 8), when the animal remains within the directional range of the head direction cell (HDC) (Taube et al., 1990). The PC-to-MC synapse is perfectly tuned to function in the context of a sustained head direction signal, as its very low initial transfer rate acts as a high pass filter (Abbott and Regehr, 2004), insensitive to sharp increases, but enhanced over time. We predict that MCs should not be recruited during fast head turns that don't involve a sustained activation of a HDC. We show that inhibition by a MC does not have much inhibitory effect on PC discharge induced by somatic DC injection. However, the inhibitory effect may be higher in dendrites. Presubicular pyramidal cell dendrites may produce electrical regenerative events (Simonnet and Fricker, unpublished) which may be affected by MC inhibition similar to the inhibition of dendritic spikes by MCs (Larkum et al., 1999; Murayama et al., 2009). When persistently signaling a head direction, the inhibition of dendritic excitatory inputs is likely to be enhanced, which may

function as a homeostatic process avoiding over-excitation in the intrinsic network (Isaacson and Scanziani, 2011). At the same time, dendritic inhibition should not abolish output firing rate, which is consistent with the fact that no adaptation was reported for HDC firing (Taube et al., 1990). MC inhibition could however help to synchronize spiking activity of neurons with the same or very close tuning properties, opening time windows for dendritic excitation.

Feedback inhibition mediated by MCs may be particularly important to improve the accuracy of head direction signal. We found that inhibition had a lower effect if it was synchronized with the AHP, namely when it corresponded to self-induced feedback inhibition (PC1 fires a MC that reciprocally inhibits PC1). Thus, self-induced feedback inhibition (on PC1) should be weaker than lateral inhibition (on PC2). Continuous attractor network models suggests that the best-tuned HDC fires at maximum frequency, neighboring HDCs fire less, and a feedback inhibition limits the overall activity (McNaughton et al., 2006). Based on PC-to-MC synapse dynamics, we assume that PC1 may be the best to recruit a MC. In turn, the MC may mediate a global feedback inhibition affecting PC2 and to a lesser extent PC1, because inhibition is time locked to PC1 firing. Hence, the activity-dependent recruitment of Martinotti cells by the presubicular intrinsic recurrent network could make an ideal inhibitory feedback loop, perfectly tuned to refine the rate coding of the Head Direction Cells.

## **Figure Legends**

### **Figure 1. Electrophysiological intrinsic properties of Martinotti cells and pyramidal cells in superficial layers.**

**(A)** Current clamp recordings of a MC (green) and a PC (blue) at resting membrane potential (RMP), and **(B)** the values for 32 MCs and 28 PCs. **(C)** Typical responses of a MC and a PC to negative and positive current step injection of 800 ms, and the corresponding IV curves **(D)**. **(E)** Compared input resistance for 32 MCs and 28 PCs. **(F)** Input-Output curves of the firing rate (Hz) as a function of injected currents revealed **(G)** a lower threshold current and higher input-output (I-O) gain in MCs than in PCs. **(H)** The high sag ratio is typical for MCs. Note there are fewer values for sag ratio (27 for MCs, 18 for PCs) compared to other parameters, because it is calculated for steady-state potential values comprised within a -90 to -100 mV range (Nassar et al. in preparation), not always reached in our recordings. In B, E and H, orange horizontal bars indicate the mean value.

### **Figure 2. Compared morphology of Martinotti and pyramidal cells and their connectivity in the slice preparation.**

**(A)** Neurolucida reconstruction of a reciprocally connected pair in layer 3, disposed on a picture of the corresponding slice during the recording. PC dendrites covered layer 1 and 3, the preferentially targeted area of the MC axon (**inset**), whereas the PC axon mainly innervates layer 3, where MC dendrites are found (**inset**). DG: dentate gyrus, Pas: Parasubiculum **(B)** Proportion of unilaterally and reciprocally connected pairs. Number of tested connection may vary because they were not always tested in both directions.

### **Figure 3. Properties of Martinotti cell inhibitory synapses.**

**(A)** Single action potentials were elicited at 0.5 Hz in a MC (green trace) and individual inhibitory currents were recorded in a connected PC clamped at -50 mV, then averaged (av, 74 traces). **(B)** Corresponding IPSC amplitude (black) and noise (white) histograms. The transfer rate was calculated with a threshold corresponding to 1.6 times the RMS of noise. **(C)** Average amplitudes (including failures) for n = 22 paired. **(D)** Dynamic of synaptic responses for 10 action potentials triggered at 50 Hz. The average amplitude (av, 40 traces) depressed during repetitive stimuli, likely due to an increase of failure rate over time, visible on individual trials.

**Figure 4. Timing dependent inhibitory effect of Martinotti cells.**

**(A)** Firing was induced at 30 – 40 Hz in a PC with current step injection (blue) and single spikes were elicited in a connected MC (green) using 2 ms pulses of 1.5 nA. IPSP, triggered by a MC action potential is clearly visible on the top trace (arrow), but less so in the bottom trace (arrow) because it is almost synchronized with the trough of the afterhyperpolarization (AHP). *MC delay* is the delay of MC firing from PC firing as indicated; *post/ISI* is the inter-spike-interval during which MC fires; *pre/ISI* is the previous one. The magnitude of the inhibitory effect was calculated as  $1 - \text{post/ISI/pre/ISI}$  and plotted as a function *MC delay* **(B)**. Note that the inhibitory effect is relatively weak, but tends to be stronger as *MC delay* increases. **(C)** For a reciprocally connected pair, inhibition is triggered by the PC spike with very short latency and boosts the PC AHP, as indicated by red filled areas.

**Figure 5. Repetitive stimulus un-mutes the pyramidal cell to Martinotti cell excitatory synapses.**

**(A)** 30 action potentials were elicited at 30 Hz in a PC while a connected MC was recorded in voltage clamp mode at -65 mV. Note that there are more EPSCs (apparent as vertical descending lines) at the end of the stimulation. The synaptic transfer rate was determined with two different methods (see methods) exposed in this figure. **(B)** Synaptic transfer raster plots, each line representing on trial. Blue bars indicate presynaptic action potentials and red dots represent EPSCs that were triggered within a monosynaptic delay of less than 3 ms. Early and late transfer rates were calculated from action potential 1 to 5 and from action potential 26 to 30, respectively. **(C)** The late transfer rate was systematically and significantly (Wilcoxon signed rank test,  $p = 0.0078$ ;  $n = 7$  pairs) higher than the early transfer rate. The EPSC amplitudes were significantly (Wilcoxon signed rank test,  $p=0.0391$ ) higher as well, but the amplitude increase was observed in 5 out of 7 pairs only. **(D)** Early and late action potentials were detected and aligned at their peak. Average synaptic responses are higher for late action potentials, which translates the increase in transfer rate apparent in traces of individual responses. **(E)** Corresponding EPSC and noise amplitude histograms. The indicated transfer rate was calculated with a threshold corresponding to 1.6 times the RMS of noise (see methods). **(F)** Transfer rate deduced from peak amplitude measurement was plotted as a function of transfer rate obtained with EPSC detection. Early transfer rate is depicted in orange, late transfer rate in purple. The two methods give comparable results.

**Figure 6. Frequency-dependent synaptic transfer from pyramidal cell to Martinotti cell.**

**(A)** 30 action potentials were elicited at either 10 or 30 Hz in a PC while a connected MC was recorded in voltage clamp mode at -65 mV. **(B)** Synaptic transfer raster plots, each line representing on trial. Blue bars indicate presynaptic action potentials and red dots represent EPSCs that were triggered within a monosynaptic delay of less than 3 ms. Note that there are more EPSCs elicited during the 30 Hz train. **(C)** Frequency dependent enhancement of transfer rate for  $n = 9$  pairs (\*\* Wilcoxon signed rank test,  $p=0.002$ ). **(D)** Similar result obtained with a protocol of step current injections of increasing amplitude in the PC. Again, synaptic transfer, calculated for the 10 first action potentials, was enhanced by the increasing firing frequency of the PC; in this example, the MC was recorded in current clamp mode at resting membrane potential ( $\sim -55$  mV) and summation of synaptic potentials for high frequency firing of the PC initiated 1 action potential in the MC. **(E)** Transfer rate increases with increasing presynaptic firing frequency; gray traces are individual cells, black trace represents the average of individual from 25 to 40 Hz.

**Figure 7. Low firing frequencies can efficiently transfer information, depending on past activity of pyramidal cell.**

**(A)** A sequence, including a 10 Hz stimulus (pre 10 Hz) followed by an un-muting stimulus, followed by another 10 Hz stimulus (post 10 Hz), was applied in a PC, as the MC was recorded in voltage clamp mode at -65 mV. **(B)** Synaptic transfer raster plots show a clear enhancement after the un-muting stimulation. **(C)** Summary data from  $n = 3$  pairs. **(D)** and **(E)** Maintained current injections were applied to induce maintained firing in a PC while a MC was recorded in current clamp mode. The top graphs show the evolution of presynaptic instantaneous frequency with time of stimulation (blue +). Instantaneous frequency was calculated for each spike as the inverse of the previous inter-spike interval. Red dots indicate the monosynaptic EPSPs in the postsynaptic MC. The lower graphs (gray line) show the evolution of transfer rate as a function of time. For the two stimuli, firing frequency adapted, from 20 to 10 Hz in **(D)** and from  $\sim 50$  to 20 Hz in **(E)**. In **(D)**, the initial frequency did not enhance transfer rate, which therefore stayed low (0 – 0.25). In **(E)**, the initial frequency unmuted and locked synaptic transfer at higher level (0.2 - 0.5), even if presynaptic frequency diminished. **(F)** Results for  $n = 3$  pairs: with an initial low frequency stimulation (orange dashed-line), synapses remain quite un-efficient (orange line); with a higher initial frequency (bleu dashed-line), synapses are enhanced and transfer rate (blue line) stays high even if firing frequency diminishes.

**Figure 8. Recruitment of Martinotti cells during natural discharge of pyramidal cells.**

**(A)** Polar plot of a head direction cell, representing the firing frequency (Hz) as a function of head direction (°). **(B)** Raster plots showing the firing pattern of this head direction cell within its directional firing range. Note that the firing is highly irregular. **(C)** Histogram of the instantaneous frequencies as the animals turned its head within the directional firing range. **(D)** Sample period during which a sustained firing occurred (282 - 286 s) as the head remained within the directional firing range (200 - 240°). **(E)** This firing pattern was injected in a PC, while a connected MC was recorded either in current clamp mode at RMP, or in voltage clamp mode at -65 mV. **(F)** Transfer rates plotted for each presynaptic action potential; on the top (example shown above), pair that had a high basal transfer rate; on the bottom, a pair that had a lower initial transfer rate. Downward red lines indicate a transfer rate of 0. **(G)** and **(H)**, “burst” of activity underlined by the gray box in (E) and (F) at shorter time scale. The initial transfer was null, then progressively increased so this single PC was able to reliably fire the MC at the end of the bursting period (5/5); the transfer rate remained elevated during the subsequent firing at lower frequencies. The synapse with lower transfer rate followed the same dynamics, at a lower level.

Figure 1

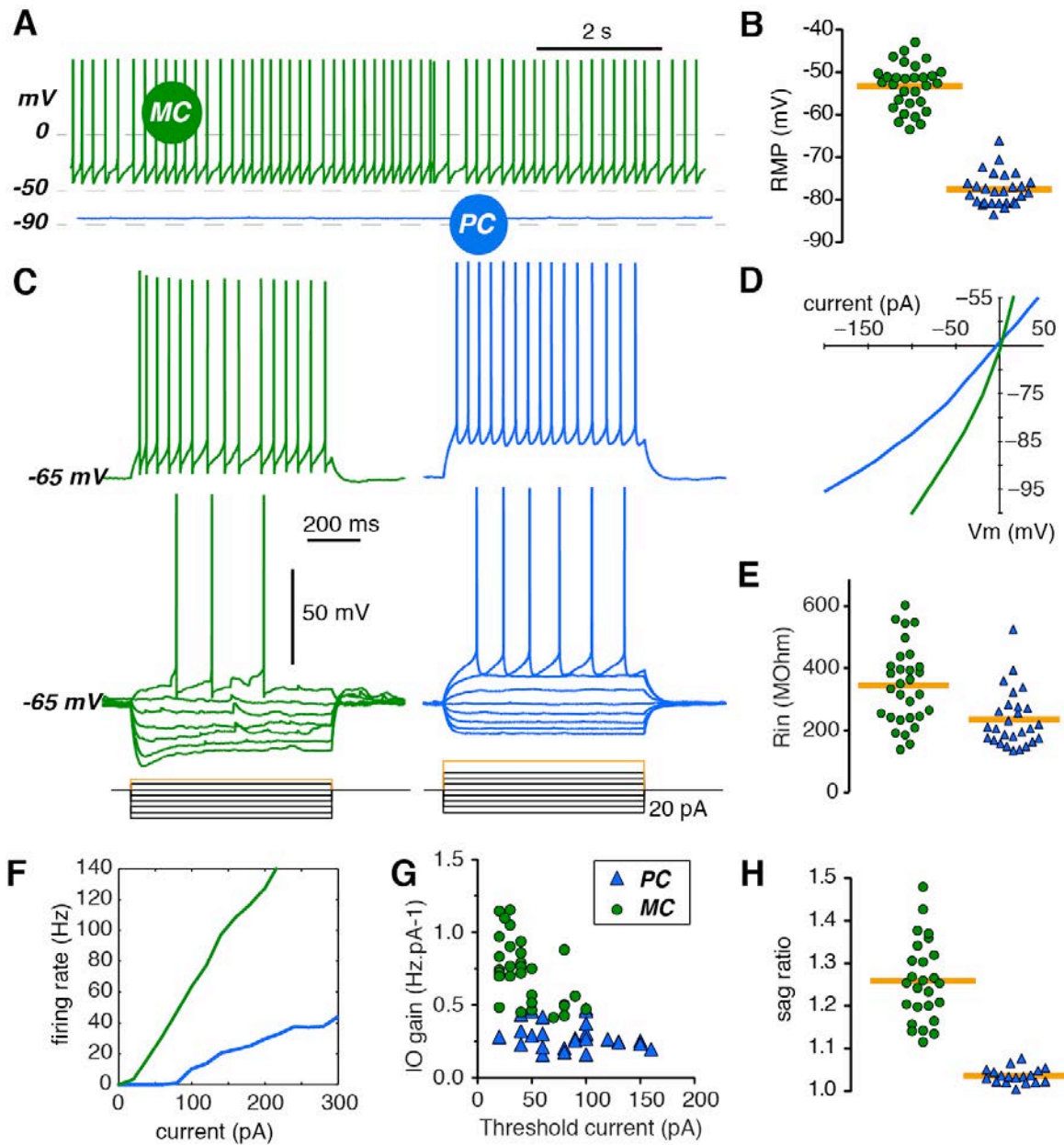


**Figure 1. Electrophysiological intrinsic properties of Martinotti cells and pyramidal cells in superficial layers of presubiculum.**

(A) Current clamp recordings of a MC (green) and a PC (blue) at resting membrane potential (RMP), and (B) the values for 32 MCs and 28 PCs. (C) Typical responses of a MC and a PC to negative and positive current step injection of 800 ms, and the corresponding IV curves (D). (E) Compared input resistance for 32 MCs and 28 PCs. (F) Input-Output curves of the firing rate (Hz) as a function of injected currents revealed (G) a lower threshold current and higher input-output (I-O) gain in MCs than in PCs. (H) The high sag ratio is typical for MCs. Note there are fewer values for sag ratio (27 for MCs, 18 for PCs) compared to other parameters, because it is calculated for steady-state potential values comprised within a -90 to -100 mV range (Nassar et al. in preparation), not always reached in our recordings. In B, E and H, orange horizontal bars indicate the mean value.

Figure 2

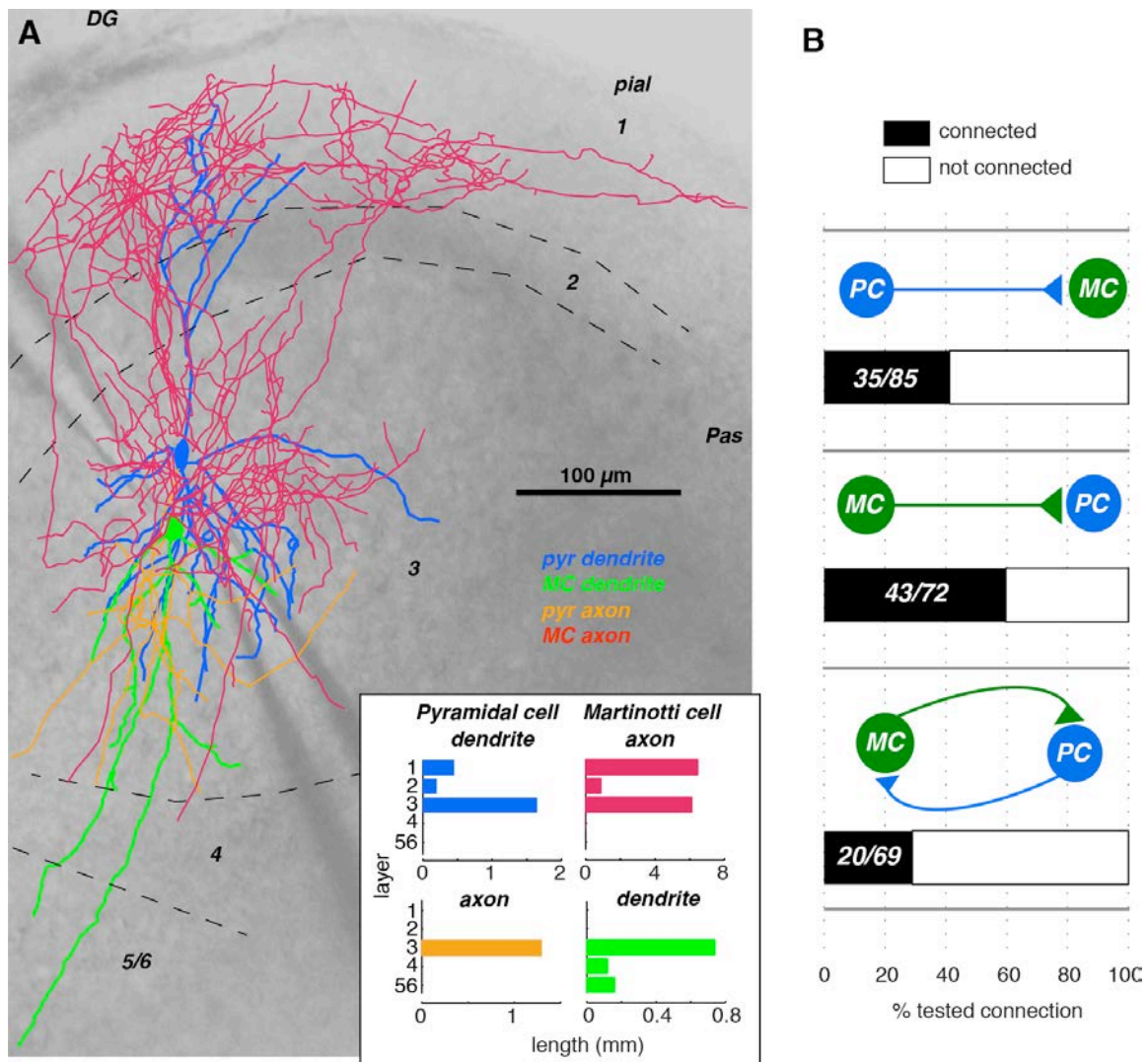


**Figure 2. Compared morphology of Martinotti and pyramidal cells and their connectivity in the slice preparation.**

**(A)** Neurolucida reconstruction of a reciprocally connected pair in layer 3, disposed on a picture of the corresponding slice during the recording. PC dendrites covered layer 1 and 3, the preferentially targeted area of the MC axon (**inset**), whereas the PC axon mainly innervates layer 3, where MC dendrites are found (**inset**). DG: dentate gyrus, Pas: Parasubiculum **(B)** Proportion of unilaterally and reciprocally connected pairs. Number of tested connection may vary because they were not always tested in both directions.

Figure 3

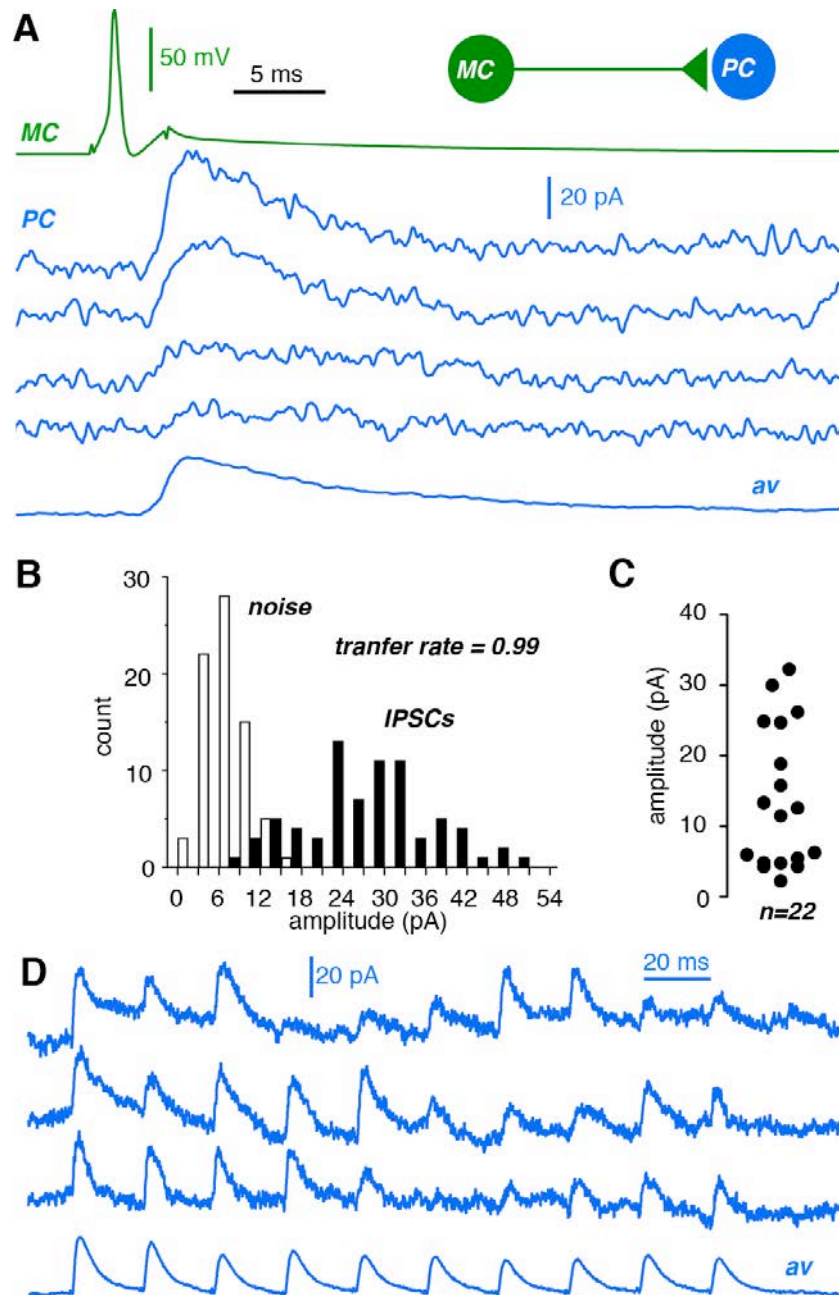


**Figure 3. Properties of Martinotti cell inhibitory synapses.**

(A) Single action potentials were elicited at 0.5 Hz in a MC (green trace) and individual inhibitory currents were recorded in a connected PC clamped at -50 mV, then averaged (av, 74 traces). (B) Corresponding IPSC amplitude (black) and noise (white) histograms. The transfer rate was calculated with a threshold corresponding to 1.6 times the RMS of noise. (C) Average amplitudes (including failures) for n = 22 paired. (D) Dynamic of synaptic responses for 10 action potentials triggered at 50 Hz. The average amplitude (av, 40 traces) depressed during repetitive stimuli, likely due to an increase of failure rate over time, visible on individual trials.

Figure 4

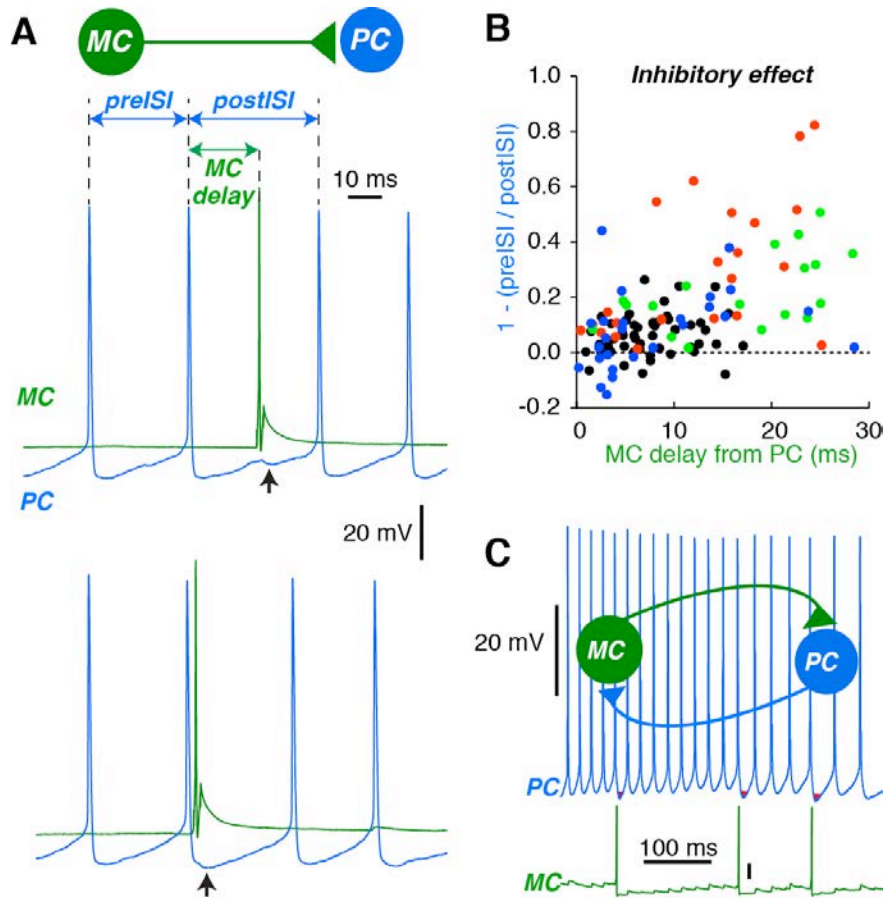


**Figure 4. Timing dependent inhibitory effect of Martinotti cells.**

(A) Firing was induced at 30 – 40 Hz in a PC with current step injection (blue) and single spikes were elicited in a connected MC (green) using 2 ms pulses of 1.5 nA. IPSP, triggered by a MC action potential is clearly visible on the top trace (arrow), but less so in the bottom trace (arrow) because it is almost synchronized with the trough of the afterhyperpolarization (AHP). *MC delay* is the delay of MC firing from PC firing as indicated; *postISI* is the inter-spike-interval during which MC fires; *preISI* is the previous one. The magnitude of the inhibitory effect was calculated as  $1 - \text{postISI}/\text{preISI}$  and plotted as a function *MC delay* (B). Note that the inhibitory effect is relatively weak, but tends to be stronger as *MC delay* increases. (C) For a reciprocally connected pair, inhibition is triggered by the PC spike with very short latency and boosts the PC AHP, as indicated by red filled areas.

**Figure 5**

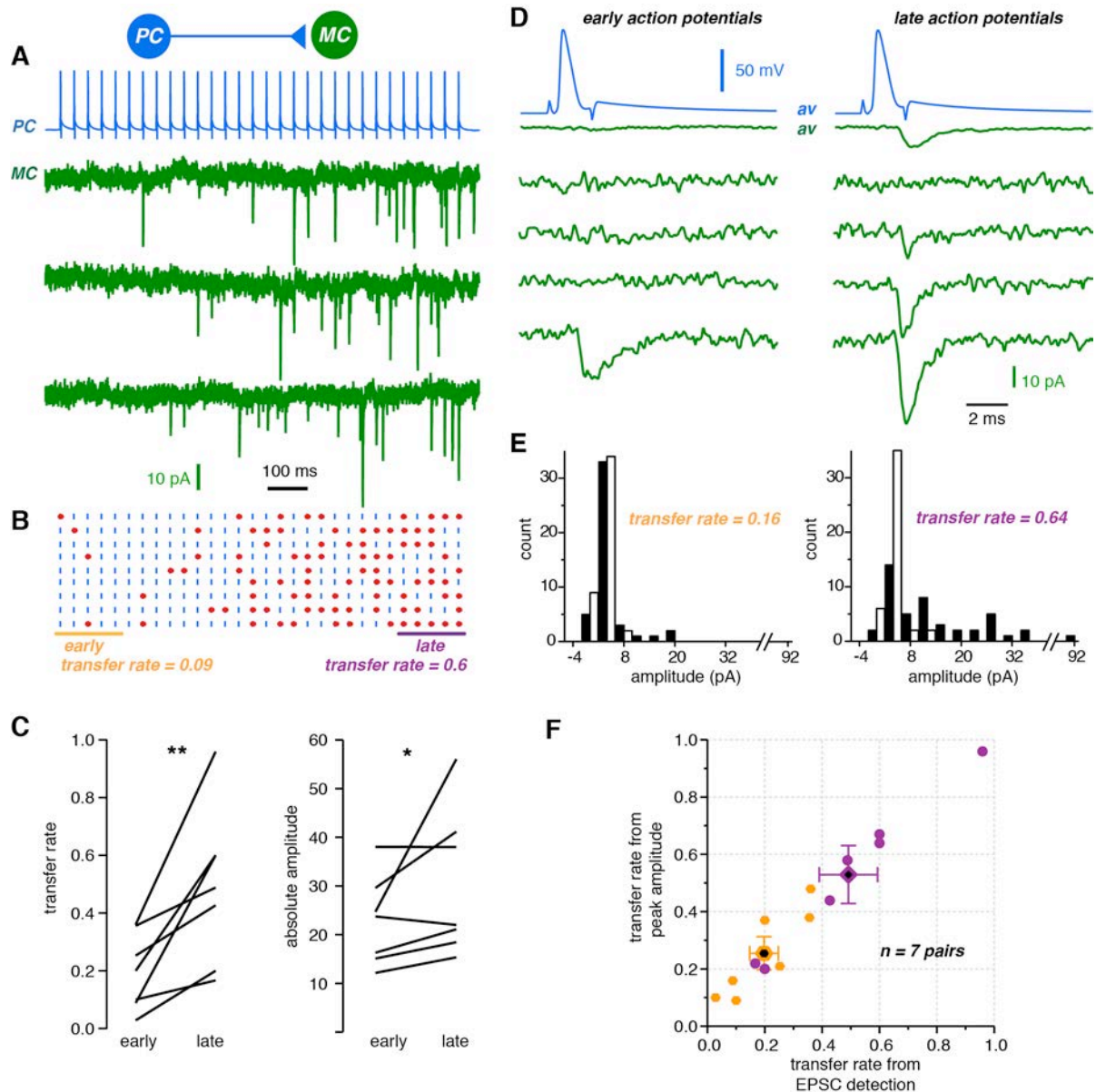


**Figure 5. Repetitive stimulus unmutes the pyramidal cell to Martinotti cell excitatory synapses.** (A) 30 action potentials were elicited at 30 Hz in a PC while a connected MC was recorded in voltage clamp mode at -65 mV. Note that there are more EPSCs (apparent as vertical descending lines) at the end of the stimulation. The synaptic transfer rate was determined with two different methods (see methods) exposed in this figure. (B) Synaptic transfer raster plots, each line representing on trial. Blue bars indicate presynaptic action potentials and red dots represent EPSCs that were triggered within a monosynaptic delay of less than 3 ms. Early and late transfer rates were calculated from action potential 1 to 5 and from action potential 26 to 30, respectively. (C) The late transfer rate was systematically and significantly (Wilcoxon signed rank test,  $p = 0.0078$ ;  $n = 7$  pairs) higher than the early transfer rate. The EPSC amplitudes were significantly (Wilcoxon signed rank test,  $p = 0.0391$ ) higher as well, but the amplitude increase was observed in 5 out of 7 pairs only. (D) Early and late action potentials were detected and aligned at their peak. Average synaptic responses are higher for late action potentials, which translates the increase in transfer rate apparent in traces of individual responses. (E) Corresponding EPSC and noise amplitude histograms. The indicated transfer rate was calculated with a threshold corresponding to 1.6 times the RMS of noise (see methods). (F) Transfer rate deduced from peak amplitude measurement was plotted as a function of transfer rate obtained with EPSC detection. Early transfer rate is depicted in orange, late transfer rate in purple. The two methods give comparable results.

Figure 6

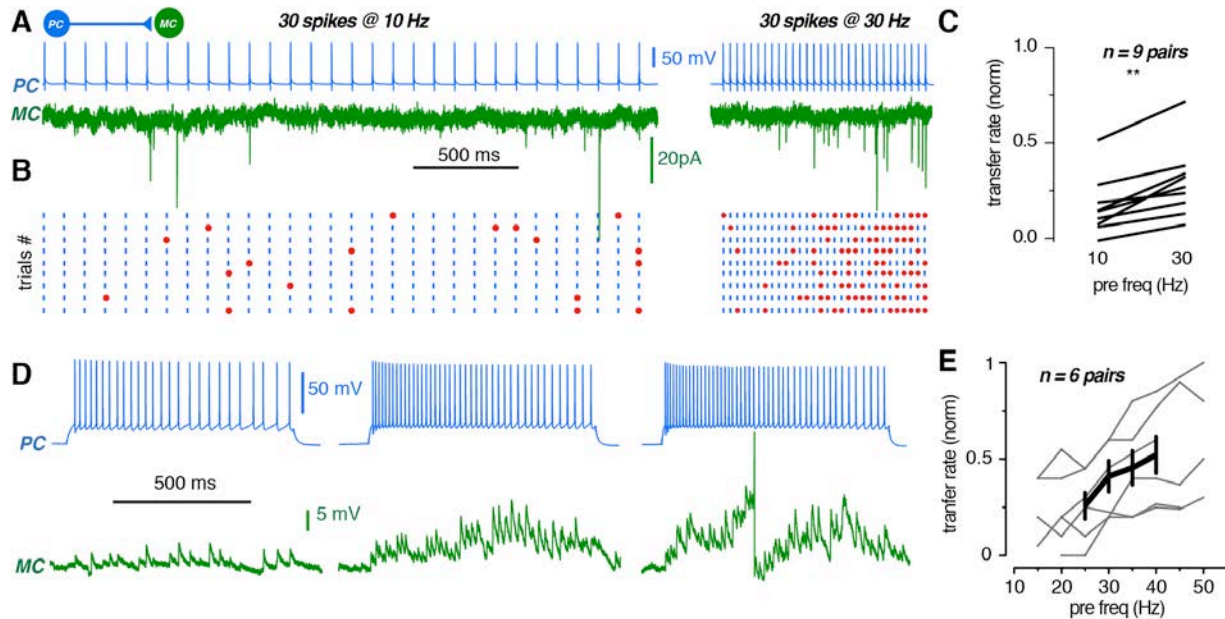


**Figure 6. Frequency-dependent synaptic transfer from pyramidal cell to Martinotti cell.**

(A) 30 action potentials were elicited at either 10 or 30 Hz in a PC while a connected MC was recorded in voltage clamp mode at  $-65$  mV. (B) Synaptic transfer raster plots, each line representing on trial. Blue bars indicate presynaptic action potentials and red dots represent EPSCs that were triggered within a monosynaptic delay of less than 3 ms. Note that there are more EPSCs elicited during the 30 Hz train. (C) Frequency dependent enhancement of transfer rate for  $n = 9$  pairs (\*\* Wilcoxon signed rank test,  $p=0.002$ ). (D) Similar result obtained with a protocol of step current injections of increasing amplitude in the PC. Again, synaptic transfer, calculated for the 10 first action potentials, was enhanced by the increasing firing frequency of the PC; in this example, the MC was recorded in current clamp mode at resting membrane potential ( $\sim -55$  mV) and summation of synaptic potentials for high frequency firing of the PC initiated 1 action potential in the MC. (E) Transfer rate increases with increasing presynaptic firing frequency; gray traces are individual cells, black trace represents the average of individual from 25 to 40 Hz.

**Figure 7**

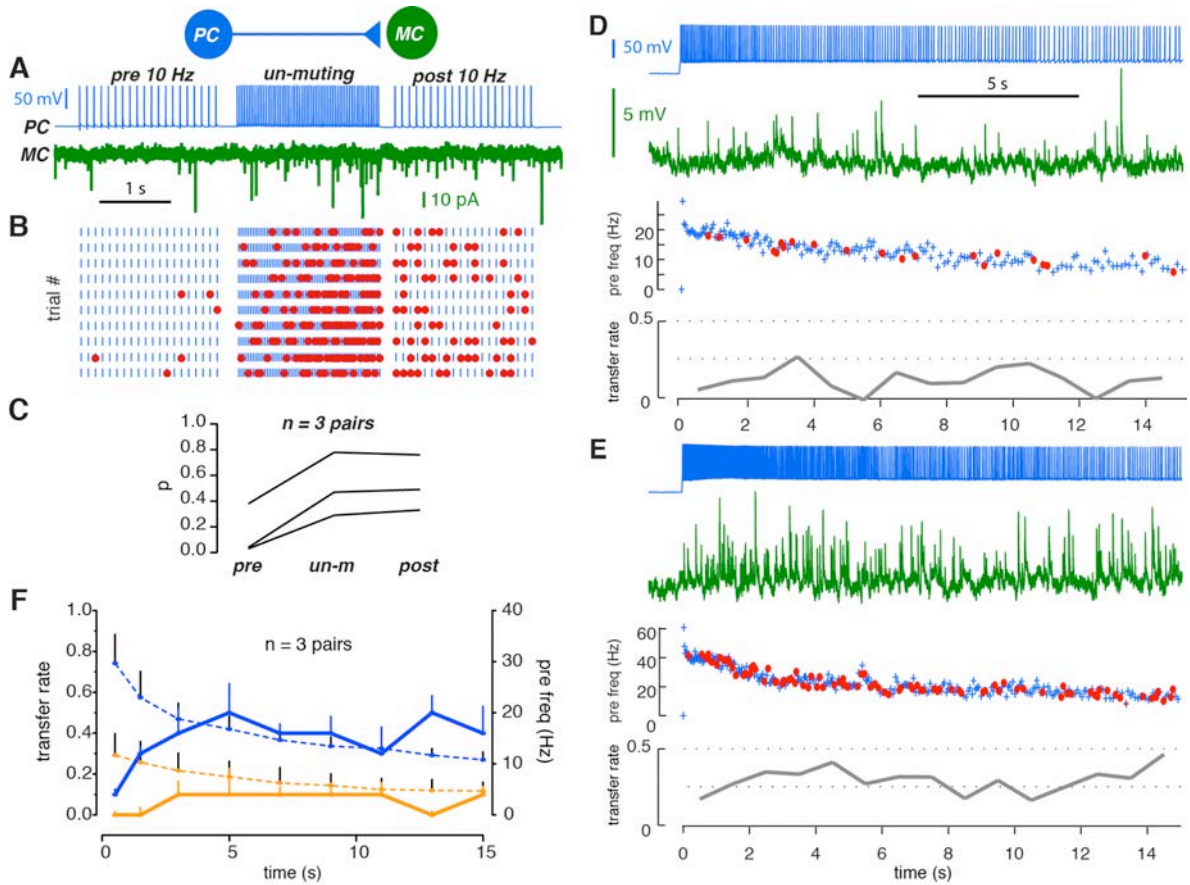


**Figure 7. Low firing frequencies can efficiently transfer information, depending on past activity of pyramidal cell.**

(A) A sequence, including a 10 Hz stimulus (pre 10 Hz) followed by an un-muting stimulus, followed by another 10 Hz stimulus (post 10 Hz), was applied in a PC, as the MC was recorded in voltage clamp mode at -65 mV. (B) Synaptic transfer raster plots show a clear enhancement after the un-muting stimulation. (C) Summary data from  $n = 3$  pairs. (D) and (E) Maintained current injections were applied to induce maintained firing in a PC while a MC was recorded in current clamp mode. The top graphs show the evolution of presynaptic instantaneous frequency with time of stimulation (blue +). Instantaneous frequency was calculated for each spike as the inverse of the previous inter-spike interval. Red dots indicate the monosynaptic EPSPs in the postsynaptic MC. The lower graphs (gray line) show the evolution of transfer rate as a function of time. For the two stimuli, firing frequency adapted, from 20 to 10 Hz in (D) and from ~50 to 20 Hz in (E). In (D), the initial frequency did not enhance transfer rate, which therefore stayed low (0 – 0.25). In (E), the initial frequency unmuted and locked synaptic transfer at higher level (0.2 - 0.5), even if presynaptic frequency diminished. (F) Results for  $n = 3$  pairs: with an initial low frequency stimulation (orange dashed-line), synapses remain quite un-efficient (orange line); with a higher initial frequency (bleu dashed-line), synapses are enhanced and transfer rate (blue line) stays high even if firing frequency diminishes.

**Figure 8**

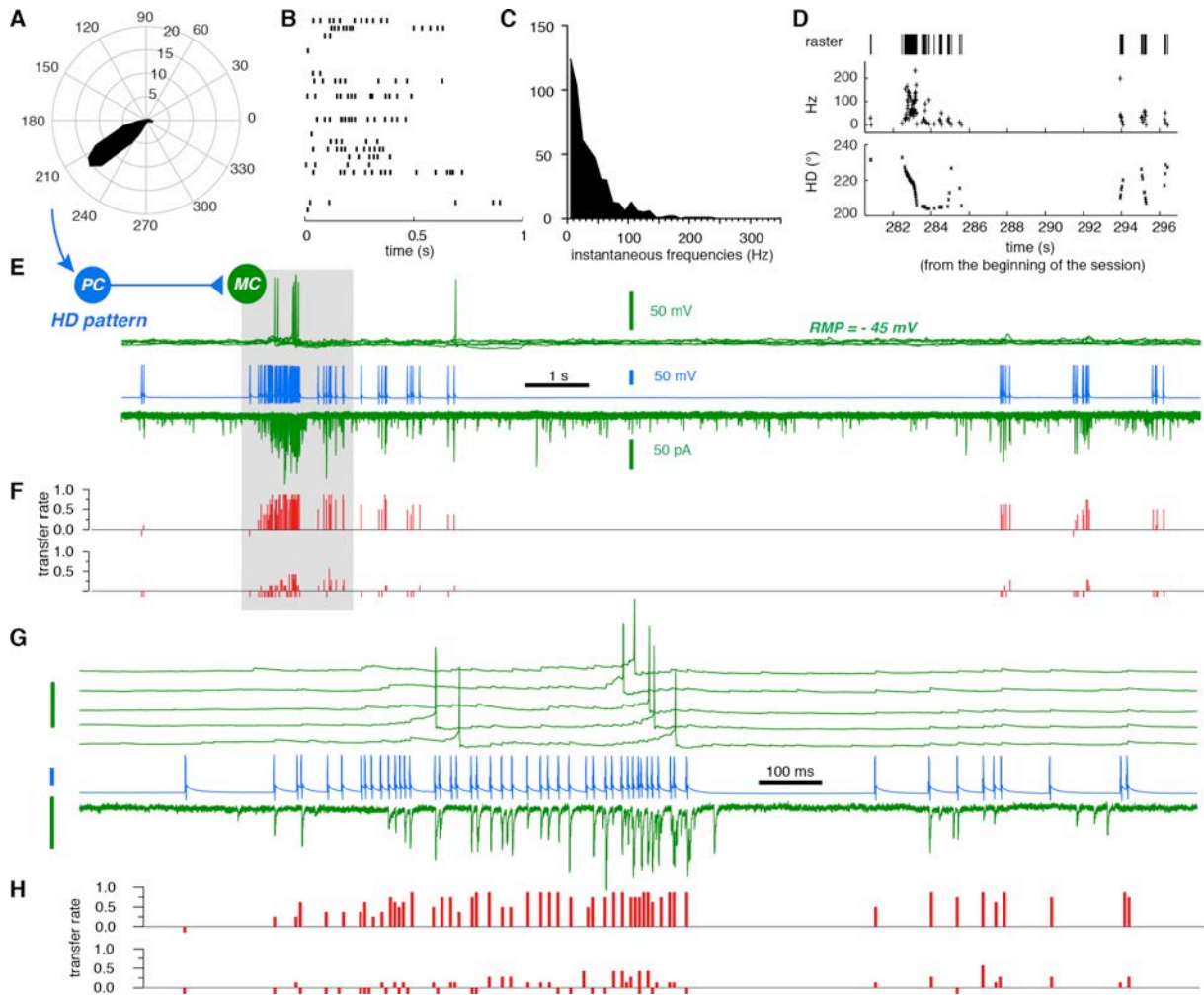


**Figure 8. Recruitment of Martinotti cells during natural discharge of pyramidal cells.**

(A) Polar plot of a head direction cell, representing the firing frequency (Hz) as a function of head direction ( $^{\circ}$ ). (B) Raster plots showing the firing pattern of this head direction cell within its directional firing range. Note that the firing is highly irregular. (C) Histogram of the instantaneous frequencies as the animals turned its head within the directional firing range. (D) Sample period during which a sustained firing occurred (282 - 286 s) as the head remained within the directional firing range (200 - 240 $^{\circ}$ ). (E) This firing pattern was injected in a PC, while a connected MC was recorded either in current clamp mode at RMP, or in voltage clamp mode at -65 mV. (F) Transfer rates plotted for each presynaptic action potential; on the top (example shown above), pair that had a high basal transfer rate; on the bottom, a pair that had a lower initial transfer rate. Downward red lines indicate a transfer rate of 0. (G) and (H), "burst" of activity underlined by the gray box in (E) and (F) at shorter time scale. The initial transfer was null, then progressively increased so this single PC was able to reliably fire the MC at the end of the bursting period (5/5); the transfer rate remained elevated during the subsequent firing at lower frequencies. The synapse with lower transfer rate followed the same dynamics, at a lower level.

## Tables

**Table 1. Electrophysiological properties of presubicular pyramidal cells and Martinotti cells.**

	Pyramidal cells			Martinotti cells		
	mean	std	n	mean	std	n
resting membrane potential (mV)	<b>-77.5</b>	0.7	28	<b>-53.3</b>	0.9	32
time constant (ms)	<b>25.8</b>	2.4	25	<b>36.7</b>	3.7	26
input resistance (M $\Omega$ )	<b>233.8</b>	16.9	28	<b>342.4</b>	22.3	31
sag ratio	<b>1.03</b>	0.00	18	<b>1.26</b>	0.02	27
rheobase (pA)	<b>88.6</b>	7.0	28	<b>44.2</b>	4.3	32
input-output gain (Hz/pA)	<b>0.296</b>	0.019	28	<b>0.728</b>	0.040	31
firing frequency @ 2x rheobase (Hz)	<b>36.0</b>	3.1	28	<b>31.2</b>	2.5	32
action potential rising amplitude (mV)	<b>82.9</b>	1.3	28	<b>81.6</b>	1.1	32
action potential half duration (ms)	<b>0.561</b>	0.019	28	<b>0.282</b>	0.005	32
AP rising phase speed (V/s)	<b>507.6</b>	17.6	28	<b>575.2</b>	14.6	32
AP falling phase speed (V/s)	<b>-135.9</b>	4.6	28	<b>-335.6</b>	9.7	32

**Table 2: Increasing transfer rate at the PC-to-MC synapse during repetitive firing.** Calculated early and late transfer rates during trains of 30 spikes at either 10 or 30 Hz. Early and late transfer rates were calculated from action potential 1 to 5 and from action potential 26 to 30, respectively. The variation between late and early was calculated for each frequency, as well as the increase between early and late phase between frequencies. Sometimes, the increase cannot be calculated if initial transfer rate is null, so the mean value can be underestimated.

	Transfer rates				Transfer rate variations			
	10Hz		30Hz		Late / Early		30Hz / 10Hz	
	Early	Late	Early	Late	10Hz	30Hz	Early	Late
pair_13o08c1c2	0.21	0.30	0.36	0.49	1.4	1.4	1.7	1.6
pair_13o11c4c5	0.00	0.16	0.10	0.17	inf	1.7	inf	1.0
pair_13o23c6c7	0.06	0.30	0.14	0.60	4.8	4.4	2.2	2.0
pair_13o25c3c5	0.02	0.16	0.09	0.60	7.0	6.7	4.0	3.9
pair_13n26c4c5	0.00	0.00	0.03	0.20	inf	7.0	inf	inf
pair_13d16c1c2	0.32	0.66	0.36	0.96	2.1	2.7	1.1	1.5
pair_13d16c10c11	0.20	0.12	0.25	0.43	0.6	1.7	1.3	3.6
pair_13d19c11c12	0.00	0.33	0.07	0.33	inf	5.0	inf	1.0
<b>MEAN</b>	<b>0.10</b>	<b>0.25</b>	<b>0.17</b>	<b>0.47</b>	<b>3.17</b>	<b>3.81</b>	<b>2.05</b>	<b>2.08</b>
<b>SD</b>	0.12	0.20	0.13	0.26	2.66	2.30	1.17	1.17
<b>SEM</b>	0.04	0.07	0.05	0.09	1.19	0.81	0.52	0.44
<b>N</b>	8	8	8	8	5	8	5	7

**Table 3: Frequency dependent transfer rate at the PC-to-MC synapse.** Calculated transfer rate over trains of 30 spikes (\* for this pair, spike train had 25 spikes) at 10 or 30 Hz. The 30Hz/10Hz column shows the variation between the two frequencies. Transfer rate per second was calculated by multiplying transfer rate with presynaptic frequency. Note that high increases between 10 and 30 Hz are often associated with very low transfer rates for 10 Hz (†).

	Transfer rates			Transfer rate per second		
	10Hz	30Hz	30Hz/10Hz	10Hz	30Hz	30Hz/10Hz
pair_13925c1c3 *	0.10	0.19	0.1	1.04	5.66	5.4
pair_13o08c1c2	0.28	0.39	1.4	2.81	11.67	4.2
pair_13o11c4c5	0.06	0.13	2.2	0.60	4.00	6.7
pair_13o23c6c7	0.24	0.42	1.8	2.39	12.67	5.3
pair_13o25c3c5	0.08	0.33	4.2	0.78	9.89	12.7
pair_13n26c4c5†	0.005	0.09	18.0	0.05	2.57	54.0
pair_13d16c1c2	0.51	0.73	1.4	5.13	22.00	4.3
pair_13d16c10c11	0.17	0.31	1.8	1.71	9.33	5.5
pair_13d19c11c12	0.21	0.27	1.3	2.11	8.00	3.8
<b>MEAN</b>	<b>0.18</b>	<b>0.32</b>	<b>3.58</b>	<b>1.85</b>	<b>9.53</b>	<b>11.31</b>
<b>SD</b>	0.15	0.19	5.52	1.53	5.77	16.23
<b>SEM</b>	0.05	0.06	1.84	0.51	1.92	5.41
<b>N</b>	9	9	9	9	9	9

- Abbasi S, Kumar SS (2013) Electrophysiological and morphological characterization of cells in superficial layers of rat presubiculum. *J Comp Neurol* 521:3116–3132.
- Abbott LF, Regehr WG (2004) Synaptic computation. *Nature* 431:796–803.
- Ali AB, Deuchars J, Pawelzik H, Thomson AM (1998) CA1 pyramidal to basket and bistratified cell EPSPs: dual intracellular recordings in rat hippocampal slices. *The Journal of Physiology* 507 ( Pt 1):201–217.
- Ali AB, Thomson AM (1998) Facilitating pyramid to horizontal oriens-alveus interneurone inputs: dual intracellular recordings in slices of rat hippocampus. *The Journal of Physiology* 507 ( Pt 1):185–199.
- Amaral DG, Witter MP (1989) The three-dimensional organization of the hippocampal formation: a review of anatomical data. *NSC* 31:571–591.
- Beierlein M, Gibson JR, Connors BW (2003) Two dynamically distinct inhibitory networks in layer 4 of the neocortex. *Journal of Neurophysiology* 90:2987–3000.
- Berger TK, Perin R, Silberberg G, Markram H (2009) Frequency-dependent disynaptic inhibition in the pyramidal network: a ubiquitous pathway in the developing rat neocortex. *The Journal of Physiology* 587:5411–5425.
- Boccaro CN, Sargolini F, Thoresen VH, Solstad T, Witter MP, Moser EI, Moser M-B (2010) Grid cells in pre- and parasubiculum. *Nature Publishing Group* 13:987–994.
- Debanne D, Bialowas A, Rama S (2013) What are the mechanisms for analogue and digital signalling in the brain? *Nat Rev Neurosci* 14:63–69.
- Fanselow EE, Richardson KA, Connors BW (2008) Selective, State-Dependent Activation of Somatostatin-Expressing Inhibitory Interneurons in Mouse Neocortex. *Journal of Neurophysiology* 100:2640–2652.
- Fino E, Yuste R (2011) Dense inhibitory connectivity in neocortex. *Neuron* 69:1188–1203.
- Funahashi M, Stewart M (1997) Presubicular and parasubicular cortical neurons of the rat: functional separation of deep and superficial neurons in vitro. *The Journal of Physiology* 501 ( Pt 2):387–403.
- Goodridge JP, Taube JS (1997) Interaction between the postsubiculum and anterior thalamus in the generation of head direction cell activity. *J Neurosci* 17:9315–9330.
- Gupta A, Wang Y, Markram H (2000) Organizing principles for a diversity of GABAergic interneurons and synapses in the neocortex. *Science* 287:273–278.
- Honda Y, Umitsu Y, Ishizuka N (2008) Organization of connectivity of the rat presubiculum: II. Associational and commissural connections. *J Comp Neurol* 506:640–658.
- Isaacson JS, Scanziani M (2011) How Inhibition Shapes Cortical Activity. *Neuron* 72:231–243.
- Kapfer C, Glickfeld LL, Atallah BV, Scanziani M (2007) Supralinear increase of recurrent inhibition during sparse activity in the somatosensory cortex. *Nat Neurosci* 10:743–753.
- Koester HJ (2005) Target Cell-Dependent Normalization of Transmitter Release at Neocortical Synapses. *Science* 308:863–866.
- Larkum ME, Zhu JJ, Sakmann B (1999) A new cellular mechanism for coupling inputs arriving at different cortical layers. *Nature* 398:338–341.
- Ma Y, Hu H, Berrebi AS, Mathers PH, Agmon A (2006) Distinct subtypes of somatostatin-containing neocortical interneurons revealed in transgenic mice. *Journal of Neuroscience* 26:5069–5082.
- Markram H, Lübke J, Frotscher M, Roth A, Sakmann B (1997) Physiology and anatomy of synaptic connections between thick tufted pyramidal neurones in the developing rat neocortex. *The Journal of Physiology* 500 ( Pt 2):409–440.
- Markram H, Wang Y, Tsodyks M (1998) Differential signaling via the same axon of neocortical pyramidal neurons. *Proc Natl Acad Sci USA* 95:5323–5328.

- McNaughton BL, Battaglia FP, Jensen O, Moser EI, Moser M-B (2006) Path integration and the neural basis of the “cognitive map.” *Nat Rev Neurosci* 7:663–678.
- Murayama M, Pérez-Garci E, Nevian T, Bock T, Senn W, Larkum ME (2009) Dendritic encoding of sensory stimuli controlled by deep cortical interneurons. *Nature* 457:1137–1141.
- Regehr WG (2012) Short-term presynaptic plasticity. *Cold Spring Harb Perspect Biol* 4:a005702.
- Silberberg G, Grillner S, LeBeau FEN, Maex R, Markram H (2005) Synaptic pathways in neural microcircuits. *Trends in Neurosciences* 28:541–551.
- Silberberg G, Markram H (2007) Disynaptic Inhibition between Neocortical Pyramidal Cells Mediated by Martinotti Cells. *Neuron* 53:735–746.
- Simonnet J, Eugène E, Cohen I, Miles R, Fricker D (2013) Cellular neuroanatomy of rat presubiculum. *Eur J Neurosci* 37:583–597.
- Taube JS, Muller RU, Ranck JB (1990) Head-direction cells recorded from the postsubiculum in freely moving rats. II. Effects of environmental manipulations. *J Neurosci* 10:436–447.
- van Groen T, Wyss JM (1990) The postsubicular cortex in the rat: characterization of the fourth region of the subicular cortex and its connections. *Brain Res* 529:165–177.
- van Strien NM, Cappaert NLM, Witter MP (2009) The anatomy of memory: an interactive overview of the parahippocampal–hippocampal network. *Nat Rev Neurosci* 10:272–282.
- Vogt BA, Miller MW (1983) Cortical connections between rat cingulate cortex and visual, motor, and postsubicular cortices. *J Comp Neurol* 216:192–210.
- Williams SR, Mitchell SJ (2008) Direct measurement of somatic voltage clamp errors in central neurons. *Nat Neurosci* 11:790–798.
- Williams SR, Stuart GJ (2003) Voltage- and site-dependent control of the somatic impact of dendritic IPSPs. *Journal of Neuroscience* 23:7358–7367.
- Yoder RM, Clark BJ, Taube JS (2011) Origins of landmark encoding in the brain. *Trends in Neurosciences*.
- Yoshida M, Hasselmo ME (2009) Persistent Firing Supported by an Intrinsic Cellular Mechanism in a Component of the Head Direction System. *Journal of Neuroscience* 29:4945–4952.
- Zhu J, Jiang M, Yang M, Hou H, Shu Y (2011) Membrane potential-dependent modulation of recurrent inhibition in rat neocortex. *PLoS Biol* 9:e1001032.
- Zucker RS, Regehr WG (2002) Short-term synaptic plasticity. *Annu Rev Physiol* 64:355–405.



# Discussion



# My PhD

During my PhD, I investigated the integrative properties of presubicular neurons at the anatomical, cellular and synaptic level in the context of microcircuit computation.

I studied the electrophysiological and morphological properties of presubicular principal cells in rat. I classified neurons according to different parameters reflecting their passive properties, firing patterns, action potential waveform, location, the orientation of dendrites and their repartition across layers. I applied an unsupervised clustering method using 27 descriptive parameters in total, for a dataset of 58 neurons. Neurons fell into 3 main groups in 3 different layers, with distinct morphological and electrophysiological properties. Superficial layer neurons were mainly pyramidal and all fired regularly with very little adaptation. This group constitutes a very homogeneous population. I discovered a population of intrinsically burst firing pyramidal cells in layer 4, and obtained preliminary data showing that these neurons project to lateral mammillary nucleus. Deep layer neurons were more heterogeneous, but they were all regular spiking with little adaptation, although it was a bit higher than for superficial layers. Two subgroups emerged; one corresponding to very excitable pyramidal neurons in upper layer 5, the other was composed of neurons with diverse morphologies and integrative properties. I showed that all regular spiking neurons had the intrinsic capability to maintain high frequency firing during tens of seconds. This work gave an overall view of the diversity of presubicular principal neurons.

In collaboration with Mérie Nassar, I next described the diversity of interneurons in mouse presubiculum. Similarly to my previous work, we recorded from identified fluorescent interneurons in the slice and reconstructed their anatomy. Unsupervised clustering based on electrophysiological parameters describing firing pattern, spike waveform and passive properties, revealed a continuum of diversity for PV+ and SST+ interneurons. We identified 3 groups of interneurons, partly following the expression of neurochemical markers. We found archetypal PV+ fast spiking cells and SST+ low threshold adapting interneurons. A third group of quasi-fast spiking cells lied at the transition between the two groups. In terms of morphology, dendritic and

axonal arbor of presubicular interneurons was quite coherent with the physiological classification, as the two archetypal groups displayed typical morphologies and the third one was very diverse even though anatomical features were not included in the cluster analysis. In conclusion of this work, two modalities of inhibition could exist in the presubiculum, the PV-mediated perisomatic inhibition and SST-mediated dendritic inhibition, although this still needs to be confirmed in future studies. The entire interneuronal population has not been characterized yet, but the presubicular inhibitory microcircuit is likely to possess the whole complexity of cortical areas regarding its diversity.

After the basic description of these neuronal populations, I have been interested in the synaptic interconnectivity in the presubicular microcircuit, looking at the fine interaction between pyramidal cells and Martinotti cells in superficial layers. I recorded from pairs of neurons and showed a high interconnectivity between pyramidal cells and Martinotti cells. The inhibitory synapse is reliable, but somatic inhibition is weak, probably due to the remote location of the synapse in the dendritic arbor. The inhibitory effect depends on the relative timing between synaptic event and pyramidal cell spike. Our results suggest that self-induced feedback inhibition (when the connection is reciprocal) may have less inhibitory effect than lateral inhibition. The dynamics of the pyramidal cell to Martinotti cell synapse is dependent on the presynaptic activity pattern. While this synapse is almost silent during sparse spiking activity, it facilitates strongly during sustained high frequency firing, and this effect persists for several seconds. We have not identified the mechanism underlying this synaptic un-muting yet. We suggest that this feedback inhibitory loop counterbalances excitation and preserves tuning of the head direction signal during prolonged discharge. I therefore defined the dynamics of a feedback inhibitory loop in the presubiculum.

# 1 | Building blocks of the presubiculum

The description of principal neurons and interneurons of the presubicular microcircuit is the basis for a better understanding of this understudied cortical area. My PhD work constitutes the first extensive study of electrophysiological and morphological properties of both major neuronal populations in the presubicular cortex. Indeed, little had been known about the cellular and anatomical substrates of presubicular components (Funahashi and Stewart, 1997a; Yoshida and Hasselmo, 2009; Fricker et al., 2009; Menendez de la Prida et al., 2003).

## 1.1 Did we correctly address the whole diversity of principal neurons?

In the wake of my publication on principal cell diversity in the presubiculum (Simmonet et al., 2013), another group published a similar study focused specifically on superficial layers (Abbasi and Kumar, 2013). The comparison of the two articles is a good way to appreciate the strengths, but also some weaknesses, of my work.

Both studies used unsupervised cluster analysis to classify presubicular neurons into distinct groups. Our dataset included 58 neurons located across all the presubicular cortex, completely characterized by both electrophysiological and morphological parameters. Putative interneurons were not included in our analysis. Abbasi and Kumar (2013) based their cluster analysis on electrophysiological parameters only, with a total number of 177 recorded neurons in the superficial layers. Morphology was obtained for a subset of neurons only, and correlated with the physiological classification at a subsequent time. Both studies found a majority of regular spiking neurons: 62% of the neurons in Abbasi's study were regular spiking neurons, with properties similar to those that we had described previously, representing 78% of all neurons in layer 3 and 56% in layer 2. Abbasi certainly better addressed the neuronal diversity in layer 2 compared to layer 3, as most neurons included in their study came from layer 2 (128). On the contrary, most of our recordings were coming from layer 3. Because the exact limit between layer 2 and 3 is not always obvious, we

had defined an objective measurement of depth and lateral position. The homogeneity of the neuronal properties that we described for superficial layer neurons largely reflects the properties of layer 3 neurons. As an example for diversity in layer 2, cell 174 in our Fig 3 (Simonnet et al., 2013) displayed distinct electrophysiological and morphological properties compared to the other neurons; this cell was grouped with other neurons of layer 2 with cluster analysis (84, 175, 63 in Fig 2), and we probably should have emphasized the existence of subpopulations in superficial layers as well.

One weakness of the work published by Abbasi and Kumar (2013) is the lower quality of their dataset compared to ours. Dendrites and axons can be damaged by the slicing procedure. In our study we had excluded low quality electrophysiological recordings and also cells with non-recovered dendritic arborization, which allowed us to get a high quality dataset, even though of rather modest size (58 neurons) compared to the number of initially recorded neurons (133 neurons). Abbasi and Kumar (2013) recorded 177 cells, filled 118 cells, recover 89 dendritic arborization and 42 axonal projections. Consequently, half of their recordings have no morphological correlate and three quarter may correspond to neurons with no or very limited axonal projections. The integrity of the proximal axon, which contains the axon initial segment, up to the first node in myelinated axons ( $100 \mu\text{m}$  from the soma) highly regulates subthreshold and firing properties (Kole, 2011; Battfeld et al., 2014, Rama et al. 9th FENS forum of Neuroscience 2014). Consequently, part of the diversity described by Abbasi and Kumar (2013) may reflect an experimental bias. It is worth noting that we also had neurons with limited axonal arborization ( $< 100 \mu\text{m}$ , 30%), which could have biased our results, but certainly not account for the heterogeneity of deep layer neurons as only 4 of these 26 neurons had a limited axonal length. The diversity of principal neurons in deep layers will deserve further investigation, and the identification of projecting neurons could be an elegant way to address this question.

As Abbasi and Kumar (2013) recorded many neurons in a confined area, their description of electrophysiological properties of neurons in superficial layers covered much of the existing diversity, even though it was not systematically correlated with morphology. In contrast, the strength, and the initial purpose, of our work was to describe neurons of all layers, in order to shed light on the overall organization of the circuit. We may have missed part of the diversity because of our limited dataset. Our approach has demonstrated that, like in other periallocortical or neocortical areas, the cellular properties of presubicular neurons follow their laminar organization.

## 1.2 Interneuron diversity

Cortical GABAergic interneurons represent only 20 % of cortical neurons, but they constitute a very heterogeneous population in terms of function, electrophysiological properties, dendritic and axonal projections (Isaacson and Scanziani, 2011; Gentet, 2012; Klausberger and Somogyi, 2008; Parra et al., 1998).

Parvalbumin (PV) positive interneurons and somatostatin (SOM) positive interneurons appear as two distinct computational elements of microcircuits (Gentet, 2012). They are often opposed in terms of function (perisomatic versus dendritic inhibition), morphologies (Basket cells versus Martinotti Cells) or intrinsic electrophysiological properties (fast spiking cells versus adapting cells).

We characterized the diversity of electrophysiological and morphological properties of these two major interneuron subtypes in the presubiculum, as described and discussed earlier. To summarize, PV+ and SOM+ interneurons formed a structured continuum of diversity, as we found two groups of archetypes (PV+ and SOM+) as well as a third group of intermediate neurons, lying at the frontier between archetypes (Battaglia et al., 2013).

The choice of parameters used for unsupervised cluster analysis has a high impact on the resulting classification (Cauli et al., 2000), therefore the results have to be interpreted carefully. Our classification is based on electrophysiological properties of neurons only, although anatomical features seemed quite specific within the different populations (Fig 5, Nassar et al.). One might think that using more or different parameters could have helped to better define the populations (Cauli et al., 2000). However, it is more important to include parameters that distinguish functional populations and we used independent parameters to obtain a non-biased classification. Too many parameters may water down the classification if included parameters are equally variable across all populations.

The molecular properties of SST+ and PV+ interneurons could have been revealed, using single cell RT-PCR (Cauli et al., 2000; Cabezas et al., 2013), or immunohistochemistry (Perrenoud et al., 2012).

PV+ and SOM+ neurons together with the 5HT3a+ cells are thought to represent all the cortical interneurons (Rudy et al., 2010). Consequently, in order to define the entire diversity of presubicular interneurons, the properties of 5HT3a interneurons should also be addressed.



## 2 | Perspective: from neuronal diversity to function

The morphological properties of principal neurons and interneurons indicate what kind of inputs they may receive, by comparing their dendritic morphology (Simonnet et al., 2013: Fig. 7; Nassar et al.: Fig. 5) with our knowledge on the laminar specificity of afferences and the projections of local axons (Simonnet et al., 2013: Fig. 7; Nassar et al.: Fig. 5) (Peters and Feldman, 1976). The integrative properties suggest how these neurons convert input into output (Simonnet et al., 2013: Fig. 8; Nassar et al.: Fig 4).

In fact, the description of neuronal features brought a lot of questions. We therefore defined hypotheses about the information flows and their regulation in the presubiculum, from afferences to microcircuit to efferences. For example, it is relevant to ask the question of the target-specificity of afferences. Are all the cells with dendrites in superficial layers (layer 2/3 pyramidal cells and interneurons, layer 4 and layer 5/6 pyramidal cells?) differentially or similarly targeted by a distinct input into superficial layers (e.g. thalamus)? Does a homogeneous population (e. g. layer 3 pyramidal cells) receive distinct inputs from distinct afferences targeting the same area (thalamus, retrosplenial cortex, visual cortex...)?

Preliminary results, obtained with optogenetic stimulation of afferences (Petreanu et al., 2007), showed that pyramidal cells and Pvalb-Cre RFP+ interneurons, but not Sst-Cre RFP+ interneurons in superficial layers were directly recruited by thalamic inputs (Mathon, Nassar, Simonnet and Fricker, unpublished). The direct recruitment of PV interneurons by long-range projections indicates a feedforward inhibitory circuit, whereas the SST interneuron may provide feedback inhibition (Cruikshank et al., 2010; Lee et al., 2013). Moreover, deep layer cells seem to be not directly targeted, but rather receive recurrent excitation. These results suggest that (1) superficial layer neurons are the main targets of thalamus, (2) they regulate information with inhibitory feedback and feedforward circuits, (3) they send the integrated information towards deep layers. The functional impact of the recruitment of interneurons in superficial layers will stay unclear as long as their specific targets

remain unknown.

Functional mapping, using caged glutamate photolysis (Beed et al., 2013; Fino and Yuste, 2011; Packer and Yuste, 2011) or optogenetic activation of identified neuronal populations (Zhao et al., 2011; Kätzel et al., 2010) are two ways to determine the local inhibitory connectivity. The Pvalb-Cre- or Sst-Cre- mice may be used to specifically induce the expression of channelrhodopsin-2 (Nagel et al., 2003) in these two specific subpopulations, allowing their specific light-induced activation in the presubicular microcircuit.

Ultimately, the functional implication of the different subtypes of interneurons in tuning the Head direction cells could be addressed *in vivo*, using specific inactivation of specific sub-population with halorhodopsins (Zhang et al., 2007). Tuning properties of head direction cells should be affected differently by distinct interneurons.

### **3 | Neurons that project to lateral mammillary (LMN) and anterodorsal thalamus (ADN): implication for the visual update of the head direction signal**

The LMN projecting neurons have been thought to be the preferential route for the visual update of the subcortical head direction signal (Yoder et al., 2011); different elements had been considered. The visual cortex sends direct projections to the superficial layers of presubiculum (Vogt and Miller, 1983). Thus, Yoder and Taube (2011) suggested that layer 4 pyramidal neurons could be their preferential targets, considering their prominent dendritic arborization that extends in superficial layers. The visual information necessary for presubicular action onto subcortical nuclei seems primarily mediated by these projections, as the indirect pathway via the retrosplenial cortex has less influence on visual update of subcortical head direction cells (Clark et al., 2010; Calton et al., 2008).

Our findings cast more doubt on these assumptions. Indeed, both ADN and LMN projecting neurons extend their dendrites in superficial layers, and superficial layer and layer 4 neurons send descending axons to deep layers (Simonnet et al., 2013), and might recruit ADN projecting neurons. Additional knowledge about the integration of visual cortical information in the presubicular microcircuit is necessary to predict how the presubiculum could operate visual control.

Nonetheless, LMN projecting neurons have interesting integrative properties to operate the fast visual update. It was shown that visual update was effective within very short latency (80 ms) in thalamus (Zugaro et al., 2003), suggesting that the integration in Visual cortex  $\rightarrow$  PrS  $\rightarrow$  LMN  $\rightarrow$  ADN or Visual cortex  $\rightarrow$  PrS  $\rightarrow$  ADN pathways should be very fast. We hypothesize that the fast integrative properties and the intrinsically burst firing behavior of LMN projecting neurons favor fast transfer of information, in both pathways. Efficient excitatory drive (burst) would be rapidly sent in parallel, to the LMN, and to neurons projecting to ADN via recurrent

axons (Simonnet et al., 2013). Thus, convergent information from the presubiculum and LMN may update head direction signal in thalamus. Yet, recurrent excitation of LMN projecting neurons onto ADN projecting neurons remains to be demonstrated.

Furthermore, the anticipation of future head direction is a characteristic of LMN (Stackman and Taube, 1998) and ADN (Goodridge and Taube, 1997) head direction cells, and modeling suggested that visual update should be delivered at low frequencies ( $< 1\text{Hz}$ ) to not disrupt the anticipatory time interval (van der Meer et al., 2007). Single spikes or intrinsically burst firing of LMN projecting layer 4 neurons may provide the necessary sparse coding as they do not sustain high frequency firing (Simonnet et al., 2013).

The diversity of ADN projecting and LMN projecting neurons has to be addressed further to complete these results and confirm their different integrative properties.

In a next step, we propose to test whether these populations are recruited by afferences from visual cortex or not. We will combine the retrograde tracing technique with stimulation of the visual afferences with optogenetics. We will (1) inject retrobeads in LMN or ADN to assist the selection of neurons in the presubicular slice; and (2) inject viral constructions expressing channelrhodopsin (Nagel et al., 2003) in the visual cortex that will let us stimulate corresponding fibers in slices (Petreanu et al., 2007). It is possible that neither, one or both populations receive direct input from the visual cortex fibers, and it is probable that other neurons, such as layer 3 neurons, or interneurons will also be recruited. In any case, this will shed light on the specific targets of visual cortex in the presubiculum; it will confirm or refute our hypothesis about the central role of layer 4 intrinsically bursting neurons in the relay of visual information from visual cortex to subcortical areas.

## 4 | Memory of past activity at the pyramidal cell-to-Martinotti cell synapse: properties and mechanisms

### 4.1 Better define the dynamics of the plasticity, its specificity and variability

The dynamics of the activity dependent increase of synaptic strength expressed at the PC-to-MC synapse are still awaiting further study. In this part, I will detail several issues that will need to be addressed in order to better define some aspects of this unusual form of synaptic plasticity: the time-course, the un-muting stimulus, the synapse specificity and the variability of transfer rate.

**The time-course.** The decay is one major parameter of all the plasticity processes as it characterizes the type of plasticity, that is, if it is a long-term process or a short-term process. We already know that the increase of transfer rate that we describe corresponds to a short term dynamic, but so far we ignore its precise time course. I therefore propose to perform continuous stimulation at low frequency (0.2- 0.5 Hz), as a probe of transfer rate, then to un-mute synaptic transfer at some point (with a high frequency stimulus) to subsequently determine the time-course of the decaying transfer rate.

**The un-muting stimulus.** I have already shown that un-muting depends on the number of presynaptic action potentials and their frequency. However, I have only tested some selected frequencies (10 Hz and 30 Hz). An un-muting index may be defined, corresponding to the number spikes necessary to increase the transfer rate by 2, 3, etc. By defining this for many frequencies (from 1 to 100 Hz), it should be possible to establish a representation of the transfer rate evolution as a function of stimulation duration and frequency, allowing a quantification of the un-muting requirements at the PC-to-MC synapse. My guess is that with increasing duration

and frequency, un-muting will be more efficient. Saturation may be reached at some point, as it was shown for the frequency dependence of short term facilitation in neocortex (Markram et al., 1998). Last, the activity dependent synaptic transfer at the PC-to-MC synapse could be modeled.

**Synapse specificity.** The PC-to-MC synapse was the only excitatory synapse that I have studied in the presubiculum so far. Short term dynamics of synapses have been shown to be synapse-specific in other cortical areas (Markram et al., 1998; Pouille and Scanziani, 2004, so it should be interesting to test the excitatory synapses that target other postsynaptic cells in the presubiculum as well. One obvious candidate would be the pyramidal cell-to-parvalbumin-positive interneuron synapse. My hypothesis is that the dynamics should be opposite. This is actually a crucial point, as it has important consequences concerning the specific role of Martinotti cells compared to other populations of interneurons in the presubiculum.

**Variability.** We noticed a rather high variability for initial transfer rates, differing from pair to pair (e.g. Fig. 4). This could possibly be due to the number of contacts made by the PC axon onto the MC. The numbers of putative contacts could be estimated by light microscopy of labeled neurons. However, electron microscopy is required to determine precisely the number of synaptic contacts (Markram et al., 1997). In the work by Markram et al. (1997) the number of synaptic contacts was not correlated with the amplitude of post synaptic events, but in fact the number of synapses was not very different (from 5 to 8) between neurons. More recently, number and size of active zones was shown to be a main determinant of release probability (Holderith et al., 2012). Light microscopy may therefore not be precise enough to determine the number of contacts; ultimately, analysis with electron microscopy will be required

## 4.2 Mechanisms of activity dependent synaptic transfer at the pyramidal cell to Martinotti cell synapse?

In this part, I will discuss possible mechanisms explaining the dynamics at the the pyramidal cell to Martinotti cell (PC-to-MC) synapse, and the experiments that could unveil those mechanisms.

### 4.2.1 Activity dependent action potential broadening

Activity dependent action potential broadening in the axon and the presynaptic terminal is known to increase calcium influx at the synapse, which enhances synaptic transfer (Geiger and Jonas, 2000; Sabatini and Regehr, 1997). I observed action potential broadening in the pyramidal cell during repetitive stimuli, and it was more pronounced for high frequencies (not shown). This phenomenon is primarily mediated by the activity dependent inactivation of potassium conductances implicated in action potential repolarization, including the D-type current, in neocortical layer 5 pyramidal cells (Foust et al., 2011; Kole et al., 2007; Shu et al., 2007) and CA3 pyramidal cells (Saviane et al., 2003), the A-type current in mossy fiber boutons (Geiger and Jonas, 2000) or the BK current in CA3 pyramidal cell synapses (Hu et al., 2001; Raffaelli et al., 2004). The presence of one, or several of these conductances in pyramidal cells of the presubiculum could explain the dynamics of synaptic transfer at the PC-to-MC synapse, although the release probability at the PC-to-MC synapse of the presubiculum remains much lower than those described in studies implicating these conductances.

**What does induce spike broadening?** The expressions of  $I_D$  and BK currents at the CA3-CA3 synapse was shown to keep low the initial transfer rate. Their pharmacological inactivation dramatically increases spike width at the soma and decreases failure rate (Saviane et al., 2003; Raffaelli et al., 2004). Besides, the initial transfer rate at the PC-to-MC synapse is much lower than in CA3 - this could be explained by the short action potential (0.6 ms) of the presubicular pyramidal cells, compared to CA3 pyramidal cells (> 1 ms). Consequently, a high expression of these K channels could explain the short spike width and the low transfer probability at the MC-to-PC synapse.

In neocortical layer 5 pyramidal cells, action potentials have quite similar widths (0.5 - 0.7 ms) (Kole et al., 2007; Shu et al., 2007) compared to the presubiculum, but their synapses are much more efficient (Kole et al., 2007; Zhu et al., 2011). These neurons are rather different from CA3 cells, as activity dependent spike broadening occurs in the soma, but unrelated to  $I_D$  inactivation (Kole et al., 2007; Shu et al., 2007). In contrast,  $I_D$  is expressed in the axon initial segment, where it normalizes the spike waveform. Indeed, it maintains a short width even if somatic spike broadening occurs, especially during intrinsic burst firing at the soma (Kole et al., 2007). However, somatic depolarization can be transferred to the proximal axon and slowly inactivate  $I_D$ , resulting in gradual spike broadening (Foust et al., 2011; Kole et al., 2007) and synaptic enhancement remaining several seconds after hyperpolarization

(Kole et al., 2007; Shu et al., 2006, 2007).

In terms of kinetics, the transfer of the PC-to-MC synapse resembles this voltage dependent increase of synaptic strength although it is difficult to evaluate, as the stimulation protocols are very different. While our pulse protocols did not induce tonic depolarization of somatic membrane potential, we cannot exclude that depolarization may occur in the axon, due to an activity dependent activation of depolarizing current (Fricker et al., 2009). We don't have evidence in favor of the expression of a D-type potassium current in presubicular pyramidal neurons, such as the depolarizing ramp at the onset of depolarizing DC injection (Saviane et al., 2003), but a possible axonal or synaptic expression would not be visible at the soma anyway (Foust et al., 2011; Kole et al., 2007; Shu et al., 2007).

Patch clamp recordings of mossy fiber boutons revealed an activity dependent spike broadening mechanism, mediated by the cumulative inactivation of a A-type potassium current, which activated and inactivated rapidly, and which recovered slowly from inactivation (Geiger and Jonas, 2000). After a high frequency stimulus, spike width returned to its initial value within several seconds, suggesting that the enhancement of synaptic strength followed the same dynamics. As the synaptic spike broadening cannot be addressed with somatic patch clamp recording, it is difficult to pin down the implication of a specific synaptic K conductance (Geiger and Jonas, 2000). But action potential broadening in presubicular pyramidal neurons is certainly a candidate mechanism to explain the frequency dependent recruitment of Martinotti cells.

**Testing the spike broadening hypothesis.** In a next step I will determine if action potential broadening is an enhancer of synaptic transfer at the PC-to-MC synapse in presubiculum.

I will therefore test the implication of the above-described currents using a comparative pharmacological approach. D-type and A-type currents can be blocked by 4-aminopyridine (4-AP), or tetraethylammonium (TEA). Adjusting the concentrations can help to differentiate A- from D-types conductance, as low concentration of 4-AP (20  $\mu$ M) are known to block preferentially D-type current (Boudkkazi et al., 2011; Storm, 1990). Axonal D-type current can be specifically blocked by DTX-I sensitive Kv1 channel subunits (Kv1.1, Kv1.2 and Kv1.6 subunits) (Boudkkazi et al., 2011; Kole et al., 2007; Shu et al., 2007). BK conductances can be specifically blocked by Paxilline or Iberotoxine (Raffaelli et al., 2004).

I will first address the effect on somatic spike broadening; even a small change can attest of the presence of these K<sup>+</sup> currents. However, their axonal or synaptic

expression may not be detected in somatic recordings (Kole et al., 2007), so I will directly address their potential effect on synaptic transfer using paired recordings (Boudkkazi et al., 2011). Using low frequency stimulation (0.2 – 0.5 Hz), I might observe an increase of transfer rate after pharmacological blockade. If one of the above drugs enhances synaptic transmission, I should check the location of the involved conductance by local puff application of the blocker (Kole et al., 2007), while recording from a postsynaptic neuron and looking for a change of transfer rate. Alternatively, I may look at spike broadening by direct axonal recordings, in whole cell (Kole et al., 2007), in cell attached (Sasaki et al., 2011) or using calcium imaging (Foust et al., 2011).

The presence of these channels in the axon initial segment could be checked by immunocytochemistry. It has already been done for Kv1 channels, which were co-localized with the axon initial segment or nodal molecules, such as Ankyrin-G and Nav channels (Goldberg et al., 2008; Lőrincz and Nusser, 2008).

#### 4.2.2 Modulation at the synapse

Neurotransmitter release probability depends on the expression of short term plasticity mechanisms (Regehr, 2012), the organization of the presynaptic active zone that conditions release mode (Kaesler and Regehr, 2014) and the activation of presynaptic receptors, such as G protein-coupled receptors that can enhance or depress synaptic transfer (Castillo et al., 2012; Debanne et al., 2013; Parnas and Parnas, 2010).

**Short term synaptic plasticity.** Many mechanisms of short and medium term plasticity, responsible for paired-pulse facilitation and augmentation, may explain the increase of synaptic transfer. All the mechanisms that were implicated in facilitation or augmentation require an elevation of intracellular calcium level (residual calcium) (Regehr, 2012). The use of ethylene glycol tetraacetic acid (EGTA, 10 mM), a slow calcium buffer, in the patch pipette should disrupt the expression of plasticity but not normal release (Manseau et al., 2010).

**Cannabinoids.** Among the synaptic regulation of release probability, the tonic block of the synapse by endocannabinoids is one candidate mechanism that could explain the activity dependent un-muting that we observe at the PC-to-MC synapse. Persistently active presynaptic cannabinoid receptors were reported for the inhibitory synapses made by CCK interneurons onto CA3 pyramidal cells (Losonczy et al., 2004), but not for excitatory synapses. Even so, the described dynamics closely

resemble those of the PC-to-MC synapse. The transfer rate is null at the stimulus onset and for a “moderate” frequency (25 Hz) and gradually starts releasing GABA during a high frequency (100 Hz) stimulus. The tonic activation of cannabinoid receptors was demonstrated, as the type 1 cannabinoid receptor antagonist, AM251, released the synaptic block. The implication of other GPCR was tested, such as GABA<sub>B</sub> receptors, metabotropic glutamate receptors, muscarinic receptor, but the effect was specific of cannabinoids (Losonczy et al., 2004). This is not really an activity dependent mechanism of enhancement, but rather an override of a muting mechanism by a high frequency stimulus. In the future, the cannabinoid dependence should be tested at the PC-to-MC synapse by the application of AM251.

### **4.2.3 The transfer rate increase may results from a synergistic mechanism**

The dynamic of the PC-to-MC synaptic transfer in presubiculum may result from the expression of different kinds of activity dependent mechanisms. The synapses could express a form of short-term facilitation, coupled to another mechanism of activity-dependent un-muting. This is actually the case for neocortical layer 5 pyramidal cell synapses (Zhu et al., 2011). The pyramidal-to-pyramidal connection is gradually enhanced during “up-state” depolarization of somatic membrane potential (Shu et al., 2006), due to the inactivation of ID in the proximal axon (Kole et al., 2007; Shu et al., 2007). In the meantime, the same cell possesses facilitating synapses onto Martinotti cells and depressing synapses onto fast spiking interneurons and pyramidal cells (Markram et al., 1998; Silberberg and Markram, 2007). Zhu et al. (2011) have demonstrated that the two mechanisms are important for the recruitment of Martinotti cells in neocortex.

## **General conclusion**



During my PhD, I studied the rodent presubiculum, a six-layered cortex in the parahippocampal area involved in spatial cognition. The presubiculum contains head direction cells, which fire persistently as a function of an animal's directional heading. The neuronal network generating this signal has been understudied and my PhD work has been developed to clarify the physiology of this cortical area.

I revealed the overall organization of principal neurons contained across the six layers of the presubiculum. The presubiculum possesses a laminar specificity of neuronal integrative properties. This area possesses the high computational power of cortical areas, as it contains different neuronal populations in the different layers that are likely to play distinct roles.

Following this idea, I showed that neurons projecting to lateral mammillary nucleus (LMN) and anterodorsal thalamus (ADN) had different morphological and electrophysiological properties. LMN projecting neurons correspond to layer 4 intrinsic burst firing pyramidal neurons. ADN projecting neurons seem to correspond to a homogeneous population in deep layers. The identification of specific postsynaptic targets should therefore be further considered to address the functional diversity in the presubiculum. Similarly, the local interconnectivity should vary for different neuronal populations and is likely to be a key component in the generation and the regulation of presubicular spatial signals.

More specifically, local inhibition plays a major role in regulating information processing in cortical areas. I therefore investigated the electrophysiological and morphological properties of different populations of GABAergic interneurons in the presubiculum. Our results suggest that inhibition in presubiculum is likely to be as complex as in other cortical areas. The functional role of the different interneurons remains to be address to understand how the inhibitory network influence information processing in the presubiculum.

I started to answer this question by focusing on one specific aspect: the recruitment of the presubicular Martinotti cells, typical dendrite-targeting interneurons. These cells are not recruited during sparse activity, but only during persistent and high frequency firing of pyramidal cells. This matches with the dynamics of similar synapses in other cortical areas and might be used to modulate persistent head direction signaling in the presubiculum. Nonetheless, I noticed that the pyramidal cell to Martinotti cell synapse had a much lower initial transfer rate compared to similar

synapses in the neocortex or the hippocampus. The mechanism behind this particular synapse dynamics remains to be identified. In the future, the other synapses should be investigated to fully understand the dynamics of information flows and their regulation in the presubicular network.

To conclude, my PhD work constitutes an essential contribution to the understanding of the presubicular information processing, a first step to elucidate the coding of orientation signals by this cortical area.

# Collaboration



## ARTICLE

# Cellular anatomy, physiology and epileptiform activity in the CA3 region of Dcx knockout mice: a neuronal lamination defect and its consequences

The purpose of the present study was the characterization of animals with an inactivated doublecortin gene. These mice presented an abnormality of lamination in CA3 of the hippocampus, associated with an epileptic phenotype. I had to characterize the intrinsic electrophysiological properties and the morphologies of the pyramidal neurons contained within the delaminated *stratum pyramidale* of CA3. I showed that neurons in animals with inactivated doublecortin gene were more excitable, had abnormal dendritic trees and misplaced dendritic spines compared to wild types. These features could contribute to the enhanced susceptibility to epileptiform activity in slices.



## NEUROSYSTEMS

# Cellular anatomy, physiology and epileptiform activity in the CA3 region of *Dcx* knockout mice: a neuronal lamination defect and its consequences

Michael Bazelot,<sup>1,2,\*</sup> Jean Simonnet,<sup>1,2,\*</sup> Céline Dinocourt,<sup>1,2,\*</sup> Elodie Bruel-Jungerman,<sup>2,3,4</sup> Richard Miles,<sup>1,2</sup> Desdemona Fricker<sup>1,2</sup> and Fiona Francis<sup>2,3,4</sup>

<sup>1</sup>INSERM UMR-S975, CRICM, CHU Pitié-Salpêtrière, UPMC, 105 boulevard de l'Hôpital, Paris 75013, France

<sup>2</sup>Université Pierre et Marie Curie, Paris 75005, France

<sup>3</sup>INSERM UMR-S839, Paris 75005, France

<sup>4</sup>Institut du Fer à Moulin, Paris 75005, France

**Keywords:** CA3 region, doublecortin, epilepsy, hippocampus, lamination defect, migration disorder, synaptic targeting

## Abstract

We report data on the neuronal form, synaptic connectivity, neuronal excitability and epileptiform population activities generated by the hippocampus of animals with an inactivated doublecortin gene. The protein product of this gene affects neuronal migration during development. Human doublecortin (DCX) mutations are associated with lissencephaly, subcortical band heterotopia, and syndromes of intellectual disability and epilepsy. In *Dcx*<sup>-/-</sup> mice, CA3 hippocampal pyramidal cells are abnormally laminated. The lamination defect was quantified by measuring the extent of the double, dispersed or single pyramidal cell layer in the CA3 region of *Dcx*<sup>-/-</sup> mice. We investigated how this abnormal lamination affected two groups of synapses that normally innervate defined regions of the CA3 pyramidal cell membrane. Numbers of parvalbumin (PV)-containing interneurons, which contact peri-somatic sites, were not reduced in *Dcx*<sup>-/-</sup> animals. Pyramidal cells in double, dispersed or single layers received PV-containing terminals. Excitatory mossy fibres which normally target proximal CA3 pyramidal cell apical dendrites apparently contact CA3 cells of both layers in *Dcx*<sup>-/-</sup> animals but sometimes on basilar rather than apical dendrites. The dendritic form of pyramidal cells in *Dcx*<sup>-/-</sup> animals was altered and pyramidal cells of both layers were more excitable than their counterparts in wild-type animals. Unitary inhibitory field events occurred at higher frequency in *Dcx*<sup>-/-</sup> animals. These differences may contribute to a susceptibility to epileptiform activity: a modest increase in excitability induced both interictal and ictal-like discharges more effectively in tissue from *Dcx*<sup>-/-</sup> mice than from wild-type animals.

## Introduction

Molecules that interact with microtubules during development affect neuronal migration (Kerjan & Gleeson, 2007; Conde & Cáceres, 2009; Jaglin & Chelly, 2009). Mutations of molecules, including doublecortin (DCX; Francis *et al.*, 1999; Gleeson *et al.*, 1998), the platelet-activating factor acetylhydrolase (LIS1, Hattori *et al.*, 1994; Reiner *et al.*, 1993) and  $\alpha$ - and  $\beta$ -tubulin (TUBA, TUBB; Keays *et al.*, 2007; Jaglin *et al.*, 2009) are linked to disordered cortical lamination. Lamination defects are associated with inherited syndromes involving intellectual disability and epilepsy (Schwartzkroin & Walsh, 2000; Guerrini & Parrini, 2010).

DCX binds to microtubules in migrating cells (Friocourt *et al.*, 2003; Schaar *et al.*, 2004), facilitating neuronal migration by limiting the number of leading processes (Kappeler *et al.*, 2006; Koizumi *et al.*, 2006). When this protein is absent, or mutated in mouse, migration is disorganized (Corbo *et al.*, 2002; Kappeler *et al.*, 2006) and retarded (Friocourt *et al.*, 2007). DCX mutations in human produce a disorganized, unfolded cortex, with band heterotopia, where some neurons remain in cortical white matter and do not reach the cortex (Kerjan & Gleeson, 2007; Leger *et al.*, 2008; Jaglin & Chelly, 2009).

Two approaches have been used to explore how abnormal lamination due to DCX mutations produces an epileptic phenotype. Suppressing *Dcx* expression by RNA interference results in animals with subcortical band heterotopias (Bai *et al.*, 2003; Ackman *et al.*, 2009). In contrast, genetic deletion of *Dcx* produces mice (*Dcx*<sup>-/-</sup>) with a heterotopia restricted to the CA3 region of the hippocampus (Corbo *et al.*, 2002; Kappeler *et al.*, 2006, 2007). Possibly, gene compensation occurs in these *Dcx* knockout (KO) animals (Deuel *et al.*, 2006). However, these mutant animals exhibit seizures,

Correspondence: R. Miles, <sup>1</sup>INSERM UMR-S975, as above.  
E-mail: richard.miles@upmc.fr

\*Present address: Institut de Radioprotection et Sécurité Nucléaire, Fontenay aux Roses 92262, France.

<sup>†</sup>M.B., J.S. and C.D. contributed equally to this study.

Received 6 September 2011, revised 2 November 2011, accepted 10 November 2011

suggesting a hippocampal perturbation may suffice to generate them (Nosten-Bertrand *et al.*, 2008; Kerjan *et al.*, 2009).

It remains unclear why disorders of migration and lamination favour epileptiform activities (Schwartzkroin & Walsh, 2000). Defective migration might alter the adult proportion of excitatory cells and GABAergic interneurons (Friocourt *et al.*, 2007; Kerjan *et al.*, 2009). Ectopically located neurons might not develop beyond immature, pro-epileptic phenotypes (Ackman *et al.*, 2009). Changes in the synaptic connectivity of ectopically situated cells might favour epileptiform syndromes (Fleck *et al.*, 2000; Ackman *et al.*, 2009). Synaptic function might be compromised by altered microtubule transport to terminals (Fleck *et al.*, 2000; Deuel *et al.*, 2006).

The CA3 region of  $Dcx^{-/Y}$  animals may help to understand the consequences of lamination defects. Synaptic connectivity in this region is well established (Johnston & Amaral, 1997). Here, we explored the perturbed lamination in the CA3 region of  $Dcx^{-/Y}$  mice. We searched for changes in synaptic targets of inhibitory or excitatory fibres that normally innervate precise regions of the CA3 pyramidal cell membrane. We compared the physiology and anatomy of pyramidal cells from both regions of the double pyramidal cell layer and attempted to induce epileptiform activities. Interictal and ictal-like activities were provoked by moderate increases in cellular excitability in tissue from  $Dcx^{-/Y}$  but not from wild-type (WT) animals.

## Materials and methods

### Animals

$Dcx^{-/Y}$  mice and their WT littermates, aged 1–6 months, were used for anatomical and electrophysiological studies. The KO mice were maintained on an *Sv129Pas* background with more than ten generations of backcrosses and genotyped to verify that the *Dcx* gene was inactivated (Kappeler *et al.*, 2006, 2007). They were anaesthetized by intraperitoneal injection of a mixture of ketamine (80 mg/kg) and xylazine (12 mg/kg; Sigma, Lyon, France). All work was performed in accordance with the European Communities Council Directive (86/809/EEC) on the care and use of animals for experimental procedures and was approved by local ethical committees.

### Anatomy

For anatomy, mice were perfused intracardially under ketamine/xylazine anaesthesia with 4% paraformaldehyde in 0.12 M sodium phosphate buffer (PB, pH 7.4). Brains were removed, immersed in paraformaldehyde solution for 1 h, rinsed in PB and cryoprotected overnight in 20% sucrose in PB at 4 °C. Forebrain blocks were frozen and sectioned coronally at 40  $\mu$ m. Sections were rinsed in phosphate-buffered saline (PBS, 0.12 M) and stored at –20 °C in an ethylene glycol-based solution. Before immunohistochemistry, free-floating sections were rinsed in potassium phosphate-buffered saline (KPBS). For immunostaining, we used three WT and four  $Dcx^{-/Y}$  animals.

### Immunohistochemical labelling

Immunostaining was performed for the neuron-specific nuclear marker NeuN, for the interneuron marker parvalbumin (PV) for the vesicular GABA transporter (vGAT) which labels some GABAergic terminals (Dumoulin *et al.*, 1999) and for the zinc transporter 3 (ZnT3) which is enriched in mossy fibre terminals (Palmiter *et al.*, 1996).

Sections were first incubated in KPBS containing 0.3% Triton X-100 and 2% milk protein (KPBS-Triton-Milk) for 1 h. Double immunostaining was made by an overnight incubation in a NeuN antibody

(1 : 10000, Chemicon) together with a PV antibody (1 : 8000, Swant) or a vGAT antibody (1 : 5000, gift from B. Gasnier) in KPBS-Triton-Milk. They were then rinsed in KPBS before incubation for 1 h in biotinylated horse anti-rabbit IgG (Vector Laboratories) diluted 1 : 400 in KPBS-Triton-Milk for PV and vGAT staining. After several rinses, sections were then incubated for 30 min with A488-conjugated streptavidin (1 : 400, Molecular Probes) for PV and vGAT staining and Cy3-conjugated goat anti-mouse (1 : 200, Jackson ImmunoResearch) for NeuN staining in KPBS-Triton-Milk. Double immunostaining for NeuN and ZnT3 was performed by incubation in an Alexa-488-conjugated NeuN antibody (1 : 500, Chemicon) and a ZnT3 antibody (1 : 1000, gift from R. Palmiter) in KPBS-Triton-Milk. Sections were then rinsed in KPBS and incubated for 30 min in Cy3-conjugated donkey anti-rabbit (1 : 400, Jackson ImmunoResearch) in KPBS-Triton-Milk. After immunostaining, sections were rinsed in KPBS and mounted with an antifade agent (ProLong Gold; Invitrogen, Eugene, OR, USA).

### Microscopy and image quantification

Images were acquired and analysed by an investigator blind to the nature of the animal from which tissue was obtained. They were made with an inverted microscope (Olympus IX81), an Optigrad II (Thales Optem) and camera (QImaging Retiga EXI) using an acquisition, scanning and measurement system (Volocity, Improvision, Coventry, UK). The Optigrad system permitted acquisition of structured images and subsequent three-dimensional reconstruction. Stacks of images of the CA3 region were acquired with a 10  $\times$  objective of NA 0.8 (30–45 images at intervals of 1  $\mu$ m with a voxel size of 0.64  $\mu$ m) or with a 40  $\times$  objective of NA 1.3 (40–70 images at 0.4  $\mu$ m with a voxel size of 0.16  $\mu$ m).

### Electrophysiology: multi-electrode records from tissue in an interface chamber

Slices were prepared after removing the forebrain from  $Dcx^{-/Y}$  mice or WT littermates anaesthetized with ketamine/xylazine. Brain tissue was immersed in a solution containing (mM) 250 sucrose, 1 KCl, 26 NaHCO<sub>3</sub>, 10 D-glucose, 1 CaCl<sub>2</sub> and 10 MgCl<sub>2</sub>, at 2–8 °C and bubbled with 5% CO<sub>2</sub> in O<sub>2</sub>. Transverse slices of 400  $\mu$ m thickness including the hippocampus and cortex were cut in a coronal plane with a vibratome (HM 650 V; Microm, Walldorf, Germany). They were transferred to an interface recording chamber where they were perfused with a solution containing (mM) 124 NaCl, 3.5 KCl, 26 NaHCO<sub>3</sub>, 10 D-glucose, 2 CaCl<sub>2</sub> and 2 MgCl<sub>2</sub>, heated to 34–36 °C with their upper surface exposed to a humidified 5% CO<sub>2</sub>/95% O<sub>2</sub> atmosphere. Recordings were made in an interface chamber from slices of brain tissue prepared from ten WT and 13  $Dcx^{-/Y}$  mice.

Intracellular records were made with glass electrodes filled with 4 M KAc and bevelled to a final resistance of 50–80 M $\Omega$ . Signals were amplified and filtered (high-pass, 3 kHz) with an Axoclamp 2B amplifier (Axon, Molecular Devices, Sunnyvale, CA, USA) operated in current-clamp mode. Extracellular records were made with linear arrays of 8–12 nichrome electrodes of 50  $\mu$ m diameter with a separation between electrode centres of  $\sim$ 100  $\mu$ m (Bazot *et al.*, 2010). Electrode arrays were positioned by a manipulator to contact slices from above and so record from sites along the somato-dendritic axis of CA3 pyramidal cells. Extracellular signals were amplified and filtered with pass-band of 0.1 Hz to 20 kHz using a non-commercialized 16-channel amplifier (Dr. F. Dubois, Dipsi, Chatillon, France). Intracellular and extracellular signals were digitized at 10–20 kHz by a 12-bit, 16-channel analog-to-digital converter (Digidata 1200A;

Axon Instruments, Molecular Devices), and visualized on a PC with the program Axoscope (Axon, Molecular Devices).

Multi-electrode records of spontaneous field events with variable spatial distributions were analysed with routines written in Matlab (The Mathworks, Natick, MA, USA). The amplitude of each field event was measured at its peak from all electrodes, the time-to-peak was measured from 10 to 90% of peak amplitude, and the decay from 90 to 10% of amplitude. After a principal component analysis, a *k*-means clustering algorithm was used to separate distinct field inhibitory postsynaptic potentials (IPSPs; Bazelot *et al.*, 2010). Starting with an excess of clusters, Euclidean distances between cluster centroids were calculated and visualized as a dendrogram. Clusters were coalesced when their centroids were separated by a Euclidean distance of < 10. Cluster coherence was confirmed visually and only well-merged clusters were analysed further. Current source density analysis was used (Bazelot *et al.*, 2010) to derive spatial and temporal variations in transmembrane currents associated with different field IPSP clusters.

In some experiments, GABA<sub>A</sub> receptor-mediated signalling was suppressed by picrotoxin (50  $\mu$ M), or bicuculline (20  $\mu$ M; both from Ascent Scientific, Bristol, UK).

#### *Electrophysiology: whole-cell records from slices in a submerged chamber*

For whole-cell records from single neurons, the forebrain was dissected after anaesthetizing *Dcx*<sup>-/-Y</sup> animals or their WT littermates aged 21–35 days with ketamine (80 mg/kg) and xylazine (12 mg/kg). Transverse slices of 300  $\mu$ m thickness containing the CA3 region of the hippocampus were prepared with a vibratome (Microm HM 650 V) in a solution containing (mM) 110 choline chloride, 2.5 KCl, 25 NaHCO<sub>3</sub>, 1.25 NaH<sub>2</sub>PO<sub>4</sub>, 7 D-glucose, 0.5 CaCl<sub>2</sub> and 7 MgCl<sub>2</sub>. The solution was cooled to 2–6 °C and equilibrated with 5% CO<sub>2</sub> in O<sub>2</sub>. Slices were stored for at least 1 h at 22–25 °C in a chamber containing (in mM) 124 NaCl, 2.5 KCl, 26 NaHCO<sub>3</sub>, 1 NaH<sub>2</sub>PO<sub>4</sub>, 2 CaCl<sub>2</sub>, 2 MgCl<sub>2</sub> and 11 D-glucose bubbled with 5% CO<sub>2</sub> in O<sub>2</sub> (pH 7.3, 305–315 mOsm/L). Recordings were made after transferring slices to a chamber of ~2 mL, at 32–34 °C, mounted on an Axioskop 2 FS microscope (Zeiss, Le Pecq, France). Slices were prepared from eight WT and ten *Dcx*<sup>-/-Y</sup> mice.

Neurons were visualized with a Luca EMCCD camera (Andor) using infrared differential interference contrast. Whole-cell records were made from CA3 pyramidal cells with glass pipettes of 3–6 M $\Omega$ . Pipettes were pulled from borosilicate glass 1.5 mm of external diameter (Hilgenberg, Germany) using a Brown-Flaming electrode puller (Sutter Instruments). They were filled with a solution containing (mM) 130 K-gluconate, 5 KCl, 10 HEPES, 10 EGTA, 2 MgCl<sub>2</sub>, 4 MgATP, 0.4 Tris-GTP, 10 Na<sub>2</sub>-phosphocreatine and 2.5 biocytin. Records were made with an Axopatch 200A amplifier (Axon, Molecular Devices) operated in current clamp fast mode. A chloride-coated silver wire contacted the pipette solution and a 3 M KCl agar bridge contacted the bath, yielding an estimated junction potential of ~15 mV, which was not corrected.

Patch clamp recordings were analysed with Axograph-X (Axograph Scientific, Sydney, Australia) Spikoscope (created by Dr. I. Cohen in Labview, National Instruments, Nanterre, France) and routines written in Matlab (The Mathworks). Neuronal input resistance (*R*<sub>in</sub>) was measured from the linear range of slope resistance in voltage responses to small step current injections of 800 ms from a holding voltage of -65 mV. Membrane time constants ( $\tau$ ) were obtained by fitting single or double exponentials to potential changes induced by these injections. Action potential (AP) threshold was

measured as the point where  $dV/dt > 10$  mV/ms (Fricker *et al.*, 1999). AP height was measured as the difference between the peak potential of the spike and the maximal afterhyperpolarization, for a period of 20 ms after the AP peak. The AP rising magnitude was defined as the voltage difference between the threshold and AP peak. The current threshold was defined as the minimum current step of 800 ms that initiated an AP. Input–output curves were made by plotting injected current against the mean AP frequency, measured as the reciprocal of the interspike interval.

Electrophysiological parameters were measured only from neurons that were subsequently identified morphologically. For this, biocytin was added to the pipette solution at 1 mg/mL. Slices were fixed in 4% paraformaldehyde in 0.12 M PB (pH 7.4, 4 °C). They were rinsed in PB and cryo-protected in 30% sucrose. Membranes were permeabilized by three freeze–thaw cycles over dry ice. Biocytin-filled neurons were revealed with a streptavidin–Cy3 conjugate (1 : 500, Invitrogen). Images were acquired using the microscope and camera system described above. Somato-dendritic forms of neurons were reconstructed in two dimensions with the NeuroLucida program (MicroBrightfield, Williston, VT, USA), which provided estimates of dendritic lengths.

#### *Statistical analyses*

Data were analysed by an unpaired Student's *t*-test, and analyses of variance (ANOVA) to assess interactions between genotype and time. Non-normally distributed variables were analysed with the Mann–Whitney rank sum test. Significance was established at *P* < 0.05. Errors were given as SEM or SD as noted.

## Results

### *Characterization of pyramidal cell layering abnormalities in the CA3 region*

NeuN-stained sections (Fig. 1) revealed three distinct patterns of pyramidal cell lamination in the CA3 region of *Dcx*<sup>-/-Y</sup> mice (*n* = 4). First, a dual layer with separate external (closer to the fimbria) and internal groups of pyramidal cell somata was evident at some sites (Fig. 1B). Layers were separated by ~100  $\mu$ m and somata were usually less dense in the internal layer. At other sites, the cell body layer was dispersed (Fig. 1C) with a width similar to that occupied by two distinct layers when they were present. Finally, at some sites CA3 pyramidal cell somata were arranged in a single layer of similar thickness and somatic density to that of WT animals (Fig. 1D; *n* = 2 WT mice).

We examined the distribution of these different lamination patterns within the CA3 region and along the rostral–caudal axis of the hippocampus in four *Dcx*<sup>-/-Y</sup> animals. Figure 1E shows the fraction of the linear extent of the CA3a, b and c regions consisting of a double, dispersed or a single layer. The CA3c region included both double and dispersed layers (double 46  $\pm$  15%, dispersed 48  $\pm$  14%, single 6  $\pm$  5%), the CA3b region was largely a double and dispersed layer (double 62  $\pm$  19%, dispersed 34  $\pm$  19%, single 4  $\pm$  3%), while the CA3a pyramidal cell layer was mostly a single layer (single layer 76  $\pm$  13%, dispersed 24  $\pm$  12%). Lamination patterns varied from dorsal to ventral hippocampus, but there was no clear trend.

### *Innervation of the dual CA3 layer by interneurons targeting pyramidal cell somata*

Basket and axo-axonic interneurons target the soma and axon initial segment of pyramidal cells and often contain the inhibitory cell

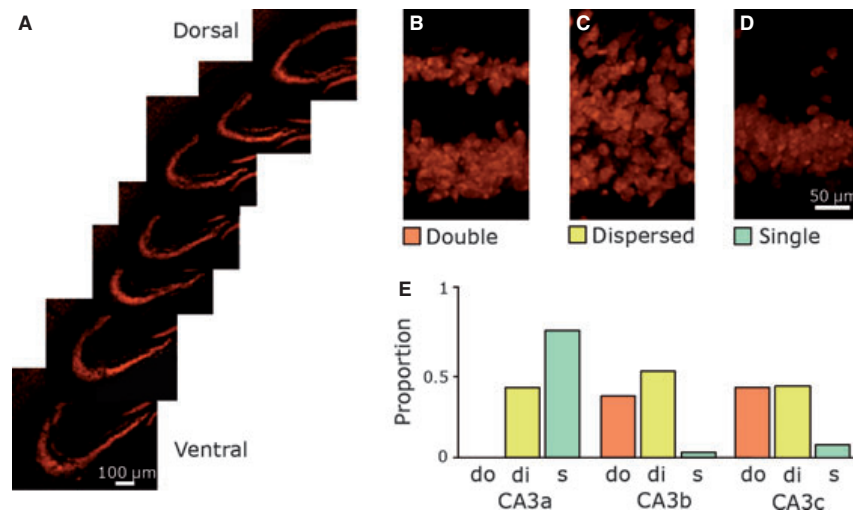


FIG. 1. Perturbation of the CA3 pyramidal cell layer in  $Dcx^{-/Y}$  mice. (A) NeuN staining for neuronal somata in seven sections of  $40 \mu\text{m}$  thickness taken at intervals of  $200 \mu\text{m}$  to cover the entire dorso-ventral extent of dorsal hippocampus. A distinct dual pyramidal cell layer is most evident in the CA3c region closest to the dentate gyrus. (B) A double CA3 pyramidal cell layer, (C) a dispersed cell layer, and (D) a single layer from NeuN-stained sections. (E) The proportion of the CA3a, CA3b and CA3c regions that comprise a double (do), dispersed (di) or single (s) pyramidal cell layer (from seven sections of each of  $n = 4$   $Dcx^{-/Y}$  mice).

marker PV. Perturbed interneuron migration (Kappeler *et al.*, 2006; Friocourt *et al.*, 2007) and abnormal lamination of the CA3 region in  $Dcx^{-/Y}$  animals might result in an aberrant inhibitory innervation of peri-somatic regions of pyramidal cells. We compared the density (number of cells/ $\text{mm}^2$ ) and location of PV-immunopositive cells and their axonal terminals in WT and  $Dcx^{-/Y}$  mice to see whether the inhibitory innervation of CA3 pyramidal cells was compromised (Fig. 2).

We compared the location and density of PV-immunopositive cell bodies (Fig. 2A–C) in the CA3 region of WT ( $n = 3$ ) and  $Dcx^{-/Y}$  mice ( $n = 4$ ). In WT animals, 18% ( $73 \pm 23$ ,  $n = 3$ ) of PV-positive cell somata were located in stratum oriens, between the fimbria and stratum pyramidale, whereas in  $Dcx^{-/Y}$  mice 10% ( $37 \pm 8$ ,  $n = 4$ ) of PV-positive somata were located in stratum oriens. In WT mice, 14% ( $57 \pm 10$ ) of the somata of PV-positive cells were located in stratum radiatum, while in  $Dcx^{-/Y}$  animals, 13% ( $45 \pm 8$ ) of PV-positive somata were located in this layer, between the internal pyramidal cell layer and the stratum lacunosum-moleculare. In WT animals, the remaining 68% ( $281 \pm 37$ ) of PV-positive somata were located in stratum pyramidale. In  $Dcx^{-/Y}$  animals, 77% ( $277 \pm 30$ ) of PV-positive somata were situated in the external and internal layers and the space between them. Of PV-positive somata, 47% ( $169 \pm 20$ ) were associated with the external cell body layer, 24% ( $85 \pm 16$ ) with the internal layer and the somata of 6% ( $23 \pm 2$ ) of the total PV-positive cell population were situated between the two layers. Thus, the density and distribution of PV-positive neurons (Fig. 2C) are comparable in  $Dcx^{-/Y}$  and WT mice.

Synaptic terminals contacting peri-somatic sites provide a punctate PV immunostaining that surrounds NeuN-stained CA3 cell somata of WT animals. In  $Dcx^{-/Y}$  mice, PV staining was detected around NeuN-positive pyramidal cell somata of both single, internal and external cell layers and between the layers (Fig. 2D and E). The presence of vGAT confirmed the staining of synaptic terminals of peri-somatic interneurons. Immunostaining for vGAT and PV was aligned with NeuN-labelled CA3 pyramidal cell somata in both the double layer (Fig. 2D) and the single layer (Fig. 2E) of  $Dcx^{-/Y}$  animals as in WT animals (data not shown).

#### Interneuron activity in the CA3 region of slices from $Dcx^{-/Y}$ and WT animals

The above data suggest that the density of PV-positive interneurons is similar in  $Dcx^{-/Y}$  and adult WT mice (Friocourt *et al.*, 2007), and that their terminals innervate pyramidal cells of both internal and external layers in  $Dcx^{-/Y}$  animals. We next used extracellular records of inhibitory field events to compare activity in inhibitory circuits of  $Dcx^{-/Y}$  and WT mice (Bazelot *et al.*, 2010).

Records were made with extracellular electrode arrays (Fig. 3) aligned along the somato-dendritic axis of CA3 pyramidal cells. In  $Dcx^{-/Y}$  animals, records were made from regions of a double pyramidal cell layer ( $n = 9$  slices from four animals), and in WT animals orthogonally to the single pyramidal cell layer ( $n = 7$  slices from three animals). This configuration (Bazelot *et al.*, 2010) allowed us to distinguish between inhibitory events with distinct somatic or dendritic spatial profiles, but did not permit separation of events generated by distinct single peri-somatic or dendritic targeting interneurons. Figure 3A compares field IPSPs recorded from the stratum pyramidale of  $Dcx^{-/Y}$  and WT mice. These events were typically correlated with inhibitory events in intracellular records (Fig. 3B; Bazelot *et al.*, 2010).

The frequency of spontaneous field IPSPs (Fig. 3C) from slices of  $Dcx^{-/Y}$  animals was  $25.7 \pm 5.5$  Hz (mean  $\pm$  SD,  $n = 9$ ), significantly higher than that,  $10.5 \pm 6.1$  Hz, of events recorded from slices of WT animals (mean  $\pm$  SD,  $n = 7$ ,  $P = 0.0013$ ). The mean amplitude of field IPSPs (Fig. 3C), measured at the electrode with the largest signal, in slices from  $Dcx^{-/Y}$  animals was  $25.3 \pm 2.7 \mu\text{V}$  (mean  $\pm$  SD,  $n = 9$ ), larger than that,  $18.9 \pm 2.4 \mu\text{V}$  (mean  $\pm$  SD,  $n = 7$ ,  $P = 0.0025$ ), from WT mice. The time-to-peak of averaged field IPSPs was similar:  $1.1 \pm 0.2$  ms (mean  $\pm$  SD,  $n = 9$ ) in records from slices of  $Dcx^{-/Y}$  animals and  $1.2 \pm 0.1$  ms (mean  $\pm$  SD,  $n = 7$ ,  $P = 0.33$ ) in slices from WT mice. The decay of averaged field IPSPs (Fig. 3C) measured from 90 to 10% of peak amplitude was  $6.2 \pm 1.0$  ms in slices from  $Dcx^{-/Y}$  animals (mean  $\pm$  SD,  $n = 9$ ), shorter than the value of  $7.9 \pm 0.1$  ms (mean  $\pm$  SD,  $n = 7$ ,  $P = 0.03$ ) from WT animals. Dendritic field IPSPs occurred at a frequency  $< 5\%$  that of somatic

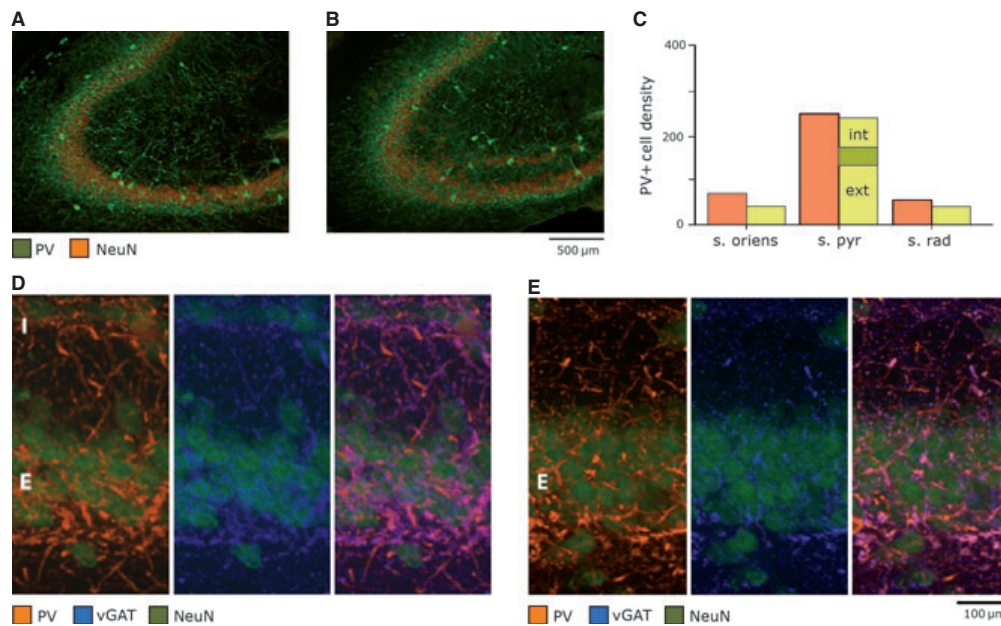


FIG. 2. Parvalbumin-positive interneurons and terminals in *Dcx*<sup>-/-</sup> and WT mice. Parvalbumin immunostaining (green) with a NeuN counterstain (red) for neuronal somata in the CA3 region of (A) wild-type and (B) *Dcx*<sup>-/-</sup> mice. (C) The density of PV-positive somata (number of cells/mm<sup>2</sup>) in stratum oriens, stratum pyramidale (st. pyr, both internal and external layers in *Dcx*<sup>-/-</sup> mice), and in stratum radiatum (st. rad.), in WT (orange) and *Dcx*<sup>-/-</sup> animals (yellow). (D, E) Staining for perisomatic interneuron terminals with antibodies against parvalbumin (orange) and the vesicular GABA transporter (blue) with NeuN (green) to reveal CA3 cell somata. Both internal (D) and external (E) cell layers appear to be innervated in regions with a double layer (D) as in regions with a single CA3 pyramidal cell layer (E). In D and E, labelling is from left to right: PV + NeuN, NeuN + vGAT and PV + NeuN + vGAT.

events in slices from both *Dcx*<sup>-/-</sup> and WT animals (data not shown). Thus, inhibitory circuits are more active in *Dcx*<sup>-/-</sup> than in WT mice. This enhanced activity might depend on an enhanced excitability of interneurons or of the pyramidal cells that excite them.

Fields generated if an interneuron innervates both layers of CA3 pyramidal cells in *Dcx*<sup>-/-</sup> animals should be spatially larger than those associated with a single layer. Figure 3D shows a current source density analysis for spontaneous peri-somatic field IPSPs from a zone with a dual cell body layer in a slice from a *Dcx*<sup>-/-</sup> animal. Similar analysis is shown for a field IPSP from a WT mouse in Fig. 3E. The current source indicates the site of active inhibitory terminals for the *Dcx*<sup>-/-</sup> animal was more intense, with a larger extent along the somato-dendritic axis, than for slices from WT mice. The difference in source dimensions was confirmed in comparing mean current profiles for 23 field event clusters isolated from records in five *Dcx*<sup>-/-</sup> slices and 17 inhibitory field clusters from five WT slices (Fig. 3F). A wider current source suggests some, and possibly all, perisomatic interneurons form synaptic contacts with pyramidal cells in both internal and external layers of *Dcx*<sup>-/-</sup> mice (cf. Fig. 2).

#### Innervation of the dual CA3 pyramidal cell layer by mossy fibre axons

Mossy fibre axons of dentate granule cells synapse with large spines on proximal dendrites of CA3 pyramidal cells (Claiborne *et al.*, 1986). We used immunostaining for the vesicular zinc transporter ZnT3, highly expressed in mossy fibre terminals, to determine whether mossy fibre innervation was altered in *Dcx*<sup>-/-</sup> animals (Fig. 4; *n* = 4 *Dcx*<sup>-/-</sup> mice).

The extent of ZnT3 staining was compared in regions of *Dcx*<sup>-/-</sup> animals where a double CA3 stratum pyramidale was evident and in

regions where there was just a single layer (Fig. 4A). In regions with a double layer, the width of ZnT3 immunostaining (Fig. 4B), associated with both internal and external layers, was  $245 \pm 12 \mu\text{m}$  (13 of 27 segments in seven sections from four animals) or  $200 \pm 17 \mu\text{m}$  when ZnT3 staining was associated with the external layer but not the internal layer (14 of 27 segments). When there was only a single CA3 pyramidal cell layer in *Dcx*<sup>-/-</sup> mice, the width of ZnT3 staining was reduced,  $150 \pm 4 \mu\text{m}$  (five segments), similar to that in WT animals. Thus, the space occupied by mossy fibres is wider in regions with a double layer than in those with a single CA3 pyramidal cell layer.

These findings suggest mossy fibres might innervate proximal apical dendrites of pyramidal cells with somata located in either internal or external cell layers. Closer examination revealed a more complex situation. In regions with a clear double layer, ZnT3 staining (Fig. 4A) extended from the external layer up to and even beyond the internal layer of somata in 11 of 31 segments of the CA3c region (seven sections from four animals). In these cases, mossy fibres may have terminated on apical dendrites of pyramidal cells of both the internal and external layers. In other cases (20 of 31 segments in CA3c), ZnT3 staining did not extend beyond the internal layer of CA3 pyramidal cell bodies. If these cells were innervated, mossy fibres must have formed contacts with basilar dendrites (Claiborne *et al.*, 1986; Kerjan *et al.*, 2009). In four of 28 CA3b segments examined, ZnT3 staining did not extend to the internal layer of NeuN-stained pyramidal cell somata: these cells were either innervated on distant basilar dendrites or received no mossy fibre inputs. Innervation of other CA3b segments was similar to that of CA3c, with mossy fibres extending to (13 of 28 segments) or beyond the internal pyramidal cell layer (11 of 28 segments).

The form of single CA3 pyramidal cells filled with biocytin during whole-cell records gave more detail on mossy fibre innervation

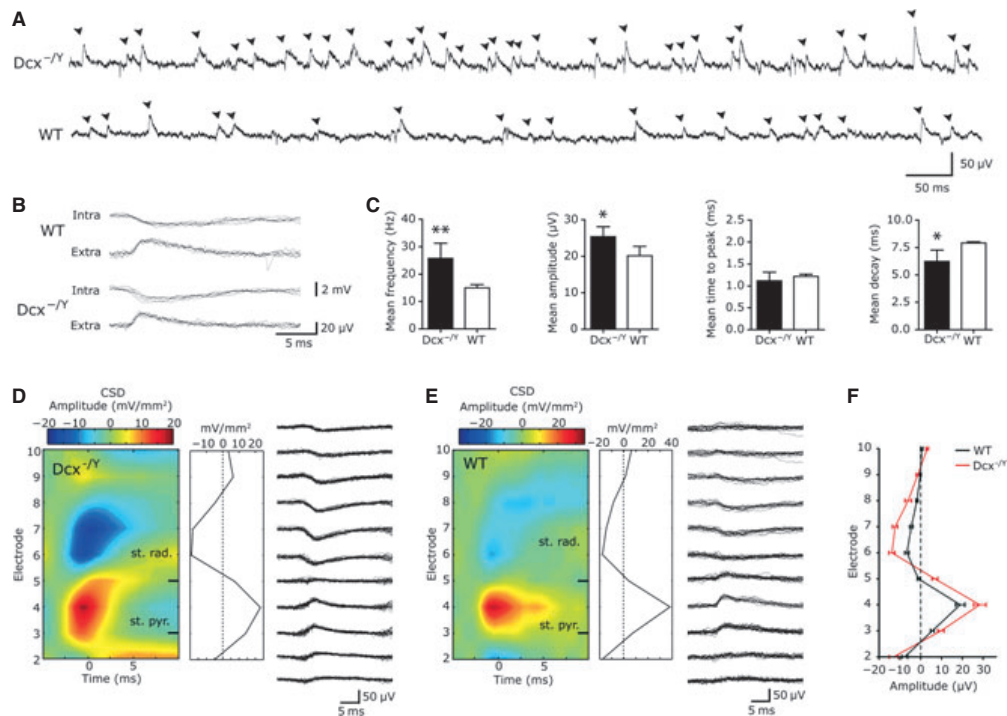


FIG. 3. Spontaneous field IPSCs from  $Dcx^{-/Y}$  and WT mice. (A) Inhibitory field potentials recorded spontaneously from the stratum pyramidale of  $Dcx^{-/Y}$  and WT animals. (B) Extracellular field events correspond to intracellular IPSPs recorded from a WT and a  $Dcx^{-/Y}$  slice (five overlaid traces). (C) Inhibitory fields from  $Dcx^{-/Y}$  ( $n = 9$  slices, four animals) and WT mice ( $n = 7$  slices, three animals). The mean frequency (first panel) and mean amplitude of field IPSPs (second panel) were larger in  $Dcx^{-/Y}$  than in WT mice. Times to peak (third panel) were similar and averaged field IPSCs decayed somewhat more quickly (fourth panel) in  $Dcx^{-/Y}$  animals. (D, E) Multi-electrode records (right panel, ten superimposed traces) and current source density plotted against time (left panel) for a peri-somatic field IPSP from a  $Dcx^{-/Y}$  mouse (D) and a WT animal (E). Warm colours (red max.) in these current source density plots indicate sources and cool colours current sinks (blue max.). The middle panel shows the amplitude profile of the current source density at the peak of the event. (F) Summed data show consistently wider sources in  $Dcx^{-/Y}$  than in WT animals (Mann–Whitney  $U$  test,  $*P < 0.05$ ,  $**P < 0.01$ ).

(Fig. 4C–F). Mossy fibre terminals contact unusually large spines 3–6  $\mu\text{m}$  in size on proximal dendrites (Claibourne *et al.*, 1986; Gonzales *et al.*, 2001). Large spines in well-filled CA3b,c pyramidal cells of WT animals ( $n = 5$ , not shown) were limited to the most proximal 35–85  $\mu\text{m}$  of apical dendrites. The expression of large spines differed for pyramidal cells with somata in the external layer of  $Dcx^{-/Y}$  animals. In three cells (Fig. 4C and D), large spines were evident on the most proximal apical dendrites, then were absent from apical dendrites for a distance of about 25  $\mu\text{m}$ , corresponding to somata of the internal pyramidal cell layer, and re-appeared beyond this layer. Such separate groups of large spines covered a total length of about 80  $\mu\text{m}$  on the apical dendrites of cells in the external CA3 layer. The distribution of large spines also differed for pyramidal cells of the internal layer of  $Dcx^{-/Y}$  animals (Fig. 4E and F,  $n = 4$  well-filled cells). Large spines were present not only on the proximal 20–60  $\mu\text{m}$  of apical dendrites but also on basilar dendrites located between internal and external cell layers. Thus, mossy fibre innervation is disturbed for CA3 cells of both internal and external layers of  $Dcx^{-/Y}$  mice.

#### Properties of pyramidal cells in the internal and external CA3 layers in $Dcx^{-/Y}$ animals

Dendritic form as well as somatic position is abnormal for neurons in some animals with migration defects (Fleck *et al.*, 2000). We compared biocytin-filled pyramidal cells from both internal and

external cell layers of  $Dcx^{-/Y}$  mice with those of CA3 pyramidal cells from wild-type mice.

We compared dendritic arborizations of biocytin-filled pyramidal cells from the CA3b, c region of WT animals (Fig. 5A,  $n = 4$ ) with well-filled cells from the external layer (Fig. 5B,  $n = 3$ ) and the internal layer (Fig. 5C and D,  $n = 4$ ) or cells from regions with a dispersed CA3 stratum pyramidale (data not shown,  $n = 4$ ). All cells had a pyramidal-shaped soma. While most cells possessed typically oriented apical and basilar dendrites, one neuron from the internal CA3c layer of a  $Dcx^{-/Y}$  animal possessed few if any basilar dendrites (Fig. 5D).

Apical dendrites of pyramidal cells in the external layer of  $Dcx^{-/Y}$  mice were typically shorter than those of WT pyramidal cells (Fig. 5B and E), while basilar dendrites of cells of the internal layer were less profuse (Fig. 5C and E). This observation was quantified by dividing the total, summed length of apical dendrites by that of basilar dendrites (Fig. 5E). The resulting ratio was 1.60 for CA3c pyramidal cells from WT animals ( $n = 4$ ), 1.41 for cells from the external layer of  $Dcx^{-/Y}$  mice ( $n = 4$ ) and 3.78 for cells from the internal layer ( $n = 4$ ). Thus, the total dendritic length for pyramidal cells from  $Dcx^{-/Y}$  animals is typically shorter than that of WT cells (Fig. 5F). If the density of dendritic synapses were similar,  $Dcx^{-/Y}$  pyramidal cells would be expected to receive fewer excitatory synapses than those of WT animals.

Neurons in brains with migration defects may remain in an immature physiological state (Colombo *et al.*, 2007; Fallet-Bianco *et al.*, 2008; Ackman *et al.*, 2009). We compared the physiology of

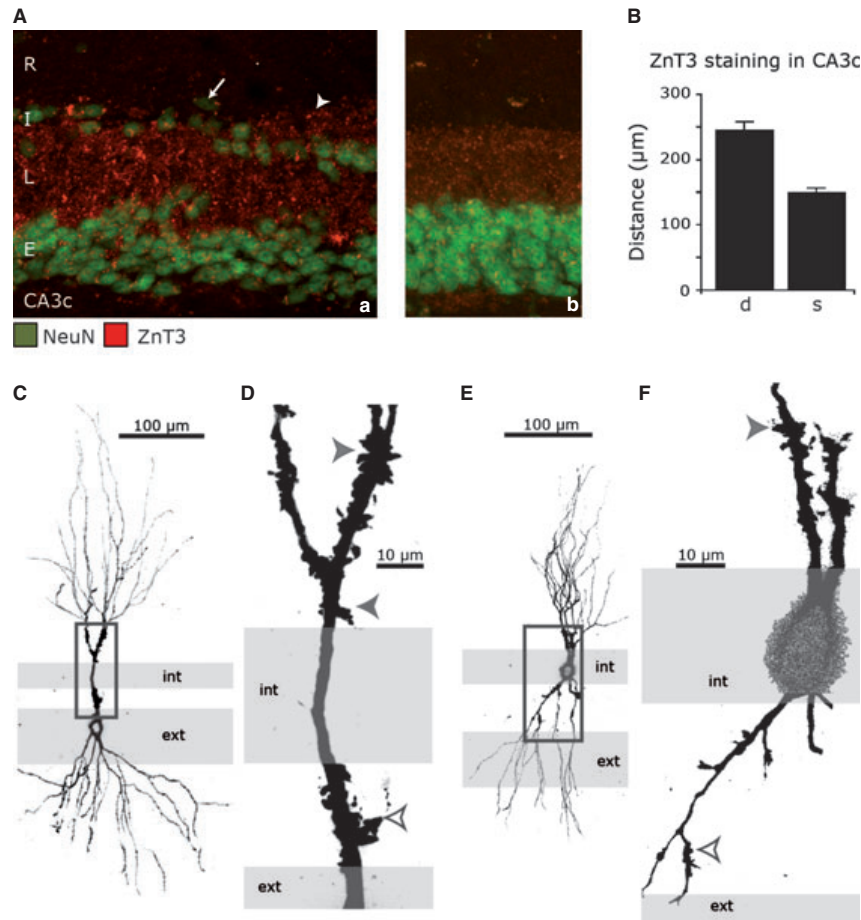


FIG. 4. Innervation of CA3 pyramidal cells by mossy fibres. (A) Double immunostaining for the zinc-transporter ZnT3 (red) and for NeuN (green), in zones of the CA3c region of  $Dcx^{-/Y}$  mice with, (a) a dual pyramidal cell layer or (b) a single layer. (B) Summary of the mean width of ZnT3 staining, corresponding to the mossy fibre layer, in regions with a dual or a single pyramidal cell layer. (C–F) Large post-synaptic spines in biocytin fills of single CA3 pyramidal cells with somata situated in the external (C and D) or the internal (E and F) layers. A cell of the external layer (C and D) with large, thorny excrescence-like spines at two separate sites on apical dendrites, before (white arrow) and after (grey arrow) the internal pyramidal cell layer. A cell with soma in the internal cell layer (E and F) exhibited large excrescence-like spines both on proximal apical (grey arrow) and on proximal basilar dendrites (white arrow).

identified pyramidal cells of the internal and external cell layers of  $Dcx^{-/Y}$  mice with that of WT pyramidal cells (Fig. 6). Resting potential, input resistance and membrane time constant were similar for pyramidal cells from  $Dcx^{-/Y}$  and from WT animals (Table 1, Fig. 6A–C). Similarly, AP properties including voltage threshold, amplitude and duration at half-height duration were comparable for pyramidal cells of  $Dcx^{-/Y}$  and WT animals (Table 1).

The most striking difference was that pyramidal cells from  $Dcx^{-/Y}$  animals were more excitable than those from WT mice. CA3 pyramidal cells in both WT and mutant animals rarely fired at resting potential. However, firing was induced (Fig. 6D and E) at a lower current threshold,  $67 \pm 14$  pA ( $n = 11$ ), in  $Dcx^{-/Y}$  CA3 cells than in WT CA3 pyramidal cells,  $109 \pm 18$  pA ( $n = 7$ ,  $P = 0.01$ ). The slope of the relationship between injected current and firing frequency was steeper,  $158 \pm 18$  Hz/nA, for cells of  $Dcx^{-/Y}$  animals ( $n = 11$ ), compared with  $97 \pm 12$  Hz/nA in WT mice ( $n = 7$ ,  $P > 0.01$ ; Fig. 6E). Firing frequency induced by a given current injection (Fig. 6F), and firing rate gain (Fig. 6E and H) were higher in cells from  $Dcx^{-/Y}$  animals while the threshold current was lower in  $Dcx^{-/Y}$  animals than in WT mice (Fig. 6G). Cells from  $Dcx^{-/Y}$  animals

tended to cluster in a low-threshold – high-gain region in threshold vs. firing rate gain plots (Fig. 6I).

We next investigated if excitability differed between cells with different locations in the CA3 region of  $Dcx^{-/Y}$  animals. The current threshold of pyramidal cells from WT animals was  $109 \pm 18$  pA ( $n = 7$ ). In pyramidal cells of the internal cell layer it was  $94 \pm 32$  pA ( $n = 4$ ), in cells of a dispersed layer it was  $53 \pm 32$  pA ( $n = 3$ ) while in pyramidal cells of the external layer the current threshold was  $51 \pm 11$  pA ( $n = 4$ ). Steeper slopes of current/firing relationships suggested that  $Dcx^{-/Y}$  cells of all groups were more excitable than WT cells. In WT animals the slope was  $97 \pm 12$  Hz/nA ( $n = 7$ ), while it was  $140 \pm 34$  Hz/nA for pyramidal cells of the internal layer ( $n = 4$ ),  $133 \pm 9$  Hz/nA for cells of the external layer ( $n = 4$ ) and  $217 \pm 37$  Hz/nA for dispersed pyramidal cells ( $n = 3$ ). Thus, a step depolarization of 200 pA from resting potential induced WT firing at  $6 \pm 4$  Hz for pyramidal cells, at  $17 \pm 9$  Hz in cells of the internal layer and at  $23 \pm 2$  Hz in cells of the external layer.

The absence of DCX might modify neuronal excitability independently of its actions on neuronal migration. To test this we compared

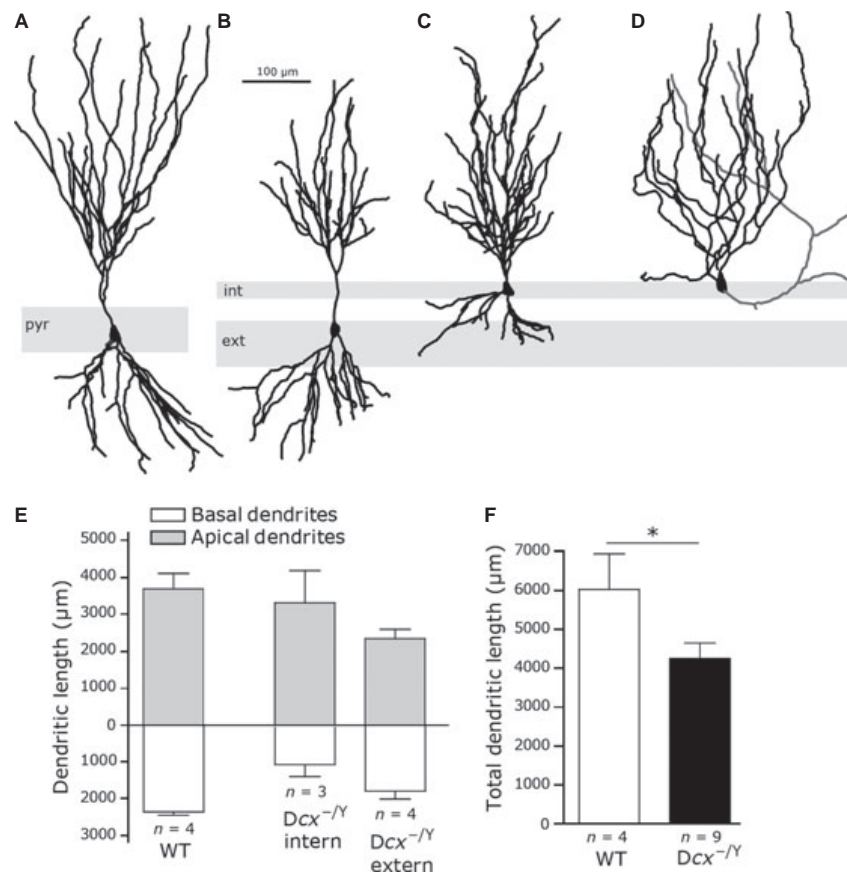


FIG. 5. Modified dendritic form of CA3 pyramidal cells from  $Dcx^{-/Y}$  mice. (A) Two-dimensional reconstruction of a biocytin-filled CA3c pyramidal cell of a WT mouse. (B–D) Reconstructions of CA3c pyramidal cells with somata in the external (B) or internal (C and D) pyramidal cell layer of  $Dcx^{-/Y}$  animals. The cell in D was apparently well filled, but few or no basilar dendrites were evident. (E) Total length of apical (grey) and basilar dendrites (clear) for CA3c pyramidal cells of WT and for cells of the internal and external pyramidal cell layers of  $Dcx^{-/Y}$  animals. A reduction in total length was apparent for basilar dendrites of cells in the internal layer and the apical dendrites of cells in the external pyramidal cell layer. (F) Total dendritic length was significantly less ( $*P > 0.05$ ) for well-filled cells ( $n = 9$ ) of  $Dcx^{-/Y}$  animals than for WT pyramidal cells ( $n = 4$ ).

CA1 pyramidal cell excitability in  $Dcx^{-/Y}$  and WT animals. The CA1 pyramidal cell layer is a little less tightly organized in  $Dcx^{-/Y}$  than in WT animals but never forms a double layer (Kappeler *et al.*, 2007). The current needed to induce an AP in WT CA1 pyramidal cells was  $99.3 \pm 18.1$  pA (mean  $\pm$  SEM;  $n = 7$ ) while it was significantly less in pyramidal cells from  $Dcx^{-/Y}$  animals, at  $56.3 \pm 8.9$  pA (mean  $\pm$  SEM;  $n = 8$ ;  $P = 0.036$ ). Neither input resistance nor resting potential were significantly different. In WT CA1 pyramidal cells, resting potential was  $-64 \pm 2$  mV (mean  $\pm$  SEM;  $n = 7$ ) and in pyramidal cells from  $Dcx^{-/Y}$  animals it was  $-69 \pm 2$  mV (mean  $\pm$  SEM;  $n = 8$ ;  $P = 0.120$ ), while the input resistance of WT CA1 pyramidal cells was  $236 \pm 30$  M $\Omega$  (mean  $\pm$  SEM;  $n = 7$ ) and in cells from  $Dcx^{-/Y}$  animals it was  $256 \pm 33$  M $\Omega$  (mean  $\pm$  SEM;  $n = 8$ ;  $P = 0.750$ ).

#### Induced epileptiform activity in the CA3 region of $Dcx^{-/Y}$ and WT animals

We compared the susceptibility to epileptiform activities of slices from WT and  $Dcx^{-/Y}$  animals. Records were made from slices maintained in an interface chamber at low divalent cation concentrations (Ca<sup>2+</sup> and Mg<sup>2+</sup> both reduced from 2 to 1 mM) to increase neuronal excitability. Both interictal and ictal-like discharges were detected in

simultaneous records made from single cells and with extracellular electrode arrays.

Interictal-like events, often with multiple burst components, were detected in 27 out of 30 slices from nine  $Dcx^{-/Y}$  animals, but in only four of 22 slices from seven WT animals (cf. Nosten-Bertrand *et al.*, 2008). Their mean total duration was  $332 \pm 42$  ms and they recurred at a frequency of  $0.38 \pm 0.17$  Hz (Fig. 7A and B). Field potentials were evident in all layers of the CA3 region. Pyramidal cells of both internal and external layers of  $Dcx^{-/Y}$  animals always received synaptic events and often fired during interictal-like events. Intracellular records suggested that pyramidal cells received strong inhibitory inputs during interictal events (Fig. 7A). Further evidence for a contribution from hyperpolarizing GABAergic inputs was obtained by showing the GABA<sub>A</sub> receptor antagonist bicuculline (10  $\mu$ M,  $n = 6$ ) increased the amplitude and duration of interictal field events. These data suggest that depolarizing GABAergic signalling did not contribute to interictal-like activities.

Ictal-like events (Fig. 7C and D) were induced in some slices exposed to reduced levels of divalent cations. They occurred spontaneously in 11/30 slices from nine  $Dcx^{-/Y}$  animals, but were never detected in 22/22 slices of seven WT animals. Ictal-like events were typically preceded by pre-ictal events and recurred at intervals

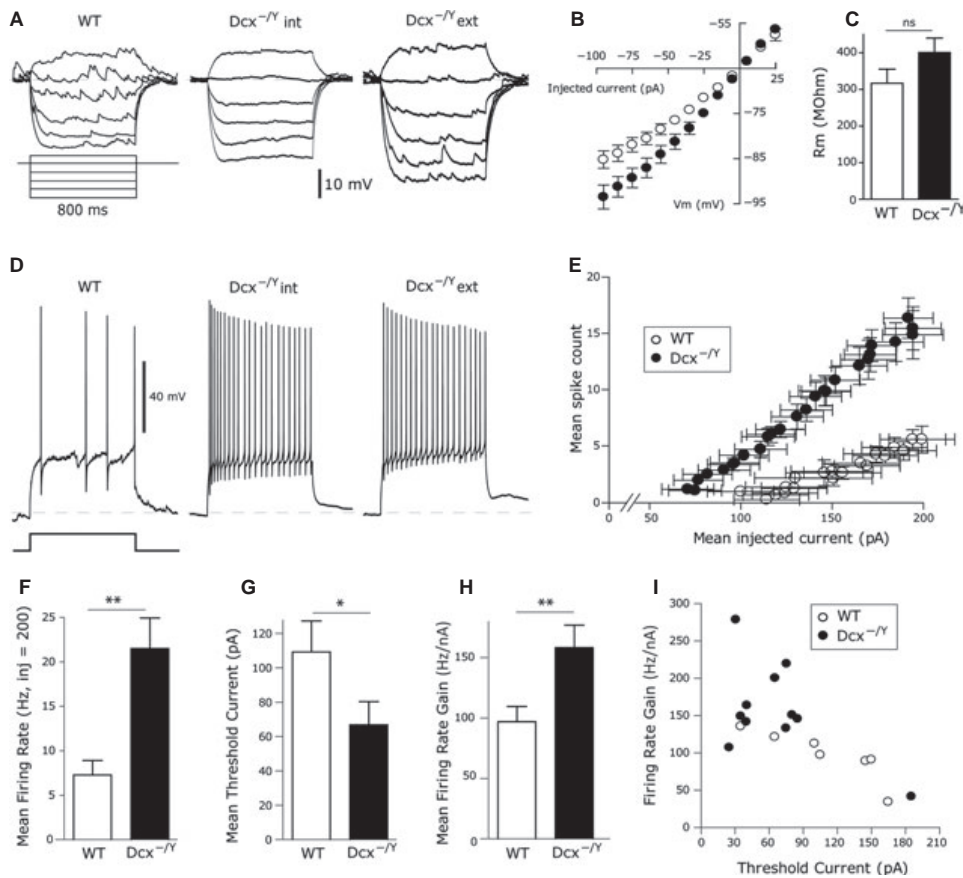


FIG. 6. Pyramidal cells of  $Dcx^{-/-}$  mice are more excitable than WT pyramidal cells. (A) Responses to current injections of a WT pyramidal cell, a pyramidal cell of the internal layer and a pyramidal cell of the external cell layer of a  $Dcx^{-/-}$  animal (left-to-right). Step currents of 600 ms duration and  $-100$ ,  $-75$ ,  $-50$ ,  $-25$ ,  $0$  and  $+25$  pA amplitude. Input resistance and membrane time constant of  $Dcx^{-/-}$  cells were not significantly different from those of WT cells. (B) Averaged current–voltage relationships and (C) similar input resistances of WT and  $Dcx^{-/-}$  animals. (D, E) Cells of  $Dcx^{-/-}$  animals were more excitable than those of WT animals. They fired at higher frequencies (D) in response to identical depolarizing current injection. (E) Input–output curves relating firing frequency to injected current differed between WT (white circles) and  $Dcx^{-/-}$  (black circles) pyramidal cells. (F) Current injections (200 pA, 600 ms) induced significantly higher firing frequencies in  $Dcx^{-/-}$  cells. (G) The minimum current needed to trigger an action potential was lower in  $Dcx^{-/-}$  cells. (H) An enhanced cellular excitability was evident as a steeper slope of the input/output relationship (mean firing rate gain) in  $Dcx^{-/-}$  cells. (I) The firing rate gain plotted against the threshold current for each cell (Mann–Whitney  $U$  test,  $*P < 0.05$ ,  $**P < 0.01$ , ns not significant).

ranging from 1–2 s to 30 min. They consisted of an initial event succeeded by repeated burst discharges for a duration of 20–60 s (Fig. 7C). Current density analysis (Fig. 7D) showed the initial event was associated with a sink in stratum radiatum and a shorter duration sink in stratum oriens. Succeeding bursts showed a rather different arrangement with a sink predominating in stratum oriens but present to a lesser extent in radiatum. It was hard to distinguish an initiation site in either external and internal cell layers as ictal-like events were infrequent and latency differences were small and variable.

## Discussion

We have examined the extent and consequences of a lamination defect in the CA3 hippocampal region of  $Dcx^{-/-}$  animals. It consists of a dual or dispersed layer of pyramidal cell somata, typically in the CA3b and c regions (Fig. 1). We asked whether this lamination disorder perturbs synaptic targeting by excitatory and inhibitory systems that normally contact specific sites on the CA3 pyramidal cell membrane. Both peri-somatic interneurons (Figs 2 and 3) and mossy

fibres that normally excite proximal dendrites of CA3 cells (Fig. 4) tended to contact appropriate zones on neurons of both layers in  $Dcx^{-/-}$  mice, although aberrant connectivity was sometimes evident. Pyramidal cells of both layers were somewhat smaller (Fig. 5), with a reduced total dendritic length (Fleck *et al.*, 2000). Pyramidal cells of both layers were more excitable than WT cells (Fig. 6). Thus, the absence of DCX affects dendritic form and synaptic connectivity and results in an enhanced pyramidal cell excitability. These factors may underlie the enhanced susceptibility to epileptiform activities of slices (Fig. 7) and  $Dcx^{-/-}$  animals (Nosten-Bertrand *et al.*, 2008; Kerjan *et al.*, 2009).

### Site and form of CA3 pyramidal cells in $Dcx^{-/-}$ mice

We found the double, or dispersed, pyramidal cell layer was largely restricted to the CA3b, c regions of  $Dcx^{-/-}$  mice maintained on the *Sv129Pas* background (Corbo *et al.*, 2002; Kappeler *et al.*, 2007). In double mutant animals for DCX and DCX-like kinase (*Dclk*), lamination of both the CA3 and the CA1 regions is defective,

TABLE 1. Electrical properties of pyramidal cells of WT and *Dcx*<sup>-/-</sup> animals

Electrical property	WT	<i>Dcx</i> <sup>-/-</sup>	Mann–Whitney <i>U</i> test
Resting membrane potential (mV)	-68 ± 5 (7)	-71 ± 3 (11)	NS
Input resistance (MΩ)	317 ± 39 (7)	401 ± 39 (11)	NS
Membrane time constant (ms)	54 ± 7 (6)	72 ± 9 (10)	NS
Threshold potential (mV)	-40 ± 1 (7)	-40 ± 1 (11)	NS
Action potential amplitude (mV)	-94 ± 2 (7)	-93 ± 2 (7)	NS
Action potential width (ms)	0.75 ± 0.03 (7)	0.81 ± 0.03 (7)	NS
Threshold current (pA)	109 ± 18 (7)	67 ± 14 (11)	<i>P</i> < 0.05
Firing rate gain (Hz/pA)	97 ± 12 (7)	158 ± 18 (11)	<i>P</i> < 0.01

For each parameter the mean and standard error on the mean are given with the number of observations in parentheses. According to the Mann–Whitney *U*-test, there were no significant differences in resting membrane potential, input resistance or membrane time constant. Similarly, parameters describing action potentials, including threshold, amplitude and duration at half-height, were similar. The threshold current for action potential initiation was significantly lower and the firing rate gain (Fig. 6E) was higher in *Dcx*<sup>-/-</sup> mice.

suggesting *Dclk* can assume some functions of *Dcx* in the CA1 subfield (Deuel *et al.*, 2006; Kerjan *et al.*, 2009; but see Kappeler *et al.*, 2007). Both CA1 and CA3 subfields are also severely disorganized in *Lis1* mutant animals (Fleck *et al.*, 2000).

Factors underlying the formation of a double or dispersed CA3 pyramidal cell layer in *Dcx*<sup>-/-</sup> mice are not well understood. CA3 pyramidal cell neurogenesis peaks at about embryonic day 14.5 and neurons reach the neuronal plate after 4–5 days (Altman & Bayer, 1990a; Nakahira & Yuasa, 2005). As well as normally sited hippocampal plate cells, a heterotopic band has been observed in

the intermediate zone of *Dcx*<sup>-/-</sup> animals that later becomes stratum oriens (Kappeler *et al.*, 2007). Possibly, these post-mitotic neurons sense components of the stop signal for migration too soon or mis-read motogenic and guidance signals (Hack *et al.*, 2002; Guerrini & Parrini, 2010). In the cortex, delayed *Dcx* expression reinitiates migration of mis-positioned cells (Manent *et al.*, 2009). However, we did not find evidence for the coexistence of an ectopic CA3 cell body layer and a correctly sited layer. Instead, neurons of both internal and external layers (Fig. 1) were malformed (Fig. 5) with an enhanced excitability (Fig. 6), suggesting that the absence of *Dcx* affects CA3 cell development regardless of their final position. The enhanced excitability of CA1 pyramidal cells from *Dcx*<sup>-/-</sup> animals also supports this idea.

Our data suggest that the absence of DCX affects not only migration but also the maturation and form of CA3 pyramidal cell dendrites. The total dendritic length of CA3 pyramidal cells from *Dcx*<sup>-/-</sup> animals was about 20–30% less than that of cells from WT animals. The basal dendrites of CA1 pyramidal cells from *Lis1*<sup>-/-</sup> animals are somewhat more severely stunted (Fleck *et al.*, 2000). In *Dcx*<sup>-/-</sup>*Dclk2*<sup>-/-</sup> double mutants, the secondary apical dendrites of CA1 cells are reduced in length and complexity (Kerjan *et al.*, 2009). No alteration in dendritic complexity was explicitly described for ectopic cortical cells from animals in which *Dcx* expression was reduced by RNA interference (Ackman *et al.*, 2009). Biocytin filling sometimes revealed extreme dendritic forms (Fig. 5D), but deformation of pyramidal cell dendrites tended to be homogeneous. Basilar dendrites of cells of the internal layer were poorly developed, while apical dendrites of external layer cells were stunted. Thus, cells of both layers in *Dcx*<sup>-/-</sup> animals possessed shorter total dendritic lengths, implying a reduced global synaptic excitation due to fewer spines, even if inhibitory innervation of pyramidal cell dendrites was presumably also reduced.

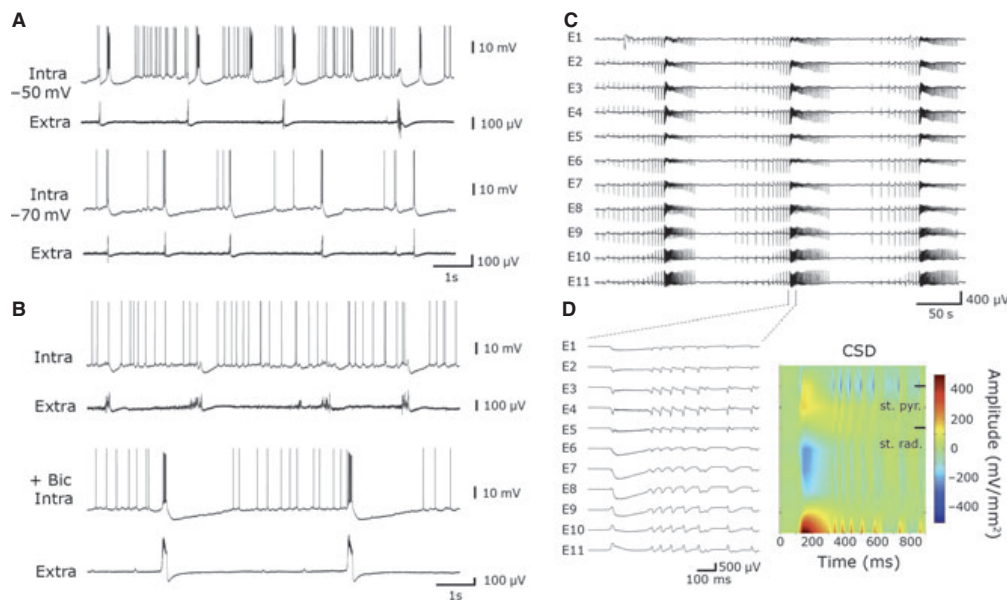


FIG. 7. Interictal and ictal-like activity recorded from slices of *Dcx*<sup>-/-</sup> animals. (A) Intra- and extracellular records of interictal-like events from the external layer of the CA3 region of a *Dcx*<sup>-/-</sup> slice in the presence of 1 mM  $Ca^{2+}$  and 1 mM  $Mg^{2+}$ . Holding pyramidal cell membrane potential at -50 mV (upper traces) and then at -70 mV (lower traces) revealed a fast inhibitory component of interictal-like events. (B) An inhibitory contribution was confirmed by the increase in amplitude and duration of population events induced by the GABA<sub>A</sub> receptor antagonist bicuculline (20 μM). Intracellular and field records from the external cell layer of a *Dcx*<sup>-/-</sup> slice. (C) Ictal-like activity recorded with a multi-electrode array aligned along the somato-dendritic axis of CA3 pyramidal cells. E1–3, stratum oriens; E4–5, stratum pyramidale; E6–9, stratum radiatum. (D) The initial 800 ms of an ictal event, and a current source density analysis. This analysis points to a major current sink for the initial part of the event in stratum radiatum, while for later events the sink was more widely distributed across stratum oriens and radiatum.

### Peri-somatic interneurons and the dual CA3 pyramidal cell layer in $Dcx^{-/Y}$ mice

PV-positive interneurons normally establish synapses on restricted peri-somatic regions of CA3 pyramidal cells (Freund & Katona, 2007). We found that numbers of PV-immunopositive cells were not reduced in  $Dcx^{-/Y}$  animals. Even if migration is perturbed and may be retarded (Kappeler *et al.*, 2006; Friocourt *et al.*, 2007), these inhibitory cells eventually reach sites similar to those in the hippocampus of WT animals (Fig. 2A–C). This situation differs in the CA1 region of *Lis1* mutant animals, where PV-expressing interneurons terminate in the stratum radiatum (Jones & Baraban, 2009).

Interneurons arrive in the CA3 region at embryonic day 16 (Pleasure *et al.*, 2000; Danglot *et al.*, 2006; Manent *et al.*, 2006) invading the hippocampal plate with similar timing to that of pyramidal cells (Soriano *et al.*, 1986; Altman & Bayer, 1990a,b). Destinations and connections of interneurons and pyramidal cells may then be coordinately regulated (Manent *et al.*, 2006). Molecular determinants of the selective innervation of specific subregions of pyramidal cell membrane by distinct inhibitory cells during this coordinated synaptogenesis remain to be completely understood (Danglot *et al.*, 2006). Our data suggest cells of both the internal and the external cell layers express molecules needed for the formation of appropriately sited peri-somatic contacts by PV-immunopositive interneurons. Furthermore, current source density distributions from array records of field IPSPs (Bazelot *et al.*, 2010) implied that the same interneuron may synapse with cells of both the internal and the external cell layers (Fig. 3D–F). Either dual records from peri-somatic inhibitory cells and pyramidal cell targets in both layers or tracing axonal arbors of single filled interneurons could confirm this point. Such records could also let us test whether interneuron excitability was enhanced in  $Dcx^{-/Y}$  mice, as in *Lis1* KO animals (Jones & Baraban, 2007), or whether the increased frequency of field IPSPs (Fig. 3A) resulted instead from an increased pyramidal cell excitability (Fig. 6). Other interneurons, such as axo-axonic cells, target distinct, specific sites of pyramidal cell membranes. Studies on the spatial specificity of their synaptic contacts with  $Dcx^{-/Y}$  pyramidal cells could provide insights into mechanisms underlying the formation of precise inhibitory connections in the hippocampus.

### Mossy fibre excitation of a dual CA3 pyramidal cell layer in $Dcx^{-/Y}$ mice

As the growth and migration of CA3 interneurons and principal cells occur in a temporally coordinated sequence, so too does the mossy fibre innervation of CA3 pyramidal cells (Deguchi *et al.*, 2011). Mouse dentate granule cells are born from embryonic stages until postnatally (Angevine, 1965; Altman & Bayer, 1990b), and generally reach their final destination later than CA3 pyramidal cells (Danglot *et al.*, 2006). Some early mossy fibre contacts with CA3 cells may be formed close to birth (Amaral & Dent, 1981) but most innervation, including an infrapyramidal bundle (Bagri *et al.*, 2003), is established later. We used ZnT3 immunostaining (Fig. 4A and B) to define mossy fibre trajectories and large post-synaptic spines (Claiborne *et al.*, 1986; Gaiarsa *et al.*, 1992) as an indication of sites of mossy fibre contacts. Our data suggest mossy fibre targeting of CA3 pyramidal cells is perturbed, but most cells of both internal and external layers of  $Dcx^{-/Y}$  mice are innervated on proximal apical or basilar dendrites. Cells of the internal layer tended to be innervated by a maintained infra-pyramidal projection (Fig. 4E and F; Gaarskjaer, 1986; Kerjan *et al.*, 2009) even if it terminates sometimes on distant basilar dendrites. Infra-pyramidal mossy fibre projections are coupled to

thorny excrescences on basilar dendrites, as we found (Fig. 4), in animals with CA3 pyramidal cell lamination defects other than those associated with *Dcx* (Nowakowski & Davis, 1985). As for inhibitory contacts, mossy fibre pathfinding and synaptogenesis may result from coordinately regulated pre- and post-synaptic processes of attraction and repulsion (Qin *et al.*, 2001; Förster *et al.*, 2006; Xu & Henkemeyer, 2009). In particular, the absence of large spines on dendrites of cells from the external layer as they cross zones of internal layer somata (Fig. 4C and D) suggests CA3 cell bodies may repel mossy fibre contacts (Seki & Rutishauser, 1998).

The shift in location of mossy fibre contacts from apical to basilar sites (Gonzales *et al.*, 2001) could enhance the efficacy of mossy fibre excitation of pyramidal cells of the internal layer of  $Dcx^{-/Y}$  mice. The smaller diameters of basilar dendrites should favour excitatory postsynaptic potential propagation to the soma (Carnevale *et al.*, 1997), thus assuring a greater influence of basilar mossy fibre inputs on somatic potential than for contacts made with thicker apical dendrites.

### CA3 pyramidal cell excitability and epileptiform activities in $Dcx^{-/Y}$ mice

Our data suggest that CA3 pyramidal cells may make a primary contribution to the epileptic phenotype of  $Dcx^{-/Y}$  animals. The excitability of pyramidal cells in both layers was increased with a reduced current threshold and an increase in the gain of the relationship between injected current and the frequency of firing to injected current. This enhanced excitability may depend in part on the higher input resistance of the smaller pyramidal cells of mutant animals (Zhu, 2000). Alternatively, the expression of voltage-independent currents (Taverna *et al.*, 2005) might be changed, although we detected no major change in subthreshold input resistance. Voltage-dependent currents might also change to compensate for a reduced excitatory drive due to reduced dendritic length (Desai *et al.*, 1999). Homeostatic control of cellular excitability in a healthy brain functions to counter changes in network activity (O'Leary *et al.*, 2010). In the pathologically changed CA3 network of  $Dcx^{-/Y}$  mice, might such compensatory mechanisms aggravate aberrant patterns of network activity so that seizures beget further seizures (Ben-Ari *et al.*, 2008)? Interestingly, we noted that in the absence of a dual layer (Kappeler *et al.*, 2007), CA1 pyramidal cells from  $Dcx^{-/Y}$  animals were also more excitable than their counterparts from WT mice. Further work is needed to define factors controlling this cell-autonomous enhanced excitability of  $Dcx^{-/Y}$  pyramidal cells.

The interictal-like behaviour (Fig. 7A and B) presumably results from interactions between an enhanced pyramidal cell excitability and recurrent synaptic connectivity in the CA3 region. We did not test explicitly whether recurrent connectivity was enhanced or whether the efficacy of single recurrent excitatory synapses was altered in  $Dcx^{-/Y}$  animals. Our data on field IPSPs (Fig. 3) and the activation of a strong synaptic inhibition during inter-ictal-like events suggests that Cl-homeostasis was not compromised (Shimizu-Okabe *et al.*, 2007). As in other slice models, ictal-like events occurred much less frequently than interictal ones (Avoli *et al.*, 2002). There seemed to be a genuine difference in susceptibility between slices from WT and  $Dcx^{-/Y}$  animals, suggesting that modified cellular and circuit properties in the CA3 region of the hippocampus can suffice to generate ictal-like activity. The reduced divalent cation stimulus used to induce this activity seems likely to have further increased CA3 cell excitability while reducing the efficacy of excitatory and inhibitory synapses.

## Conclusions

*Dcx*<sup>-Y</sup> animals were known to possess a double layer of CA3 pyramidal cells. These data show that cells in both layers have simplified dendritic arbors and an increased excitability as do cells of the less disorganized CA1 region. This situation recalls that described for the CA1 region of *Lis1* KO animals (Fleck *et al.*, 2000). Thus, defects in pyramidal cell form and function are associated with migration disorders in two animal models of dis-lamination, disorganization and seizures, linked to two distinct microtubule-associated molecules.

## Acknowledgements

We thank Ivan Cohen for help with analysis of the whole-cell electrophysiology and Emmanuel Eugene for help with anatomy. We thank Jamel Chelly for support during the creation of *Dcx* KO mice. We acknowledge Dr Bruno Gasnier (Institut de Biologie Physico-Chimique, Paris) for a gift of the vGAT antibody and Dr Richard Palmier (University of Washington, Seattle) for a gift of the ZnT3 antibody. We are grateful for financial support from the Agence Nationale de Recherche (ANR- 08-MNP-013; F.F. and R.M.), the European Community (EPICURE, LSH-037315; R.M.) as well as from INSERM, including the Avenir programme (F.F.), the Fondation pour la Recherche Médicale (R.M.), the FRC (R.M.), the Fondation Bettencourt Schueller (F.F.), the Ile-de-France region (NERF; E.B.J., F.F.) and the Fondation Jérôme Lejeune (F.F.).

## Abbreviations

AP, action potential; CA3, cornu ammonis region 3; Cy3, cyanine 3; DCX, doublecortin; IPSP, inhibitory postsynaptic potential; KO, knockout; KPBS, potassium phosphate-buffered saline; NA, numerical aperture; PB, sodium phosphate buffer; PBS, phosphate-buffered saline; PV, parvalbumin; vGAT, vesicular GABA transporter; WT, wild-type; ZnT3, zinc transporter 3.

## References

Ackman, J.B., Aniksztejn, L., Crépel, V., Becq, H., Pellegrino, C., Cardoso, C., Ben-Ari, Y. & Represa, A. (2009) Abnormal network activity in a targeted genetic model of human double cortex. *J. Neurosci.*, **29**, 313–327.

Altman, J. & Bayer, S.A. (1990a) Prolonged sojourn of developing pyramidal cells in the intermediate zone of the hippocampus and their settling in the stratum pyramidale. *J. Comp. Neurol.*, **301**, 343–364.

Altman, J. & Bayer, S.A. (1990b) Migration and distribution of two populations of hippocampal granule cell precursors during the perinatal and postnatal periods. *J. Comp. Neurol.*, **301**, 365–381.

Amaral, D.G. & Dent, J.A. (1981) Development of the mossy fibers of the dentate gyrus: I. A light and electron microscopic study of the mossy fibers and their expansions. *J. Comp. Neurol.*, **195**, 51–86.

Angevine, J.B. Jr (1965) Time of neuron origin in the hippocampal region. An autoradio-graphic study in the mouse. *Exp. Neurol. Suppl.*, **1965**, 1–70.

Avoli, M., D'Antuono, M., Louvel, J., Köhling, R., Biagini, G., Pumain, R., D'Arcangelo, G. & Tancredi, V. (2002) Network and pharmacological mechanisms leading to epileptiform synchronization in the limbic system in vitro. *Prog. Neurobiol.*, **68**, 167–207.

Bagri, A., Cheng, H.J., Yaron, A., Pleasure, S.J. & Tessier-Lavigne, M. (2003) Stereotyped pruning of long hippocampal axon branches triggered by retraction inducers of the semaphorin family. *Cell*, **113**, 285–299.

Bai, J., Ramos, R.L., Ackman, J.B., Thomas, A.M., Lee, R.V. & LoTurco, J.J. (2003) RNAi reveals doublecortin is required for radial migration in rat neocortex. *Nat. Neurosci.*, **6**, 1277–1283.

Bazelot, M., Dinocourt, C., Cohen, I. & Miles, R. (2010) Inhibitory field potentials in the CA3 region of rat hippocampus. *J. Physiol.*, **588**, 2077–2090.

Ben-Ari, Y., Crepel, V. & Represa, A. (2008) Seizures beget seizures in temporal lobe epilepsies: the boomerang effects of newly formed aberrant kainatergic synapses. *Epilepsy Curr.*, **8**, 68–72.

Carnevale, N.T., Tsai, K.Y., Claiborne, B.J. & Brown, T.H. (1997) Comparative electrotonic analysis of three classes of rat hippocampal neurons. *J. Neurophysiol.*, **78**, 703–720.

Claiborne, B.J., Amaral, D.G. & Cowan, W.M. (1986) A light and electron microscopic analysis of the mossy fibers of the rat dentate gyrus. *J. Comp. Neurol.*, **246**, 435–458.

Colombo, E., Collombat, P., Colasante, G., Bianchi, M., Long, J., Mansouri, A., Rubenstein, J.L. & Broccoli, V. (2007) Inactivation of *Arx*, the murine ortholog of the X-linked lissencephaly with ambiguous genitalia gene, leads to severe disorganization of the ventral telencephalon with impaired neuronal migration and differentiation. *J. Neurosci.*, **27**, 4786–4798.

Conde, C. & Cáceres, A. (2009) Microtubule assembly, organization and dynamics in axons and dendrites. *Nat. Rev. Neurosci.*, **10**, 319–332.

Corbo, J.C., Deuel, T.A., Long, J.M., LaPorte, P., Tsai, E., Wynshaw-Boris, A. & Walsh, C.A. (2002) Doublecortin is required in mice for lamination of the hippocampus but not the neocortex. *J. Neurosci.*, **22**, 7548–7557.

Danglot, L., Triller, A. & Marty, S. (2006) The development of hippocampal interneurons in rodents. *Hippocampus*, **16**, 1032–1060.

Deguchi, Y., Donato, F., Galimberti, I., Cabuy, E. & Caroni, P. (2011) Temporally matched subpopulations of selectively interconnected principal neurons in the hippocampus. *Nat. Neurosci.*, **14**, 495–504.

Desai, N.S., Rutherford, L.C. & Turrigiano, G.G. (1999) Plasticity in the intrinsic excitability of cortical pyramidal neurons. *Nat. Neurosci.*, **2**, 515–520.

Deuel, J.C., Yoo, T.A., Liu, J.S., Corbo, S.Y., Rorke-Adams, L.B. & Walsh, C.A. (2006) Genetic interactions between doublecortin and doublecortin-like kinase in neuronal migration and axon outgrowth. *Neuron*, **49**, 41–53.

Dumoulin, A., Rostaing, P., Bedet, C., Lévi, S., Isambert, M.F., Henry, J.P., Triller, A. & Gasnier, B. (1999) Presence of the vesicular inhibitory amino acid transporter in GABAergic and glycinergic synaptic terminal boutons. *J. Cell Sci.*, **112**, 811–823.

Fallet-Bianco, C., Loeuillet, L., Poirier, K., Loget, P., Chapon, F., Pasquier, L., Saillour, Y., Beldjord, C., Chelly, J. & Francis, F. (2008) Neuropathological phenotype of a distinct form of lissencephaly associated with mutations in *TUBA1A*. *Brain*, **131**, 2304–2320.

Fleck, M.W., Hirotsune, S., Gambello, M.J., Phillips-Tansey, E., Soares, G., Mervis, R.F., Wynshaw-Boris, A. & McBain, C.J. (2000) Hippocampal abnormalities and enhanced excitability in a murine model of human lissencephaly. *J. Neurosci.*, **20**, 2439–2450.

Förster, E., Zhao, S. & Frotscher, M. (2006) Laminating the hippocampus. *Nat. Rev. Neurosci.*, **7**, 259–267.

Francis, F., Koulakoff, A., Boucher, D., Chafey, P., Schaar, B., Vinet, M.C., Friocourt, G., McDonnell, N., Reiner, O., Kahn, A., McConnell, S.K., Berwald-Netter, Y., Denoulet, P. & Chelly, J. (1999) Doublecortin is a developmentally regulated, microtubule-associated protein expressed in migrating and differentiating neurons. *Neuron*, **23**, 247–256.

Freund, T.F. & Katona, I. (2007) Perisomatic inhibition. *Neuron*, **56**, 33–42.

Fricker, D., Verheugen, J.A. & Miles, R. (1999) Cell-attached measurements of the firing threshold of rat hippocampal neurons. *J. Physiol.*, **517**, 791–804.

Friocourt, G., Koulakoff, A., Chafey, P., Boucher, D., Fauchereau, F., Chelly, J. & Francis, F. (2003) Doublecortin functions at the extremities of growing neuronal processes. *Cereb. Cortex*, **13**, 620–626.

Friocourt, G., Liu, J.S., Antypa, M., Rakic, S., Walsh, C.A. & Parnavelas, J.G. (2007) Both doublecortin and doublecortin-like kinase play a role in cortical interneuron migration. *J. Neurosci.*, **27**, 3875–3883.

Gaarskjaer, F.B. (1986) The organization and development of the hippocampal mossy fiber system. *Brain Res.*, **396**, 335–357.

Gaiarsa, J.L., Beaudoin, M. & Ben-Ari, Y. (1992) Effect of neonatal degranulation on the morphological development of rat CA3 pyramidal neurons: inductive role of mossy fibers on the formation of thorny excrescences. *J. Comp. Neurol.*, **321**, 612–625.

Gleeson, J.G., Allen, K.M., Fox, J.W., Lamperti, E.D., Berkovic, S., Scheffer, I., Cooper, E.C., Dobyns, W.B., Minnerath, S.R., Ross, M.E. & Walsh, C.A. (1998) Doublecortin, a brain-specific gene mutated in human X-linked lissencephaly and double cortex syndrome, encodes a putative signaling protein. *Cell*, **92**, 63–72.

Gonzales, R.B., DeLeon Galvan, C.J., Rangel, Y.M. & Claiborne, B.J. (2001) Distribution of thorny excrescences on CA3 pyramidal neurons in the rat hippocampus. *J. Comp. Neurol.*, **430**, 357–368.

Guerrini, R. & Parrini, E. (2010) Neuronal migration disorders. *Neurobiol. Dis.*, **38**, 154–166.

Hack, I., Bancila, M., Loulier, K., Carroll, P. & Cremer, H. (2002) Reelin is a detachment signal in tangential chain-migration during postnatal neurogenesis. *Nat. Neurosci.*, **5**, 939–945.

Hattori, M., Adachi, H., Tsujimoto, M., Arai, H. & Inoue, K. (1994) Miller-Dieker lissencephaly gene encodes a subunit of brain platelet-activating factor acetylhydrolase. *Nature*, **370**, 216–218.

- Jaglin, X.H. & Chelly, J. (2009) Tubulin-related cortical dysgeneses: microtubule dysfunction underlying neuronal migration defects. *Trends Genet.*, **25**, 555–566.
- Jaglin, X.H., Poirier, K., Saillour, Y., Buhler, E., Tian, G., Bahi-Buisson, N., Fallet-Bianco, C., Phan-Dinh-Tuy, F., Kong, X.P., Bomont, P., Castelnaud-Ptakhine, L., Odent, S., Loget, P., Kossorotoff, M., Snoeck, I., Plessis, G., Parent, P., Beldjord, C., Cardoso, C., Represa, A., Flint, J., Keays, D.A., Cowan, N.J. & Chelly, J. (2009) Mutations in the beta-tubulin gene TUBB2B result in asymmetrical polymicrogyria. *Nat. Genet.*, **41**, 746–752.
- Johnston, D. & Amaral, D.G. (1997) The hippocampus. In: Shepherd, G.M. (Ed.), *The Synaptic Organization of the Brain*. Oxford University Press, New York, pp. 455–498.
- Jones, D.L. & Baraban, S.C. (2007) Characterization of inhibitory circuits in the malformed hippocampus of *Lis1* mutant mice. *J. Neurophysiol.*, **98**, 2737–2746.
- Jones, D.L. & Baraban, S.C. (2009) Inhibitory inputs to hippocampal interneurons are reorganized in *Lis1* mutant mice. *J. Neurophysiol.*, **102**, 648–658.
- Kappeler, C., Saillour, Y., Baudoin, J.P., Tuy, F.P., Alvarez, C., Houbron, C., Gaspar, P., Hamard, G., Chelly, J., Métin, C. & Francis, F. (2006) Branching and nucleokinesis defects in migrating interneurons derived from doublecortin knockout mice. *Hum. Mol. Genet.*, **15**, 1387–1400.
- Kappeler, C., Dhenain, M., Tuy Phan Dinh, F., Saillour, Y., Marty, S., Fallet-Bianco, C., Souville, I., Souil, E., Pinard, J.M., Meyer, G., Encha-Razavi, F., Volk, A., Beldjord, C., Chelly, J. & Francis, F. (2007) Magnetic resonance imaging and histological studies of corpus callosal and hippocampal abnormalities linked to doublecortin deficiency. *J. Comp. Neurol.*, **500**, 239–254.
- Keays, D.A., Tian, G., Poirier, K., Huang, G.J., Siebold, C., Cleak, J., Oliver, P.L., Fray, M., Harvey, R.J., Molnár, Z., Piñon, M.C., Dear, N., Valdar, W., Brown, S.D., Davies, K.E., Rawlins, J.N., Cowan, N.J., Nolan, P., Chelly, J. & Flint, J. (2007) Mutations in alpha-tubulin cause abnormal neuronal migration in mice and lissencephaly in humans. *Cell*, **128**, 45–57.
- Kerjan, G. & Gleeson, J.G. (2007) Genetic mechanisms underlying abnormal neuronal migration in classical lissencephaly. *Trends Genet.*, **23**, 623–630.
- Kerjan, G., Koizumi, H., Han, E.B., Dubé, C.M., Djakovic, S.N., Patrick, G.N., Baram, T.Z., Heinemann, S.F. & Gleeson, J.G. (2009) Mice lacking doublecortin and doublecortin-like kinase 2 display altered hippocampal neuronal maturation and spontaneous seizures. *Proc. Natl. Acad. Sci. USA*, **106**, 6766–6771.
- Koizumi, H., Higginbotham, H., Poon, T., Tanaka, T., Brinkman, B.C. & Gleeson, J.G. (2006) Doublecortin maintains bipolar shape and nuclear translocation during migration in the adult forebrain. *Nat. Neurosci.*, **9**, 779–786.
- Leger, P.L., Souville, I., Boddaert, N., Elie, C., Pinard, J.M., Plouin, P., Moutard, M.L., des Portes, V., Van Esch, H., Joriot, S., Renard, J.L., Chelly, J., Francis, F., Beldjord, C. & Bahi-Buisson, N. (2008) The location of DCX mutations predicts malformation severity in X-linked lissencephaly. *Neurogenetics*, **9**, 277–285.
- Manent, J.B., Jorquera, I., Ben-Ari, Y., Aniksztejn, L. & Represa, A. (2006) Glutamate acting on AMPA not NMDA receptors modulates migration of hippocampal interneurons. *J. Neurosci.*, **26**, 5901–5909.
- Manent, J.B., Wang, Y., Chang, Y., Paramasivam, M. & LoTurco, J.J. (2009) *Dcx* re-expression reduces subcortical band heterotopia and seizure threshold in an animal model of neuronal migration disorder. *Nat. Med.*, **15**, 84–90.
- Nakahira, E. & Yuasa, S. (2005) Neuronal generation, migration, and differentiation in the mouse hippocampal primordium as revealed by enhanced green fluorescent protein gene transfer by means of in utero electroporation. *J. Comp. Neurol.*, **483**, 329–340.
- Nosten-Bertrand, M., Kappeler, C., Dinocourt, C., Denis, C., Germain, J., Tuy Phan Dinh, F., Verstraeten, S., Alvarez, C., Métin, C., Chelly, J., Giros, B., Miles, R., Depaulis, A. & Francis, F. (2008) Epilepsy in *Dcx* knockout mice associated with discrete lamination defects and enhanced excitability in the hippocampus. *PLoS ONE*, **3**, e2473.
- Nowakowski, R.S. & Davis, T.L. (1985) Dendritic arbors and dendritic excrescences of abnormally positioned neurons in area CA3c of mice carrying the mutation ‘‘hippocampal lamination defect’’. *J. Comp. Neurol.*, **239**, 267–275.
- O’Leary, T., van Rossum, M.C. & Wyllie, D.J. (2010) Homeostasis of intrinsic excitability in hippocampal neurons: dynamics and mechanism of the response to chronic depolarization. *J. Physiol.*, **588**, 157–170.
- Palmiter, R.D., Cole, T.B., Quaife, C.J. & Findley, S.D. (1996) ZnT-3, a putative transporter of zinc into synaptic vesicles. *Proc. Natl. Acad. Sci. USA*, **93**, 14934–14939.
- Pleasure, S.J., Anderson, S., Hevner, R., Bagri, A., Marin, O., Lowenstein, D.H. & Rubenstein, J.L. (2000) Cell migration from the ganglionic eminences is required for the development of hippocampal GABAergic interneurons. *Neuron*, **28**, 727–740.
- Qin, L., Marrs, G.S., McKim, R. & Dailey, M.E. (2001) Hippocampal mossy fibers induce assembly and clustering of PSD95-containing postsynaptic densities independent of glutamate receptor activation. *J. Comp. Neurol.*, **440**, 284–298.
- Reiner, O., Carrozzo, R., Shen, Y., Wehnert, M., Faustinella, F., Dobyns, W.B., Caskey, C.T. & Ledbetter, D.H. (1993) Isolation of a Miller-Dieker lissencephaly gene containing G protein beta-subunit-like repeats. *Nature*, **364**, 717–721.
- Schaar, B.T., Kinoshita, K. & McConnell, S.K. (2004) Doublecortin microtubule affinity is regulated by a balance of kinase and phosphatase activity at the leading edge of migrating neurons. *Neuron*, **41**, 203–213.
- Schwartzkroin, P.A. & Walsh, C.A. (2000) Cortical malformations and epilepsy. *Ment. Retard. Dev. Disabil. Res. Rev.*, **6**, 268–280.
- Seki, T. & Rutishauser, U. (1998) Removal of polysialic acid-neuronal cell adhesion molecule induces aberrant mossy fiber innervation and ectopic synaptogenesis in the hippocampus. *J. Neurosci.*, **18**, 3757–3766.
- Shimizu-Okabe, C., Okabe, A., Kilb, W., Sato, K., Luhmann, H.J. & Fukuda, A. (2007) Changes in the expression of cation-Cl<sup>-</sup> cotransporters, NKCC1 and KCC2, during cortical malformation induced by neonatal freeze-lesion. *Neurosci. Res.*, **59**, 288–295.
- Soriano, E., Cobas, A. & Fairén, A. (1986) Asynchronism in the neurogenesis of GABAergic and non-GABAergic neurons in the mouse hippocampus. *Brain Res.*, **395**, 88–92.
- Taverna, S., Tkatch, T., Metz, A.E. & Martina, M. (2005) Differential expression of TASK channels between horizontal interneurons and pyramidal cells of rat hippocampus. *J. Neurosci.*, **25**, 9162–9170.
- Xu, N.J. & Henkemeyer, M. (2009) Ephrin-B3 reverse signaling through Grb4 and cytoskeletal regulators mediates axon pruning. *Nat. Neurosci.*, **12**, 268–276.
- Zhu, J.J. (2000) Maturation of layer 5 neocortical pyramidal neurons: amplifying salient layer 1 and layer 4 inputs by Ca<sup>2+</sup> action potentials in adult rat tuft dendrites. *J. Physiol.*, **526**, 571–587.



## List of Figures

1	Representations of the hippocampal formation, the parahippocampal region and retrosplenial cortex in rat brain . . . . .	16
2	Layers and afferent fibers in the presubiculum . . . . .	18
3	Basic features of presubicular head direction cells. . . . .	21
4	The Head direction circuit . . . . .	23
5	A continuous attractor network model of head direction signal generation . . . . .	25
6	Entorhinal-hippocampal circuit and function . . . . .	28
7	Landmark control of spatial signals. . . . .	30
8	Cellular properties in presubiculum . . . . .	32
9	Presubicular intrinsic connectivity . . . . .	34
10	Laminar specificity of afferences and efferences in presubiculum . . . . .	36
11	Studying the network. Same neurons, different methods . . . . .	40
12	Firing patterns of neocortical neurons . . . . .	45
13	Firing patterns of cortical interneurons . . . . .	46
14	Action potential broadening enhances synaptic efficiency in mossy fiber boutons . . . . .	52
15	Cortical chemical synapse . . . . .	55
16	Schematic of neurotransmitter release . . . . .	57
17	Impact of fast spiking interneuron-mediated synchronous and asynchronous GABA release onto neocortical pyramidal cell firing . . . . .	59
18	Short term presynaptic plasticity . . . . .	62
19	Synaptic transmission in the mammalian hippocampus . . . . .	65



# Bibliography

- Abbasi, S. and Kumar, S. S. (2013). Electrophysiological and morphological characterization of cells in superficial layers of rat presubiculum. *The Journal of Comparative Neurology*, 521(13):3116–3132.
- Abbott, L. F. and Regehr, W. G. (2004). Synaptic computation. *Nature*, 431(7010):796–803.
- Adams, D. J., Takeda, K., and Umbach, J. A. (1985). Inhibitors of calcium buffering depress evoked transmitter release at the squid giant synapse. *The Journal of Physiology*, 369:145–159.
- Adler, E. M., Augustine, G. J., Duffy, S. N., and Charlton, M. P. (1991). Alien intracellular calcium chelators attenuate neurotransmitter release at the squid giant synapse. *The Journal of neuroscience : the official journal of the Society for Neuroscience*, 11(6):1496–1507.
- Adrian, E. D. (1920). The recovery process of excitable tissues: Part I. *The Journal of Physiology*, 54(1-2):1–31.
- Alger, B. E. and Kim, J. (2011). Supply and demand for endocannabinoids. *Trends in Neurosciences*, 34(6):304–315.
- Ali, A. B., Deuchars, J., Pawelzik, H., and Thomson, A. M. (1998). CA1 pyramidal to basket and bistratified cell EPSPs: dual intracellular recordings in rat hippocampal slices. *The Journal of Physiology*, 507 ( Pt 1):201–217.
- Ali, A. B. and Thomson, A. M. (1998). Facilitating pyramid to horizontal oriens-alveus interneurone inputs: dual intracellular recordings in slices of rat hippocampus. *The Journal of Physiology*, 507 ( Pt 1):185–199.
- Alle, H. (2006). Combined Analog and Action Potential Coding in Hippocampal Mossy Fibers. *Science*, 311(5765):1290–1293.
- Alle, H. and Geiger, J. R. (2008). Analog signalling in mammalian cortical axons. *Current opinion in neurobiology*, 18(3):314–320.
- Allen, G. V. and Hopkins, D. A. (1989). Mamillary body in the rat: topography and synaptology of projections from the subicular complex, prefrontal cortex, and midbrain tegmentum. *The Journal of Comparative Neurology*, 286(3):311–336.
- Amaral, D. G. and Witter, M. P. (1989). The three-dimensional organization of the hippocampal formation: a review of anatomical data. *NSC*, 31(3):571–591.

- Angevine, J. B. and Sidman, R. L. (1961). Autoradiographic study of cell migration during histogenesis of cerebral cortex in the mouse. *Nature*, 192:766–768.
- Angulo, M. C., Staiger, J. F., Rossier, J., and Audinat, E. (1999). Developmental synaptic changes increase the range of integrative capabilities of an identified excitatory neocortical connection. *The Journal of neuroscience : the official journal of the Society for Neuroscience*, 19(5):1566–1576.
- Ascoli, G. A., Alonso-Nanclares, L., Anderson, S. A., Barrionuevo, G., Benavides-Piccione, R., Burkhalter, A., Buzsáki, G., Cauli, B., DeFelipe, J., Fairén, A., Feldmeyer, D., Fishell, G., Fregnac, Y., Freund, T. F., Gardner, D., Gardner, E. P., Goldberg, J. H., Helmstaedter, M., Hestrin, S., Karube, F., Kisvárdy, Z. F., Lambolez, B., Lewis, D. A., Marin, O., Markram, H., Muñoz, A., Packer, A., Petersen, C. C. H., Rockland, K. S., Rossier, J., Rudy, B., Somogyi, P., Staiger, J. F., Tamas, G., Thomson, A. M., Toledo-Rodriguez, M., Wang, Y., West, D. C., and Yuste, R. (2008). Petilla terminology: nomenclature of features of GABAergic interneurons of the cerebral cortex. *Nature Reviews Neuroscience*, 9(7):557–568.
- Atluri, P. P. and Regehr, W. G. (1998). Delayed release of neurotransmitter from cerebellar granule cells. *The Journal of neuroscience : the official journal of the Society for Neuroscience*, 18(20):8214–8227.
- Bacci, A. and Huguenard, J. R. (2006). Enhancement of Spike-Timing Precision by Autaptic Transmission in Neocortical Inhibitory Interneurons. *Neuron*, 49(1):119–130.
- Baginskas, A., Palani, D., Chiu, K., and Raastad, M. (2009). The H-current secures action potential transmission at high frequencies in rat cerebellar parallel fibers. *European Journal of Neuroscience*, 29(1):87–96.
- Bartasaghi, R. and Gessi, T. (1990). Electrophysiological analysis of the hippocampal output to the presubiculum. *NSC*, 37(2):335–345.
- Bassett, J. P., Tullman, M. L., and Taube, J. S. (2007). Lesions of the Tegmentomammillary Circuit in the Head Direction System Disrupt the Head Direction Signal in the Anterior Thalamus. *Journal of Neuroscience*, 27(28):7564–7577.
- Battaglia, D., Karagiannis, A., Gallopin, T., Gutch, H. W., and Cauli, B. (2013). Beyond the frontiers of neuronal types. *Frontiers in neural circuits*, 7:13.
- Battefeld, A., Tran, B. T., Gavrilis, J., Cooper, E. C., and Kole, M. H. P. (2014). Heteromeric Kv7.2/7.3 channels differentially regulate action potential initiation and conduction in neocortical myelinated axons. *Journal of Neuroscience*, 34(10):3719–3732.
- Bayer, S. A. (1980). Development of the hippocampal region in the rat. I. Neurogenesis examined with 3H-thymidine autoradiography. *The Journal of Comparative Neurology*, 190(1):87–114.
- Bean, B. P. (2007). The action potential in mammalian central neurons. *Nature Reviews Neuroscience*, 8(6):451–465.
- Beckstead, R. M. (1978). Afferent connections of the entorhinal area in the rat as demonstrated by retrograde cell-labeling with horseradish peroxidase. *Brain research*, 152(2):249–264.

- Beed, P., Gundlfinger, A., Schneiderbauer, S., Song, J., Böhm, C., Burgalossi, A., Brecht, M., Vida, I., and Schmitz, D. (2013). Inhibitory Gradient along the Dorsoventral Axis in the Medial Entorhinal Cortex. *Neuron*, 79(6):1197–1207.
- Beierlein, M., Gibson, J. R., and Connors, B. W. (2003). Two dynamically distinct inhibitory networks in layer 4 of the neocortex. *Journal of Neurophysiology*, 90(5):2987–3000.
- Best, A. R. and Regehr, W. G. (2009). Inhibitory regulation of electrically coupled neurons in the inferior olive is mediated by asynchronous release of GABA. *Neuron*, 62(4):555–565.
- Betz, W. J. (1970). Depression of transmitter release at the neuromuscular junction of the frog. *The Journal of Physiology*, 206(3):629–644.
- Bezudnaya, T. and Keller, A. (2008). Laterodorsal nucleus of the thalamus: A processor of somatosensory inputs. *The Journal of Comparative Neurology*, 507(6):1979–1989.
- Bischofberger, J., Engel, D., Li, L., Geiger, J. R., and Jonas, P. (2006). Patch-clamp recording from mossy fiber terminals in hippocampal slices. *Nature Protocols*, 1(4):2075–2081.
- Blackstad, T. W. (1956). Commissural connections of the hippocampal region in the rat, with special reference to their mode of termination. *The Journal of Comparative Neurology*, 105(3):417–537.
- Blair, H. T. and Sharp, P. E. (1995). Anticipatory head direction signals in anterior thalamus: evidence for a thalamocortical circuit that integrates angular head motion to compute head direction. *The Journal of neuroscience : the official journal of the Society for Neuroscience*, 15(9):6260–6270.
- Boccaro, C. N., Sargolini, F., Thoresen, V. H., Solstad, T., Witter, M. P., Moser, E. I., and Moser, M.-B. (2010). Grid cells in pre- and parasubiculum. *Nature Publishing Group*, 13(8):987–994.
- Bonnevie, T., Dunn, B., Fyhn, M., Hafting, T., Derdikman, D., Kubie, J. L., Roudi, Y., Moser, E. I., and Moser, M.-B. (2013). Grid cells require excitatory drive from the hippocampus. *Nature Neuroscience*, 16(3):309–317.
- Boucheny, C., Brunel, N., and Arleo, A. (2005). A continuous attractor network model without recurrent excitation: maintenance and integration in the head direction cell system. *Journal of computational neuroscience*, 18(2):205–227.
- Boudkazi, S., Fronzaroli-Molinieres, L., and Debanne, D. (2011). Presynaptic action potential waveform determines cortical synaptic latency. *The Journal of Physiology*, 589(Pt 5):1117–1131.
- Brager, D. H., Cai, X., and Thompson, S. M. (2003). Activity-dependent activation of presynaptic protein kinase C mediates post-tetanic potentiation. *Nature Neuroscience*, 6(6):551–552.
- Brodmann, K. (1909). Vergleichende Lokalisationslehre der Grosshirnrinde in ihren Prinzipien dargestellt aufgrund des Zellenbaues.
- Bucher, D. and Goaillard, J.-M. (2011). Beyond faithful conduction: Short-term dynamics, neuromodulation, and long-term regulation of spike propagation in the axon. *Progress in neurobiology*, 94(4):307–346.

- Buetfering, C., Allen, K., and Monyer, H. (2014). Parvalbumin interneurons provide grid cell-driven recurrent inhibition in the medial entorhinal cortex. *Nature Publishing Group*, 17(5):710–718.
- Bullock, T. H. (1951). Facilitation of conduction rate in nerve fibres. *The Journal of Physiology*, 114(1-2):89–97.
- Bullock, T. H. (2005). The Neuron Doctrine, Redux. *Science*, 310(5749):791–793.
- Bush, D., Barry, C., and Burgess, N. (2014). What do grid cells contribute to place cell firing? *Trends in Neurosciences*, 37(3):136–145.
- Cabezas, C., Irinopoulou, T., Cauli, B., and Ponce, J. C. (2013). Molecular and functional characterization of GAD67-expressing, newborn granule cells in mouse dentate gyrus. *Frontiers in neural circuits*, 7:60.
- Caillard, O., Moreno, H., Schwaller, B., Llano, I., Celio, M. R., and Marty, A. (2000). Role of the calcium-binding protein parvalbumin in short-term synaptic plasticity. *Proceedings of the National Academy of Sciences of the United States of America*, 97(24):13372–13377.
- Calton, J. L., Stackman, R. W., Goodridge, J. P., Archey, W. B., Dudchenko, P. A., and Taube, J. S. (2003). Hippocampal place cell instability after lesions of the head direction cell network. *Journal of Neuroscience*, 23(30):9719–9731.
- Calton, J. L., Turner, C. S., Cyrenne, D.-L. M., Lee, B. R., and Taube, J. S. (2008). Landmark control and updating of self-movement cues are largely maintained in head direction cells after lesions of the posterior parietal cortex. *Behavioral neuroscience*, 122(4):827–840.
- Campanac, E., Gassel, C., Baude, A., Rama, S., Ankri, N., and Debanne, D. (2013). Enhanced Intrinsic Excitability in Basket Cells Maintains Excitatory-Inhibitory Balance in Hippocampal Circuits. *Neuron*, 77(4):712–722.
- Canto, C. B., Koganezawa, N., Beed, P., Moser, E. I., and Witter, M. P. (2012). All Layers of Medial Entorhinal Cortex Receive Presubicular and Parasubicular Inputs. *Journal of Neuroscience*, 32(49):17620–17631.
- Carter, A. G., Vogt, K. E., Foster, K. A., and Regehr, W. G. (2002). Assessing the role of calcium-induced calcium release in short-term presynaptic plasticity at excitatory central synapses. *Journal of Neuroscience*, 22(1):21–28.
- Castillo, P. E., Younts, T. J., Chávez, A. E., and Hashimoto, Y. (2012). Endocannabinoid Signaling and Synaptic Function. *Neuron*, 76(1):70–81.
- Cauli, B., Porter, J. T., Tsuzuki, K., Lambolez, B., Rossier, J., Quenet, B., and Audinat, E. (2000). Classification of fusiform neocortical interneurons based on unsupervised clustering. *Proceedings of the National Academy of Sciences of the United States of America*, 97(11):6144–6149.
- Cenquizca, L. A. and Swanson, L. W. (2007). Spatial organization of direct hippocampal field CA1 axonal projections to the rest of the cerebral cortex. *Brain Research Reviews*, 56(1):1–26.

- Chagnac-Amitai, Y. and Connors, B. W. (1989). Synchronized excitation and inhibition driven by intrinsically bursting neurons in neocortex. *Journal of Neurophysiology*, 62(5):1149–1162.
- Chen, X. and Johnston, D. (2004). Properties of single voltage-dependent K<sup>+</sup> channels in dendrites of CA1 pyramidal neurones of rat hippocampus. *The Journal of Physiology*, 559(Pt 1):187–203.
- Chevaleyre, V. and Castillo, P. E. (2004). Endocannabinoid-Mediated Metaplasticity in the Hippocampus. *Neuron*, 43(6):871–881.
- Chevaleyre, V. and Siegelbaum, S. A. (2010). Strong CA2 pyramidal neuron synapses define a powerful disinaptic cortico-hippocampal loop. *Neuron*, 66(4):560–572.
- Cho, J. and Sharp, P. E. (2001). Head direction, place, and movement correlates for cells in the rat retrosplenial cortex. *Behavioral neuroscience*, 115(1):3–25.
- Clark, B. J., Bassett, J. P., Wang, S. S., and Taube, J. S. (2010). Impaired head direction cell representation in the anterodorsal thalamus after lesions of the retrosplenial cortex. *Journal of Neuroscience*, 30(15):5289–5302.
- Clark, B. J. and Taube, J. S. (2012). Vestibular and attractor network basis of the head direction cell signal in subcortical circuits. *Frontiers in neural circuits*, 6:7.
- Connors, B. W. and Gutnick, M. J. (1990). Intrinsic firing patterns of diverse neocortical neurons. *Trends in Neurosciences*, 13(3):99–104.
- Couey, J. J., Witoelar, A., Zhang, S.-J., Zheng, K., Ye, J., Dunn, B., Czajkowski, R., Moser, M.-B., Moser, E. I., Roudi, Y., and Witter, M. P. (2013). Recurrent inhibitory circuitry as a mechanism for grid formation. *Nature Publishing Group*, 16(3):318–324.
- Cruikshank, S. J., Lewis, T. J., and Connors, B. W. (2007). Synaptic basis for intense thalamo-cortical activation of feedforward inhibitory cells in neocortex. *Nature Neuroscience*.
- Cruikshank, S. J., Urabe, H., Nurmikko, A. V., and Connors, B. W. (2010). Pathway-Specific Feed-forward Circuits between Thalamus and Neocortex Revealed by Selective Optical Stimulation of Axons. *Neuron*, 65(2):230–245.
- Cummings, D. D., Wilcox, K. S., and Dichter, M. A. (1996). Calcium-dependent paired-pulse facilitation of miniature EPSC frequency accompanies depression of EPSCs at hippocampal synapses in culture. *The Journal of neuroscience : the official journal of the Society for Neuroscience*, 16(17):5312–5323.
- David, G. and Barrett, E. F. (2003). Mitochondrial Ca<sup>2+</sup> uptake prevents desynchronization of quantal release and minimizes depletion during repetitive stimulation of mouse motor nerve terminals. *The Journal of Physiology*, 548(2):425–438.
- Debanne, D. (2004). Information processing in the axon. *Nature Reviews Neuroscience*, 5(4):304–316.
- Debanne, D., Bialowas, A., and Rama, S. (2013). What are the mechanisms for analogue and digital signalling in the brain? *Nature Reviews Neuroscience*, 14(1):63–69.

- Debanne, D., Campanac, E., Bialowas, A., Carlier, E., and Alcaraz, G. (2011). Axon Physiology. *Physiological Reviews*, 91(2):555–602.
- Debanne, D., Guérineau, N. C., Gähwiler, B. H., and Thompson, S. M. (1996). Paired-pulse facilitation and depression at unitary synapses in rat hippocampus: quantal fluctuation affects subsequent release. *The Journal of Physiology*, 491 ( Pt 1):163–176.
- Debanne, D., Guérineau, N. C., Gähwiler, B. H., and Thompson, S. M. (1997). Action-potential propagation gated by an axonal I(A)-like K<sup>+</sup> conductance in hippocampus. *Nature*, 389(6648):286–289.
- Dekel, N., Priest, M. F., Parnas, H., Parnas, I., and Bezanilla, F. (2012). Depolarization induces a conformational change in the binding site region of the M2 muscarinic receptor. *Proceedings of the National Academy of Sciences of the United States of America*, 109(1):285–290.
- Deleuze, C., Paziienti, A., and Bacci, A. (2014). Autaptic self-inhibition of cortical GABAergic neurons: Synaptic narcissism or useful introspection? *Current opinion in neurobiology*, 26:64–71.
- Devaux, J. J., Kleopa, K. A., Cooper, E. C., and Scherer, S. S. (2004). KCNQ2 is a nodal K<sup>+</sup> channel. *Journal of Neuroscience*, 24(5):1236–1244.
- Dias, R. B., Rombo, D. M., Ribeiro, J. A., Henley, J. M., and Sebastião, A. M. (2013). Adenosine: setting the stage for plasticity. *Trends in Neurosciences*, 36(4):248–257.
- Ding, S.-L. (2013). Comparative anatomy of the prosubiculum, subiculum, presubiculum, postsubiculum, and parasubiculum in human, monkey, and rodent. *The Journal of Comparative Neurology*, 521(18):4145–4162.
- Ding, S.-L. and Rockland, K. (2001). Modular organization of the monkey presubiculum. *Experimental Brain Research*, 139(3):255–265.
- Domnisoru, C., Kinkhabwala, A. A., and Tank, D. W. (2013). Membrane potential dynamics of grid cells. *Nature*.
- Dumitriu, D., Cossart, R., Huang, J., and Yuste, R. (2007). Correlation between axonal morphologies and synaptic input kinetics of interneurons from mouse visual cortex. *Cerebral cortex (New York, N.Y. : 1991)*, 17(1):81–91.
- Dunwiddie, T. V. and Masino, S. A. (2001). The role and regulation of adenosine in the central nervous system. *Annual Review of Neuroscience*, 24:31–55.
- Epsztein, J., Brecht, M., and Lee, A. K. (2011). Intracellular determinants of hippocampal CA1 place and silent cell activity in a novel environment. *Neuron*, 70(1):109–120.
- Faas, G. C., Schwaller, B., Vergara, J. L., and Mody, I. (2007). Resolving the fast kinetics of cooperative binding: Ca<sup>2+</sup> buffering by calretinin. *PLoS biology*, 5(11):e311.
- Fanselow, E. E., Richardson, K. A., and Connors, B. W. (2008). Selective, State-Dependent Activation of Somatostatin-Expressing Inhibitory Interneurons in Mouse Neocortex. *Journal of Neurophysiology*, 100(5):2640–2652.

- Few, A. P., Nanou, E., Watari, H., Sullivan, J. M., Scheuer, T., and Catterall, W. A. (2012). Asynchronous Ca<sup>2+</sup> current conducted by voltage-gated Ca<sup>2+</sup> (CaV)-2.1 and CaV2.2 channels and its implications for asynchronous neurotransmitter release. *Proceedings of the National Academy of Sciences of the United States of America*, 109(7):E452–60.
- Filimonoff, I. N. (1947). A rational subdivision of the cerebral cortex. *Archives of neurology and psychiatry*, 58(3):296–311.
- Fino, E. and Yuste, R. (2011). Dense inhibitory connectivity in neocortex. *Neuron*, 69(6):1188–1203.
- Fisher, S. A., Fischer, T. M., and Carew, T. J. (1997). Multiple overlapping processes underlying short-term synaptic enhancement. *Trends in Neurosciences*, 20(4):170–177.
- Fiumara, F., Milanese, C., Corradi, A., Giovedì, S., Leitinger, G., Menegon, A., Montarolo, P. G., Benfenati, F., and Ghirardi, M. (2007). Phosphorylation of synapsin domain A is required for post-tetanic potentiation. *Journal of cell science*, 120(Pt 18):3228–3237.
- Forsythe, I. D., Tsujimoto, T., Barnes-Davies, M., Cuttle, M. F., and Takahashi, T. (1998). Inactivation of presynaptic calcium current contributes to synaptic depression at a fast central synapse. *Neuron*, 20(4):797–807.
- Foust, A. J., Yu, Y., Popovic, M., Zecevic, D., and McCormick, D. A. (2011). Somatic Membrane Potential and Kv1 Channels Control Spike Repolarization in Cortical Axon Collaterals and Presynaptic Boutons. *Journal of Neuroscience*, 31(43):15490–15498.
- Fricker, D., Dinocourt, C., Eugène, E., Wood, J. N., Wood, J., and Miles, R. (2009). Pyramidal cells of rodent presubiculum express a tetrodotoxin-insensitive Na<sup>+</sup> current. *The Journal of Physiology*, 587(Pt 17):4249–4264.
- Funahashi, M., Harris, E., and Stewart, M. (1999). Re-entrant activity in a presubiculum-subiculum circuit generates epileptiform activity in vitro. *Brain research*, 849(1-2):139–146.
- Funahashi, M. and Stewart, M. (1997a). Presubicular and parasubicular cortical neurons of the rat: electrophysiological and morphological properties. *Hippocampus*, 7(2):117–129.
- Funahashi, M. and Stewart, M. (1997b). Presubicular and parasubicular cortical neurons of the rat: functional separation of deep and superficial neurons in vitro. *The Journal of Physiology*, 501 ( Pt 2):387–403.
- Fyhn, M., Molden, S., Witter, M. P., Moser, E. I., and Moser, M.-B. (2004). Spatial representation in the entorhinal cortex. *Science*, 305(5688):1258–1264.
- Gabernet, L., Jadhav, S. P., Feldman, D. E., Carandini, M., and Scanziani, M. (2005). Somatosensory Integration Controlled by Dynamic Thalamocortical Feed-Forward Inhibition. *Neuron*, 48(2):315–327.
- García-López, P., García-Marín, V., and Freire, M. (2007). The discovery of dendritic spines by Cajal in 1888 and its relevance in the present neuroscience. *Progress in neurobiology*, 83(2):110–130.

- Geiger, J. R. and Jonas, P. (2000). Dynamic control of presynaptic Ca(2+) inflow by fast-inactivating K(+) channels in hippocampal mossy fiber boutons. *Neuron*, 28(3):927–939.
- Genc, O., Kochubey, O., Toonen, R. F., Verhage, M., and Schneggenburger, R. (2014). Munc18-1 is a dynamically regulated PKC target during short-term enhancement of transmitter release. *eLife*, 3:e01715.
- Gentet, L. J. (2012). Functional diversity of supragranular GABAergic neurons in the barrel cortex. *Frontiers in neural circuits*, 6:52.
- Goldberg, E. M., Clark, B. D., Zaghera, E., Nahmani, M., Erisir, A., and Rudy, B. (2008). K+ channels at the axon initial segment dampen near-threshold excitability of neocortical fast-spiking GABAergic interneurons. *Neuron*, 58(3):387–400.
- Goldstein, S. S. and Rall, W. (1974). Changes of Action Potential Shape and Velocity for Changing Core Conductor Geometry. *Biophysj*, 14(10):731–757.
- Golob, E. J. and Taube, J. S. (1997). Head direction cells and episodic spatial information in rats without a hippocampus. *Proceedings of the National Academy of Sciences of the United States of America*, 94(14):7645–7650.
- Golob, E. J., Wolk, D. A., and Taube, J. S. (1998). Recordings of postsubiculum head direction cells following lesions of the laterodorsal thalamic nucleus. *Brain research*, 780(1):9–19.
- Gonzalo-Ruiz, A., Alonso, A., Sanz, J. M., and Llinás, R. R. (1992). Afferent projections to the mammillary complex of the rat, with special reference to those from surrounding hypothalamic regions. *The Journal of Comparative Neurology*, 321(2):277–299.
- Goodridge, J. P., Dudchenko, P. A., Worboys, K. A., Golob, E. J., and Taube, J. S. (1998). Cue control and head direction cells. *Behavioral neuroscience*, 112(4):749–761.
- Goodridge, J. P. and Taube, J. S. (1997). Interaction between the postsubiculum and anterior thalamus in the generation of head direction cell activity. *The Journal of neuroscience : the official journal of the Society for Neuroscience*, 17(23):9315–9330.
- Grossman, Y., Parnas, I., and Spira, M. E. (1979). Differential conduction block in branches of a bifurcating axon. *The Journal of Physiology*, 295:283–305.
- Gulledge, A. T., Kampa, B. M., and Stuart, G. J. (2005). Synaptic integration in dendritic trees. *Journal of neurobiology*, 64(1):75–90.
- Habets, R. L. P. and Borst, J. G. G. (2005). Post-tetanic potentiation in the rat calyx of Held synapse. *The Journal of Physiology*, 564(Pt 1):173–187.
- Habets, R. L. P. and Borst, J. G. G. (2006). An Increase in Calcium Influx Contributes to Post-Tetanic Potentiation at the Rat Calyx of Held Synapse. *Journal of Neurophysiology*, 96(6):2868–2876.
- Hamilton, N. B. and Attwell, D. (2010). Do astrocytes really exocytose neurotransmitters? *Nature Reviews Neuroscience*, 11(4):227–238.

- Harris, K. M. and Weinberg, R. J. (2012). Ultrastructure of synapses in the mammalian brain. *Cold Spring Harbor perspectives in biology*, 4(5).
- He, L., Xue, L., Xu, J., McNeil, B. D., Bai, L., Melicoff, E., Adachi, R., and Wu, L.-G. (2009). nature07860. *Nature*, 459(7243):93–97.
- Hippenmeyer, S., Vrieseling, E., Sigrist, M., Portmann, T., Laengle, C., Ladle, D. R., and Arber, S. (2005). A developmental switch in the response of DRG neurons to ETS transcription factor signaling. *PLoS biology*, 3(5):e159.
- Hochner, B., Parnas, H., and Parnas, I. (1989). Membrane depolarization evokes neurotransmitter release in the absence of calcium entry. *Nature*, 342(6248):433–435.
- Hodgkin, A. L. and Huxley, A. F. (1952). A quantitative description of membrane current and its application to conduction and excitation in nerve. *The Journal of Physiology*, 117(4):500–544.
- Hodgkin, A. L. and Katz, B. (1949). The effect of sodium ions on the electrical activity of giant axon of the squid. *The Journal of Physiology*, 108(1):37–77.
- Holderith, N., Lőrincz, A., Katona, G., Rózsa, B., Kulik, A., Watanabe, M., and Nusser, Z. (2012). Release probability of hippocampal glutamatergic terminals scales with the size of the active zone. *Nature Neuroscience*, 15(7):988–997.
- Honda, Y., Furuta, T., Kaneko, T., Shibata, H., and Sasaki, H. (2011). Patterns of axonal collateralization of single layer V cortical projection neurons in the rat presubiculum. *The Journal of Comparative Neurology*, 519(7):1395–1412.
- Honda, Y. and Ishizuka, N. (2004). Organization of connectivity of the rat presubiculum: I. Efferent projections to the medial entorhinal cortex. *The Journal of Comparative Neurology*, 473(4):463–484.
- Honda, Y., Umitsu, Y., and Ishizuka, N. (2008). Organization of connectivity of the rat presubiculum: II. Associational and commissural connections. *The Journal of Comparative Neurology*, 506(4):640–658.
- Hosoi, N., Holt, M., and Sakaba, T. (2009). Calcium Dependence of Exo- and Endocytotic Coupling at a Glutamatergic Synapse. *Neuron*, 63(2):216–229.
- Hsu, S. F., Augustine, G. J., and Jackson, M. B. (1996). Adaptation of Ca(2+)-triggered exocytosis in presynaptic terminals. *Neuron*, 17(3):501–512.
- Hu, H., Cavendish, J. Z., and Agmon, A. (2013). Not all that glitters is gold: off-target recombination in the somatostatin-IRES-Cre mouse line labels a subset of fast-spiking interneurons. *Frontiers in neural circuits*, 7:195.
- Hu, H., Shao, L. R., Chavoshy, S., Gu, N., Trieb, M., Behrens, R., Laake, P., Pongs, O., Knaus, H. G., Ottersen, O. P., and Storm, J. F. (2001). Presynaptic Ca<sup>2+</sup>-activated K<sup>+</sup> channels in glutamatergic hippocampal terminals and their role in spike repolarization and regulation of transmitter release. *Journal of Neuroscience*, 21(24):9585–9597.

- Huxley, A. F. and Stämpfli, R. (1949). Evidence for saltatory conduction in peripheral myelinated nerve fibres. *The Journal of Physiology*, 108(3):315–339.
- Ikeda, K. and Bekkers, J. M. (2009). Counting the number of releasable synaptic vesicles in a presynaptic terminal. *Proceedings of the National Academy of Sciences of the United States of America*, 106(8):2945–2950.
- Isaacson, J. S. and Scanziani, M. (2011). How Inhibition Shapes Cortical Activity. *Neuron*, 72(2):231–243.
- Ishizuka, N. (2001). Laminar organization of the pyramidal cell layer of the subiculum in the rat. *The Journal of Comparative Neurology*, 435(1):89–110.
- Jones, B. F. and Witter, M. P. (2007). Cingulate cortex projections to the parahippocampal region and hippocampal formation in the rat. *Hippocampus*, 17(10):957–976.
- Kaesler, P. S. and Regehr, W. G. (2014). Molecular Mechanisms for Synchronous, Asynchronous, and Spontaneous Neurotransmitter Release. *Annual Review of Physiology*, 76(1):333–363.
- Karagiannis, A., Gallopin, T., David, C., Battaglia, D., Geoffroy, H., Rossier, J., Hillman, E. M. C., Staiger, J. F., and Cauli, B. (2009). Classification of NPY-Expressing Neocortical Interneurons. *Journal of Neuroscience*, 29(11):3642–3659.
- Katz, B. and Miledi, R. (1968). The role of calcium in neuromuscular facilitation. *The Journal of Physiology*, 195(2):481–492.
- Kätzel, D., Zemelman, B. V., Buetfering, C., Wölfel, M., and Miesenböck, G. (2010). The columnar and laminar organization of inhibitory connections to neocortical excitatory cells. *Nature Publishing Group*, 14(1):100–107.
- Kim, Y. and Spruston, N. (2011). Target-specific output patterns are predicted by the distribution of regular-spiking and bursting pyramidal neurons in the subiculum. *Hippocampus*.
- Klausberger, T. and Somogyi, P. (2008). Neuronal Diversity and Temporal Dynamics: The Unity of Hippocampal Circuit Operations. *Science*, 321(5885):53–57.
- Knierim, J. J., Kudrimoti, H. S., and McNaughton, B. L. (1995). Place cells, head direction cells, and the learning of landmark stability. *The Journal of neuroscience : the official journal of the Society for Neuroscience*, 15(3 Pt 1):1648–1659.
- Koester, H. J. (2005). Target Cell-Dependent Normalization of Transmitter Release at Neocortical Synapses. *Science*, 308(5723):863–866.
- Kohara, K., Pignatelli, M., Rivest, A. J., Jung, H.-Y., Kitamura, T., Suh, J., Frank, D., Kajikawa, K., Mise, N., Obata, Y., Wickersham, I. R., and Tonegawa, S. (2013). nm.3614. *Nature Neuroscience*, 17(2):269–279.
- Köhler, C. (1984). Morphological details of the projection from the presubiculum to the entorhinal area as shown with the novel PHA-L immunohistochemical tracing method in the rat. *Neuroscience Letters*, 45(3):285–290.

- Köhler, C. (1985). Intrinsic projections of the retrohippocampal region in the rat brain. I. The subicular complex. *The Journal of Comparative Neurology*.
- Kole, M. H. P. (2011). First node of Ranvier facilitates high-frequency burst encoding. *Neuron*, 71(4):671–682.
- Kole, M. H. P., Letzkus, J. J., and Stuart, G. J. (2007). Axon initial segment Kv1 channels control axonal action potential waveform and synaptic efficacy. *Neuron*, 55(4):633–647.
- Kole, M. H. P. and Stuart, G. J. (2012). Signal processing in the axon initial segment. *Neuron*, 73(2):235–247.
- Kononenko, N. L. and Witter, M. P. (2011). Presubiculum layer III conveys retrosplenial input to the medial entorhinal cortex. *Hippocampus*, pages n/a–n/a.
- Korogod, N., Lou, X., and Schneggenburger, R. (2005). Presynaptic Ca<sup>2+</sup> requirements and developmental regulation of posttetanic potentiation at the calyx of Held. *Journal of Neuroscience*, 25(21):5127–5137.
- Korogod, N., Lou, X., and Schneggenburger, R. (2007). Posttetanic potentiation critically depends on an enhanced Ca(2+) sensitivity of vesicle fusion mediated by presynaptic PKC. *Proceedings of the National Academy of Sciences of the United States of America*, 104(40):15923–15928.
- Kosel, K. C., Van Hoesen, G. W., and Rosene, D. L. (1983). A direct projection from the perirhinal cortex (area 35) to the subiculum in the rat. *Brain research*, 269(2):347–351.
- Krnjevic, K. and Miledi, R. (1959). Presynaptic failure of neuromuscular propagation in rats. *The Journal of Physiology*, 149:1–22.
- Langston, R. F., Ainge, J. A., Couey, J. J., Canto, C. B., Bjerknes, T. L., Witter, M. P., Moser, E. I., and Moser, M. B. (2010). Development of the Spatial Representation System in the Rat. *Science*, 328(5985):1576–1580.
- Larkum, M. E., Zhu, J. J., and Sakmann, B. (1999). A new cellular mechanism for coupling inputs arriving at different cortical layers. *Nature*, 398(6725):338–341.
- Le Duigou, C., Simonnet, J., Teleńczuk, M. T., Fricker, D., and Miles, R. (2014). Recurrent synapses and circuits in the CA3 region of the hippocampus: an associative network. *Frontiers in cellular neuroscience*, 7:262.
- Lee, D., Lee, K.-H., Ho, W.-K., and Lee, S.-H. (2007). Target cell-specific involvement of presynaptic mitochondria in post-tetanic potentiation at hippocampal mossy fiber synapses. *Journal of Neuroscience*, 27(50):13603–13613.
- Lee, J. S., Ho, W.-K., and Lee, S.-H. (2010). Post-tetanic increase in the fast-releasing synaptic vesicle pool at the expense of the slowly releasing pool. *The Journal of general physiology*, 136(3):259–272.
- Lee, S., Kruglikov, I., Huang, Z. J., Fishell, G., and Rudy, B. (2013). A disinhibitory circuit mediates motor integration in the somatosensory cortex. *Nature Neuroscience*, 16(11):1662–1670.

- Lillie, R. S. (1925). Factors affecting transmission and recovery in the passive iron nerve model. *The Journal of general physiology*, 7(4):473–507.
- Lorente De Nó, R. (1933). Studies on the structure of the cerebral cortex. I. The Area Entorhinalis. *Journal für Psychologie und Neurologie*, pages 1–58.
- Lorente de Nó, R. (1934). Studies on the structure of the cerebral cortex. II. Continuation of the study of the ammonic system. *Journal für Psychologie und Neurologie*.
- Lőrincz, A. and Nusser, Z. (2008). Cell-type-dependent molecular composition of the axon initial segment. *Journal of Neuroscience*, 28(53):14329–14340.
- Losonczy, A., Biró, Á. A., and Nusser, Z. (2004). Persistently active cannabinoid receptors mute a subpopulation of hippocampal interneurons. *Proceedings of the National Academy of Sciences of the United States of America*, 101(5):1362–1367.
- Lübke, J. and Feldmeyer, D. (2007). Excitatory signal flow and connectivity in a cortical column: focus on barrel cortex. *Brain Structure and Function*, 212(1):3–17.
- Lüscher, H. R. and Shiner, J. S. (1990). Computation of action potential propagation and presynaptic bouton activation in terminal arborizations of different geometries. *Biophysj*, 58(6):1377–1388.
- Ma, Y., Hu, H., Berrebi, A. S., Mathers, P. H., and Agmon, A. (2006). Distinct subtypes of somatostatin-containing neocortical interneurons revealed in transgenic mice. *Journal of Neuroscience*, 26(19):5069–5082.
- Madisen, L., Zwingman, T. A., Sunkin, S. M., Oh, S. W., Zariwala, H. A., Gu, H., Ng, L. L., Palmiter, R. D., Hawrylycz, M. J., Jones, A. R., Lein, E. S., and Zeng, H. (2010). A robust and high-throughput Cre reporting and characterization system for the whole mouse brain. *Nature Publishing Group*, 13(1):133–140.
- Magleby, K. L. and Zengel, J. E. (1975). A dual effect of repetitive stimulation on post-tetanic potentiation of transmitter release at the frog neuromuscular junction. *The Journal of Physiology*, 245(1):163–182.
- Magleby, K. L. and Zengel, J. E. (1976). Augmentation: A process that acts to increase transmitter release at the frog neuromuscular junction. *The Journal of Physiology*, 257(2):449–470.
- Major, G., Larkum, M. E., and Schiller, J. (2013). Active Properties of Neocortical Pyramidal Neuron Dendrites. *Annual Review of Neuroscience*, 36(1):1–24.
- Manor, Y., Koch, C., and Segev, I. (1991). Effect of geometrical irregularities on propagation delay in axonal trees. *Biophysj*, 60(6):1424–1437.
- Manseau, F., Marinelli, S., Méndez, P., Schwaller, B., Prince, D. A., Huguenard, J. R., and Bacci, A. (2010). Desynchronization of Neocortical Networks by Asynchronous Release of GABA at Autaptic and Synaptic Contacts from Fast-Spiking Interneurons. *PLoS biology*, 8(9):e1000492.

- Markram, H., Lübke, J., Frotscher, M., Roth, A., and Sakmann, B. (1997). Physiology and anatomy of synaptic connections between thick tufted pyramidal neurones in the developing rat neocortex. *The Journal of Physiology*, 500 ( Pt 2):409–440.
- Markram, H., Wang, Y., and Tsodyks, M. (1998). Differential signaling via the same axon of neocortical pyramidal neurons. *Proceedings of the National Academy of Sciences of the United States of America*, 95(9):5323–5328.
- Marozzi, E. and Jeffery, K. J. (2012). Place, space and memory cells. *Current biology : CB*, 22(22):R939–42.
- Martina, M., Schultz, J. H., Ehmke, H., Monyer, H., and Jonas, P. (1998). Functional and molecular differences between voltage-gated K<sup>+</sup> channels of fast-spiking interneurons and pyramidal neurons of rat hippocampus. *The Journal of neuroscience : the official journal of the Society for Neuroscience*, 18(20):8111–8125.
- McBain, C. J. and Fisahn, A. (2001). Interneurons unbound. *Nature Reviews Neuroscience*, 2(1):11–23.
- McNaughton, B. L., Battaglia, F. P., Jensen, O., Moser, E. I., and Moser, M.-B. (2006). Path integration and the neural basis of the 'cognitive map'. *Nature Reviews Neuroscience*, 7(8):663–678.
- Menendez de la Prida, L., Suarez, F., and Pozo, M. A. (2003). Electrophysiological and morphological diversity of neurons from the rat subicular complex in vitro. *Hippocampus*, 13(6):728–744.
- Michael Wyss, J. (1981). An autoradiographic study of the efferent connections of the entorhinal cortex in the rat. *The Journal of Comparative Neurology*, 199(4):495–512.
- Mizumori, S. J. and Williams, J. D. (1993). Directionally selective mnemonic properties of neurons in the lateral dorsal nucleus of the thalamus of rats. *The Journal of neuroscience : the official journal of the Society for Neuroscience*, 13(9):4015–4028.
- Mochida, S., Few, A. P., Scheuer, T., and Catterall, W. A. (2008). Regulation of Presynaptic CaV2.1 Channels by Ca<sup>2+</sup> Sensor Proteins Mediates Short-Term Synaptic Plasticity. *Neuron*, 57(2):210–216.
- Morris, R., Garrud, P., Rawlins, J., and O'Keefe, J. (1982). Place navigation impaired in rats with hippocampal lesions. *Nature*.
- Moser, E. I. and Moser, M.-B. (2013). Grid Cells and Neural Coding in High-End Cortices. *Neuron*, 80(3):765–774.
- Muir, G. M., Brown, J. E., Carey, J. P., Hirvonen, T. P., Della Santina, C. C., Minor, L. B., and Taube, J. S. (2009). Disruption of the Head Direction Cell Signal after Occlusion of the Semicircular Canals in the Freely Moving Chinchilla. *Journal of Neuroscience*, 29(46):14521–14533.

- Nagel, G., Szellas, T., Huhn, W., Kateriya, S., Adeishvili, N., Berthold, P., Ollig, D., Hegemann, P., and Bamberg, E. (2003). Channelrhodopsin-2, a directly light-gated cation-selective membrane channel. *Proceedings of the National Academy of Sciences of the United States of America*, 100(24):13940–13945.
- Nishikawa, S., Goto, S., Hamasaki, T., Yamada, K., and Ushio, Y. (2002). Involvement of reelin and Cajal-Retzius cells in the developmental formation of vertical columnar structures in the cerebral cortex: evidence from the study of mouse presubicular cortex. *Cerebral cortex (New York, N.Y. : 1991)*, 12(10):1024–1030.
- O’Keefe, J. and Dostrovsky, J. (1971). The hippocampus as a spatial map. Preliminary evidence from unit activity in the freely-moving rat. *Brain research*, 34(1):171–175.
- O’Mara, S. M., Commins, S., Anderson, M., and Gigg, J. (2001). The subiculum: a review of form, physiology and function. *Progress in neurobiology*, 64(2):129–155.
- Otsu, Y., Shahrezaei, V., Li, B., Raymond, L. A., Delaney, K. R., and Murphy, T. H. (2004). Competition between phasic and asynchronous release for recovered synaptic vesicles at developing hippocampal autaptic synapses. *Journal of Neuroscience*, 24(2):420–433.
- Packer, A. M. and Yuste, R. (2011). Dense, unspecific connectivity of neocortical parvalbumin-positive interneurons: a canonical microcircuit for inhibition? *Journal of Neuroscience*, 31(37):13260–13271.
- Panatier, A., Vallée, J., Haber, M., Murai, K. K., Lacaille, J.-C., and Robitaille, R. (2011). Astrocytes Are Endogenous Regulators of Basal Transmission at Central Synapses. *Cell*, 146(5):785–798.
- Parnas, I. and Parnas, H. (2010). Control of neurotransmitter release: From Ca<sup>2+</sup> to voltage dependent G-protein coupled receptors. *Pflügers Archiv European Journal of Physiology*, 460(6):975–990.
- Parra, P., Gulyás, A. I., and Miles, R. (1998). How many subtypes of inhibitory cells in the hippocampus? *Neuron*, 20(5):983–993.
- Pascual, O. (2005). Astrocytic Purinergic Signaling Coordinates Synaptic Networks. *Science*, 310(5745):113–116.
- Perrenoud, Q., Geoffroy, H., Gauthier, B., Rancillac, A., Alfonsi, F., Kessaris, N., Rossier, J., Vitalis, T., and Gallopin, T. (2012). Characterization of Type I and Type II nNOS-Expressing Interneurons in the Barrel Cortex of Mouse. *Frontiers in neural circuits*, 6:36.
- Perrenoud, Q., Rossier, J., Geoffroy, H., Vitalis, T., and Gallopin, T. (2013). Diversity of GABAergic Interneurons in Layer VIa and VIb of Mouse Barrel Cortex. *Cerebral Cortex*, 23(2):423–441.
- Peters, A. and Feldman, M. L. (1976). The projection of the lateral geniculate nucleus to area 17 of the rat cerebral cortex. I. General description. *Journal of neurocytology*, 5(1):63–84.

- Peters, H. C., Hu, H., Pongs, O., Storm, J. F., and Isbrandt, D. (2004). Conditional transgenic suppression of M channels in mouse brain reveals functions in neuronal excitability, resonance and behavior. *Nature Neuroscience*, 8(1):51–60.
- Petreaunu, L., Huber, D., Sobczyk, A., and Svoboda, K. (2007). Channelrhodopsin-2-assisted circuit mapping of long-range callosal projections. *Nature Neuroscience*, 10(5):663–668.
- Po, S., Roberds, S., Snyders, D. J., Tamkun, M. M., and Bennett, P. B. (1993). Heteromultimeric assembly of human potassium channels. Molecular basis of a transient outward current? *Circulation research*, 72(6):1326–1336.
- Pouille, F. and Scanziani, M. (2004). Routing of spike series by dynamic circuits in the hippocampus. *Nature*, 429(6993):717–723.
- Puopolo, M., Raviola, E., and Bean, B. P. (2007). Roles of Subthreshold Calcium Current and Sodium Current in Spontaneous Firing of Mouse Midbrain Dopamine Neurons. *Journal of Neuroscience*, 27(3):645–656.
- Raffaelli, G., Saviane, C., Mohajerani, M. H., Pedarzani, P., and Cherubini, E. (2004). BK potassium channels control transmitter release at CA3-CA3 synapses in the rat hippocampus. *The Journal of Physiology*, 557(Pt 1):147–157.
- Rakic, P. (1974). Neurons in rhesus monkey visual cortex: systematic relation between time of origin and eventual disposition. *Science*, 183(4123):425–427.
- Ramon y Cajal, S. (1899). *Textura del sistema nervioso del hombre y de los vertebrados*. Oxford Univ Press.
- Ranck, Jr, J. B. (1984). Head direction cells in the deep cell layer of dorsal presubiculum in freely moving rats. *Soc Neurosci Abstr*.
- Rasmussen, H. B., Frøkjær-Jensen, C., Jensen, C. S., Jensen, H. S., Jørgensen, N. K., Misonou, H., Trimmer, J. S., Olesen, S.-P., and Schmitt, N. (2007). Requirement of subunit co-assembly and ankyrin-G for M-channel localization at the axon initial segment. *Journal of cell science*, 120(Pt 6):953–963.
- Ray, S., Naumann, R., Burgalossi, A., Tang, Q., Schmidt, H., and Brecht, M. (2014). Grid-Layout and Theta-Modulation of Layer 2 Pyramidal Neurons in Medial Entorhinal Cortex. *Science*, 343(6173):891–896.
- Redish, A. D., Elga, A. N., and Touretzky, D. S. (1996). A coupled attractor model of the rodent head direction system. *Network: Computation in ...*, 7(4):671–685.
- Regehr, W. G. (2012). Short-term presynaptic plasticity. *Cold Spring Harbor perspectives in biology*, 4(7):a005702.
- Rizzoli, S. O. and Betz, W. J. (2005). Synaptic vesicle pools. *Nature Reviews Neuroscience*, 6(1):57–69.
- Roberts, W. M. (1993). Spatial calcium buffering in saccular hair cells. *Nature*, 363(6424):74–76.

- Rose, J. E. and Woolsey, C. N. (1948). Structure and relations of limbic cortex and anterior thalamic nuclei in rabbit and cat. *The Journal of Comparative Neurology*, 89(3):279–347.
- Rose, M. (1926). Der Allocortex bei Mensch und Tier ; 1. Teil.
- Rowland, D. C., Weible, A. P., Wickersham, I. R., Wu, H., Mayford, M., Witter, M. P., and Kentros, C. G. (2013). Transgenically Targeted Rabies Virus Demonstrates a Major Monosynaptic Projection from Hippocampal Area CA2 to Medial Entorhinal Layer II Neurons. *Journal of Neuroscience*, 33(37):14889–14898.
- Rudy, B., Fishell, G., Lee, S., and Hjerling-Leffler, J. (2010). Three groups of interneurons account for nearly 100GABAergic neurons. *Developmental Neurobiology*, 71(1):45–61.
- Sabatini, B. L. and Regehr, W. G. (1997). Control of neurotransmitter release by presynaptic waveform at the granule cell to Purkinje cell synapse. *The Journal of neuroscience : the official journal of the Society for Neuroscience*, 17(10):3425–3435.
- Sakaba, T. and Neher, E. (2001). Calmodulin mediates rapid recruitment of fast-releasing synaptic vesicles at a calyx-type synapse. *Neuron*, 32(6):1119–1131.
- Sargolini, F., Fyhn, M., Hafting, T., McNaughton, B. L., Witter, M. P., Moser, M.-B., and Moser, E. I. (2006). Conjunctive representation of position, direction, and velocity in entorhinal cortex. *Science*, 312(5774):758–762.
- Sasaki, T. (2013). The axon as a unique computational unit in neurons. *Neuroscience Research*, 75(2):83–88.
- Sasaki, T., Matsuki, N., and Ikegaya, Y. (2011). Action-Potential Modulation During Axonal Conduction. *Science*, 331(6017):599–601.
- Sasaki, T., Matsuki, N., and Ikegaya, Y. (2012). Effects of axonal topology on the somatic modulation of synaptic outputs. *Journal of Neuroscience*, 32(8):2868–2876.
- Sätzler, K., Söhl, L. F., Bollmann, J. H., Borst, J. G. G., Frotscher, M., Sakmann, B., and Lübke, J. H. R. (2002). Three-dimensional reconstruction of a calyx of Held and its postsynaptic principal neuron in the medial nucleus of the trapezoid body. *Journal of Neuroscience*, 22(24):10567–10579.
- Saviane, C., Mohajerani, M. H., and Cherubini, E. (2003). An ID-like current that is downregulated by Ca<sup>2+</sup> modulates information coding at CA3-CA3 synapses in the rat hippocampus. *The Journal of Physiology*, 552(Pt 2):513–524.
- Saviane, C. and Silver, R. A. (2006). Fast vesicle reloading and a large pool sustain high bandwidth transmission at a central synapse. *Nature*, 439(7079):983–987.
- Scanziani, M., Gähwiler, B. H., and Charpak, S. (1998). Target cell-specific modulation of transmitter release at terminals from a single axon. *Proceedings of the National Academy of Sciences of the United States of America*, 95(20):12004–12009.

- Schikorski, T. and Stevens, C. F. (1999). Quantitative fine-structural analysis of olfactory cortical synapses. *Proceedings of the National Academy of Sciences of the United States of America*, 96(7):4107–4112.
- Schikorski, T. and Stevens, C. F. (2001). Morphological correlates of functionally defined synaptic vesicle populations. *Nature Neuroscience*, 4(4):391–395.
- Schmidt-Hieber, C. and Häusser, M. (2013). Cellular mechanisms of spatial navigation in the medial entorhinal cortex. *Nature Neuroscience*, 16(3):325–331.
- Scott, R., Ruiz, A., Henneberger, C., Kullmann, D. M., and Rusakov, D. A. (2008). Analog modulation of mossy fiber transmission is uncoupled from changes in presynaptic Ca<sup>2+</sup>. *Journal of Neuroscience*, 28(31):7765–7773.
- Shadlen, M. N. and Newsome, W. T. (1995). Is there a signal in the noise? *Current opinion in neurobiology*, 5(2):248–250.
- Shah, M. M., Migliore, M., Valencia, I., Cooper, E. C., and Brown, D. A. (2008). Functional significance of axonal Kv7 channels in hippocampal pyramidal neurons. *Proceedings of the National Academy of Sciences of the United States of America*, 105(22):7869–7874.
- Sharp, P. E., Blair, H. T., and Cho, J. (2001a). The anatomical and computational basis of the rat head-direction cell signal. *Trends in Neurosciences*, 24(5):289–294.
- Sharp, P. E., Tinkelman, A., and Cho, J. (2001b). Angular velocity and head direction signals recorded from the dorsal tegmental nucleus of gudden in the rat: implications for path integration in the head direction cell circuit. *Behavioral neuroscience*, 115(3):571–588.
- Sheng, M. and Kim, E. (2011). The postsynaptic organization of synapses. *Cold Spring Harbor perspectives in biology*, 3(12).
- Sheng, M., Liao, Y. J., Jan, Y. N., and Jan, L. Y. (1993). Presynaptic A-current based on heteromultimeric K<sup>+</sup> channels detected in vivo. *Nature*, 365(6441):72–75.
- Shepherd, G. M. and Harris, K. M. (1998). Three-dimensional structure and composition of CA3→CA1 axons in rat hippocampal slices: implications for presynaptic connectivity and compartmentalization. *The Journal of neuroscience : the official journal of the Society for Neuroscience*, 18(20):8300–8310.
- Shipley, M. T. (1975). The topographical and laminar organization of the presubiculum’s projection to the ipsi- and contralateral entorhinal cortex in the guinea pig. *The Journal of Comparative Neurology*, 160(1):127–145.
- Shu, Y., Hasenstaub, A., Duque, A., Yu, Y., and McCormick, D. A. (2006). Modulation of intracortical synaptic potentials by presynaptic somatic membrane potential. *Nature*, 441(7094):761–765.
- Shu, Y., Yu, Y., Yang, J., and McCormick, D. A. (2007). Selective control of cortical axonal spikes by a slowly inactivating K<sup>+</sup> current. *Proceedings of the National Academy of Sciences of the United States of America*, 104(27):11453–11458.

- Silberberg, G., Grillner, S., LeBeau, F. E. N., Maex, R., and Markram, H. (2005). Synaptic pathways in neural microcircuits. *Trends in Neurosciences*, 28(10):541–551.
- Silberberg, G. and Markram, H. (2007). Disynaptic Inhibition between Neocortical Pyramidal Cells Mediated by Martinotti Cells. *Neuron*, 53(5):735–746.
- Simonnet, J., Eugène, E., Cohen, I., Miles, R., and Fricker, D. (2013). Cellular neuroanatomy of rat presubiculum. *The European journal of neuroscience*, 37(4):583–597.
- Skaggs, W. E., Knierim, J. J., Kudrimoti, H. S., and McNaughton, B. L. (1995). A model of the neural basis of the rat’s sense of direction. *Advances in neural information processing systems*, 7:173–180.
- Slomianka, L. and Geneser, F. A. (1991). Distribution of acetylcholinesterase in the hippocampal region of the mouse: I. Entorhinal area, parasubiculum, retrosplenial area, and presubiculum. *The Journal of Comparative Neurology*, 303(3):339–354.
- Soleng, A. F., Chiu, K., and Raastad, M. (2003). Unmyelinated axons in the rat hippocampus hyperpolarize and activate an H current when spike frequency exceeds 1 Hz. *The Journal of Physiology*, 552(Pt 2):459–470.
- Solstad, T., Boccara, C. N., Kropff, E., Moser, M.-B., and Moser, E. I. (2008). Representation of geometric borders in the entorhinal cortex. *Science*, 322(5909):1865–1868.
- Stackman, R. W. and Taube, J. S. (1998). Firing properties of rat lateral mammillary single units: head direction, head pitch, and angular head velocity. *The Journal of neuroscience : the official journal of the Society for Neuroscience*, 18(21):9020–9037.
- Storm, J. F. (1990). Potassium currents in hippocampal pyramidal cells. *Prog. brain Res.*
- Südhof, T. C. (2013). Neurotransmitter Release: The Last Millisecond in the Life of a Synaptic Vesicle. *Neuron*, 80(3):675–690.
- Sugar, J., Witter, M. P., van Strien, N. M., and Cappaert, N. L. M. (2011). The retrosplenial cortex: intrinsic connectivity and connections with the (para)hippocampal region in the rat. An interactive connectome. *Frontiers in neuroinformatics*, page 7.
- Sullivan, J. M. (2007). A Simple Depletion Model of the Readily Releasable Pool of Synaptic Vesicles Cannot Account for Paired-Pulse Depression. *Journal of Neurophysiology*, 97(1):948–950.
- Suzuki, N. and Bekkers, J. M. (2010). Inhibitory neurons in the anterior piriform cortex of the mouse: Classification using molecular markers. *The Journal of Comparative Neurology*, 518(10):1670–1687.
- Swadlow, H. A. and Gusev, A. G. (2002). Receptive-field construction in cortical inhibitory interneurons. *Nature Neuroscience*, 5(5):403–404.
- Swanson, L. W. and Cowan, W. M. (1977). An autoradiographic study of the organization of the efferent connections of the hippocampal formation in the rat. *The Journal of Comparative Neurology*, 172(1):49–84.

- Talbot, J. D. (2003). Inhibition of Mitochondrial Ca<sup>2+</sup> Uptake Affects Phasic Release From Motor Terminals Differently Depending on External [Ca<sup>2+</sup>]. *Journal of Neurophysiology*, 90(1):491–502.
- Tamamaki, N., Yanagawa, Y., Tomioka, R., Miyazaki, J.-I., Obata, K., and Kaneko, T. (2003). Green fluorescent protein expression and colocalization with calretinin, parvalbumin, and somatostatin in the GAD67-GFP knock-in mouse. *The Journal of Comparative Neurology*, 467(1):60–79.
- Taniguchi, H., He, M., Wu, P., Kim, S., Paik, R., Sugino, K., Kvitsiani, D., Kvitsani, D., Fu, Y., Lu, J., Lin, Y., Miyoshi, G., Shima, Y., Fishell, G., Nelson, S. B., and Huang, Z. J. (2011). A resource of Cre driver lines for genetic targeting of GABAergic neurons in cerebral cortex. *Neuron*, 71(6):995–1013.
- Tasaki, I. (1939). The electro-saltatory transmission of the nerve impulse and the effect of narcosis upon the nerve fiber. *The American Journal of Physiology*, 127:211–227.
- Taube, J. S. (1995). Head direction cells recorded in the anterior thalamic nuclei of freely moving rats. *The Journal of neuroscience*.
- Taube, J. S. (2007). The Head Direction Signal: Origins and Sensory-Motor Integration. *Annual Review of Neuroscience*, 30(1):181–207.
- Taube, J. S., Kesslak, J. P., and Cotman, C. W. (1992). Lesions of the rat postsubiculum impair performance on spatial tasks. *Behavioral and neural biology*, 57(2):131–143.
- Taube, J. S., Muller, R. U., and Ranck, J. B. (1990a). Head-direction cells recorded from the postsubiculum in freely moving rats. I. Description and quantitative analysis. *The Journal of neuroscience : the official journal of the Society for Neuroscience*, 10(2):420–435.
- Taube, J. S., Muller, R. U., and Ranck, J. B. (1990b). Head-direction cells recorded from the postsubiculum in freely moving rats. II. Effects of environmental manipulations. *The Journal of neuroscience : the official journal of the Society for Neuroscience*, 10(2):436–447.
- Thorndike, R. L. (1953). Who belongs in the family? *Psychometrika*, 18(4):267–276.
- Toledo-Rodriguez, M., El Manira, A., Wallén, P., Svirskis, G., and Hounsgaard, J. (2005). Cellular signalling properties in microcircuits. *Trends in Neurosciences*, 28(10):534–540.
- van der Meer, M. A. A., Knierim, J. J., Yoganarasimha, D., Wood, E. R., and van Rossum, M. C. W. (2007). Anticipation in the rodent head direction system can be explained by an interaction of head movements and vestibular firing properties. *Journal of Neurophysiology*, 98(4):1883–1897.
- van Groen, T. and Wyss, J. M. (1990a). Connections of the retrosplenial granular a cortex in the rat. *The Journal of Comparative Neurology*, 300(4):593–606.
- van Groen, T. and Wyss, J. M. (1990b). The connections of presubiculum and parasubiculum in the rat. *Brain research*, 518(1-2):227–243.

- van Groen, T. and Wyss, J. M. (1990c). The postsubicular cortex in the rat: characterization of the fourth region of the subicular cortex and its connections. *Brain research*, 529(1-2):165–177.
- van Groen, T. and Wyss, J. M. (1992a). Connections of the retrosplenial dysgranular cortex in the rat. *The Journal of Comparative Neurology*, 315(2):200–216.
- van Groen, T. and Wyss, J. M. (1992b). Projections from the laterodorsal nucleus of the thalamus to the limbic and visual cortices in the rat. *The Journal of Comparative Neurology*, 324(3):427–448.
- van Groen, T. and Wyss, J. M. (1995). Projections from the anterodorsal and anteroventral nucleus of the thalamus to the limbic cortex in the rat. *The Journal of Comparative Neurology*, 358(4):584–604.
- van Haeften, T., Wouterlood, F. G., Jorritsma-Byham, B., and Witter, M. P. (1997). GABAergic presubicular projections to the medial entorhinal cortex of the rat. *The Journal of neuroscience : the official journal of the Society for Neuroscience*, 17(2):862–874.
- van Strien, N. M., Cappaert, N. L. M., and Witter, M. P. (2009). The anatomy of memory: an interactive overview of the parahippocampal–hippocampal network. *Nature Reviews Neuroscience*, 10(4):272–282.
- Vervaeke, K., Gu, N., Agdestein, C., Hu, H., and Storm, J. F. (2006). Kv7/KCNQ/M-channels in rat glutamatergic hippocampal axons and their role in regulation of excitability and transmitter release. *The Journal of Physiology*, 576(Pt 1):235–256.
- Vogt, B. A. and Miller, M. W. (1983). Cortical connections between rat cingulate cortex and visual, motor, and postsubicular cortices. *The Journal of Comparative Neurology*, 216(2):192–210.
- Vyleta, N. P. and Jonas, P. (2014). Loose coupling between Ca<sup>2+</sup> channels and release sensors at a plastic hippocampal synapse. *Science*, 343(6171):665–670.
- Waldeck, R. F., Pereda, A., and Faber, D. S. (2000). Properties and plasticity of paired-pulse depression at a central synapse. *The Journal of neuroscience : the official journal of the Society for Neuroscience*, 20(14):5312–5320.
- Ward Jr, J. (1963). Hierarchical grouping to optimize an objective function. *Journal of the American statistical association*.
- Wiener, S. I. and Taube, J. S. (2005). *Head direction cells and the neural mechanisms of spatial orientation*. The MIT Press.
- Wills, T. J., Cacucci, F., Burgess, N., and O’Keefe, J. (2010). Development of the Hippocampal Cognitive Map in Prewaning Rats. *Science*, 328(5985):1573–1576.
- Wu, L. G. and Borst, J. G. (1999). The reduced release probability of releasable vesicles during recovery from short-term synaptic depression. *Neuron*, 23(4):821–832.
- Wyss, J. M. and van Groen, T. (1992). Connections between the retrosplenial cortex and the hippocampal formation in the rat: a review. *Hippocampus*, 2(1):1–11.

- Xu, J., He, L., and Wu, L.-G. (2007). Role of Ca<sup>2+</sup> channels in short-term synaptic plasticity. *Current opinion in neurobiology*, 17(3):352–359.
- Xu, J. and Wu, L.-G. (2005). The Decrease in the Presynaptic Calcium Current Is a Major Cause of Short-Term Depression at a Calyx-Type Synapse. *Neuron*, 46(4):633–645.
- Xue, L. and Wu, L.-G. (2010). Post-tetanic potentiation is caused by two signalling mechanisms affecting quantal size and quantal content. *The Journal of Physiology*, 588(Pt 24):4987–4994.
- Yoder, R. M., Clark, B. J., and Taube, J. S. (2011). Origins of landmark encoding in the brain. *Trends in Neurosciences*.
- Yoder, R. M. and Taube, J. S. (2009). Head Direction Cell Activity in Mice: Robust Directional Signal Depends on Intact Otolith Organs. *Journal of Neuroscience*, 29(4):1061–1076.
- Yoder, R. M. and Taube, J. S. (2011). Projections to the anterodorsal thalamus and lateral mammillary nuclei arise from different cell populations within the postsubiculum: Implications for the control of head direction cells. *Hippocampus*, 21(10):1062–1073.
- Yoshida, M. and Hasselmo, M. E. (2009). Persistent Firing Supported by an Intrinsic Cellular Mechanism in a Component of the Head Direction System. *Journal of Neuroscience*, 29(15):4945–4952.
- Zhang, F., Wang, L.-P., Brauner, M., Liewald, J. F., Kay, K., Watzke, N., Wood, P. G., Bamberg, E., Nagel, G., Gottschalk, A., and Deisseroth, K. (2007). Multimodal fast optical interrogation of neural circuitry. *Nature*, 446(7136):633–639.
- Zhang, S. J., Ye, J., Miao, C., Tsao, A., Cerniauskas, I., Ledergerber, D., Moser, M. B., and Moser, E. I. (2013). Optogenetic Dissection of Entorhinal-Hippocampal Functional Connectivity. *Science*, 340(6128):1232627–1232627.
- Zhao, S., Ting, J. T., Atallah, H. E., Qiu, L., Tan, J., Gloss, B., Augustine, G. J., Deisseroth, K., Luo, M., Graybiel, A. M., and Feng, G. (2011). Cell type-specific channelrhodopsin-2 transgenic mice for optogenetic dissection of neural circuitry function. *Nature methods*, 8(9):745–752.
- Zhu, J., Jiang, M., Yang, M., Hou, H., and Shu, Y. (2011). Membrane potential-dependent modulation of recurrent inhibition in rat neocortex. *PLoS biology*, 9(3):e1001032.
- Zucker, R. S. and Regehr, W. G. (2002). Short-term synaptic plasticity. *Annual Review of Physiology*, 64:355–405.
- Zugaro, M. B., Arleo, A., Berthoz, A., and Wiener, S. I. (2003). Rapid spatial reorientation and head direction cells. *Journal of Neuroscience*, 23(8):3478–3482.



## Abstract

Cognitive functions rely on the generation and regulation of information in specialized neuronal networks. The presubiculum, a cortical area located between the hippocampus and the entorhinal cortex, is involved in signaling the sense of orientation in animals as well as in humans. Most presubicular neurons are Head Direction Cells, that is, they fire as a function of directional heading. The presubiculum constitutes a crucial crossroad for spatial information. Very few data exist on the functional organization of the presubiculum, but its 6-layered cytoarchitecture suggests that signals are not passively relayed but rather actively integrated and refined.

During my PhD, I studied the microcircuit elements of rodent presubiculum in the slice preparation, linking structure and physiology using patch clamp records.

First, I focused on rat principal neurons and distinguished 3 groups: a homogeneous population of regular spiking neurons in superficial layers, mostly pyramidal; intrinsically burst firing neurons of layer 4; and a very heterogeneous population of regular spiking neurons in deep layers. These populations constitute the primary elements for information processing in the presubiculum, and their diversity suggests a high computational power.

Then, I addressed the question of the inhibitory control in the presubiculum. Recordings were performed from slices of transgenic mouse strains that express fluorescent proteins in interneurons. We showed a continuum of diversity for parvalbumin- (PV) and somatostatin- (SST) containing interneurons, from the archetypical PV-positive fast spiking basket cells to the SST-positive low-threshold spiking Martinotti cells. Regarding the inhibition, the presubiculum seems to possess the complexity of all cortical areas.

Finally, I investigated the synaptic interactions of pyramidal cells and Martinotti cells in superficial layers, using dual patch clamp recordings. Martinotti cells provide low amplitude but reliable inhibition onto pyramidal cell dendrites. I found that the strength at the excitatory synapse was enhanced following repetitive stimulation at high frequency. Consequently, dendritic inhibition by presubicular Martinotti cells may act as a homeostatic response to sustained excitation.

My PhD work brought essential knowledge about the presubicular microcircuit. It has shed light on the different populations of principal neurons and GABAergic interneurons and has uncovered a feedback inhibitory loop that is recruited during sustained but not transient activity.

## Résumé

Les fonctions cognitives dépendent de la génération et du traitement de l'information dans des réseaux neuronaux spécialisés. Le présubiculum, une aire corticale située entre l'hippocampe et le cortex entorhinal, est impliqué dans le sens de l'orientation aussi bien chez l'animal que chez l'Homme. La plupart des neurones du présubiculum sont des cellules de direction de la tête, elles déchargent en fonction de la direction prise par la tête de l'animal. Peu de données existent sur l'organisation fonctionnelle du présubiculum, mais les 6 couches suggèrent que les informations n'y sont pas relayées passivement, mais qu'elles y sont plutôt activement intégrées et raffinées. J'ai étudié les éléments du microcircuit presubiculaire sur tranche aigüe de rongeur, liant structure et physiologie en utilisant la technique de patch clamp.

Je me suis d'abord intéressé aux neurones principaux, chez le rat, et j'ai identifié 3 groupes : une population homogène de neurones pyramidaux à décharge régulière dans les couches superficielles ; des neurones pyramidaux à décharge en bouffée dans la couche 4 ; une population hétérogène de neurones à décharge régulière située en couches profondes. Ces populations neuronales constituent la base cellulaire du codage de l'information, et leur diversité suggère une puissance computationnelle avancée dans le traitement du signal nerveux au niveau du présubiculum.

Je me suis ensuite intéressé au contrôle inhibiteur dans le présubiculum en étudiant les propriétés des interneurones à partir de souris transgéniques exprimant une protéine fluorescente dans les interneurones. Nous avons montré qu'il existait un continuum au niveau de la diversité des interneurones, depuis des cellules en panier à décharge rapide et exprimant la parvalbumine, jusqu'au cellules de Martinotti à bas seuil d'activation et exprimant la somatostatine. Concernant l'inhibition, le présubiculum semble posséder la complexité de toute aire corticale.

Finalement, j'ai étudié les interactions synaptiques entre les cellules pyramidales et les cellules de Martinotti dans couches superficielles, en réalisant des doubles enregistrements en patch clamp. Les cellules de Martinotti procurent une inhibition fiable au niveau des dendrites des cellules pyramidales. L'efficacité de la synapse excitatrice s'améliorait lors de stimulations répétées à haute fréquence. L'inhibition dendritique délivrée par les cellules de Martinotti du présubiculum pourrait constituer un processus homéostatique répondant à une stimulation soutenue.

Mon travail de thèse a apporté des connaissances essentielles sur le microcircuit du présubiculum. Il a fait la lumière sur les différentes populations de neurones principaux et d'interneurones et a révélé une boucle de rétrocontrôle inhibiteur qui est recruté préférentiellement lors d'activités maintenues.